

BLDSC no:- DX 231681



**Pilkington Library**

Author/Filing Title ..... MATAW .....

Vol. No. .... Class Mark ..... ● T .....

**Please note that fines are charged on ALL  
overdue items.**

**FOR REFERENCE ONLY**

0402509579





**FILLER SURFACE CHARACTERISATION AND ITS  
RELATION TO THE MECHANICAL PROPERTIES OF  
POLYMER COMPOSITES**


**By**

**David Maton**

Phd.

2000

Loughborough

 Loughborough University Library
Date: Major
Class:
Acc No. 040254957

## **Abstract**

The formation of stearate on precipitated calcium carbonate (PCC) and magnesium hydroxide has been examined. The object of coating the filler surface is to achieve improved mechanical properties in the resulting composite material. The coating of a filler with stearate allows the modification of the energies of interaction so as to improve dispersion and alter the mechanical properties of the interphase region. In this work the use of Fourier transform infra-red spectroscopy (FTIR), X-ray photoelectron spectroscopy (XPS), nitrogen adsorption isotherm analysis, thermal gravimetric analysis (TGA) and carbon-hydrogen-nitrogen combustion analysis (CHN) have been used to characterise the stearate on the surface of the calcium carbonate filler. New methods for the estimation of fractional coverage and coating thickness calculation have been developed. Using dynamic mechanical thermal analysis (DMTA) the effects of the coating on the interphase region of the composite have been demonstrated.

## Acknowledgements

This work was completed as part of a CASE award, awarded to the Chemistry Department, Loughborough University, sponsored jointly by the EPSRC and Solvay (formerly part of Zeneca Resins).

I must thank all the members of the departments of Chemistry, Physics, IPTME and Chemical Engineering who have helped me with different areas of the project. Also my fellow students, past and present, from the Polymer and Surface Chemistry Group.

My special thanks must go to my industrial supervisor Dr. David Harrison of Solvay. My university supervisor, Dr. Ian Sutherland, for all the support he has given me in the last 5 years, and finally my parents for their never ending support and encouragement.

# Table of Contents

<b>ABSTRACT .....</b>	<b>2</b>
<b>ACKNOWLEDGEMENTS .....</b>	<b>3</b>
<b>TABLE OF CONTENTS.....</b>	<b>4</b>
Table of Figures.....	10
Table of Tables .....	17
<b>CHAPTER 1 INTRODUCTION .....</b>	<b>19</b>
1.1 General Background.....	19
1.2 Objectives.....	20
<b>CHAPTER 2 LITERATURE REVIEW .....</b>	<b>21</b>
2.1 Polymer Composites .....	21
2.2 Industrial Application .....	22
2.2.1 Industrial Plastics .....	22
2.2.2 Industrial Fillers .....	24
2.2.2.1 Calcium Carbonate.....	26
2.2.2.2 Magnesium Hydroxide.....	27
2.2.3 Industrial Filler Coatings .....	29
2.2.3.1 Coating Methods .....	32
2.2.3.2 Stearate based coatings .....	33
2.3 Polymer-Filler Interactions.....	34
2.3.1 Wetting.....	36

2.3.2 Adhesion .....	38
2.3.3 Dispersion .....	41
2.3.3.1 Dispersion Analysis .....	42
2.3.4 Surface and Interfacial Energies .....	43
2.3.5 Polymer Adsorption .....	46
<b>2.4 Filler, Polymer Interphase .....</b>	<b>47</b>
<b>2.5 Mechanical Properties .....</b>	<b>50</b>
2.5.1 Filler Loading .....	51
2.5.2 Industrial Processing Parameters .....	52
2.5.3 Coating Effects .....	54
2.5.4 Engineering Models .....	55
2.5.5 Filler Particle Size Theory .....	58
2.5.5.1 Bound Matrix Fraction .....	59
<b>2.6 Filler Coating Theory .....</b>	<b>62</b>
2.6.1 A 'Monolayer' Coating .....	62
2.6.2 Surface Reactive Sites .....	63
2.6.3 w/w v's Monolayer-Surface Area Relationship .....	64
2.6.4 The Coating Reaction .....	65
2.6.4.1 Aqueous Phase Reaction .....	67
2.6.4.2 Non-Aqueous Phase Reaction .....	71
2.6.4.3 Dry Coating Reaction .....	71
<b>2.7 Filler Surface Characterisation .....</b>	<b>72</b>
2.7.1 Electron Microscopy .....	74
2.7.2 Classical Analysis .....	74
2.7.3 Gas Adsorption Isotherm Analysis .....	75
2.7.3.1 Langmuir Adsorption Isotherm .....	77
2.7.3.2 BET Adsorption Isotherm .....	78
2.7.3.3 Surface Heterogeneity .....	79
2.7.4 Infrared Spectroscopy .....	81
2.7.4.1 FTIR Spectrometer .....	81
2.7.4.2 DRIFT Apparatus .....	82



2.7.4.3 DRIFT Theory .....	84
2.7.4.4 Infrared Application .....	86
2.7.5 X-ray Photoelectron Spectroscopy .....	89
2.7.5.1 XPS Apparatus .....	90
2.7.5.2 XPS Analysis .....	90
2.7.6 X-ray Diffraction .....	95
2.7.7 Dynamic Mechanical Analysis (DMA) .....	97
<b>CHAPTER 3 EXPERIMENTAL.....</b>	<b>105</b>
<b>3.1 Experimental Coating.....</b>	<b>105</b>
3.1.1 Coating Levels .....	105
<b>3.2 Experimental Preparations .....</b>	<b>105</b>
3.2.1 Wet Coating Preparations .....	106
3.2.1.1 Ammonium Stearate Coating .....	106
3.2.1.2 Stearic Acid Coatings.....	106
3.2.1.3 Sodium Stearate Coating.....	107
3.2.2 Organic Solution Coating Preparations .....	107
3.2.3 Dry Coating Preparations.....	107
3.2.4 Polymer Composite Preparation .....	108
<b>3.3 Experimental Analysis.....</b>	<b>110</b>
3.3.1 Electron Microscopy .....	110
3.3.1.1 Scanning Electron Microscopy .....	110
3.3.1.2 Transmission Electron Microscopy.....	110
3.3.2 Thermal Analysis .....	110
3.3.2.1 CHN Experimental Analysis.....	110
3.3.2.2 Thermogravimetric Experimental Analysis .....	110
3.3.3 Gas Adsorption Isotherm Analysis .....	111
3.3.4 Infrared Spectroscopy .....	111
3.3.4.1 DRIFT Experimental.....	111
3.3.5 X-Ray Photoelectron Spectroscopy .....	112
3.3.6 X-Ray Diffraction .....	113
3.3.7 DMTA Experimental Analysis .....	113

<b>CHAPTER 4 RESULTS .....</b>	<b>114</b>
<b>4.1 Electron Microscopy .....</b>	<b>114</b>
4.1.1 Calcium Carbonate.....	114
4.1.1.1 Scanning Electron Microscopy .....	114
4.1.1.2 Transmission Electron Microscopy.....	116
4.1.2 Magnesium Hydroxide.....	<b>Error! Bookmark not defined.</b>
4.1.2.1 Scanning Electron Microscopy .....	<b>Error! Bookmark not defined.</b>
4.1.2.2 Transmission Electron Microscopy.....	<b>Error! Bookmark not defined.</b>
<b>4.2 Thermal Analysis .....</b>	<b>122</b>
4.2.1 CHN Analysis .....	122
4.2.1.1 Calcium Carbonate.....	122
4.2.1.2 Magnesium Hydroxide.....	125
4.2.2 Thermogravimetric Analysis .....	126
4.2.2.1 Zeneca Batch Coated Samples .....	126
4.2.2.2 Sodium Stearate Coated Samples.....	129
4.2.2.3 Stearic Acid Coated Samples .....	130
4.2.2.4 Dry Stearic Acid Coated Samples.....	131
<b>4.3 Gas Adsorption Results .....</b>	<b>133</b>
4.3.1 Dual BET Adsorption Isotherm Theory .....	134
4.3.1.1 Single Site Adsorption .....	134
4.3.1.2 Multi Site Adsorption .....	135
4.3.2 Dual BET Adsorption Isotherm Validation.....	137
4.3.3 Calcium Carbonate - Sodium Stearate Coatings.....	138
<b>4.4 DRIFT Results.....</b>	<b>140</b>
4.4.1 Calcium Carbonate.....	140
4.4.1.1 Ammonium Stearate .....	142
4.4.1.2 Sodium Stearate .....	144
4.4.1.3 Stearic Acid Coatings.....	146
4.4.1.4 Zeneca Ammonium Stearate Coatings .....	147
4.4.1.5 Stearic Acid Dry Coated .....	147
4.4.1.6 Sodium Stearate Blended.....	148
4.4.1.7 Comparison Of Wet Coating Methods.....	149
4.4.1.8 Comparison Of Coating Material Peaks.....	151

4.4.1.9 Comparison Of Coating Peaks.....	152
4.4.2 Magnesium Hydroxide.....	157
4.4.2.1 Sodium Stearate .....	157
<b>4.5 XPS Results.....</b>	<b>160</b>
4.5.1 XPS Thickness Models.....	162
4.5.1.1 Geometric XPS Theory.....	162
4.5.1.2 'First' Generation Models .....	169
4.5.1.3 'Second' Generation Models.....	169
4.5.1.4 'Third' Generation Models .....	170
4.5.1.5 'Fourth' Generation Models .....	172
4.5.1.6 Effect of Density .....	179
4.5.1.7 Effect of Escape Depth .....	181
4.5.1.8 Model Summary.....	182
4.5.2 Calcium Carbonate.....	183
4.5.2.1 Ammonium Stearate Coatings .....	183
4.5.2.2 Sodium Stearate Coatings .....	184
4.5.2.3 Comparison Alternative Coating Methods.....	191
4.5.2.4 Sample charging.....	192
4.5.3 Magnesium Hydroxide.....	193
4.5.3.1 Sodium Stearate Coatings .....	194
<b>4.6 XRD.....</b>	<b>198</b>
4.6.1 Sodium & Calcium Stearate.....	198
4.6.2 Calcium Carbonate.....	199
<b>4.7 DMTA Analysis.....</b>	<b>201</b>
4.7.1. Dynamic Mechanical Response of uPVC.....	201
4.7.2 Dynamic Response of uPVC Composites.....	202
4.7.2.1 Dynamic Response as a function of filler loading .....	202
4.7.2.2 Dynamic Response as a function of coating level.....	204
<b>CHAPTER 5 DISCUSSION.....</b>	<b>207</b>
<b>5.1 Electron Microscopy.....</b>	<b>207</b>
5.1.1 Electron Microscopy and Gas Adsorption Analysis.....	207

<b>5.2 Thermal analysis .....</b>	<b>208</b>
<b>5.3 Gas Adsorption Analysis .....</b>	<b>209</b>
<b>5.4 IR analysis .....</b>	<b>211</b>
5.4.1 Quantitative IR analysis.....	211
5.4.2 Surface Chemistry.....	211
5.4.3 FTIR and Gas Adsorption Analysis.....	213
<b>5.5 XPS analysis .....</b>	<b>215</b>
5.5.1 Coating Characterisation.....	215
5.5.2 Coating Thickness Characterisation .....	215
5.5.3 XPS and Gas Adsorption Analysis .....	216
5.5.4 XPS and FTIR Coating Characterisation.....	218
<b>5.6 XRD analysis .....</b>	<b>219</b>
<b>5.7 Mechanical Properties .....</b>	<b>220</b>
<b>CHAPTER 6 CONCLUSION .....</b>	<b>223</b>
<b>CHAPTER 7 APPENDICES.....</b>	<b>225</b>
Appendix 1 Presentations & Publications .....	225
Appendix 2 Visual Basic XPS Thickness Calculation Program .....	227
<b>CHAPTER 8 REFERENCES.....</b>	<b>236</b>

## Table of Figures

Figure 1 ASTM definition of interface and interphase region.....	34
Figure 2 Schematic representation of a liquid drop at a surface.....	36
Figure 3 Liquid resin wetting a porous surface. When this solidifies on cooling or curing, a mechanically interlocking interface is formed.....	40
Figure 4 A diagram showing the interactions of chains grafted to the filler surface with free polymer chains.....	48
Figure 5 Summary of the relationship between many physical properties and the filler content in a composite.....	52
Figure 6 Effect of particle radius on the surface area per unit of calcite .....	58
Figure 7 Effect of calcite particle radius on the percentage volume composition of a uPVC-calcite composite (simple cubic model).....	60
Figure 8 Effect of calcite particle radius on the percentage mass composition of a uPVC-calcite composite (simple cubic model).....	61
Figure 9 Graph showing the bound matrix fraction generated by different calcite particles (simple cubic model).....	61
Figure 10 Pictorial representation of the monolayer assumption .....	62
Figure 11 2D Graphical representation of the coating coverage limiting factor, the area per reactive site or the footprint area of the coating molecule (Ignoring chain mobility).....	64
Figure 12 Effect of the specific surface area on the w/w – monolayer relationship. ....	65
Figure 13 Schematic of the chemical reaction at the surface.....	66
Figure 14 Diagram of the reactions that occur between the chemical species produced when calcium carbonate dissolves .....	68
Figure 15 Gas adsorption, Type I to V isotherm classification .....	76
Figure 16 Schematic diagram of a Michelson interferometer based FTIR machine .....	82
Figure 17 Schematic diagram of a Spectra Tech Inc. diffuse reflectance infrared (DRIFT) cell.....	83

Figure 18 Schematic diagram of X-ray induced photoemission.....	89
Figure 19 Schematic diagram of an XPS system.....	90
Figure 20 Schematic representation of Bragg's law of the 'reinforced reflection'	96
Figure 21 Schematic representation of the response of viscoelastic material to an applied sinusoidal stress.....	98
Figure 22 Mechanical head of a PL-DMTA showing the essential features of sample mounting, vibrator system and transducer.....	103
Figure 23 Dual cantilever clamping of small rectangular bar sample .....	104
Figure 24 Diagram of apparatus and timings used in the preparation of coated calcium carbonate samples .....	106
Figure 25 Variation in processing temperature as a function of time for the Waring blender (External Heat – 10 minutes onwards, Speed 3 – 7000RPM). .....	108
Figure 26 Schematic diagram of the 'ideal' polymer composite production process .....	109
Figure 27 Scanning electron micrograph of precipitated calcium carbonate .....	115
Figure 28 Scanning electron micrograph of ammonium stearate coated precipitated calcium carbonate .....	115
Figure 29 Transmission electron micrograph of precipitated calcium carbonate (Scale 1:150,000) .....	117
Figure 30 Transmission electron micrograph of badly precipitated calcium carbonate (Scale 1:150,000).....	<b>Error! Bookmark not defined.</b>
Figure 31 Particle size analysis of transmission electron micrograph of precipitated calcium carbonate .....	<b>Error! Bookmark not defined.</b>
Figure 32 A comparison of transmission electron micrograph particle size analysis distributions of 'good' and 'bad' precipitated calcium carbonate	<b>Error!</b>
	<b>Bookmark not defined.</b>
Figure 33 SEM photo-micrograph showing uncoated magnesium hydroxide (Scale 1:20,000) .....	<b>Error! Bookmark not defined.</b>
Figure 34 Theoretical CHN decomposition profile for stearic acid coated calcium carbonate (assuming empirical composition) .....	123
Figure 35 Coating level estimation by carbon CHN analysis of stearic acid coated calcium carbonate .....	124

Figure 36 Coating level estimation by hydrogen CHN analysis of stearic acid coated calcium carbonate.....	125
Figure 37 Coating level estimation by carbon CHN analysis of stearic acid coated magnesium hydroxide.....	126
Figure 38 Thermogravimetric analysis of uncoated calcium carbonate .....	127
Figure 39 Thermogravimetric analysis of coated calcium carbonate .....	128
Figure 40 Coating level calculated by thermogravimetric analysis of ammonium stearate coated calcium carbonate.....	129
Figure 41 Coating level calculated by thermogravimetric analysis of sodium stearate coated calcium carbonate.....	130
Figure 42 Coating level calculated by thermogravimetric analysis of stearic acid coated calcium carbonate.....	131
Figure 43 Thermogravimetric analysis of dry stearic acid coated calcium carbonate .....	132
Figure 44 Calculated BET adsorption isotherms for a uncoated, partially coated and coated filler.....	133
Figure 45 Diagrammatic representation of the ‘coating equivalence’. A partially coated filler can be experimentally compared to a mixture of coated and uncoated fillers.....	137
Figure 46 Validation of the dual BET adsorption isotherm model using mixtures of coated and uncoated calcium carbonate .....	138
Figure 47 Figure showing the level of coverage calculated for fillers coated with different amounts of sodium stearate using the Dual Adsorption BET Isotherm .....	139
Figure 48 DRIFT spectra of stearate coated and uncoated calcium carbonate....	141
Figure 49 Quantitative DRIFT for ammonium stearate coated calcium carbonate showing the increase in C-H bands with coating level.....	142
Figure 50 Effect of the quantity of coating material added (as ammonium stearate) on the FTIR absorbance ratio (C-H band (3000-2800 $\text{cm}^{-1}$ ) divided by the carbonate band (2450-2650 $\text{cm}^{-1}$ )).....	143
Figure 51 Comparison of the absorbance and Kubelka-Munk ratios calculated during FTIR analysis (C-H band (3000-2800 $\text{cm}^{-1}$ ) divided by the carbonate	

band (2450-2650 $\text{cm}^{-1}$ ) .....	144
Figure 52 Effect of the quantity of coating material added (as sodium stearate) on the FTIR absorbance ratio (C-H band (3000-2800 $\text{cm}^{-1}$ ) divided by the carbonate band (2450-2650 $\text{cm}^{-1}$ )).....	145
Figure 53 Effect of temperature on the FTIR absorbance ratio (C-H band (3000-2800 $\text{cm}^{-1}$ ) divided by the carbonate band (2450-2650 $\text{cm}^{-1}$ )) produced when sufficient sodium stearate is added to produce a coating equivalent to a monolayer .....	145
Figure 54 Effect of the quantity of coating material added (as stearic acid) on the FTIR absorbance ratio (C-H band (3000-2800 $\text{cm}^{-1}$ ) divided by the carbonate band (2450-2650 $\text{cm}^{-1}$ )) .....	146
Figure 55 Effect of the quantity of coating material added (as ammonium stearate) on the FTIR absorbance ratio (C-H band (3000-2800 $\text{cm}^{-1}$ ) divided by the carbonate band (2450-2650 $\text{cm}^{-1}$ )) when produced on a batch scale.....	147
Figure 56 DRIFT spectra of dry stearate coated and uncoated calcium carbonate .....	148
Figure 57 Diagram showing the FTIR absorbance ratio of a sodium stearate/calcium carbonate mixture compared to a wet coated sodium stearate sample .....	149
Figure 58 Comparison of stearate coatings produced by different methods measured by FTIR absorbance ratio (C-H band (3000-2800 $\text{cm}^{-1}$ ) divided by the carbonate band (2450-2650 $\text{cm}^{-1}$ )).....	150
Figure 59 Comparison of the FTIR absorbance ratios (C-H band (3000-2800 $\text{cm}^{-1}$ ) divided by the carbonate band (2450-2650 $\text{cm}^{-1}$ )) produced, by the varying quantities of sodium and ammonium stearate added .....	151
Figure 60 DRIFT spectra of different coating compounds. (Please note peak sizes are not comparable (SA = Sigma Aldrich)).....	152
Figure 61 Comparison of the carbon-oxygen bond absorption frequency as a function of the stearate coating process .....	153
Figure 62 Comparison of the carbonyl bond absorption frequency for different coating conditions .....	154
Figure 63 Comparison of the sodium stearate coated calcium carbonate, C=O	



bond absorption frequency, as a function of the washing process.....	154
Figure 64 DRIFT spectra (4000 – 1000 cm <sup>-1</sup> ) of sodium stearate coated and uncoated magnesium hydroxide .....	157
Figure 65 DRIFT spectra (2000 – 1000 cm <sup>-1</sup> ) of magnesium carbonate, sodium stearate coated and uncoated magnesium hydroxide, and the resultant spectral subtraction.....	158
Figure 66 DRIFT ratio analysis of sodium stearate coated magnesium hydroxide (C-H band (3000-2800 cm <sup>-1</sup> ) divided by the hydroxide band (3750-3600 cm <sup>-1</sup> )).....	159
Figure 67 Diagram representing the photoemission from a flat coated surface ..	163
Figure 68 Diagram representing the photoemission from a coated sphere.....	165
Figure 69 Diagram representing the photoemission of the infinitely small ring .	167
Figure 70 Diagram showing the origins of photoelectron peaks analysed using the simple flat and spherical models.....	172
Figure 71 Diagram showing the origins of photoelectron peaks analysed using the ‘fourth’ generation (part 1) flat and spherical models .....	173
Figure 72 Diagram showing the origins of photoelectron peaks analysed using the ‘fourth’ generation (part 2) flat and spherical models .....	175
Figure 73 Effect of the fractional coverage on the ‘fourth’ generation flat model XPS carbon/carbon ratio .....	177
Figure 74 Effect of the fractional coverage on the ‘fourth’ generation spherical model XPS carbon/carbon ratio .....	178
Figure 75 Graph showing the effect of coating density on the thickness estimated from a carbon/carbon XPS ratio calculated for the flat model .....	179
Figure 76 Graph showing the effect of coating density on the thickness estimated from a carbon/carbon XPS ratio calculated for the spherical model .....	180
Figure 77 Effect of method used to calculate the escape depth of a photoelectron (IMFP. or AL ).....	181
Figure 78 Broad scan XPS spectra of ammonium stearate coated and uncoated calcium carbonate .....	183
Figure 79 Atomic composition calculated by XPS of a precipitated calcium carbonate filler coated with sodium stearate.....	184

Figure 80 Coating thickness of sodium stearate coated calcium carbonate calculated using the <i>'first'</i> generation XPS model .....	185
Figure 81 Coating thickness of sodium stearate coated calcium carbonate calculated using the <i>'third'</i> generation flat XPS model.....	187
Figure 82 Coating thickness of sodium stearate coated calcium carbonate calculated using the <i>'third'</i> generation spherical XPS model.....	187
Figure 83 Coating thickness of sodium stearate coated calcium carbonate calculated using the carbon/carbon ratio and the <i>'fourth'</i> generation (part 1) XPS models.....	189
Figure 84 Coating thickness of sodium stearate coated calcium carbonate calculated using the <i>'fourth'</i> generation (part 2) flat XPS model.....	190
Figure 85 Coating thickness of sodium stearate coated calcium carbonate calculated using the <i>'fourth'</i> generation (part 2) spherical XPS model.....	191
Figure 86 Comparison of the coating thickness produced using different coating methods calculated using the carbon/carbon ratio and the <i>'second'</i> generation model.....	192
Figure 87 Coated Precipitated calcium carbonate, organic carbon peak charging referenced to adventitious carbon at 284.6 eV.....	193
Figure 88 Broad scan XPS spectra of sodium stearate coated and magnesium hydroxide .....	194
Figure 89 Atomic composition calculated by XPS of a magnesium hydroxide filler coated with sodium stearate .....	195
Figure 90 Coating thickness of sodium stearate coated magnesium hydroxide calculated using carbon/magnesium ratio and the <i>'second'</i> generation models .....	196
Figure 91 Coating thickness of sodium stearate coated magnesium hydroxide calculated using carbon/oxygen ratio and the <i>'second'</i> generation models.	196
Figure 92 X-Ray diffraction pattern of sodium and calcium stearate.....	198
Figure 93 X-Ray diffraction pattern of sodium and calcium stearate.....	199
Figure 94 X-Ray diffraction pattern of sodium stearate coated calcium carbonate (0 -2 monolayers) .....	199
Figure 95 X-Ray diffraction pattern of sodium stearate coated calcium carbonate	

(4 –12 monolayers) .....	200
Figure 96 Dynamic mechanical response of uPVC .....	201
Figure 97 E' Component of the dynamic mechanical response of uPVC – uncoated filler composites (Filler composition varying as a weight filler/weight polymer) .....	202
Figure 98 E'' Component of the dynamic mechanical response of uPVC – uncoated filler composites (Filler composition varying as a weight filler/weight polymer) .....	203
Figure 99 Tan $\delta$ of the dynamic mechanical response of uPVC – uncoated filler composites (Filler composition varying as a weight filler/weight polymer) .....	204
Figure 100 E' Component of the dynamic mechanical response of uPVC – filler composites (50/50 Filler/Polymer loading, coating levels in w/w%).....	205
Figure 101 E'' Component of the dynamic mechanical response of uPVC – filler composites (50/50 Filler/Polymer loading, coating levels in w/w%).....	205
Figure 102 Tan $\delta$ component of the dynamic mechanical response of uPVC – filler composites (50/50 Filler/Polymer loading, coating levels in w/w%)	206
Figure 103 Possible coating confirmation scenarios and the effect on the coverage L calculated using the BET dual adsorption isotherm equation .....	210
Figure 104 Summary of the XPS and dual BET results expected for different coating configuration .....	217

## Table of Tables

Table 1 Summary of commercial polymers used and their applications .....	24
Table 2 A summary of the main industrial minerals used in plastics and their functions.....	25
Table 3 Industrial uses of calcium carbonate fillers .....	26
Table 4 A summary of coating reagents used for the modification of the filler surface .....	31
Table 5 The physical effects of filler addition to a polymer.....	50
Table 6 Surface Energies of fillers and plastics .....	54
Table 7 Maximum packing fraction of selected fillers .....	59
Table 8 Tables of solubility data .....	66
Table 9 Tables of physical constants .....	67
Table 10 Table summarising the gas adsorption isotherm classification .....	76
Table 11 Summary of equations for electron inelastic mean free paths (IMFP) (as defined) or effective attenuation length (EAL) .....	91
Table 12 Summary of equations for attenuation lengths (AL) (as defined) .....	92
Table 13 Summary of dynamic mechanical analysis terms.....	99
Table 14 Summary of parameters affecting the mobility of polymer chains in composites.....	100
Table 15 Particle size analysis of transmission electron micrograph of precipitated calcium carbonate .....	<b>Error! Bookmark not defined.</b>
Table 16 Summary of IR characteristic peaks of coating materials and coated precipitated calcium carbonate samples.....	155
Table 17 Summary of attenuation length calculated using the CS2 equation used in the coating thickness analysis of stearate coatings on calcium carbonate (calcite) .....	160
Table 18 Summary of attenuation length calculated using the CS2 equation used in the coating thickness analysis of stearate coatings on magnesium hydroxide (brucite).....	161
Table 19 Summary of attenuation length calculated using the CS2 equation used	

in the coating thickness analysis of stearate coatings on magnesium oxide  
(periclase)..... 161  
Table 20 Summary of XPS models..... 182  
Table 21 Proposed assignment of the IR characteristic coating peaks .....212

# Chapter 1 Introduction

## 1.1 General Background

The plastics industry provides a vast and lucrative market for industrial fillers. This has grown an average of 9% per year over the past decade into a \$23 billion global business, with over 37% of all thermoplastics, thermosets and elastomers being compounded and reinforced with fillers and fibers. The industry is both demanding and competitive. To remain competitive any mineral supplier must be prepared to make sure their product meets stringent specifications. The need to invest in research and development in order to keep in line with market requirements is becoming evident.

Fillers are added at the compounding stage as low cost inert fillers, extenders, or reinforcement or functional fillers. The addition of inorganic material in the form of minerals offers both benefits and disadvantages to the polymer system. The disadvantages that result from the incompatibility of the filler and the polymer phases can often be reduced or eliminated by the use of surface coatings. To optimise the polymer composite properties it is necessary to control the interaction of the surface and the polymer. By producing fillers of a known composition, particle size and distribution, morphology and coating we are at a point at which we are able to begin to quantify the effects of the above factors on the mechanical properties of the polymer composite. When this correlation of surface characteristics with composite properties has been achieved, the need for the 'blind' engineering of composites will be eliminated. Commercially this will make the filler industry more dynamic. They can become proactive rather than reactive in responding to the needs of the plastics industry.

Research has mainly been directed at improving the composite with a coated filler rather than a co-ordinated approach of a complete fundamental surface analysis, industrial process optimisation and mechanical analysis. Improvements in

composite properties are most easily achieved by altering the processing conditions. The alteration of processing conditions does not though allow a detailed determination of the effects of surface modification. In this work, we concentrate on the surface and interfacial chemistry of the system.

## **1.2 Objectives**

The objective of this study is to characterise the mineral surface, prior to and after coating. From this the coating structures can then correlated with the mechanical properties of the resulting polymer composites.

The research can be divided into three sections

- The characterisation of the level and extent of coating.
- The elucidation of the effect of filler coating on the interphase region of the polymer composite.
- The correlation of surface characteristics with the mechanical properties.

The fillers used are calcium carbonate and magnesium hydroxide. These have been coated with either stearic acid or a stearic acid salt. Incorporating the calcium carbonate into an unplasticised grade poly(vinylchloride) (uPVC) has produced 'ideal' composite materials.

# Chapter 2 Literature Review

## 2.1 Polymer Composites

A composite is defined as a mixture of two different component phases which are separated by an interface or interphase region. The interaction across the interface plays an important role in controlling the mechanical characteristics of the composite. Research in the field of composites<sup>1,2</sup> and filled polymers<sup>3,4</sup> is well documented.



## **2.2 Industrial Application**

Pure polymers are not generally the optimum materials for the best performance of the final product; additives are frequently employed to enhance a particular property. The blend of polymer and suitable additives, of which fillers are a particular group, when compounded together, are generally known as plastics.

The selective use of fillers allows the unfilled material to be enhanced. As a result fillers are employed to obtain the following effects:

- Added stiffness, rigidity and hardness
- Controlled thermal expansion and shrinkage
- Improved heat resistance
- Increased strength and reduce creep
- Modified rheological properties
- Improved surface quality
- Modified flow and processing characteristics
- Reduced cost

The selection of polymer and filler for the final plastic is dictated by the cost of the manufactured product. A summary of the main industrial plastics, fillers, and coatings can be found in the following sections.

### **2.2.1 Industrial Plastics**

The plastics industry continues to introduce new and modified polymers into the plastics market. A summary of the most common plastics can be found in Table 1. Values for the glass transition point ( $T_g$ ) and the melting point ( $T_m$ ) given in the table are approximate and may vary with the type and quantity of additive used. It can be used though as a comparison of industrial plastics.

Polymer	T <sub>g</sub> (°C)	T <sub>m</sub> (°C)	Properties	Applications
Poly(ethylene) PE	-70	120	Insulation, chemical resistance, poor creep, opaque.	Films & sheets, wire cable and pipes injection and blow moulding.
Poly(propylene) PP	0	170	Chemical resistance, poor low temp properties, opaque.	Films, spun fibres, mouldings and extrusions.
Poly(styrene) PS	100	Am	Amorphous, transparent, poor chemical resistance, brittle.	Rigid packaging, foam products.
Poly(acrylonitrile butadiene styrene) ABS	100	Am	Opaque, better chemical resistance than PS.	Rigid packaging, plated electro parts, low cost engineering polymer.
Poly(vinylchloride) PVC	80	Am	Rigid, tough, good flame retardant properties, good chemical resistance.	Used with plasticisers to produce sheets, pipes, bottles, cables, coated fabrics.
Poly(methyl methacrylate) PMMA	110	Am	Transparent, good weathering properties, good scratch resistance, poor chemical resistance.	High strength transport glazing, signs.
Poly(carbonate) PC	150	Am	Poor weathering and chemical resistance.	Electrical goods.
Poly(amides) (Nylon 6,6)		270	Hard, opaque, good solvent resistance, good abrasion, low friction properties.	Engineering plastics, fibres.
Poly(ethylene terephthalate) PET	80	260	Amorphous or crystalline, good electrical properties.	Bottles, containers, tapes, metalized films.
Poly(formaldehyde) PF		175	Low friction, high creep resistance, high crystallinity.	General engineering applications.
Poly(tetrafluoro ethylene) PTFE		380	Good chemical resistance, poor creep resistance, opaque, good	Non-stick applications, gaskets, chemical resistant

			electrical properties.	applications, lubrication, medical applications.
Poly(sulfone)	200	285	High service temp, low flammability.	High temp light holders, electrical connectors.
Poly(ether ether ketone) PEEK	145	345	High service temp, good chemical resistance, low flammability.	High temp applications, cable insulation, valves and engine components.
Poly(urethane) PU	-	-	Main use in cross linked form.	Reactive processing, cellular foams.
Epoxy	-	-	Cross linked.	High strength applications, GRP, CRP.

(Values of  $T_g$  and  $T_m$  are approximate, and vary a great deal when additives are used, Am = Amorphous)

Table 1 Summary of commercial polymers used and their applications

### 2.2.2 Industrial Fillers

The plastics industry provides a large lucrative market for industrial fillers. By volume, the most widely used fillers in plastics are calcium carbonate (50%), talc (20%) and mica (10%). Precipitated calcium carbonate (PCC), in particular, is rapidly increasing its market share with an annual growth approaching 15%.

Vast quantities of minerals are used as functional fillers and extenders in plastics, rubbers, mastics etc. Each mineral is capable of modifying different physical and chemical properties. Variations within a mineral category can also result in variations in properties. Historically, the main use of fillers has been to reduce the cost of the polymer composite. However, the use of fillers to provide improved mechanical properties is now the most common reason. Current research is aimed at further understanding and improving the mechanical properties. Research in the areas of fillers to provide improved flame retardency and chemical resistance is also in progress. A summary of the main industrial minerals used in plastics

can be seen in Table 2.

<b>Mineral</b>	<b>Major Resins</b>	<b>Functions</b>
Aluminium trihydrate (ATH)	ABS, TPES*, LDPE, PVC, epoxy, phenolics, PU	Extender, flame retardant, smoke suppressant.
Barytes	PU	Filler & white pigment, increases SG, friction and chemical resistance.
Calcium carbonate	ABS, fluoroplastics, polyolefins, PS, PVC*, epoxy, phenolic, PU	Most widely used filler, improves flexural modulus & surface finish, controls viscosity. Natural and synthetic (PCC) forms available.
Felspar/nepheline syenite	Acrylic, cellulose, PP, PS, PVC*, epoxy	Speciality filler, easily wetted and dispersed, allows transparency, weather and chemical resistance.
Kaolin	Nylon, polyolefins, PU, PVC	Hydrous or calcined grades, largest use in wire & cable, SMC, BMC and vinyl flooring, rheological modifier, cost reduction, improves finish.
Mica	ABS, fluoroplastics, nylon, PC, PP*, polyolefins, thermosets	Flake reinforcement, improves dielectric, thermal and mechanical properties, low cost.
Silica	ABS, polyolefins, PS, PVC, PU, epoxy*	Filler, extender, reinforcement, thickens liquid systems, thixotropic agent, flattening agent, avoids plateout in PVC.
Talc	Nylon, polyolefins, PVC, phenolic, PU, PS*, PP*	Filler, extender, reinforcement, higher stiffness, improves tensile and creep resistance.
Wollastonite	Nylon, PC, PS, polyolefins, thermosets	Improves strength, lowers moisture absorption, raises heat and dimensional stability, improves electrical properties, reinforcement.

\* indicates main consuming resin

Table 2 A summary of the main industrial minerals used in plastics and their functions

### 2.2.2.1 Calcium Carbonate

It is used in both natural and synthetic forms in the rubber, plastic and paper industries. In these applications, surface properties play an important role in determining its effectiveness as a bulk filler or as functional component in the product.

Calcium carbonate filler type	Example uses
Dry ground limestone	rubbers, adhesives, putties and textural paints.
Wet ground limestone	caulk, sealants and latex based paints.
Coated limestone	all polymers.
Coated precipitated	elastomers, PVC, PU and thermosets.

Table 3 Industrial uses of calcium carbonate fillers

Calcium carbonate occurs naturally as limestone and is a consolidated sedimentary rock. The most well known types of limestone are chalk and marble. Commercially viable deposits occur throughout the world. The deposits differ considerably not only in purity, but in size and formation route. The deposits that form the limestone are usually organic in origin. Chalk formations are soft textured limestones, which were laid down in the Cretaceous period (70-130 million years ago). Marble is a metamorphic rock, formed by the recrystallisation of the limestone under extreme temperatures and pressures. They often contain large quantities of magnesium based impurities which have been introduced from the sea water in which the deposition occurred.

Calcium carbonate is also produced synthetically by a number of methods. The most common technique involves blowing carbon dioxide through a slurry of calcium hydroxide (milk of lime). The calcium carbonate can exist in three crystal forms, aragonite, calcite and vaterite, although calcite is the only form of real significance. The physical properties are summarised in greater detail in

section 2.6.4.

Research in the field of calcium carbonate based fillers is vast. The high surface energy and basic nature of calcium carbonate makes its reaction with organic acids and the associated reduction of surface energy especially interesting. The technique has been used for many years<sup>5</sup>. Investigations include not only the coating by simple organic molecules but also the coating of the filler by anionic and cationic polymers<sup>6</sup>.

Conventional coupling agents do not perform well with PCC, although coupling may be brought about by the reaction with unsaturated polymers<sup>7</sup>. Sodium polyacrylate was observed to both adsorb on and promote dissolution of polished limestone surfaces in alkaline  $\text{CaSO}_4$ , and that cationic starch adsorbed at low concentrations caused mineral dissolution at higher concentrations. It was also shown<sup>8</sup> that the surface morphology of the mineral plays a key role in the adsorption of water.

Research has shown<sup>9</sup> that precipitated calcium carbonate powders can be coated by suspension and dry coating methods. The effect of coating with monofunctional and difunctional acids has been investigated. It has been shown that varying the acid concentration and type has an effect on XPS and DRIFT spectra. It has also been shown<sup>10</sup> that varying the acid chain length or functionality also effects the coating level.

### **2.2.2.2 Magnesium Hydroxide**

Magnesium hydroxide is a white crystalline filler. Magnesium hydroxide decomposes endothermically with the evolution of inert gases at the temperatures at which polymers pyrolyse. Alumina trihydrate (ATH) is the main filler used where flame retardant properties are required. The onset of decomposition of ATH occurs at around 200 °C. This is unfortunately below the minimum process

temperatures of many thermoplastics. In comparison magnesium hydroxide is stable at these processing temperatures and starts to decompose at around 300 °C. Its main applications utilise its flame retardant properties e.g. EVA copolymers for electrical wiring. Significant flame retardant properties are only achieved at relatively high filler loading, so that the improvement of the filler-polymer interaction is of significant importance.

Three forms of magnesium hydroxide are available; natural, synthetic large crystals and synthetic sea water. Natural deposits of magnesium hydroxide exist although the high level of impurity often makes them unusable as a filler. The large synthetic crystals are produced by two main routes, hydration of magnesium oxide<sup>11</sup>, or by the precipitation of a magnesium salt by the addition of a base<sup>12,13</sup>. If these processes are controlled a pure morphologically desirable product may be obtained. The most common form of production is known as the 'sea water' type. Magnesium hydroxide is precipitated by the reaction of magnesium salts in sea water on the addition of lime. Magnesium hydroxide is an intermediate in the production of magnesium oxide refractories, so that this process is in principle fairly cheap. The quality of the filler produced (size, porosity, morphology, and impurities) can vary greatly and as a result is far from ideal. The use of 'sea water' based magnesium hydroxide is widespread, and the improvements that may be obtained by surface modification are of particular interest.

A great deal of research has been done into the use of magnesium hydroxide as a filler. Because it is industry orientated, mechanical tests are usually employed so that the system can be optimised<sup>14</sup>. Coating of the filler is widely used and there are many papers investigating the resultant properties<sup>4,14</sup>.

### 2.2.3 Industrial Filler Coatings

The need for filler surface treatment comes about as a direct result of the requirement of the plastic industry for high performance fillers for the modern market.

To optimise the composite, modification of the polymer-filler interaction is required. This can be done in three ways:

- Modification of the polymer
- Incorporation of an additional 'third party' additive
- Modification of the filler surface

Modification of the polymer may be performed by the incorporation of functional groups <sup>2</sup>. The incorporation of additional additives during compounding may result in the migration of the additives to the filler <sup>15</sup>, or alternatively the incorporation of fatty acid soaps may be used as a lubricant to somewhat rectify changes in viscosity and melt properties imposed by the use of fillers.

Filler modification provides the most controlled and varied approach to the modification of the polymer-filler interaction. The action of the coating on the polymer-filler interaction can be summarised in two areas; coupling and wetting, although the nature of coupling agents often results in reduced wettability.

Wetting agents serve to wet out the filler; to allow a stable, homogeneous dispersion to be made in the polymer matrix and to reduce the viscosity of the plastic melt. This allows higher filler loadings to be incorporated into the polymer matrix, producing cost economies and improved physical properties of the final product.

Coupling agents act by modifying the interfacial region between the inorganic filler and the organic polymer to provide a more controlled bonding between the



two. At the same time coupling agents also reduce the wettability.

The choice of using a coated filler is determined by the improvement in the mechanical property and the economic penalty incurred. As a result, when selecting a filler, one must carefully review its morphology and properties as well as its interactions with the polymer matrix.

A summary of the main categories of coating agents may be found in Table 4. Not all types are used industrially on a bulk scale.

Modification agent	Mode of action	Use
Silane <sup>16</sup> Coupling Agents	Possesses a $-Si(OR)_3$ group which can be hydrolysed to bond with the filler. At the same time an organo-functional group is available to bond to the polymer.	Silica, silicates, clays, wollastonite and alumina trihydrate. Suitable for unsaturated polyesters, epoxies and thermoplastics.
Titanate <sup>17</sup> Coupling Agents	React with free protons at the inorganic interface, resulting in monomolecular layers of organofunctionality, which in turn bond the two components.	Calcium carbonate, wollastonite. Suitable for thermo and thermoset plastics.
Zirconaluminate <sup>18</sup> Coupling Agents	Comparable to silane coupling agents, but are soluble in aqueous environments.	Silica, clay, calcium carbonate, alumina trihydrate and titanium dioxide.
Hydrophobic <sup>19</sup> Wetting Agents	These reagents wet the filler by displacing the air / water normally surrounding the filler, and encapsulating it with a chemical compatible with the organic polymer.	All minerals, but agent used is specific to the acidic/basic nature of the filler. Mainly used in blow (BMC) and sheet (SMC) moulding compounds, filled thermoplastics.
Fatty Acid Ester <sup>19</sup> Coupling / Wetting Agents	Surface treatment of filler, with the fatty acid, These reagents have been found to improve processibility and physical properties.	Can be applied as a pre-treatment, or in-situ, it has been successfully applied to calcium carbonate, aluminium trihydrate.
Organosilicone Coupling / Wetting Agents	Follow modes similar to the silane and hydrophobic wetting agents.	Calcium carbonate, mica, talc and alumina trihydrate. Successfully used with polyolefins.

Table 4 A summary of coating reagents<sup>20</sup> used for the modification of the filler surface

Comparative research looking at different coating materials has been undertaken on many occasions<sup>21</sup>. Other techniques for coating include phosphate treatment<sup>22</sup> and plasma treatment<sup>23</sup>.

### 2.2.3.1 Coating Methods

The surface treatment of the filler may occur at anyone of the three stages described below:

- Coating during filler production e.g. PCC
- Coating after filler production e.g. naturally occurring materials
- Coating during compounding e.g. in-situ coating

The third route although not a coating process does allow the modification of the interphase region. The coating processes may be divided into three categories:

- Aqueous phase coating. e.g. PCC with stearic acid in water
- Non aqueous phase coating e.g. PCC with stearic acid in toluene
- Dry coating e.g. Kaolin with stearic acid with external and shear heating

There are many advantages and disadvantages to each technique most of which are related to improved physical properties, better levels of processability or a more marketable product. Aqueous phase processes are best associated with coatings added during filler production. Dry coating processes are best associated with coatings added after filler production. Solvent-based processes are generally not used in industry because of solvent restrictions and the drive towards safer aqueous based processes. As a result these are mainly used academically for the production of controlled coatings.

### **2.2.3.2 Stearate based coatings**

Stearate coatings can be produced by all the methods described in section 2.2.3.1 Coating Methods. Both ammonium and sodium hydroxide are used industrially to produce stearate-based salts. This allows the incorporation of the cheaper natural formulations of long chain fatty acids into the reaction process as soluble stearates. Various stearate salts are commercially available. The use of a base to produce a stearate salt introduces the pH variable into the coating process.

## 2.3 Polymer-Filler Interactions

Interfaces involving polymers are generally of finite width. The polymer nearest to the filler surface may be adsorbed, and consequently differ from the bulk polymer. Filler surfaces may themselves show a gradation in properties with depth. The region around the interface over which the material differs from the bulk phase is sometimes called the interphase. In highly filled plastics the interphase may make up a significant proportion of the composite.

The 'ideal' polymer-filler interface would consist of a two dimensional plane between two homogeneous phases. However even the simplest interface, without the presence of strongly interacting groups, results in polymer being adsorbed at the interface, and the formation of an interphase region. The size of the interphase varies and is discussed later (Section 2.4 Filler, Polymer Interphase).

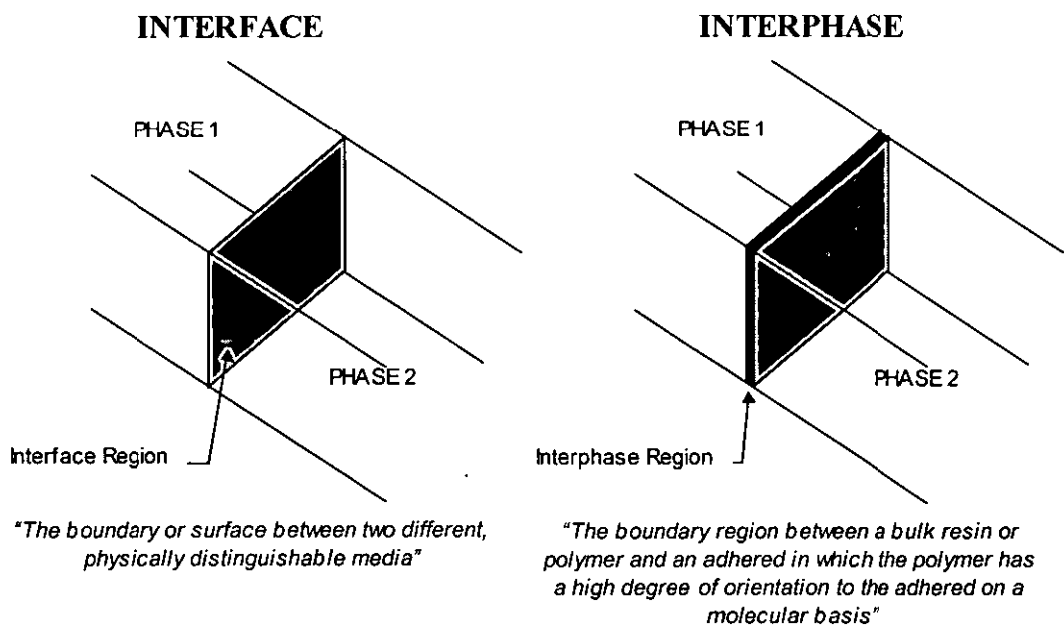


Figure 1 ASTM definition of interface and interphase region

The original purpose of adding low cost mineral fillers to high cost polymers to form composites was one of cost reduction. The extent of 'filling' is limited only by the detrimental effect of the filler on the mechanical properties of the plastic. The detrimental effect can largely be attributed to the compatibility problems associated with adding an inorganic polar solid to a largely non-polar organic matrix, resulting in poor dispersion and stability. A poor distribution of filler and a low level of dispersion can lead to the production of non-homogeneous final products.

The simplest powder dispersions are generally unstable. The stability of the dispersion depends on the rate at which the balance between interfacial tension, viscosity and density difference are achieved. For thermoplastic melts the rate at which separation of the phases might occur is insignificant. During normal processing the thermodynamic-kinetic balance is such that 'stable' dispersions are readily formed. These filled polymer melts constitute kinetically stable dispersions. Viscosities are such that filler particles do not settle out at any appreciable rate even when they form agglomerates. Nevertheless the state of the dispersion and therefore the interface properties strongly affect the final end properties.

Filler-filler interactions per unit area are stronger than polymer-polymer interactions. Because agglomerates often contain (per unit area of contact) a small number of high energy filler-filler interactions compared to the large number of low energy polymer-polymer and polymer-filler interactions, these agglomerates often constitute weak points in the composite. Agglomerates will tend to form in those melt systems in which the filler-filler energy is more favorable e.g. the polymer-filler interfacial energy is high. In industrial processes, where agglomeration occurs, particle-particle interactions are such that compounding can cause damage to the filler.

The testing of mechanical properties is fraught with problems. The relationship between interface and interphase characteristics and mechanical properties are

difficult to demonstrate due to variations in the methods of compounding, processing and testing. The lack of a complete understanding of these techniques and their relation to the exact macroscopic behavior of the polymer and its effect on any interface makes the correlation of mechanical properties to molecular characteristics very difficult.

Three concepts; wetting, adhesion and dispersion may be used to describe the filler-polymer interaction. There is a general correlation between wetting, adhesion and dispersion, although they are not a prerequisite for one another. Poor dispersion in a filled system will manifest itself in the rheology of the filled melt even when agglomerates are well wetted. An agglomerated system may nevertheless show good adhesion across the filler-polymer interface. Poor levels of wetting and adhesion often produce other detrimental properties e.g. encourages attack by moisture and other corrosives.

### 2.3.1 Wetting

Wetting of solids by liquids can be defined as the extent to which a liquid makes contact with a surface. In polymer composites it is therefore characterised by the extent of direct interfacial contact and the ease with which this is achieved.

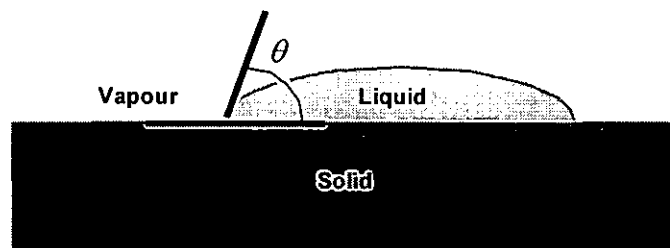


Figure 2 Schematic representation of a liquid drop at a surface

Wetting is generally quantified by the contact angle of a liquid on a surface at equilibrium. This is described by Young's equation:

$$\gamma_{SV} = \gamma_{SL} + \gamma_{LV} \cos \theta$$

Equation 1

where:

$\gamma_{SV}$  is the specific surface free energy of the solid in equilibrium with the vapour of the contact angle liquid,

$\gamma_{SL}$  is the free energy of the solid-liquid interface,

$\gamma_{LV}$  is the surface free energy of the liquid,

$\theta$  is the contact angle of the liquid drop on the surface.

Ideally, for complete wetting  $\theta$  should be zero. Analysing this equation it can be seen that this can be achieved in one of three ways;  $\gamma_{SV}$  can be raised,  $\gamma_{SL}$  lowered or  $\gamma_{LV}$  lowered.

Practically this can be achieved by:

- Reducing the surface tension ( $\gamma_{LV}$ ) by judicious choice of an additive which would diffuse to the surface.
- Modifying the energy of the interface between the two phases ( $\gamma_{SL}$ ). This may be achieved by the incorporation of interfacially active additives.
- Manipulation of the surface energy of the phase to be dispersed ( $\gamma_{SV}$ ). This may be achieved by the use of suitable surface treatments.

It must be remembered that the Young equation describes the action of wetting at equilibrium. This equilibrium is not instantaneous and is dependent on the balance between the driving force for wetting and the viscosity of the fluid. In the case of industrial processing of polymer melts, viscosities can be very high (100 - 1000 Pa s). As a result equilibrium is not easily achieved.

Various relationships have been proposed for calculating the rate of spontaneous



wetting. A widely accepted estimate of the time scale for spontaneous wetting can be made using the Washburn<sup>24</sup> equation (Equation 2) which describes the rate of fluid rise in a vertical capillary:

$$\frac{dh}{dt} = \frac{R^2}{8\eta h} \frac{2\gamma_{LV} \cos\theta}{R} \pm \rho gh$$

Equation 2

where:

$h$  is the height,

$t$  the time,

$R$  the capillary radius,

$\eta$  the viscosity,

$\gamma_{LV}$  the surface tension,

$\theta$  the contact angle,

$\rho$  the density,

$g$  the gravitational acceleration.

These calculations are for an ideal situation. In reality other factors, e.g. impurities, are involved and these perturb the contact angle to either an advancing or receding position.

### 2.3.2 Adhesion

Adhesion can be described as the intimate sticking together of surfaces so that stress can be transmitted between them.

Adhesion requires the contact of two phases. For this to occur wetting must have already occurred. From this we may conclude that the unwetted areas make no or only a small contribution to the overall adhesive strength. These areas of low strength during failure act as points at which the fracture propagation can occur.

For an ‘ideal’ interface we can use the following equations to begin to understand the relationship between the adhesion, wetting and the surface energies of the phases.

The thermodynamic work of adhesion  $W_{AD}$  may be described as the reversible work done per unit area in separating an interface. Dupré proposed therefore that  $W_{AD}$  may therefore be considered as the total of the surface free energies minus the interfacial free energy. The Dupré equation states:

$$W_{AD} = \gamma_{SV} + \gamma_{LV} - \gamma_{SL}$$

Equation 3

where:

$\gamma_{SL}$  is the interfacial free energy,

$\gamma_{SV}$  is the surface free energy of the solid component (filler),

$\gamma_{LV}$  is the surface free energies of the liquid component (polymer).

Modifications to the filler surface, incorporation of proactive compounds to produce covalent bonds or cause mechanical molecular entanglements, may lead to enhanced adhesion. Due to viscoelastic effects, these changes will be small when considering the energy to create a fracture. Surface modification can also result in a reduction of  $W_{AD}$ . This can be attributed to a reduction in bonding across the interface.

The strongest adhesion will occur when covalent bonds are formed across the interface. Interfacial modification is frequently designed to produce these. If covalent bonding does not exist, Hydrogen Bonds, Keesom (dipole-dipole interactions), Debye (dipole-induced dipole interactions) or London dispersion (transient induced dipole-induced dipole interaction) forces across the interface

must provide the means to transmit stress. These are one to two orders of magnitudes smaller in strength (energy) when compared to covalent bonding. From this we may conclude that, all other factors being equal, the stronger the molecular interactions between the phases the greater the adhesive strength.

Roughness can increase the work of adhesion by simply increasing the surface area. However it can also improve adhesion by providing sites for mechanical adhesion. This technique can be used when one of the phases is in the liquid state during processing. On curing or cooling the trapped solid can only fail by a cohesive mechanism. Given the fact that polymer composites are often formed when the polymer phase is in the liquid state this mechanism may make a very significant contribution to adhesion.

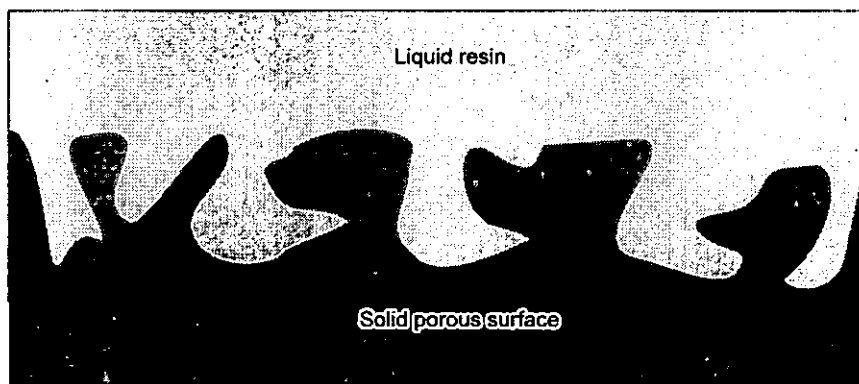


Figure 3 Liquid resin wetting a porous surface. When this solidifies on cooling or curing, a mechanically interlocking interface is formed

In composite systems in which both phases are polymeric, adhesion at the surface can also be attributed to molecular entanglements in the interphase region. On a molecular layer these are analogous to the macroscopic interlocking of chains, which provide mechanical adhesion. Adhesion of this form can only occur if thermodynamic and entropy requirements are satisfied. For this to occur the polymer chains of the 'filler' must be of a similar polymeric nature to that of the

polymer matrix. However, the presence of similar polymeric chains does not ensure the good interlocking of chains.

### 2.3.3 Dispersion

Dispersion requires the creation of large interfacial areas and is therefore easier when interfacial energy is low. As Equation 1 and Equation 3 indicate this will generally be the case in systems in which wetting is good, and the work of adhesion ( $W_{AD}$ ) is strong.

When interfacial energy is high a good level of dispersion may be obtained if extra energy is expended in the processing stage. If processing parameters are altered to provide this energy, a kinetically stable dispersion can be achieved.

The degree of dispersion describes the state of distribution of the filler in the matrix. In a filled system good dispersion corresponds to stable individual particles and poor dispersion to filler agglomeration.

Nevertheless, the state of the dispersion and therefore the interface properties strongly affect the end properties. If agglomerates contain 'weaker interactions' (the sum of all filler-filler interaction as a function of the total filler surface area) than those of the polymer interactions, then the agglomerates will constitute weak points in the composite. If an industrial plastic processing method is used, for a fixed set of processing parameters the level of dispersion achieved is generally a function of the surface energy of the filler. The optimisation of the industrial processing parameters is often not sufficient to generate similar levels of dispersion for different surface energy fillers.

Agglomerates will tend to form in those melt systems in which the polymer-filler interfacial energy is high. In industrial processes, where agglomeration occurs, particle-particle interactions are such that extreme compounding can cause damage to the filler.

If the effect of the filler surface is to be established, the level of dispersion and the treatment of the composite components must be kept constant. In this case the changes in the only property being varied, the filler surface, can be correlated directly with the mechanical properties of the composite.

The variation in mechanical properties of polymer composites is often stated to be the result of poor dispersion<sup>25,26</sup>.

### **2.3.3.1 Dispersion Analysis**

The effect of dispersion on the mechanical properties is often seen in visual observations of the failure surface. The comparative analysis of dispersion is best made prior to mechanical analysis. Methods of dispersion analysis may be split into two categories:

- Visual observations<sup>27</sup> e.g. optical microscopy, SEM, elemental maps.
- Scattering techniques e.g. small angle light scattering.

Transmission optical microscopy is often used to assess the dispersion of large filler particles. By analysing layers of 25  $\mu\text{m}$  PP it has been shown that the level of dispersion of 10-20  $\mu\text{m}$  talcs and shale could be determined<sup>28</sup>. In the case of smaller filler particles, scanning electron microscopy is used to provide higher levels of resolution. Experimental preparation is usually reliant on the samples being microtomed, although low temperature plasma etching has been used with some success<sup>29</sup>. Microtomed samples often exhibit sample damage<sup>27</sup>. This damage may often be reduced by the use of a cryomicrotome. The contrast between filler, coating and polymer, can often be improved by either dissolving the filler<sup>27</sup>, or by dissolving the coating<sup>30</sup>.

### 2.3.4 Surface and Interfacial Energies

The thermodynamic work of adhesion ( $W_{AD}$ ) is the reversible work done in separation of unit area of interface between two phases (A and B). Dupré pointed out this could be calculated by considering the interfacial energies. Good and Girafalco<sup>31,32,33,34</sup> introduced the interaction parameter  $\phi$ , with which the thermodynamic work of adhesion between two phases could be evaluated.

$$W_{AD} = 2\phi(\gamma_{SV}\gamma_{LV})^{1/2}$$

Equation 4

The interaction parameter may be estimated from the molecular properties of both phases<sup>35,36</sup>, with general values of  $\phi$  falling in the range 0.5-1.2. The difficulty with this approach is the calculation of  $\phi$  which is lengthy and requires precise knowledge of the surface being studied; this is seldom available in practice.

Fowkes proposed the theory of fractional polarity<sup>37,38,39,40</sup>. He suggested that the surface free energy of a solid could be given by the sum of several independent contributions from dispersion interactions, hydrogen bonding etc.

$$\gamma_{SV} = \gamma_S^D + \gamma_S^P + \gamma_S^H$$

Equation 5

where:

$\gamma_{SV}$  is the surface energy of the solid,

$\gamma_S^D$  is the dispersion component of surface energy,

$\gamma_S^P$  is the polar component of surface energy,

$\gamma_S^H$  is the hydrogen bonding component of surface free energy.

Often the hydrogen bonding component and polar component are encompassed in

a single term.

For interfaces involving one non-polar material, the interactions contributing to the thermodynamic work of adhesion must consist principally of dispersion forces. Fowkes suggested that for a saturated hydrocarbon and a solid surface, where only dispersion forces may operate, the thermodynamic work of adhesion could be given by the following relationship using the geometric mean approximation for dispersion force interactions.

$$W_{AD} = 2(\gamma_S^D \gamma_L^D)^{1/2}$$

Equation 6

Owens and Wendt<sup>41,42</sup> employed the theory of fractional polarity and suggested that polar interactions, including hydrogen bonds, could also be estimated by a geometric mean, leading to a more comprehensive relationship between the interfacial free energy and its components,

$$W_{AD} = 2(\gamma_S^D \gamma_L^D)^{1/2} + 2(\gamma_S^P \gamma_L^P)^{1/2}$$

Equation 7

Equation 7 is frequently used to estimate the thermodynamic work of adhesion, but is not without critics. There is some debate about whether the geometric mean approach is the best way of approximating the polar interactions at an interface. It has been suggested that the geometric mean could be replaced by the arithmetic, quadratic, anharmonic, or harmonic means<sup>43,44,45,46</sup>. Despite the approximations involved the geometric mean approximation is popular and widely used.

Fowkes has suggested that polar interactions across an interface can be thought of in terms of Lewis acid/base interactions<sup>47,48,49,50</sup>. As a consequence,  $W_{AD}$ , the

work of adhesion may be written in terms of the work of adhesion due to dispersion interactions,  $W^D$ , and the work of adhesion due to acid-base interactions,  $W^{AB}$  (Equation 8).

$$W_{AD} = W^D + W^{AB}$$

Equation 8

Drago<sup>51</sup> developed a theoretical approach for relating the enthalpy of interaction with the acidity and basicity of the interacting species, by allocating constants to define the strength of acids. These are the E and C constants, which represent the electrostatic and covalent, or hard and soft contributions to the acidity and basicity of the compound.

$$W^{AB} = C_A C_B + E_A E_B$$

Equation 9

The constants are determined from calorimetric measurements, and are applied to the acids and bases. These do not necessarily relate precisely to the electrostatic and covalent contributions of the acid-base interactions. This approach has much to commend it, and it has been used successfully. However it can be difficult to find the appropriate Drago coefficients<sup>52,53</sup> that describe the acid-base properties of the materials involved. The applicability of Drago coefficients in surface studies is also debatable.

These theories predict that coating an inorganic filler with an inert non-polar organic coating will reduce the surface energy of the filler, and the work of adhesion between filler and a non-polar polymer will fall as a result of reduced dispersion interactions. Greater reductions are predicted for inorganic fillers in polar polymers where polar and hydrogen bonding interactions need to be



considered.

Measurement of surface energies is difficult, but some measurements have been made. They are dependent on adsorbed molecules and contaminants. Estimates of the energy of interaction at filler surfaces can be obtained from gas adsorption measurements such as adsorption isotherms<sup>54</sup> and inverse gas chromatography<sup>17,55,56</sup>. These measurements have confirmed a reduction in surface energy as a result of the presence of organic coatings. Alternatively interactions may be studied in the liquid phase using contact angle measurements<sup>57,58</sup>, heats of immersion<sup>59</sup>, flow microcalorimetry<sup>60</sup>, thin layer wicking<sup>61,62</sup> and capillary rise methods<sup>63</sup>.

### **2.3.5 Polymer Adsorption**

Even the simplest filler surface with no strongly interacting groups exhibits a filler-polymer interaction.

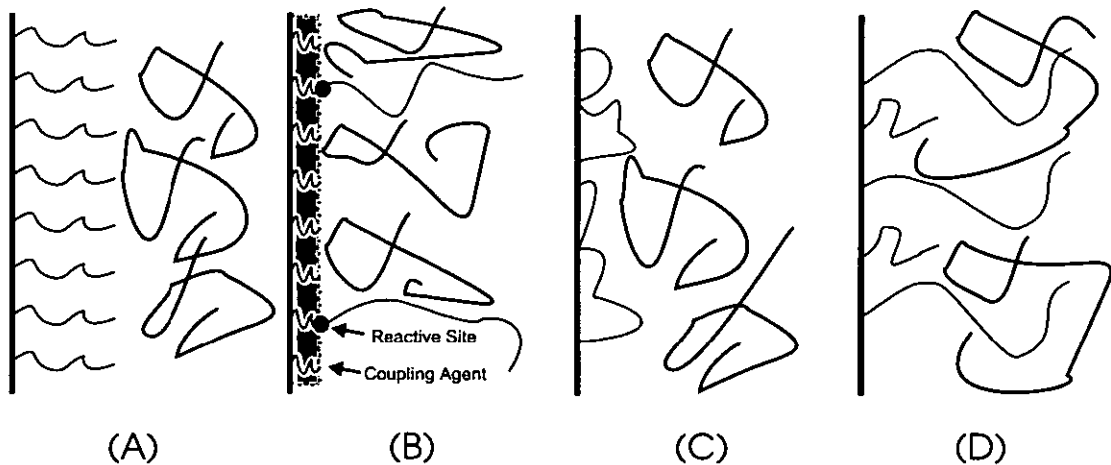
A high energy inorganic filler surface is such that polymer will be adsorbed onto the surface<sup>64</sup>. Conformational analysis would suggest that polymers adsorbed on the surface are adsorbed in more than one place. The desorption of the entire polymer chain is determined by the equilibrium of adsorption and desorption of multiple segments. Due to the probability of all the segments being desorbed at the same time, the release of the polymer molecule is unlikely. Adsorption of multiple segments would result in the formation of a phase around the filler quite different to that of the bulk.

## 2.4 Filler, Polymer Interphase

One might assume that the most compatible coating material would be an independently applied coating of the polymer itself. The benefits of this type of coating are not as well defined as one might think. The polymer-polymer interface or the coating-polymer interface is extremely complicated. The filler-polymer interaction has been previously described. (Section 2.2.3 Industrial Filler Coatings).

It has been experimentally shown that in a silica filled PE composite a 3 nm layer of bound polymer can be found on the silica after fracture<sup>65</sup>. From this we conclude that either cohesive matrix failure has occurred or a weak 'interface' between free and bound polymer exists. These hypotheses would suggest that chemically adsorbed chains and similarly free chains are not identical in character and may not be fully miscible. This is particularly significant since a common approach to filler coating is to attach polymer chains to the surface. To further utilise the ability of the filler to provide reinforcement, we must try to improve the bound polymer-polymer interface. A description of this theory and technology can be found in, Section 2.3.2 Adhesion.

As discussed in Section 2.2.3 Industrial Filler Coating, two types of coating materials can be applied to fillers; coupling agents and wetting agents. Wetting agents act to reduce the filler-filler interaction. If all other variables are constant, and there is no interaction between the filler and the polymer, then the overall adhesion between the filler and the polymer matrix will be reduced. Coupling agents provide sites at which 'bonds' between the coating and polymer can be formed, thus improving adhesion across the coating-polymer interface. The phenomena of wetting agents (stearic acid) reducing adhesion is widely reported<sup>66</sup>.



- (A) - High density of low molecular weight grafts - poor coupling. Comparable to the use of a wetting agent.
- (B) - Coupling agent coated filler, low density of high molecular weight grafts - moderate coupling.
- (C) - High surface energy filler, low density of high molecular weight grafts - poor coupling.
- (D) - Moderate density of high molecular weight grafts - good coupling

Figure 4 A diagram showing the interactions of chains grafted to the filler surface with free polymer chains

The reactive sites of the coupling agent generate chemical bonds, these bonds favour the formation of molecular entanglements (B), rather than the multiple segment adsorption that would occur in the case of an uncoated filler with a similar amount of polymer adsorbed.

The thermodynamics of the mixing of chains grafted to a surface and otherwise similar free chains has been investigated<sup>67</sup>. De Gennes predicted that, as the density of grafting increases and/or as the molecular weight of the free polymer increases, free chains will be expelled from the grafted layer. The basic driving force for this is the reduction in entropy when free chains penetrate a dense coating of attached chains. As the number of individual chains grafted per unit

area increases the constrained chains become more extended. Any free chains entering this system would have their conformational freedom reduced, and in the (unrealistic) limit of fully extended 'toothbrush like' grafted chains would themselves have to adopt an extended rod-like conformation to mix with the grafted layer. Experimental confirmation of this has been obtained for a PMMA matrix filled with glass beads system, to which PMMA has been grafted <sup>68</sup>.

The width of the interphase in a PS-PMMA system is estimated to be around 5 nm wide. For a 10% blend of PS in PMMA with an average particle size of 0.1  $\mu\text{m}$ , the interphase is calculated to constitute around 3% of the bulk polymer matrix <sup>69</sup>.

## 2.5 Mechanical Properties

The mechanical properties of a composite are determined by the filler's reinforcing ability. This is determined by the filler's size, shape, size-shape distribution, pre-treatment, method of compounding, processing and post processing operations. Usually the reinforcement is defined in terms of a particular property of interest, e.g. impact strength or modulus. Mechanical properties in filled systems are limited by the ability of the interface to transfer stress. For this reason surface modification may be introduced to promote adhesion. Thus in filled polymer composites, a surface active agent coupling the dispersed phase to the matrix is commonly present. Many properties of multicomponent systems are indirectly influenced by the interface through its influence on powder morphology.

The physical effects of filler addition are summarised in the table below.

<b>Physical Property</b>	<b>Description of changes</b>
Modulus	Increase in stiffness (creep/deformation resistance and hardness).
Yield strength	Modest increases. The strength of filled compounds is difficult to predict since it is dependent on a number of different parameters, including, dispersion, particle size and shape and the polymer-filler interaction.
Ultimate properties	Ultimate properties are difficult predict due to the complex relationships involved in the polymer-filler interaction.

Table 5 The physical effects of filler addition to a polymer

Key factors in the production of a successfully filled composite include both the compound specification (filler particle characteristics) and additional factors that are dependent on the processing conditions.

## 2.5.1 Filler Loading

The extent of filling in a polymer is limited by the detrimental effect of the filler. It is convenient to discuss filler concentrations in terms of the reduced volume.

$$\tilde{\phi} = \phi / \phi_m$$

Equation 10

Where:

$\tilde{\phi}$  is the reduced volume,

$\phi$  is the filler volume fraction (packing fraction),

$\phi_m$  the maximum filler loading.

If we consider the filler as an inert object, the volume fraction  $\phi_m$  is normally determined by the filler geometry (Section 2.5.5 Filler Particle Size Theory, Table 7).

For the majority of properties the following graph describes the variation in a property with increasing filler loading.

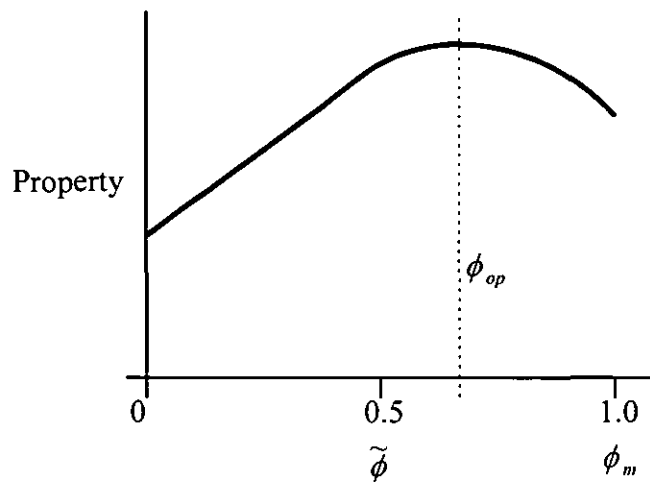


Figure 5 Summary of the relationship between many physical properties and the filler content in a composite

The optimal loading  $\phi_{op}$  is dependent on the property of interest. For modulus, compressive strength and dielectric constant optimal properties are obtained at a maximum loading ( $\tilde{\phi} = \phi_m$ ), whereas for tensile yield stress or strain, maximum strain at break and permeability the optimal loading is achieved when  $\tilde{\phi} \leq 0.5\phi_m$ .

In general the solid-solid interactions are stronger than those for the solid-liquid interface. As a consequence the solid particles tend to aggregate. Aggregation causes an apparent increase of filler loading at a given concentration. This results in an effective decrease of  $\phi_m$ . Since the interfacial properties are inversely proportional to the particle radius, the severity of aggregation tends to increase with a decrease in particle size.

## 2.5.2 Industrial Processing Parameters

Fillers can be mixed with polymer in a number of ways, depending on the nature of both ingredients. Some of the processes that must occur are defined as:

- The elimination of adsorbed volatiles e.g. H<sub>2</sub>O
- The breaking down of the aggregates, securing total wetting of each particle by the matrix
- The uniform distribution of the particles within the system without excessive attrition

Bonding may be improved by the surface treatment of the fillers, and effective dispersion is achieved by destroying any tendency towards particle agglomeration by using purpose designed screw configurations in compound extruders<sup>3</sup>.



### 2.5.3 Coating Effects

The basic role of an interfacial agent is to reduce the solid-solid interactions and to facilitate dispersion. Since agglomeration leads to higher effective volume fractions of filler at constant loading, the pre-treatment of a filler often results in a reduction in viscosity. The interfacial agents effectively remove or suppress the three dimensional composite structure responsible for yield behaviour, and lower the shear viscosity at low deformation rates by orders of magnitude. In other cases the addition of proactive coatings to the filler often cause polymer immobilisation on the filler surface thus increasing the apparent volume fraction and viscosity.

The coating of powders has been shown to reduce surface energies <sup>1,21,70</sup>. The reduction of surface energy results in a reduction in agglomeration, and an improvement in dispersion and overall filler compatibility. It can be seen that after coating the surface energy of the filler has been reduced to that comparable to the polymers in which they are to be incorporated. Values obtained for surface energies can be seen in Table 6.

Filler	Surface Energy (mJ m <sup>-2</sup> )
Diamond	10,000 *
Glass	1,200 *
Calcium carbonate	65 – 70
Stearate coated calcium carbonate	28
Polymers	15 – 60
Polypropylene	31

(\* in practice these values are never achieved)

Table 6 Surface Energies of fillers and plastics <sup>4</sup>

The addition of fillers to polymers to improve properties are widely reported. The use of coatings to enhance these mechanical properties are also well documented. For example the addition of 40 % by weight of untreated mica to PP increased the flexural modulus from 1.8 to 5.4 GPa. When mica was treated with 0.5 % silane

the modulus is further increased to 7.5 GPa <sup>71</sup>.

## 2.5.4 Engineering Models

The mathematical prediction of the filler's effect on a mechanical property of a composite, e.g. modulus, is the aim of any applied surface science experiment.

Because the modulus is a bulk property, as is viscosity, the modulus of the filled materials has been represented by a large number of equations. A number of scientists have predicted the effect of the filler on the strength of the composite.

The simplest equation is based on the rule of mixtures and has often been used as a first approximation,

$$E_c = (1 - \phi_f)E_m + \phi_f E_f$$

Equation 11

where:

$E_c$  is the modulus of elasticity of the composite,

$E_m$  is the modulus of elasticity of the matrix,

$E_f$  is the modulus of elasticity of the filler,

$\phi_f$  is the volume fraction of the filler.

Low filler concentration (Einstein <sup>72</sup>).

$$E_c = E_m(1 + 2.5\phi_f)$$

Equation 12

High filler concentration (Guth <sup>73</sup>).

$$E_c = E_m(1 + 2.5\phi_f + 14.1\phi_f^2)$$

Equation 13

A more rigorous approach was developed by Kerner <sup>74</sup>.

$$E_c = \frac{G_f \phi_f / [(7 - 5\nu)G_m + (8 - 10\nu)G_f] + \phi_f / [15(1 - \nu)]}{G_m \phi_f / [(7 - 5\nu)G_m + (8 - 10\nu)G_f] + \phi_f / [15(1 - \nu)]}$$

Equation 14

where:

$G_f$  is the shear modulus of the filler,

$G_m$  is the shear modulus of the matrix,

$\nu$  is the Poisson ratio of the polymer.

A substantial amount of work has been done attempting to predict the strength and toughness of filled plastic. However, except in a few cases, there is no general predictive theory of ultimate properties for filled polymers. Unlike fibrous composites, the prediction of particulate composite strength is a controversial subject. Although investigations have produced a large number of both theoretical and empirical equations, there is no unifying theory for general prediction <sup>75</sup>.

These simple models predict that at low filler concentrations there is a reduction in strength. This is because the simplest strength prediction models are based on the area reduction of the matrix in the presence of fillers. These models assume that there is no adhesion between the fillers and the matrix and the reduction in composite strength is due to the reduction of the matrix area:

$$\sigma_c = \sigma_m \frac{A_m}{A_c}$$

Equation 15

where:

$\sigma_c$  is the composite strength (modulus),

$\sigma_m$  is the matrix strength (modulus),

$A_m$  and  $A_c$  are the matrix area without fillers and matrix area in the presence of filler.

The area ratio may be expressed as a function of the filler volume fraction.

$$\frac{A_m}{A_c} = 1 - \alpha \phi_f^{2/3}$$

Equation 16

in which the parameter  $\alpha$  is dependent on the type of filler distribution.

Furthermore rigorous approaches have been proposed to predict the ultimate tensile strength of particulate-filled polymers<sup>76,77</sup>. The model relates the tensile strength to the volume fraction of the filler, the elastic moduli of the two phases as well as the shape, size and interfacial adhesion between the filler and the matrix.

The model also predicts that the effect of particle size is felt only when the particle diameter is greater than a critical value. The ultimate tensile strength is thus given by:

$$\sigma_n^2 = \left( \frac{12\gamma_{sl}E_m}{d} \right) \left( \frac{1}{E_c} + \phi_f \right)$$

Equation 17

where:

$\sigma^2$  is the ultimate tensile strength,

$d$  is the particle diameter,

$\gamma_{sl}$  is the work of adhesion between the filler and the polymer.

### 2.5.5 Filler Particle Size Theory

The interaction of a filler particle within a matrix has been demonstrated<sup>65</sup>. If we assume that individual polymer chains coat individual filler particles, we may assume that the bound volume fraction of polymer is dependent on the surface area / particle geometry.

The effect of particle radius on the surface area per unit mass (specific surface area) of a calcite particle is described below (Calcite density 2710 kg m<sup>-3</sup>).

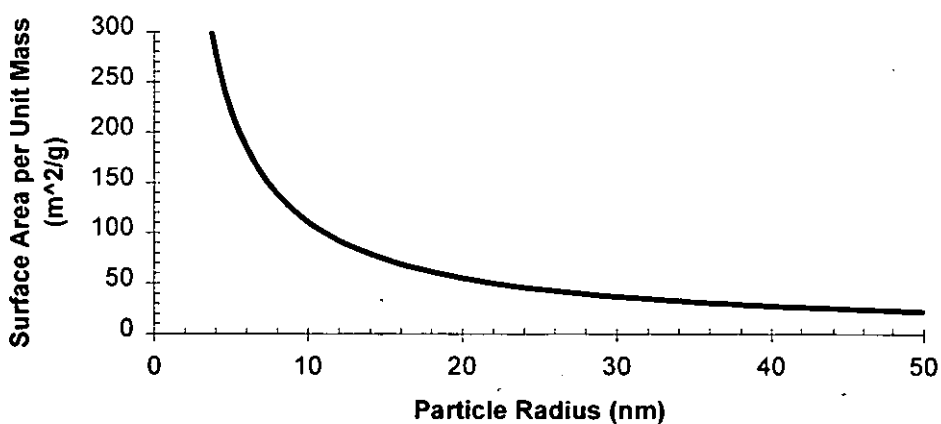


Figure 6 Effect of particle radius on the surface area per unit of calcite

If we try to pack spheres of the same size, we may consider a number of different conformations. The conformation dictates the quantity of polymer that is required before voids form within the composite. The volume fraction of the space occupied by the sphere is known as the packing fraction. The two conformations of interest are known as close packed (packing fraction 0.74) and simple cubic (packing fraction 0.52). Random loose packing is determined to be of the order of 0.64. These packing fractions can be determined for other filler types. The packing fraction becomes increasingly important as the filler geometry changes and moves further away from a sphere.

Filler Type	Packing Confirmation	Packing Fraction
Sphere	Hexagonal	0.74
Sphere	Face centered cubic	0.74
Sphere	Body centered cubic	0.60
Sphere	Simple cubic	0.52
Sphere	Random	0.64
Irregular	Random	0.64
Fibres	Random (L/D = 5:1)	0.52
Fibres	Random (L/D = 20:1)	0.20
Flakes	Random (L/t = 56:1)	0.33

Table 7 Maximum packing fraction of selected fillers<sup>78</sup>

### 2.5.5.1 Bound Matrix Fraction

If we use a simple cubic model, we can consider the effect of particle radius / surface area on the 'limiting' loading levels. From this we can show that as the particle radius increases, the volume (Figure 7) and the mass fraction (Figure 8) of bound polymer will decrease. (uPVC Density 1200 kg m<sup>-3</sup>). The figures assume that a 3 nm bound matrix layer is formed<sup>65</sup>. Estimated values of up to 20 nm have been reported in the literature<sup>79</sup>.

If particles of radius 10 nm were available, the quantity of fraction of bound

polymer (50%) could be easily detected by techniques sensitive to polymer mobility e.g. DMTA. At larger radii (smaller surface areas) the fraction of bound matrix decreases considerably, this reduces the possibility of detection. As a result composites of the highest filler loading possible are required.

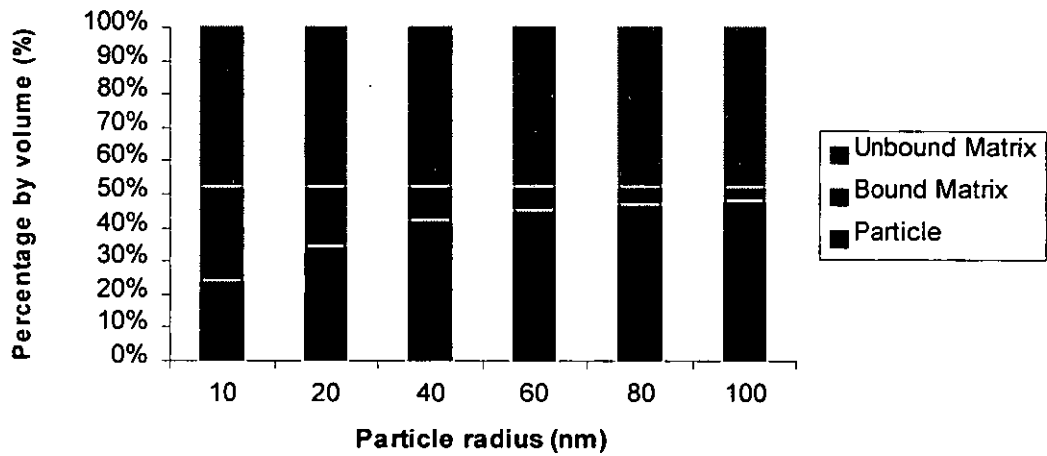


Figure 7 Effect of calcite particle radius on the percentage volume composition of a uPVC-calcite composite (simple cubic model)

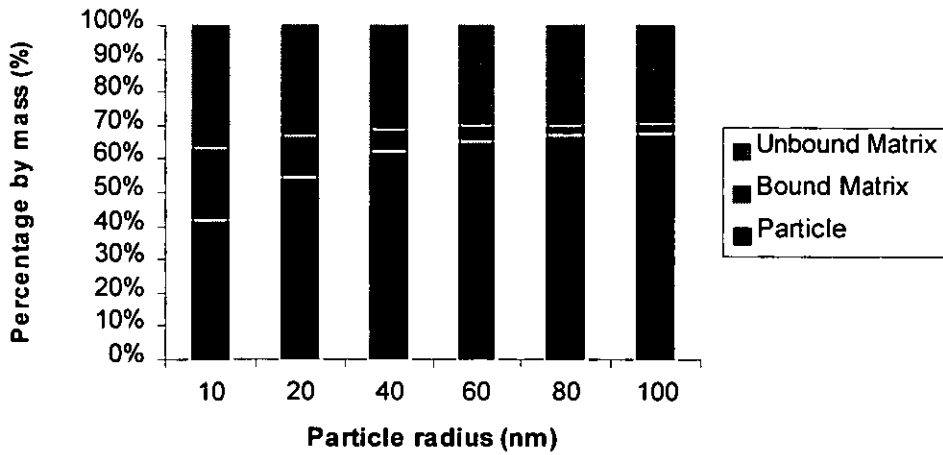


Figure 8 Effect of calcite particle radius on the percentage mass composition of a uPVC-calcite composite (simple cubic model)

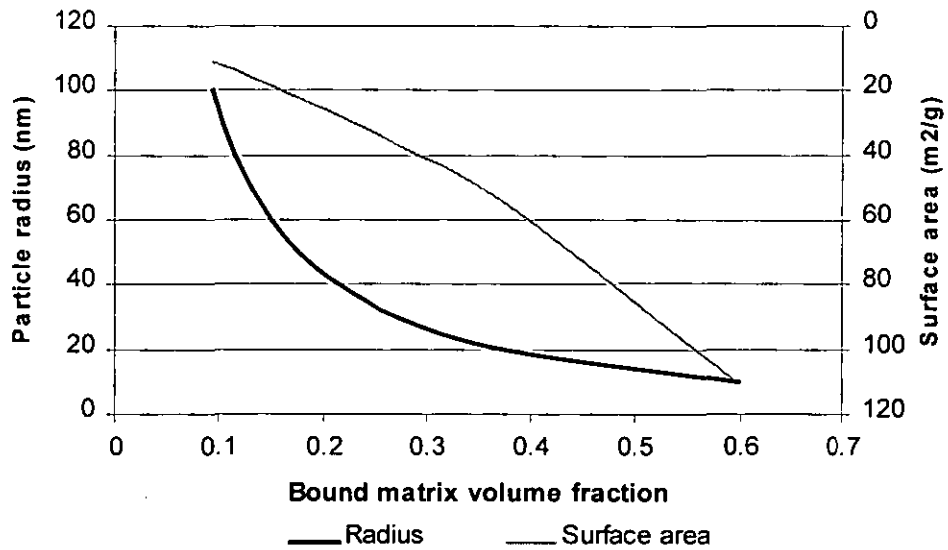


Figure 9 Graph showing the bound matrix fraction generated by different calcite particles (simple cubic model)



## 2.6 Filler Coating Theory

The quantity of coating material used is often described industrially in terms of the weight percentage of the acid added to the total material. Although this is easy to use industrially it does not allow the cross comparison between different coating materials and different fillers. The concept of a 'theoretical monolayer' is used to enable the cross comparison of results.

### 2.6.1 A 'Monolayer' Coating

When the stearate reacts with the filler, it finishes with the polar head group interacting with the surface. Theoretical analysis of the chain conformation<sup>80</sup> may allow the prediction of the space occupied by the stearate molecule.

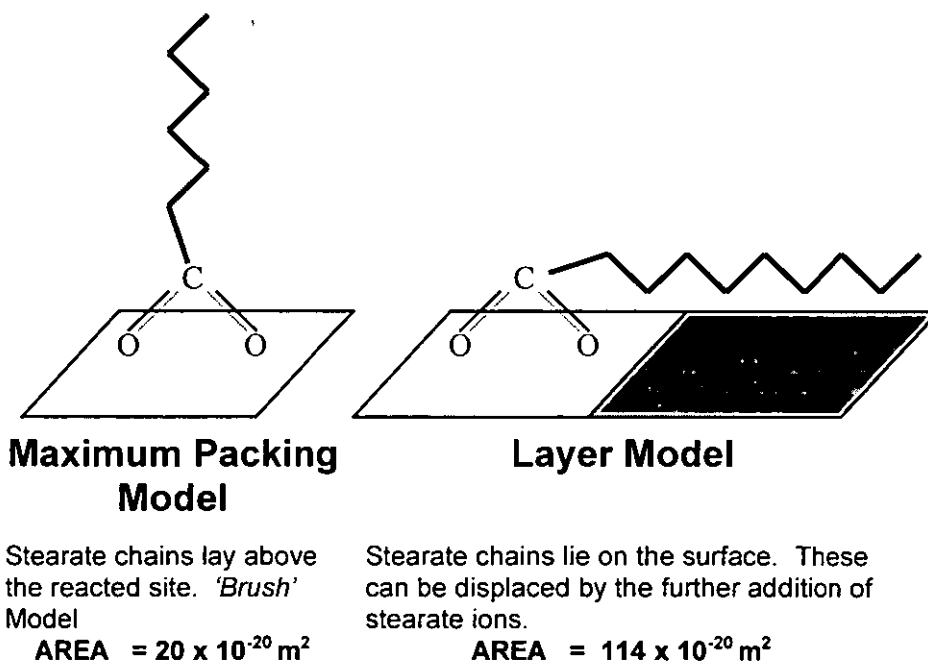


Figure 10 Pictorial representation of the monolayer assumption

If it is assumed that the stearate molecules are adsorbed in a close packed 'brush' type configuration as shown in Figure 10, with each head group occupying

$20 \times 10^{-20} \text{ m}^2$ . Knowing the specific surface area, it is possible to calculate the number of stearate molecules required to give complete coverage.

If the chain is fully extended, the length of the chain has been calculated to be equal to 2.43 nm (24.3 Å)<sup>64</sup>.

Alternative configurations must be considered when more complicated molecules are used. A looped structure may also be considered if a bi-functional acid is used.

### **2.6.2 Surface Reactive Sites**

The size of the 'footprint' of the coating molecule is only one factor in determining the quantity of coating required for a theoretical monolayer. The orientation of the coating molecule and the number of reactive sites must also be considered.

Without taking coating steric factors into consideration the completeness of the coating can be visualised (Figure 11). The completeness of the coverage can be described as a function of the number of reactive sites per unit coating footprint area i.e. a low number of reactive sites will result in an incomplete coating.

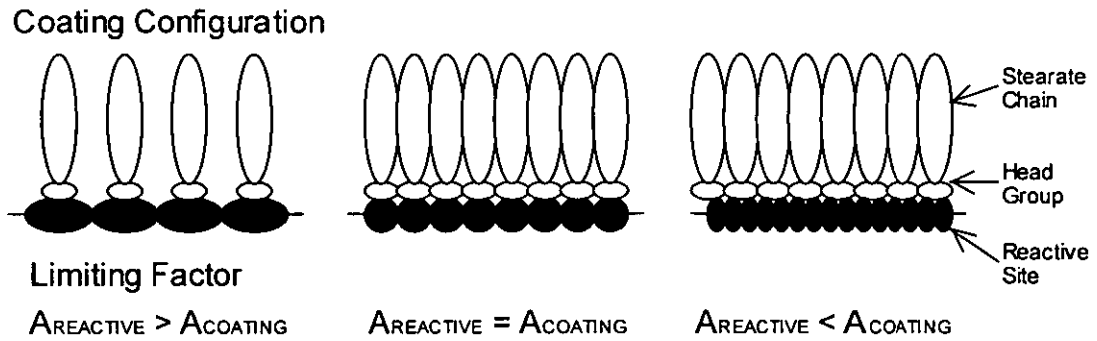


Figure 11 2D Graphical representation of the coating coverage limiting factor, the area per reactive site or the footprint area of the coating molecule (Ignoring chain mobility)

In the case of  $A_{\text{REACTIVE}} > A_{\text{COATING}}$  the chains would relax (try to lay on their sides) and form a thinner more complete coating.

### 2.6.3 w/w v's Monolayer-Surface Area Relationship

Considering the surface area in terms of the number of monolayers is helpful when trying to visualise the coating formation. The conversion between the two sets of units is simple (Figure 12). If this is taken into account materials with surface areas of  $20 \text{ m}^2/\text{g}$  and  $13 \text{ m}^2/\text{g}$  would require  $0.04724 \text{ g}$  and  $0.03071 \text{ g}$  of stearic acid respectively per gram of filler to form a single monolayer.

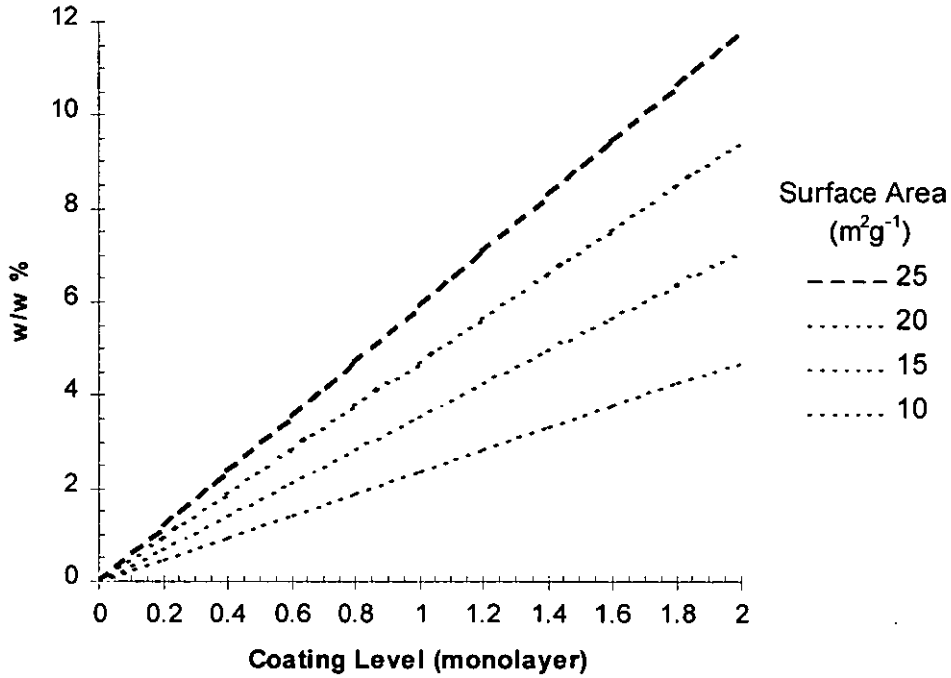
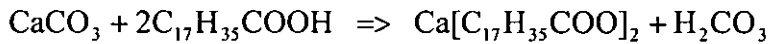


Figure 12 Effect of the specific surface area on the w/w – monolayer relationship.

### 2.6.4 The Coating Reaction

A general reaction scheme for the reaction of calcium carbonate and stearic acid may be proposed. (This must be revised when we think about the reaction at the surface).



Equation 18

This reaction is most likely to occur with the formation of a stearate salt with the cation : anion ratio of 1:1. Formation of a bound salt with the ratio 1:2 is unlikely to occur since bonding of the molecule to the surface will be sterically hindered.

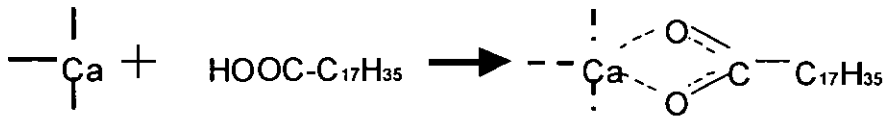


Figure 13 Schematic of the chemical reaction at the surface

The effectiveness of the coating processes defined in section 2.2.3.1 Coating Methods are dependent on the physical properties of the coating materials and the filler. The physical properties<sup>81</sup> are shown in Table 8 and Table 9.

Compound	Cold Water (g/100ml)	Hot Water (g/100ml)
Stearic acid	Insoluble	-
Ammonium stearate (Mixed)	Very Soluble	-
Sodium stearate	0.004	-
Calcium stearate	0.004	-
Magnesium stearate	0.003/0.004	0.008
Zinc stearate	Insoluble	-

Compound	Cold Water (g/100ml)	Hot Water (g/100ml)
Calcium carbonate (Calcite)	0.0014	0.0018
Calcium hydroxide	0.185	0.077
Magnesium carbonate (Magnesite)	0.0106	-
Magnesium hydroxide (Brucite)	0.0009	0.004

Table 8 Tables of solubility data<sup>81</sup>

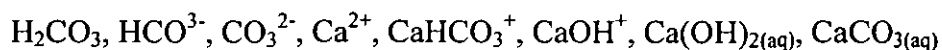
Compound	M.Wt (amu)	Density (kg m <sup>-3</sup> )	Mpt (°C)
Octadecane	254.51	776.8	28.18
Stearic acid	284.50	940.8	71.5
Ammonium stearate, stearic acid (mixed)	586.00	-	110
Sodium stearate	306.47	-	-
Calcium stearate	607.04	-	179-180
Magnesium stearate	591.27	-	86-88
Zinc stearate	632.33	-	130

Compound	M.Wt (amu)	Density (kg m <sup>-3</sup> )	Mpt (°C)
Calcium carbonate (Calcite)	100.09	2710	1339
Calcium hydroxide	74.09	2240	580
Magnesium carbonate (Magnesite)	84.32	2958	350 (decompose)
Magnesium hydroxide (Brucite)	58.33	2360	350 (decompose)
Magnesium oxide (Periclase)	40.31	3580	2800

Table 9 Tables of physical constants<sup>81</sup>

### 2.6.4.1 Aqueous Phase Reaction

When dissolved in water calcium carbonate (CaCO<sub>3(s)</sub>) will produce the following chemical species:



The chemical reactions are shown in Figure 14. The redistribution of these chemical species will, under most conditions, result in the charging of the calcite surface. The surface charging is therefore the result of ion dissolution - ion adsorption processes.

There are a large number of reaction possibilities and rate constants that describe the behavior and interaction of the chemical species produced when calcium carbonate is dissolved in water<sup>82</sup>. These can be further complicated by the presence of other ions and organic matter<sup>83</sup>. As a result the system for coating calcium carbonate from an aqueous solution is an extremely complex reaction to model.

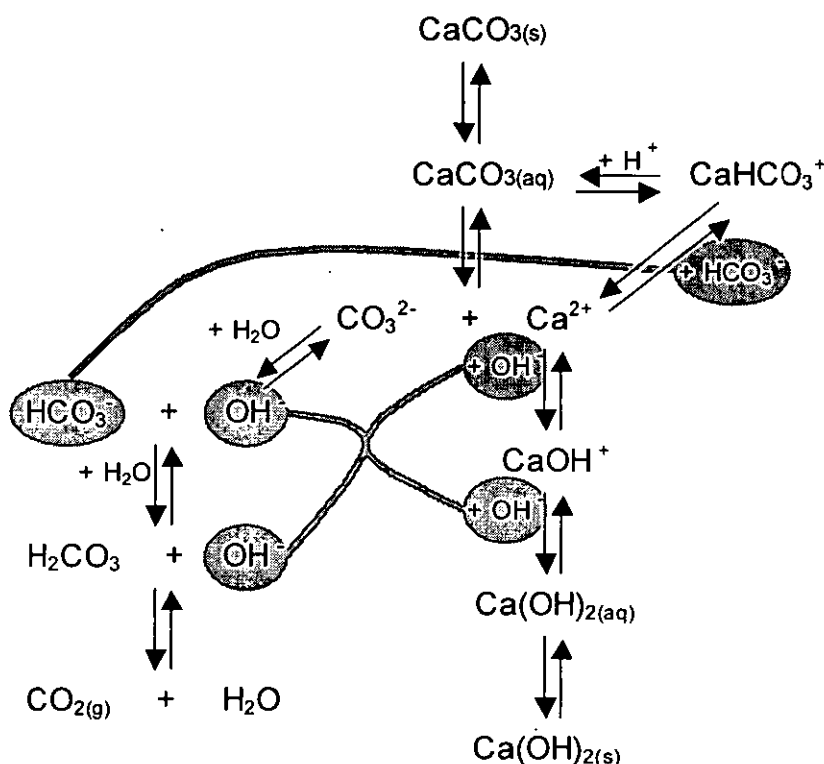


Figure 14 Diagram of the reactions that occur between the chemical species produced when calcium carbonate dissolves

The electrokinetic behavior of calcite has been studied by many authors under a wide variety of conditions. There have been many attempts made to model the calcite-water system but in general the results have been inconsistent<sup>84</sup>. The variation in results is due to the calcite reactivity which strongly influences its surface charge and, therefore its electrophoretic mobility and electrokinetic

potential. In the calcite-water system there are two important factors governing the formation of the surface charge:

- The concentration of the potential determining ions ( $\text{Ca}^{2+}$  and  $\text{CaCO}_3^{2-}$ )
- The pH, on which the concentration of the potential determining anion  $\text{CaCO}_3^{2-}$  depends

In the calcite-water system the charge balance of the chemical species described in Figure 14 can be summarised as:



where  $v + 2w = x + 2y + z$

Equation 19

In general, PCC in distilled water at concentrations greater than  $50\text{mg}/100\text{cm}^{-3}$  will undergo ion dissolution and ion adsorption to form an alkali solution (approximately pH 9) with a positively charged surface<sup>85</sup>. This surface charge can be made negative if the solution is made more alkaline. These two surface regimes are nominally the two possible states that must be considered during any coating process. The presence of organic matter in general reduces the positive nature of a charged surface<sup>83</sup>. There are a number of methods used industrially to produce the coating, most of which require the use of an alkali to generate the soluble stearate. In general in an alkaline environment the coating process occurs when the calcite is negatively charged. The presence of the stearate and the variable pH levels, in addition to the reactions described above, make the mathematical modeling of the coating process almost impossible.

The solubility of the stearates at room temperature is shown in Table 8. All show limited solubility at room temperature. Those stearate groups in solution are thought to form a mixture of free surfactant and micelles. Those that are not in solution form a liquid crystalline phase. The critical micelle concentration (CMC)



for an 18-carbon alkyl chain is very low. At higher temperatures, above the Krafft Temperature (56°C for an 18-carbon alkyl chain) the number of stearate groups in solution increases rapidly forming additional micelles.

Calcium stearate formation can be imagined to take place either at the surface or in the solution. These reactions will be competitive and will be dependent on the effects and the availability of calcium and stearate ions as described above. The differentiation of the bound and the unbound stearate is most frequently achieved by solvent extraction<sup>19</sup>. This does not allow accurate determination of the formation process.

Attempts have been made to show the effect of the filler-matrix interaction by the adsorption of surfactants<sup>86</sup>. This research was based on an industrial natural grade chalk. The use of this data in terms of generating a model for the formation of a coating in a calcite-water system is hazardous. Anionic and cationic surfactants showed different zeta potential adsorption profiles. Both surfactants at low concentrations generated negative zeta potentials whilst at higher concentrations the cationic surfactant generated a positive zeta potential possibly indicating the formation of a multilayer. When the fillers were compounded the tensile and flexural strength was found to increase to a maximum value. This maximum corresponds approximately to the formation of a monolayer. The increase may therefore be interpreted in terms of the adhesion between the components. The impact strength was shown to vary only at high coating concentrations. This may be explained either as a result of the formation of a weak interface layer, which dissipates energy in the impact tests, or the formation of a toughened matrix layer generated by filler surface effects.

#### **2.6.4.2 Non-Aqueous Phase Reaction**

A non-aqueous phase such as toluene does not allow ion dissolution or ion adsorption and as a result it forms a neutral medium under which the formation of calcium stearate can take place. Consequently the soluble acid forms the only mobile phase. The formation of calcium stearate is dependent on the rate of arrival of the stearate at the surface and the rate of reaction. This, unlike the aqueous phase reaction, is an entirely surface based reaction.

#### **2.6.4.3 Dry Coating Reaction**

This is again an entirely surface based reaction, although it is disadvantaged by the lack of mobility of the stearic acid in comparison to a non-aqueous phase process. As a result this process is often inefficient.

## 2.7 Filler Surface Characterisation

The filler and its coating may be characterised in a number of different ways. The techniques may be divided into the following groups:

- Spectroscopic & diffraction based techniques e.g. XPS, DRIFT, XRD, SEM
- Calorimetry/Adsorption techniques e.g. FMC, IGC, BET
- Classical techniques e.g. Gravimetry, acid extraction
- Measurement of molecular mobility/mechanical properties e.g. NMR, Rheological properties, DMTA

Alternatively these techniques may be described in terms of those that measure actual properties and those that measure specific interactions.

Classical and spectroscopic techniques fall into the first category. Spectroscopic techniques were used initially to describe the structure of the bulk materials. As the techniques have developed and with the introduction of computers, the application of these techniques to interface and interphase analysis, has become important<sup>87,88,89</sup>.

Those techniques that measure specific interactions allow the effect of any surface modification to be analysed in terms of the chemical or physical effects. Analysis may be either chemical, physical or mechanical.

The interaction of a probe molecule allows the change in the surface chemistry to be analysed. Flow microcalorimetry (FMC) allows the enthalpy change during the adsorption of a compound on to a surface to be measured<sup>48</sup>. The enthalpy of adsorption, may then be considered in terms of the acidic and basic characteristics of the adsorbate. When used in conjunction with an HPLC detector the technique is also capable of determining the quantity of adsorbate<sup>90</sup>. An alternative 'probe' technique is inverse gas chromatography (IGC)<sup>91,92</sup>. In IGC a small quantity of a

probe molecule is injected into a column of the material to be analysed. The time taken for the probe to elute the column, compared to that of a non-adsorbing probe is measured and is interpreted in terms of an interaction between the probe and surface of the material. A mathematical treatment can then relate this difference in elution time to the free-energy change in the adsorption process. IGC has been used to study the effect of stearic acid coating on calcium carbonate<sup>19</sup>, in which it was shown that the energy of interaction was significantly reduced by coating. The surface energy was reduced to approximately that expected for stearic acid.

Analysis of the molecular mobility of the polymer is achievable by a number of techniques, the most common being DMTA and DSC. The use of electron spin resonance (ESR) and solid state nuclear magnetic resonance (NMR) is becoming more widespread<sup>93,94</sup>. Differences in relaxation times for bound and unbound polymer have been observed<sup>95,96</sup>. The introduction of either oil or a molten polymer to the filler allows the physical interaction of the filler with the polymer to be studied. Not only can the packing fraction be determined<sup>97,98</sup>, the rheological properties can also be analysed as a function of frequency, temperature or composition.

No one technique allows a complete understanding of the coating and its formation. It is only through a multi technique approach that a better understanding of the coating can be obtained. Only those techniques used in this work are further described in the following sections.

## 2.7.1 Electron Microscopy

Electron microscopy techniques are widely used in the analysis of fillers and their interactions with polymers. When analyzing fillers, Scanning Electron Microscopy (SEM) provides an excellent method of visual analysis, whilst Transmission Electron Microscopy (TEM) provides an excellent method of high resolution 'profile' analysis. Both techniques allow limited elemental analysis. The formation of a stearic acid coating on glass beads has been studied using scanning electron microscopy<sup>99</sup>. These beads are orders of magnitude larger than the filler particles analysed in this thesis.

These techniques become especially useful when we either want to try to understand the level of dispersion or try to understand the mode of composite failure<sup>1,14</sup>.

## 2.7.2 Classical Analysis

Before the widespread use of electronic analytical instrumentation, measurements were based on either classical wet techniques, thermal or combustion analysis. The analysis of the somewhat impure starting fatty acid is also of great importance<sup>100</sup>.

Surface acid concentration was measured by dissolving the carbonate, followed by ether extraction and steam extraction. This technique, although providing a quantitative measure of the surface coating, is time consuming and has a low level of reproducibility.

The use of thermal analysis is well documented. Both thermogravimetric and combustion analysis are widespread in the analysis of the decomposition of both organic and inorganic compounds. The quantities of physisorbed and chemisorbed water are known to vary as a function of sample preparation<sup>101,102</sup> and procedural variables<sup>103</sup>. By taking this into account thermal methods have been used to analyse the modifier content of fillers modified with stearic acid

<sup>104,105</sup> and titanate coating agents <sup>104</sup>.

The use of combustion analysis or carbon-hydrogen-nitrogen elemental analysis (CHN) has been reported <sup>9,14</sup>. Treatment of experimental data relies on assumptions of substrate and material physical properties, and combustion reactions/products.

### **2.7.3 Gas Adsorption Isotherm Analysis**

The study of the adsorption of a molecule on the surface of both porous and non-porous media is well established, and has been well reviewed <sup>106,107</sup>. The relationship between the amount of gas adsorbed and the pressure at constant temperature is termed the adsorption isotherm. The majority of isotherms which result from physical adsorption may be grouped into five classes, as shown in Figure 15 and summarized by Table 10, which were originally classified by Brunauer, Deming, Deming and Teller <sup>108</sup>.

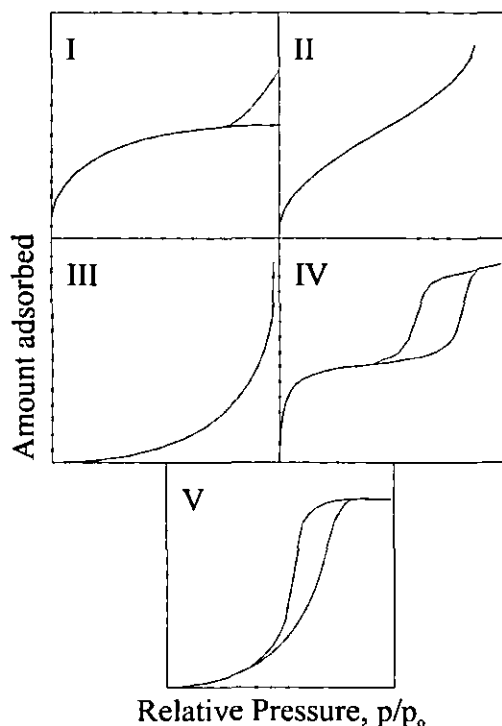


Figure 15 Gas adsorption, Type I to V isotherm classification

Type	Description	Example
I	The approach predicted by the Langmuir isotherm.	Microporous solids, having relatively little external surface, the limited uptake being governed by the accessible micropore volume, rather than by the internal surface area.
II	Unrestricted monolayer – multilayer adsorption.	Normal form obtained from a non-porous or macro porous adsorbent.
III	Multilayer formation.	This occurs on solids for which the adsorption potential is low. This is not common, and is often characteristic of a non-porous system. e.g. nitrogen on ice <sup>109</sup> .
IV	Analogue of II, on porous adsorbents.	Adsorption on porous materials, where the adsorption is limited by the volume of mesopores. They reflect condensation phenomena and may show hysteresis effects.
V	Analogue of III, on porous adsorbents.	

Table 10 Table summarising the gas adsorption isotherm classification

Pore size distribution and surface area measurements can be extracted from adsorption isotherms. The most common method for evaluating the surface area and pore size distribution is the adsorption of nitrogen at its boiling point, 77K. However, the results are extremely dependent on the model used to derive the distribution, which has resulted in many different modelling techniques.

### 2.7.3.1 Langmuir Adsorption Isotherm

Interpretation of the Type I isotherm must account for the fact that the uptake does not increase continuously as in the Type II isotherm. According to Langmuir<sup>110</sup>, this type of phenomena can be generated if the pores are so narrow that they can only accommodate a single molecular layer and thus the plateau corresponds to the completion of this monolayer.

The shape of the isotherm was explained using the ‘classical’ Langmuir model. Langmuir used a kinetic derivation considering the dynamic equilibrium between the adsorbed layer and the bulk gas phase. By using the kinetic theory of gases, and the assumption that the gas is adsorbed only at points on the surface, with no lateral gas interactions, the fractional coverage of the surface may be calculated from,

$$\frac{n}{n_m} = \frac{b(p/p_o)}{1 + b(p/p_o)}$$

Equation 20

where;

$n$  is the number of atoms/molecules adsorbed,

$n_m$  is the number of atoms/molecules required to form a monolayer,

$p$  is the gas pressure,

$p_o$  is the standard gas pressure,

$b$  is a constant and is related to the adsorption energy and is dimensionless.



The Langmuir adsorption isotherm is a good approximation for adsorption on high energy surfaces at pressures below  $p_0$ .

### 2.7.3.2 BET Adsorption Isotherm

Experimental physical adsorption isotherms have shown from the early days that adsorption did not normally stop at a monolayer and that multi layers were usually present at partial pressures of greater than around 0.1 <sup>108</sup>.

In 1938 Brunauer, Emmett and Teller <sup>111</sup> derived a kinetic theory model that accounted for the localised multi layer adsorption at low vapor pressures, which is known today as the BET model. The model has also been derived by statistical thermodynamic methods <sup>112</sup>. By considering the rates of condensation and evaporation of the individual layers the volume of gas adsorbed at specific partial pressures may be calculated from,

$$\frac{v}{v_m} = \frac{c(p/p_o)}{(1-p/p_o)(1-p/p_o + c(p/p_o))}$$

Equation 21

where:

$v$  is the volume of gas adsorbed,

$v_m$  is the volume of gas required to form a monolayer,

$p$  is the gas pressure,

$p_o$  is the standard pressure,

$c$  is a constant (defined in Equation 22).

The value of  $c$  is given by:

$$c = e^{(E_1 - E_L)/RT}$$

Equation 22

The term  $E_1 - E_L$ , the difference between the heat of adsorption in the first layer and the heat of liquefaction, is known as the 'net' heat of adsorption.

Both Langmuir and BET models may be used to calculate the surface areas<sup>113</sup> of the material if the volume occupied by a single molecule of the adsorbent gas is known.

### 2.7.3.3 Surface Heterogeneity

Various gas adsorption methods have been used in attempts to determine the distribution of adsorption potentials. Such a distribution will in part be dependent on the nature of the substrate, but there will also be an effect due to the nature of the adsorbate gas. In most cases to date the distribution of site energies is confined to the submonolayer region. In this region the adsorption or the fractional coverage can be considered to be a function  $\theta$  of  $Q$ ,  $P$  and  $T$ , where  $Q$  is an adsorption energy,  $P$  is the pressure and  $T$  is the temperature. The distribution of sites of energy  $Q$  may be considered as a distribution function  $f(Q) dQ$ . The experimentally observed adsorption isotherm will be a function  $\theta$  of  $P$  and  $T$ . And may be described as follows:

$$\theta(P, T) = \int_0^{\infty} \theta(Q, P, T) f(Q) dQ$$

Equation 23

There are in essence two approaches to solving this equation:

- To calculate theoretical isotherms from postulated distributions, and then compare these with the experimental isotherm. This technique is limited by the previously determined adsorption parameters<sup>114</sup>.

- To make successive approximations from the experimental isotherm and deduce the distribution <sup>115,116,117</sup>.

The common factor between both methods is the reliance of the method on the actual function used to describe the standard local adsorption isotherm.

## 2.7.4 Infrared Spectroscopy

Infrared (IR) spectroscopy measures the absorption of infrared radiation by the sample due to bending, stretching or wagging vibrations of the molecular bonds. Quantitative analysis can be carried out according to Beer's Law. The intensity of the absorption is proportional to the concentration of the sample.

$$A = \log \frac{I_0}{I} = \epsilon cl$$

Equation 24

where:

$A$  is the absorbance,

$I$  is the intensity,

$\epsilon$  is the molar absorption coefficient,

$c$  is the concentration,

$l$  is the path length.

IR is quantitative only under certain circumstances i.e. assuming the geometry and optics are kept constant; and the intensity of the IR is within the linear range of the detector.

### 2.7.4.1 FTIR Spectrometer

Quantitative analysis of the filler coating is essential in understanding the role of the filler-polymer interface. Infrared spectroscopy is widely used in the analysis of polymers and fillers. Koenig<sup>118</sup> and Ishida<sup>119</sup> produced extensive reviews of the principles and applications of Fourier Transform Infra Red (FTIR) analysis of polymers. Compared with dispersion infrared which utilised gratings or prisms to disperse the radiation, FTIR has the advantage of being faster and more sensitive. To overcome the disadvantage of the dispersive system, where much of the energy is lost because of the scanning nature of the detection system, a Michelson

interferometer is used. A schematic diagram of a Michelson Interferometer based FTIR machine is shown in Figure 16.

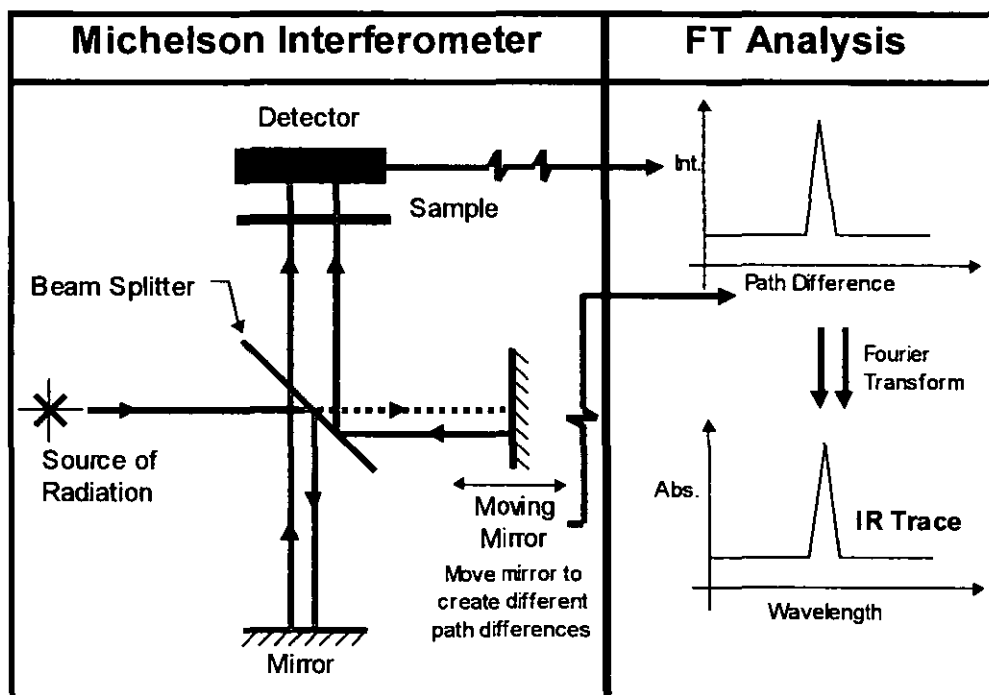


Figure 16 Schematic diagram of a Michelson interferometer based FTIR machine

The improved efficiency and radiation throughput (Jacquinot's advantage) result in a technique with a very high signal to noise ratio. This, in conjunction with faster rates of data acquisition due to the continuous analysis of all frequencies ( Fellgett's advantage) and improved accuracy in the measurement of the wavelength (Conne's advantage) result in a system superior to previous dispersive IR systems.

#### 2.7.4.2 DRIFT Apparatus

Diffuse reflection spectroscopy (DRIFT) is the preferred infra-red technique for studying organic coatings on inorganic powders. Using this technique infra-red radiation diffusely scattered from the surface of the sample is collected by an

elliptical refocusing mirror and passed to a detector (Figure 17). Steps can be taken to eliminate specular reflection<sup>120</sup>. Functional groups present in the sample are identified from their characteristic absorption frequencies. The technique appears to have some surface specificity.

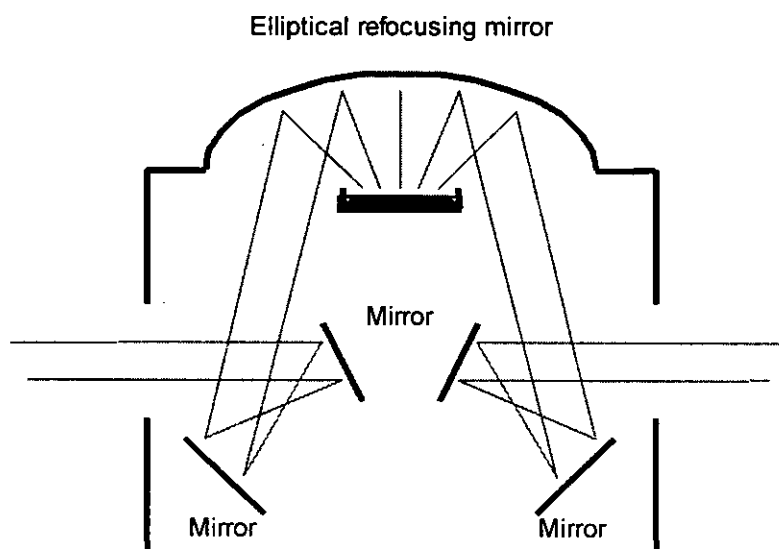


Figure 17 Schematic diagram of a Spectra Tech Inc. diffuse reflectance infrared (DRIFT) cell

When performing DRIFT experiments, the two components of the reflected radiation must be taken into consideration. If the diffuse and specular components are not taken into consideration the spectra cannot be analysed quantitatively. In high concentration analyses it was shown that a 'blocker vane' was required to eliminate all but the reflectance that had penetrated the sample, i.e. diffuse reflectance<sup>120</sup>. High concentration samples also result in the intensity of the adsorption being outside the linear range of the detector.

In order to ensure that the spectra can be quantitatively analysed, the powdered sample must be diluted in a non-IR absorbent material, i.e. KBr, KCl, NaCl. The shape and particle size of both the diluent and the sample is critical<sup>119,121</sup>. The quantitative nature of DRIFT has been studied extensively and reasons have been

reported for deviations from linearity <sup>119</sup>.

### **2.7.4.3 DRIFT Theory**

Theories of DRIFT can be divided into two categories known as continuum and statistical <sup>122</sup>. Both theories are based on the assumption that only the scattering centres of the sample analysed may adsorb radiation.

Statistical models are based upon a summation of transmittances and reflectances from individual layers or particles. Thus, some assumptions must be made about the nature of these fundamental units, and the validity of the ultimate result will depend upon how closely these assumptions correspond with reality. Only the statistical models lead to expressions from which absolute absorptivities and scattering coefficients can be calculated and related to the actual particle characteristics.

Continuum models typically describe the scattering and adsorbing properties of a given medium in terms of two phenomenological constants. These models may be regarded as varying levels of approximate solutions to the general equation of radiative transfer.

In a dense scattering medium the interaction of the radiation fields can be considered in two parts:

- Coherent part - largely due to the nearest neighbour interaction, this gives rise to the dispersion effects
- Incoherent part - multiple scattering as a sum of the interactions throughout the entire medium

The basic concept of radiative transfer theory is that each volume element is irradiated by scattering from every other volume element. The equation of radiative transfer can be simply written as,

$$\partial I = -\kappa \rho l \partial x + j \rho \partial x$$

Equation 25

where:

$\partial I$  is the change in intensity of the beam,

$-\kappa \rho l \partial x$  is equal to the radiation lost due to adsorption and scattering,

$j \rho \partial x$  is equal to that which in this direction from other directions,

$\rho$  is the density,

$\kappa$  is the attenuation coefficient,

$j$  is the scattering function,

$\partial x$  is the element of path length.

A number of different models have been used to approximate the scattering of which the most common is the Kubelka-Munk continuum theory<sup>139</sup>

Kubelka-Munk theory is based upon a model in which the radiation field is approximated by two fluxes ( $I_+$  travelling from the sample surface,  $I_-$  travelling toward the illuminated surface). As radiation travels from the surface, its intensity is decreased by scattering and adsorption processes, which are assumed to be proportional to the thickness of the medium traversed. This is partially offset by scattering of the beam travelling toward the surface. The equation for the two beams is given by,

$$\frac{\partial R}{S \partial x} = R^2 - 2aR + 1$$



Equation 26

Where S and K are phenomenological constants which describe scattering (S) and adsorption (K).

$$R = \frac{I_-}{I_+}$$

Equation 27

$$a = \frac{S + K}{S}$$

Equation 28

This can be easily integrated from  $x = 0$  to  $x = \infty$ . Resulting in the well known Kubelka-Munk function  $F(R_\infty)$ .

$$F(R_\infty) = \frac{(1 - R_\infty)^2}{2R_\infty} = \frac{K}{S}$$

Equation 29

#### 2.7.4.4 Infrared Application

Infrared is widely used in the analysis of both organic and inorganic compounds and the frequencies at which specific groups absorb are well documented<sup>123,124</sup>.

Both chemical species and chemical environment information can be obtained and this has been well documented<sup>87,119</sup>. Before the invention of the modern FTIR most infrared analysis was aimed at the assignment of the specific vibrations in terms of their symmetry properties<sup>125</sup>.

The spectra obtained for the two fillers of interest have been reported. Uncoated

precipitated calcium carbonate values agree well with those cited in the literature for calcite <sup>126,127</sup>. The experimental values determined for magnesium hydroxide are also in good agreement <sup>128,129</sup>.

The structure and the effect of the chemical environment on the IR adsorption frequency of the carboxylic acid / carboxylate group have been studied <sup>130</sup>.

The charge density of the metal ion has been shown to have an effect on the bond frequency <sup>131,132</sup>. As the charge density of the metal ion increases the IR adsorption is found to move to a longer wavelength.

The presence of electronegative substituents in the organic molecule, has been shown to result in a shift to a lower wave number <sup>133</sup>.

The effect of water on the 'external chemical environment' or the presence of hydrogen bonds <sup>132,134</sup> has been shown to result in lower stretching frequencies (lower wave number).

The effect of the external physical environment, in particular the phase type and the packing will have an effect on the frequency of adsorption <sup>132</sup>. The variables described above are inter-related and are not independent

In summary it may be concluded that the effect of the sum of the variables described above will be visible in the position of the carboxylate adsorption.

FTIR is now routinely involved in the analysis of fillers <sup>135</sup>. It has been often been applied as a tool to study the surface hydration of minerals <sup>136,137</sup>. The FTIR has generally been used in one of two modes. Either direct analysis of the filler by DRIFT <sup>138,139,140</sup> or by a 'dissolution method' <sup>17</sup>. This 'dissolution method' works by comparing unreacted or unbound material dissolved in a suitable solvent

compared to a predefined calibration curve.

DRIFT has shown that the coating reaction continues beyond that required to form one theoretical monolayer <sup>141</sup>. This additional unbound coating has been shown to be removed when exposed to a solvent extraction <sup>139</sup>.

## 2.7.5 X-ray Photoelectron Spectroscopy

XPS is now a well established surface analysis technique providing quantitative elemental analysis (all elements except hydrogen) in the outer 2-5 nm of solid surfaces. In XPS the sample is irradiated with soft X-rays and the photoelectrons generated are collected and energy analysed to yield a spectrum. The photoelectron energy is directly related to the binding energy of the electron to the core level.

$$K.E. = h\nu - B.E. - \phi_s$$

Equation 30

where:

$K.E.$  is the kinetic energy of the photoelectron,

$h\nu$  is the photon energy,

$B.E.$  is the binding energy,

$\phi_s$  is the work function of the spectrometer.

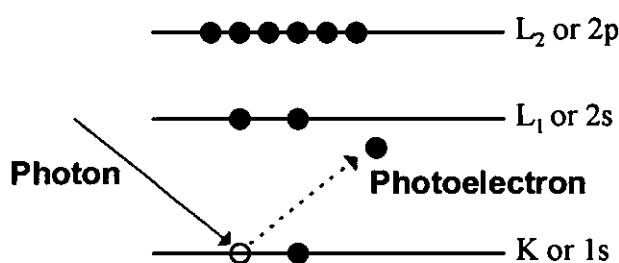


Figure 18 Schematic diagram of X-ray induced photoemission

High energy resolution spectra may be used to study the surface chemistry and identify the functional groups present at the surface in addition to providing the elemental composition. Since the technique provides quantitative data it is possible to relate the extent of coating measured by XPS to the mechanical properties of the composite.

### 2.7.5.1 XPS Apparatus

X-ray photoelectron spectroscopy makes use of soft X-rays, generally Al  $K\alpha$  (1486 eV) or Mg  $K\alpha$  (1254 eV). These X-rays penetrate the material travelling approximately 7  $\mu\text{m}$  or more. As described in section 2.7.5 X-ray Photoelectron Spectroscopy, the X-rays will induce the photoemission of photoelectrons in the solid. Electrons generated through a photoemission process from a core level have a very short inelastic mean free path (IMFP) or attenuation length, so only those generated within 2-5 nm of the surface escape. Therefore the technique is extremely surface specific. A schematic diagram of the set up required for a XPS system can be seen in Figure 19.

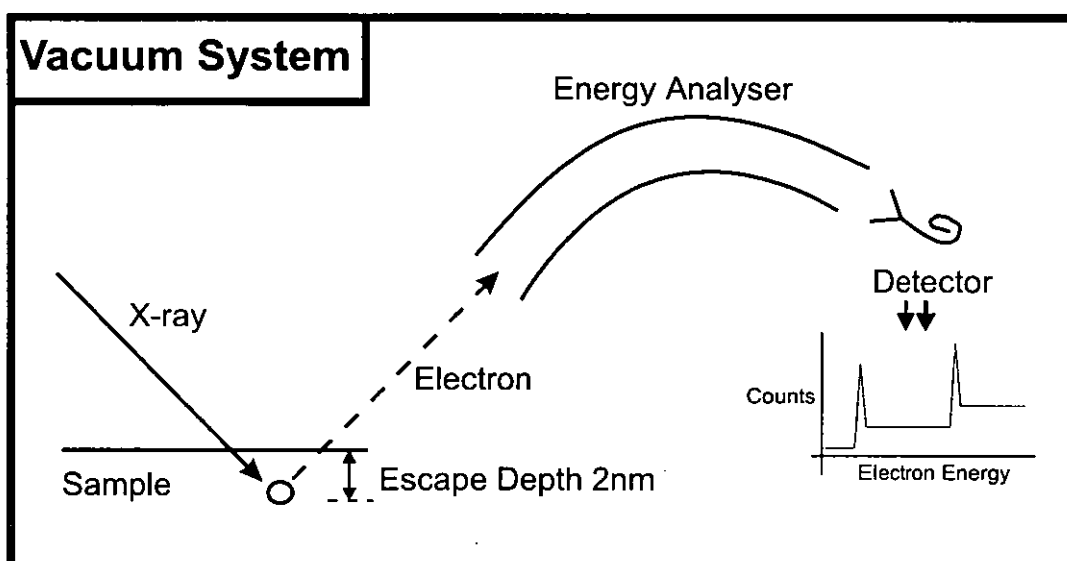


Figure 19 Schematic diagram of an XPS system

### 2.7.5.2 XPS Analysis

XPS is a commonly used technique; its photoemission energies and the nature of chemical shifts are well documented. In the beginning, quantification was achieved by considering the composition averaged over the sampling depth by relating the intensities of those measured to those of bulk reference standards <sup>142</sup>.

However, the need for the measurement of the outermost atomic layer has resulted in the need to consider more accurately the electron sampling depth. To a first approximation the electron sampling depth obeys a universal curve ( $\lambda \propto E^{1/2}$ ). Initially it was considered that the depth of analysis could be derived from the electron's inelastic mean free path (IMFP) and a knowledge of the sample geometry<sup>143</sup>. This was later referred to as the effective attenuation length (EAL)<sup>144</sup>.

This approach was summarised, to make it one equation per situation; elements, inorganic compounds, organic compounds. The equations were applicable to electron energies between 1 to 10,000 eV. The predictions are significantly more accurate for electrons above 150 eV. A summary of the equations can be found in Table 11.

Electron Source	IMFP <sup>(143)</sup> or EAL <sup>(144)</sup>
Element	$\lambda_M = \frac{538}{E^2} + 0.41(aE)^{1/2}$ monolayers
Inorganic Compound	$\lambda_M = \frac{2170}{E^2} + 0.72(aE)^{1/2}$ monolayers
Organic Compound	$\lambda_M = \frac{49}{E^2} + 0.11E^{1/2}$ mgm <sup>-2</sup>

where  $a$  is the monolayer thickness in nanometers.

Table 11 Summary of equations for electron inelastic mean free paths (IMFP) (as defined)<sup>143</sup> or effective attenuation length (EAL)<sup>144</sup>

These equations have allowed analysts to attempt to quantify overlayer thickness. The inelastic mean free path is an intrinsic property of the material under analysis. It is defined as the average of the distances measured along the trajectories, that particles of a given energy travel between inelastic collisions in a substance. This was soon considered to be inappropriate for overlayer thickness calculations. The

'attenuation length' (AL), was thought to be more appropriate. The use of ALs does allow a more accurate quantification of the system being studied in comparison to IMFP's. This is because the 'standard IMFP equations' (Table 11) do not consider the contributions of a number of secondary effects. The most notably being elastic scattering, as shown by Monte-Carlo simulations<sup>145</sup>. The ALs are typically found to be 10-25% shorter than IMFPs<sup>146</sup>. Semi-empirical equations have been developed<sup>146</sup> (CS1 and CS2) that allow easy estimation of ALs in any solid over the energy range 100-2000eV.

Matrix	Attenuation Length Equation
Lattice Parameter and Density Unkown	Equation CS1 (monolayers) $\lambda_{AL} = 0.160 \left\{ \frac{E}{Z^{0.45} [\ln(E/27) + 3]} + 4 \right\}$
Lattice Parameter and Density Known	Equation CS2 (monolayers) $\lambda_{AL} = 0.316a^{3/2} \left\{ \frac{E}{Z^{0.45} [\ln(E/27) + 3]} + 4 \right\}$

where  $a$  is the monolayer thickness in nanometers.

Table 12 Summary of equations for attenuation lengths (AL) (as defined)<sup>146</sup>

These most recent equations have also generated great interest regarding their validity. It was suggested that they did not consider the effect of photo-ionization, although recent work has shown that at an analysis angle of greater than sixty degrees, samples tend to show an insensitivity to anisotropy<sup>144</sup>. Another shortcoming of these equations is that they do not allow for different levels of back scattering. This effect typically generates a 1-3 % variation in calculated film thickness (Important in Auger Electron Spectroscopy (AES)).

A great deal of further work has been done to calculate more accurately the IMFP of elements in pure solids<sup>147</sup>. Alternative more complicated variations of these equations have been proposed by Bethe<sup>148</sup> and Tanuma et al.<sup>149</sup>. (Equation TPP-

2M). Recent work has also considered the effect of elastic scattering off nuclei<sup>150</sup>, and the use of the transport mean free path function (TrMFP) to describe it. A new term mean escape depth (MED) is introduced as a measure of surface specificity, and is defined as the average depth normal to the surface from which the specified particles or radiation escapes<sup>144</sup>.

The most accurate methods of calculating the attenuation length and the improvements in accuracy are unfortunately outweighed by other experimental considerations in overlayer thickness calculations. In the author's opinion at present the CS1 and CS2 equations proposed by Cumpson and Seah<sup>146</sup> provide the best method for estimating attenuation lengths for practical analysis.

Presently three methods are used. Two are based on the properties of the photoelectron emission, and the third is based on ion bombardment. Ion bombardment is known to result in the undesired effects such as preferential sputtering, atomic mixing and loss of chemical information.

Of the two 'photoelectron emission' methods, estimation of the coating thickness is most easily achieved by the measurement of the relative intensity of the photoelectron peaks due to coating ( $I_{\text{COATING}}$ ) and substrate ( $I_{\text{SUBSTRATE}}$ ). This is described in Section 4.5 XPS Results. The assumption that the attenuation lengths are the same in both the substrate and coating is only valid in a very few cases<sup>151</sup>. Previous practical experimental estimates have failed to allow for a variation in attenuation length or sample geometry. Failure to allow for these factors may result in the answer being in error by a factor of two or more.

If it is assumed that the coating is uniform over all the particles, the thickness can be estimated by considering the effect of the coating on the attenuation of the photoelectrons emitted from the sample. Two models have been investigated: photoemission from a coated flat sample and a coated sphere. These models may be considered to be the most extreme conditions for analysis. A true



representation of the sample geometry should lie somewhere between them.

The alternative 'photoelectron emission' approach suggested by Tougaard<sup>152</sup>, proposes that composition information may be obtained by studying the background shape of the peak. It is proposed that electrons originally excited at some depth in the solid lose energy on their way out to the solid surface. The peak shape in the measured energy spectrum is distorted as a result and the distortion depends on the path travelled. From this we may conclude that information on depth composition is contained within the region around the XPS peak.

## 2.7.6 X-ray Diffraction

This is a widely used method for determining the structure of crystals. By directing a monochromatic beam of X-Rays at a crystal and then measuring the X-Ray reflections from the atomic planes, the arrangement of atoms in the crystal can be deduced. In essence:

- X-rays are diffracted by each individual atom.
- The combined effect of all the atoms in a single plane is to produce a reflected beam at the same angle to the crystal plane as the incident beam.
- The reflections from similar planes should reinforce one another at certain angles. If this third condition is met, the following equation, known as Bragg's law, gives the angle of 'reinforced reflection'.

The positions at which diffractions occur is given by Bragg's law,

$$n\lambda = 2d \sin \theta$$

Equation 31

where:

$n$  is the order of the reflection,

$\lambda$  is the wavelength,

$d$  is the lattice plane separation.

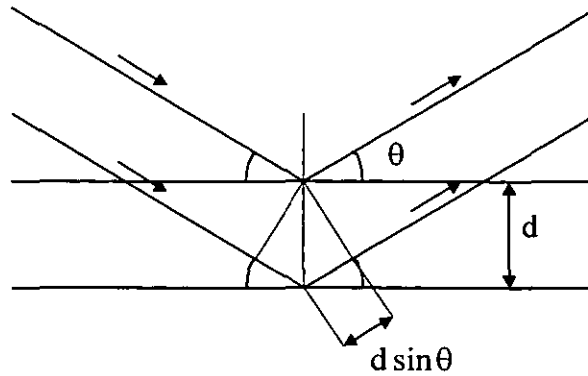


Figure 20 Schematic representation of Bragg's law of the 'reinforced reflection'

For a cubic lattice the unit cell dimension  $d$  is related to the interplanar ( $hkl$ ) spacing by the following equation where  $a$  is the lattice parameter.

$$d = \frac{a}{\sqrt{h^2 + k^2 + l^2}}$$

Equation 32

Both magnesium hydroxide and calcium carbonate have hexagonal lattices. The unit cell dimension  $d$  is related to the interplanar ( $hkl$ ) spacing by the following equation where  $a$  is the lattice parameter.

$$\sin^2 \theta_{hkl} = \frac{\lambda^2}{3a^2} (h^2 + hk + k^2) + \frac{\lambda^2}{4c^2} l^2$$

Equation 33

X-ray diffraction is used in two ways; single crystal or powder. By using a powdered sample it is assumed that we have all planes available for reflection. By altering the angle of incidence to the sample different intensities of X-ray are reflected. This variation of intensities can be recorded as a function of  $\theta$ . The

intensities corresponding to different angles may be assigned to different planes. From this assignment values of the lattice parameter ( $a$ ) can be calculated. Tables of lattice parameters and their corresponding planes can be used to identify the compound <sup>153</sup>.

Previous work has shown <sup>154</sup> that some crystalline magnesium stearate was detected in magnesium stearate coated magnesium hydroxide (5 monolayer). Diffraction analysis of magnesium stearate is common as it is used extensively as a lubricant not only in the plastics industry, but also in the pharmaceutical industry. Analysis of the magnesium stearate form on its chemical, physical and lubricant properties is extensive <sup>155,156</sup>. X-Ray diffraction patterns have been shown to vary as a function of water content, preparation method and mechanical treatment.

### **2.7.7 Dynamic Mechanical Analysis (DMA)**

Materials respond to an applied stress or strain by dissipating energy in the form of heat (viscous dissipation), storing the energy elastically, or through a combination of these two mechanisms. Dynamic mechanical testing makes it possible to measure both of these properties.

The dynamic mechanical method assesses the structure and properties of solids and viscoelastic liquids via their dynamic moduli and damping. In particular, changes in these parameters are studied as a function of temperature and applied frequency. The method has great sensitivity in detecting changes in internal molecular mobility and in probing phase structure and morphology.

When a sinusoidal stress is applied to a 'perfectly' elastic solid the deformation and hence the strain, occur exactly in phase with the stress. However, when applied to a polymer, when some internal molecular motion is occurring in the same frequency range as the impressed stress, the material responds in a viscoelastic manner and the strain response lags behind the stress.

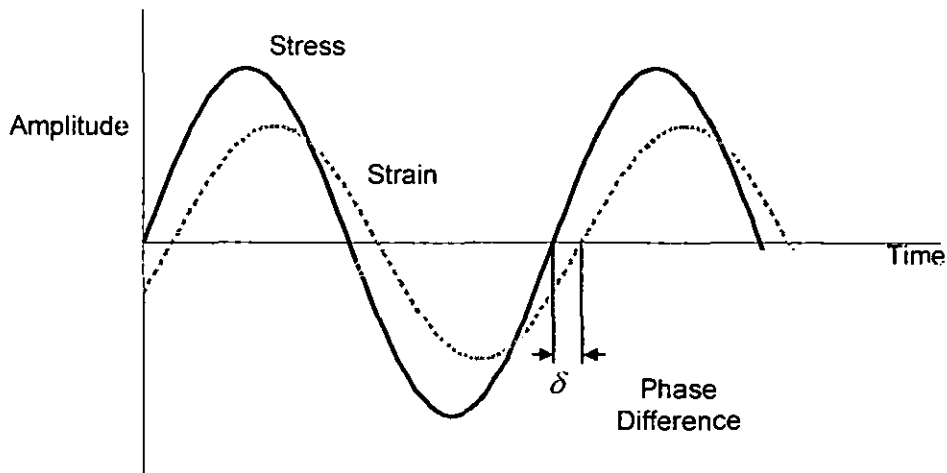


Figure 21 Schematic representation of the response of viscoelastic material to an applied sinusoidal stress

The modeling<sup>157</sup> of the viscoelastic response of the material is considered in terms of a combination of perfectly elastic and perfectly viscous responses. Hooke's law is used to describe the elastic or 'spring' like component, and Newton's law is used to describe the viscous or 'dashpot' like component of the viscoelasticity. The most common viscoelastic models consider the 'spring' and 'dashpots' either in series (Maxwell model) or parallel (Voigt model). These enable the retardation time (Voigt model – the time taken for the strain to reach  $(1-1/e)$  of the equilibrium value) and the relaxation time (Maxwell model – the time taken for the stress to decay to  $1/e$  of the original value) to be analysed. The ability to analyse the time-dependence of the retardation and the relaxation at different temperatures enables the effect known as the time-temperature superposition principle to be observed. This ability to compare a frequency to a temperature is described by the universal Williams-Landel-Ferry equation (WLF equation).

The techniques of thermal and dynamic mechanical analysis are combined in a technique known as Dynamic Mechanical Thermal Analysis (DMTA). A loss peak in the temperature plane occurs when the frequency of a motional process

coincides with the impressed (measurement) frequency. This peak may be used to characterize the molecular mobility <sup>158</sup>.

This technique detects the changes in internal molecular mobility of the polymer chains. As a result, this technique is ideal for detecting the individual effects of the components within the composite, and the interaction of the components.

The causes of the variations in the molecular mobility of the polymer chains in the composites are summarised in Table 14.

In DMTA the following can be defined <sup>159,160,161</sup>.

Symbol	Title	Description
$E^*$	Dynamic Young's modulus	This is the sum of the resolved, in and out of phase modulus components of the strain. ( $E^* = E' + iE''$ )
$E'$	Storage modulus	Is the elastic response and corresponds to completely recoverable energy.
$E''$	Loss modulus	Is the viscous response corresponding to energy lost through internal motion.
$\tan \delta$	Loss tangent	Is the tangent of the loss angle ( $\tan \delta$ ). This is dimensionless and is equal to the ratio of energy lost (dissipated as heat) to energy stored per cycle.

Table 13 Summary of dynamic mechanical analysis terms

Type	Cause	Description
Internal	Wetting	The level of contact between the two phases.
Internal	Adhesion	The adhesion between the two phases.
Internal	Dispersion	The distribution of the two phases.
Internal	Composition	The composition will alter the number/type or molecular distribution of the phases.
External	Production	The type of processing, can effect all the internal parameters.
External	Thermal History	The rate of cooling or heating can effect the crystallisation and the orientation of the polymer chains.
External	Chemical Environment	The presence of small molecules, e.g. solvents. These can act as plasticisers or 'lubricants' in composite system.
External	Physical Environment	The temperature and/or additional external sources of energy can alter the mobility of the molecules.

Table 14 Summary of parameters affecting the mobility of polymer chains in composites

All the external parameters may be said to define the extent to which the internal parameters occur, although they themselves do not alone determine the internal parameters. When attempting to analyse the effects of one of the internal causes for a difference in the internal molecular mobility it is important to ensure that all the other variables remain constant. The application of dynamic mechanical thermal analysis to the study of polymer composites is widespread <sup>161,162</sup>.

Different modes of mechanical vibration enable a wide number of materials to be studied <sup>162</sup>.

As discussed in section 2.5.5.1 Bound Matrix Fraction, the quantity of polymer in the 'interphase region' is small. As a result, variations in the external parameters must be kept to a minimum. An understanding of the interactions and the limitations of the equipment are required <sup>163,164,165</sup> if an accurate determination of the results is to be achieved.

Initial analysis of the mechanical properties of filled composites<sup>166</sup> indicated a discrepancy between theoretical predictions and experimental results. The models of Einstein and Guth discussed in section 2.5.4 Engineering Models were shown to be unable to explain the observed results. For the interpretation of these results, where it is assumed that no interaction of the two phases, the following may be considered<sup>167</sup>.

$$\tan \delta_c = \tan \delta_p (1 - \phi_f)$$

Equation 34

where:

$\delta_c$  is the damping factor of the composite,

$\delta_p$  is the damping factor of the polymer,

$\phi_f$  is the volume fraction of the filler.

A simple correction factor  $B$  has been applied to this to allow for a bound region.

$B$  is related to the effective thickness of the interphase layer.

$$\tan \delta_c = \tan \delta_p (1 - B\phi_f)$$

Equation 35

where  $B$  is given by,

$$B = \left(1 + \frac{\Delta R}{R}\right)^3$$

Equation 36

where  $R$  is the radius of the dispersed particle and  $\Delta R$  is the thickness of the bound layer.



Some results of the analysis of the interfacial interactions have shown promising results<sup>168</sup>. Composites were made from chlorinated polyethylene (CPE) and rutile fillers with differing acid base properties. The thickness of the bound layer was estimated to increase as the basicity or acidity of the filler increased. A neutral filler was still seen to have a bound layer. From this it may be concluded that acid-base interactions are not the only interactions to result in a bound layer. A maximum thickness was found to exist, suggesting that the acid-base interactions only affect the polymer up to a certain distance from the surface of the filler.

As discussed in section 2.5.5.1 Bound Matrix Fraction, the analysis of a high surface area filler will show a larger effect. On the analysis of a composite of polyethylene glycol and a high surface area silica an increase in Tg was detected<sup>169</sup>. This phenomenon has subsequently been modelled in terms of an interphase<sup>170</sup>. The modeling of this theory has shown that for glass sphere filled high density polyethylene (HDPE), the immobilised layer is smaller at higher temperatures<sup>171</sup>. The surface treatment of the glass spheres with a coupling agent was also seen to raise the temperature at which the maxima of the loss tangent occurred.

The effect of the filler on the crystallization process of the polymer in composites has been investigated. It has been shown that in the case of polypropylene (PP) and silica, the level of crystallinity increases as the filler size decreases<sup>172</sup>. A broadening of the loss peaks were assumed to occur as a result of the generated grain boundaries of the composite or the crystalline boundary in the pure PP. The coating of magnesium silicate with n-decylaldehyde in a PP matrix was observed to increase the level of crystallinity above that observed for the untreated silicate<sup>173</sup>.

The analysis of calcium carbonate filled polyethylene has taken place although the results were inconclusive<sup>174</sup>. In all work mentioned (except reference 168,

where the author acknowledges or although does not comment further) the authors have failed to take into account or have not indicated whether the parameters in Table 14 remain constant.

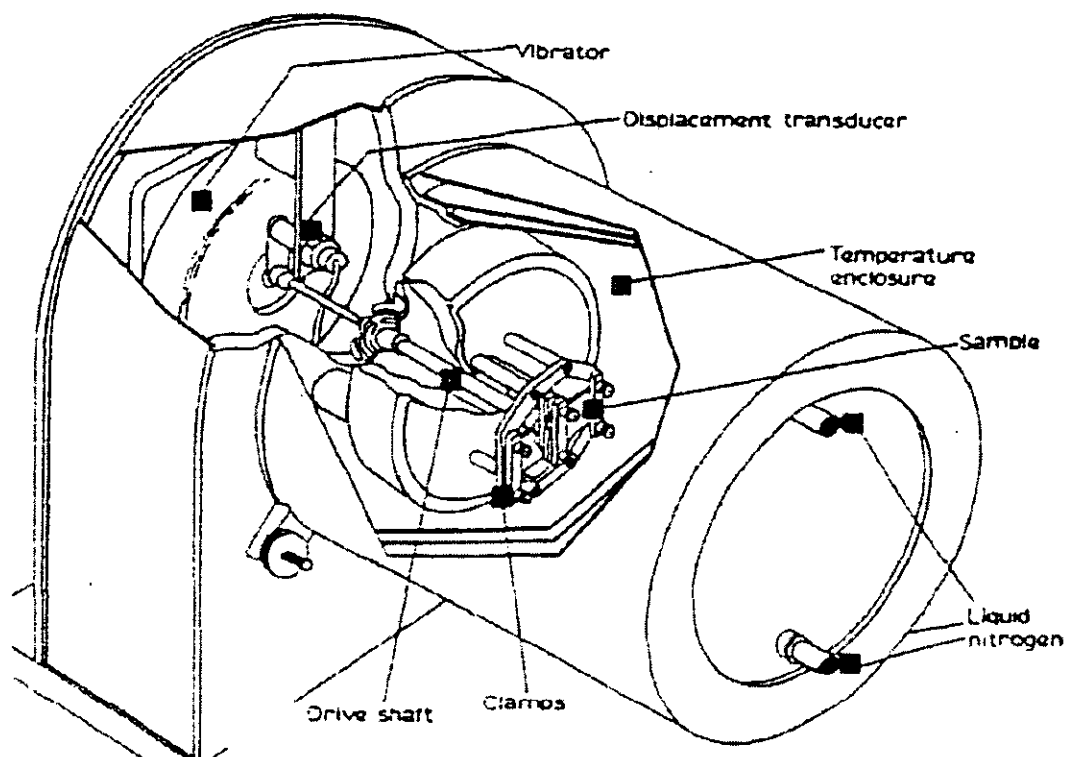


Figure 22 Mechanical head of a PL-DMTA showing the essential features of sample mounting, vibrator system and transducer

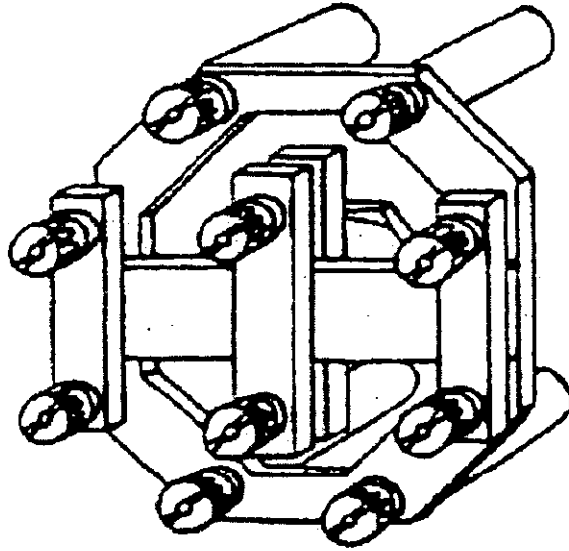


Figure 23 Dual cantilever clamping of small rectangular bar sample

## Chapter 3 Experimental

### 3.1 Experimental Coating

The precipitated calcium carbonate (PCC) grade selected was the uncoated Winnofil product supplied by Solvay Specialty Chemicals formally Zeneca Resins, The nitrogen BET surface area of this filler was of approximately  $20 \text{ m}^2\text{g}^{-1}$ .

The magnesium hydroxide grade selected was the Premier Periclase DP393. This grade is manufactured from sea water by a precipitation/recrystallisation process. The nitrogen BET surface area of this filler was approximately  $13 \text{ m}^2\text{g}^{-1}$ . A particle size of  $0.75 \mu\text{m}$  (d-50) was measured using a Coulter counter<sup>14</sup>.

Two grades of stearic acid were used. The Sigma-Aldrich SLR grade (99 %) was used for the bulk coating process, and the Sigma-Aldrich grade (99.9+ %) for the laboratory based process. A BDH (purified grade) sodium stearate was also used as an alternative to stearic acid in the coating process.

#### 3.1.1 Coating Levels

Coating levels are defined as fractions of a monolayer, as defined in Section 2.6.1 A 'Monolayer' Coating using the specific surface areas given in Section 3.1 Experimental Coating.

### 3.2 Experimental Preparations

A number of experimental techniques have been used in the preparation of coated filler particles.

### 3.2.1 Wet Coating Preparations

#### 3.2.1.1 Ammonium Stearate Coating

Stearic acid neutralised with excess ammonia was used to coat the sample. The wet coating method is based as much as possible on the industrial preparation technique used by Zeneca Resins.

For the large-scale manufacture of samples an aqueous slurry of calcium carbonate particles was placed in a water bath at a fixed temperature and coating material added. For the laboratory scale production of samples the slurry was dried and ground to determine the exact quantity of filler to be used.

The reaction process is summarised in Figure 24.

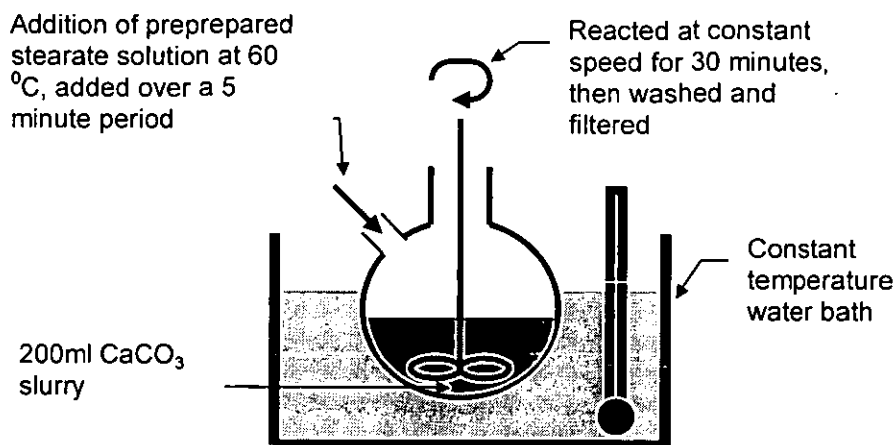


Figure 24 Diagram of apparatus and timings used in the preparation of coated calcium carbonate samples

#### 3.2.1.2 Stearic Acid Coatings

Coatings formed from stearic acid were prepared in the same way as in section 3.2.1.1 Ammonium Stearate Coating, except that the stearic acid was added directly to the reaction vessel.

### **3.2.1.3 Sodium Stearate Coating**

Coatings formed from sodium stearate were prepared in the same way as in section 3.2.1.1 Ammonium Stearate Coating, except that the sodium stearate was added directly to the reaction vessel.

### **3.2.2 Organic Solution Coating Preparations**

Previous experiments have shown<sup>19</sup> that an alternative wet coating route to the production of a coated PCC is available. The process of stearic acid adsorption is slow and equilibrium at 30<sup>0</sup>C is obtained after around 24 hours. In this system two forms of adsorption take place; physical adsorption and chemical adsorption. The two types have been differentiated by the use of a hot toluene extraction. The physical adsorption follows a type II adsorption isotherm, suggesting the formation of multilayers at high concentrations. The chemical adsorption follows a Langmuir type isotherm, indicating the formation of a monolayer of stearate.

This route has been used to produce the organic solution coated PCC samples.

### **3.2.3 Dry Coating Preparations**

The dry coating process is widely used industrially where the coating is added to the filler after production. Small scale dry coating was carried out in a Waring Blender<sup>14</sup>. The stearic acid is added to the blender over a period of five minutes. Heating takes place only after the acid has been added. The sample was heated to a maximum of 95<sup>0</sup>C at a speed of 7000 rpm. Variation in temperature of the vessel was monitored and can be seen in Figure 25.

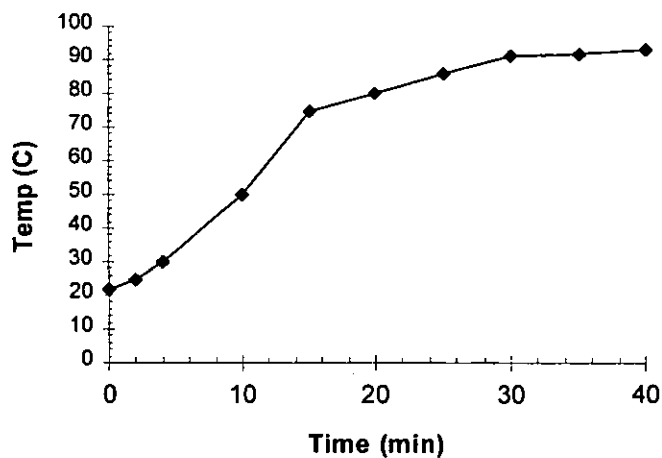


Figure 25 Variation in processing temperature as a function of time for the Waring blender (External Heat – 10 minutes onwards, Speed 3 – 7000RPM).

### 3.2.4 Polymer Composite Preparation

Polymer composite samples were produced using EVIPOL SH6520, an unplasticised polyvinylchloride (uPVC). To produce a ‘ideally’ filled polymer composite the coated and uncoated filler powder must be dispersed to a similar extent. Comparative mechanical analysis can only take place on identically dispersed composites.

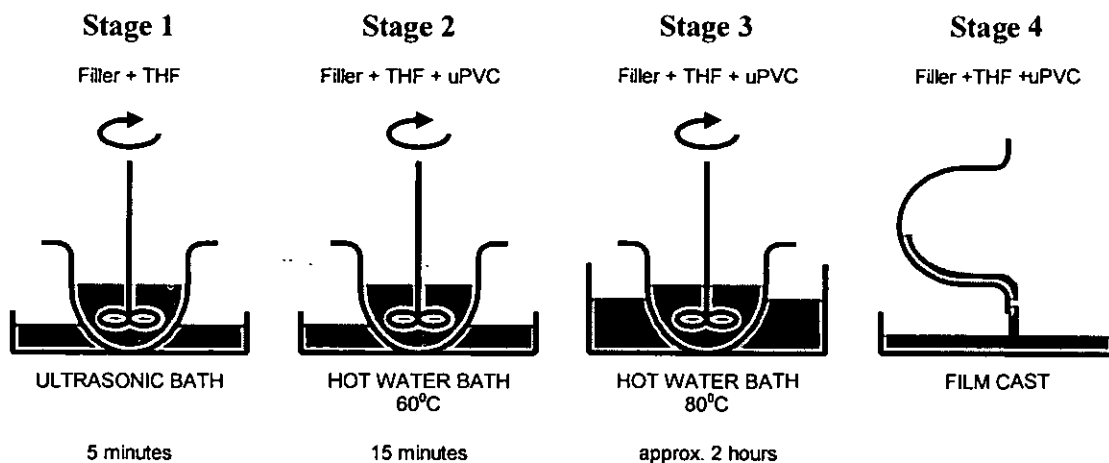


Figure 26 Schematic diagram of the 'ideal' polymer composite production process

It is hoped that a 'ideally filled' uPVC polymer has been produced by the dispersing of the filler in THF. The agglomerates in the filler powders have been removed by the use of stirring and an ultrasonic bath. The uPVC was then dissolved in the THF - filler mixture at 60 °C, uPVC was added at a rate of approximately 0.5 g s<sup>-1</sup>. Incorporation was improved by the use of further stirring. After 15 minutes the water bath was raised to 80 °C. THF was evaporated until a known volume of polymer remained. The paste was then cast and excess THF removed in an oven at 50 °C for 24 hours and then a vacuum oven at 80 °C for 24 hours.

Cast composite samples were then preheated to 90 °C for 10 minutes and pressed using a FTIR constant thickness press at 120 °C for 10 minutes. On removal of the press containing the composite, the constant thickness maker was cooled for 20 minutes using tap water, and then the pressed composite removed. DMTA test pieces were then cut from the pressed composite. Every effort was made to ensure a similar thermal history for each set of polymer composite samples. The reaction process was tested to ensure that no side reactions or coating loss was incurred during the composite production process.



### **3.3 Experimental Analysis**

#### **3.3.1 Electron Microscopy**

Electron microscopy was employed to quantitatively assess the shape, size and degree of agglomeration of the filler samples. The samples were viewed using three different electron microscopes.

##### **3.3.1.1 Scanning Electron Microscopy**

Calcium carbonate samples were analysed at ICI Wilton using a high resolution Hitachi S4000 FEG-SEM. Magnesium hydroxide samples were analysed using a Jeol JEM-100CX transmission electron microscope (TEM) in the scanning mode by F. Page from IPTME, Loughborough University . In both cases samples were mounted on aluminium stubs and gold sputtered to reduce sample charging.

##### **3.3.1.2 Transmission Electron Microscopy**

Calcium carbonate samples were analysed at ICI Wilton using a Philips 400 FEG-TEM. Transmission electron micrographs were then analysed using computer based image analysis to allow the particle size distribution to be determined.

#### **3.3.2 Thermal Analysis**

##### **3.3.2.1 CHN Experimental Analysis**

Carbon Hydrogen Nitrogen (CHN) elemental analysis was carried out on a Perkin Elemer 2400 CHN analyser in the Chemistry Department, Loughborough University by A. Daley. Complete combustion of the flammable matter occurs at 900 °C in a pure oxygen atmosphere.

##### **3.3.2.2 Thermogravimetric Experimental Analysis**

Tests were carried out using a Mettler TGA-50 linked to a TC-11 processor. Data was analysed using the TA-72 software. All tests were carried out in Zeneca,

Lostock. The test procedure was carried according to a test protocol developed by Zeneca<sup>175</sup>. This protocol relies on a two stage heating process. The first in which water is removed, and the second in which the quantity of calcium stearate is calculated.

### **3.3.3 Gas Adsorption Isotherm Analysis**

Nitrogen adsorption isotherms were measured using a Micromeritics ASAP 2010C Analyser. Samples were analysed after outgassing for 24 hours at 383 K. Weighed samples of calcium carbonate were prepared by outgassing for a minimum period of 24 hours at 110 °C on the degas ports of the analyser. Adsorption isotherms were generated by dosing nitrogen (>99.99 % purity) onto the adsorbent contained within a bath of liquid nitrogen at approximately 77 K.

### **3.3.4 Infrared Spectroscopy**

#### **3.3.4.1 DRIFT Experimental**

Infra-red spectra were recorded on a Nicolet 20 DXC spectrometer with a Spectratech diffuse reflection attachment. Samples were dispersed in ground spectroscopic grade KBr prior to analysis. The sample loading was 1% by weight in the KBr. The same batch of ground KBr was used for all samples to keep particle size consistent. The average particle size was in the region of 20 microns.

Diffuse reflection spectra can be used quantitatively, but samples must be prepared and the results interpreted with care. The infra-red spectra obtained depend strongly on the shape and size of the powder particles used and the size of the diluent particles. One practical problem is that it can be difficult to achieve the same degree of dispersion of the coated and uncoated filler in the KBr. To achieve a sufficient level of dispersion, samples were shaken for six periods of 5 minutes.

Interpretation and spectra manipulation was achieved using the Nicolet OMNIC

software. Water vapour detected in the sample spectra was subtracted, using water vapour standards created using the background KBr. All spectra have been obtained in absorbance units, and converted to Kubelka-Munk units after water vapour subtraction.

To get a measure of the coating achieved the absorbance indicative of the coating can be related to the amount of material present. In the case of calcium carbonate, an uncoated sample must be subtracted from the coated spectra, to remove the background absorbance. The extent of subtraction required was determined by the removal of the calcite ( $2650\text{-}2400\text{ cm}^{-1}$ ) peak from the resultant spectrum. The area under the C-H band ( $3000\text{-}2800\text{ cm}^{-1}$ ) can then be effectively ratioed to that under the carbonate band ( $2650\text{-}2400\text{ cm}^{-1}$ ). In the case of magnesium hydroxide the area under the C-H band ( $3000\text{-}2800\text{ cm}^{-1}$ ) can be ratioed to that under the hydroxide band ( $3750\text{-}3600\text{ cm}^{-1}$ ).

### 3.3.5 X-Ray Photoelectron Spectroscopy

Samples of powder were placed in a sample tray for XPS analysis. Spectra were recorded on a VG ESCALAB spectrometer using Al  $K\alpha$  (1486 eV) radiation. Pass energies of 100 and 20 eV were used for the broad scan and high resolution spectra respectively. Binding energies are referenced to adventitious carbon at 284.6 eV.

Peak area and composition analysis was made using the in-house XPS Data System V2.2, high resolution curve fitting was completed using XPSPEAK shareware software designed by Raymund Kwok. Curve positions were fixed relative to the adventitious carbon peak and were fitted with a 15% Lorentzian-Gaussian curve.

Quantification was achieved by measurement of peak area after subtraction of a Shirley type background, with appropriate corrections made for photoelectron cross-sections<sup>176</sup>, inelastic mean free paths<sup>143</sup>, energy analyser transmission<sup>177</sup>

and angular asymmetry in photoemission <sup>178</sup> when required. Re-analysis by XPS of several samples after the initial analysis showed no significant changes in surface composition, indicating that no significant radiation damage had occurred.

### **3.3.6 X-Ray Diffraction**

X-ray diffraction patterns were collected using a Phillips X50 diffractometer operating with copper K-alpha radiation. The diffraction data were collected over a period of 40-60 minutes using a  $2\theta$  step of 0.02 degrees between 2 to 40 degrees. Data evaluation was performed using Hilton Brookes software.

### **3.3.7 DMTA Experimental Analysis**

Dynamic mechanical responses to forced oscillations were measured using a Polymer Laboratories - DMTA MKIII analyser. The samples were analysed using a small bending frame in the dual cantilever mode, with a free sample length (L) of 5 mm. Responses are measured at three frequencies, 0.1, 1, 10 Hz. The test samples were prepared as described in section 3.2.4 Polymer Composite Preparation.

## **Chapter 4 Results**

### **4.1 Electron Microscopy**

Electron microscopy of the samples has enabled the determination of the particle morphology and particle size distribution. Scanning electron microscopy of composite materials is mainly limited to composite failure mode analysis. However it is able to provide a valuable insight into the geometric nature of the primary particles. Transmission electron microscopy provides an excellent way to analyse the particle size distribution of the filler, and also the distribution of the filler within the composite.

#### **4.1.1 Calcium Carbonate**

Samples analysed by scanning electron microscopy and transmission electron microscopy are not those used in the coating and mechanical analysis. The samples used in the experimental analysis in this thesis are comparable to the 'good' samples shown in Figure 27.

##### **4.1.1.1 Scanning Electron Microscopy**

The primary particulates produced by precipitation shown in Figure 27, are spherical or cuboid in nature. This particulate (low L:D) ratio is maintained on coating (Figure 28).



Figure 27 Scanning electron micrograph of precipitated calcium carbonate

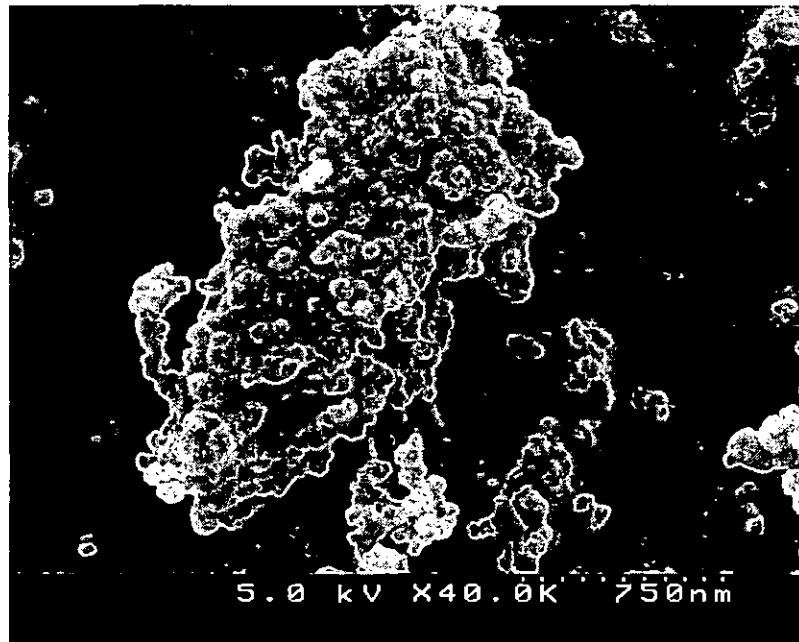


Figure 28 Scanning electron micrograph of ammonium stearate coated precipitated calcium carbonate

#### **4.1.1.2 Transmission Electron Microscopy**

The resolution obtainable through transmission electron microscopy (TEM) is approximately 10-100 times, that can be achieved by scanning electron microscopy. This increase in resolution is balanced against a loss in three dimensional spatial resolution (depth of field).

Transmission electron micrographs (Figure 29) of the filler enable an exact particle size distribution to be calculated (Figure 31).

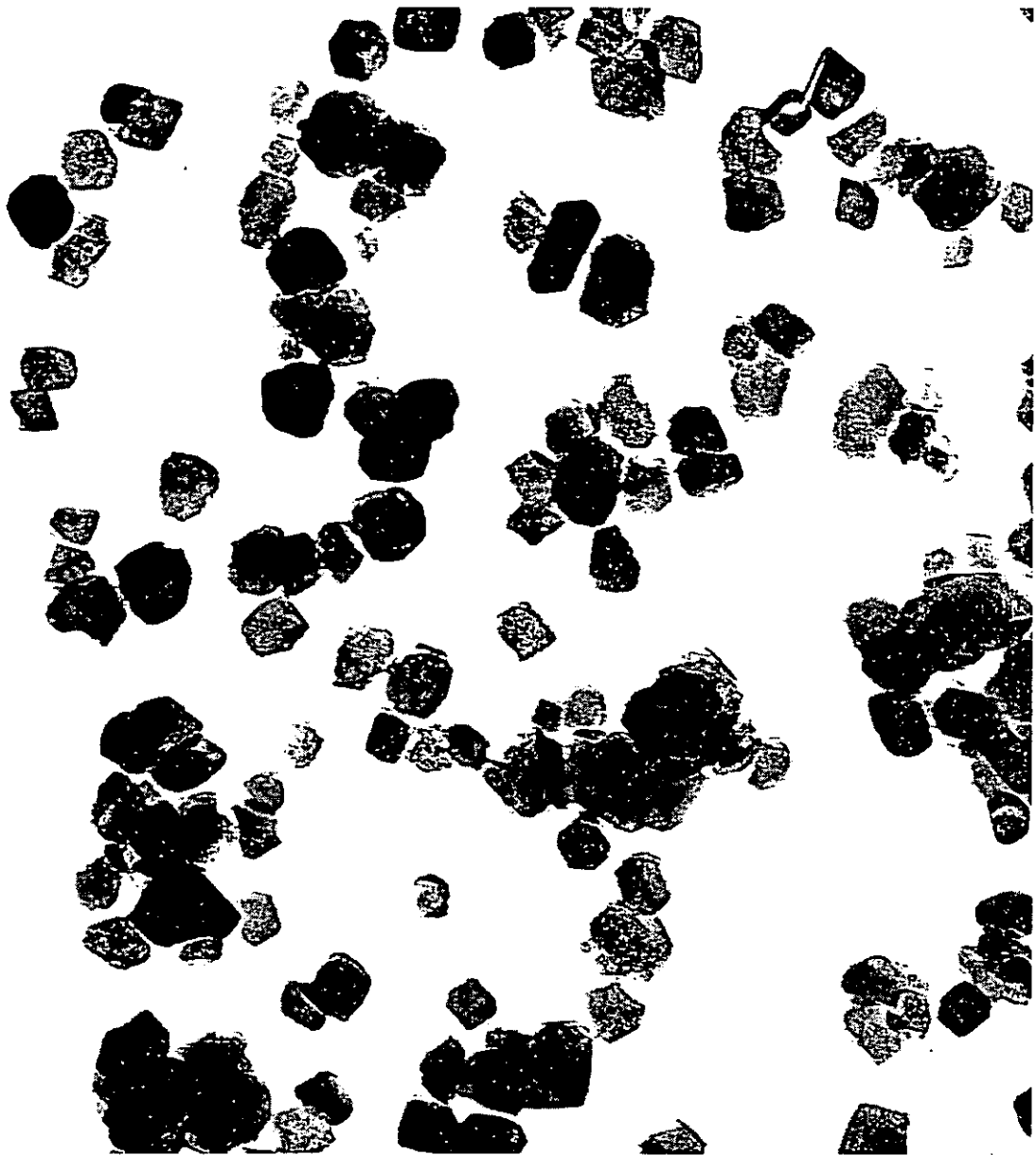


Figure 29 Transmission electron micrograph of precipitated calcium carbonate  
(Scale 1:150,000)



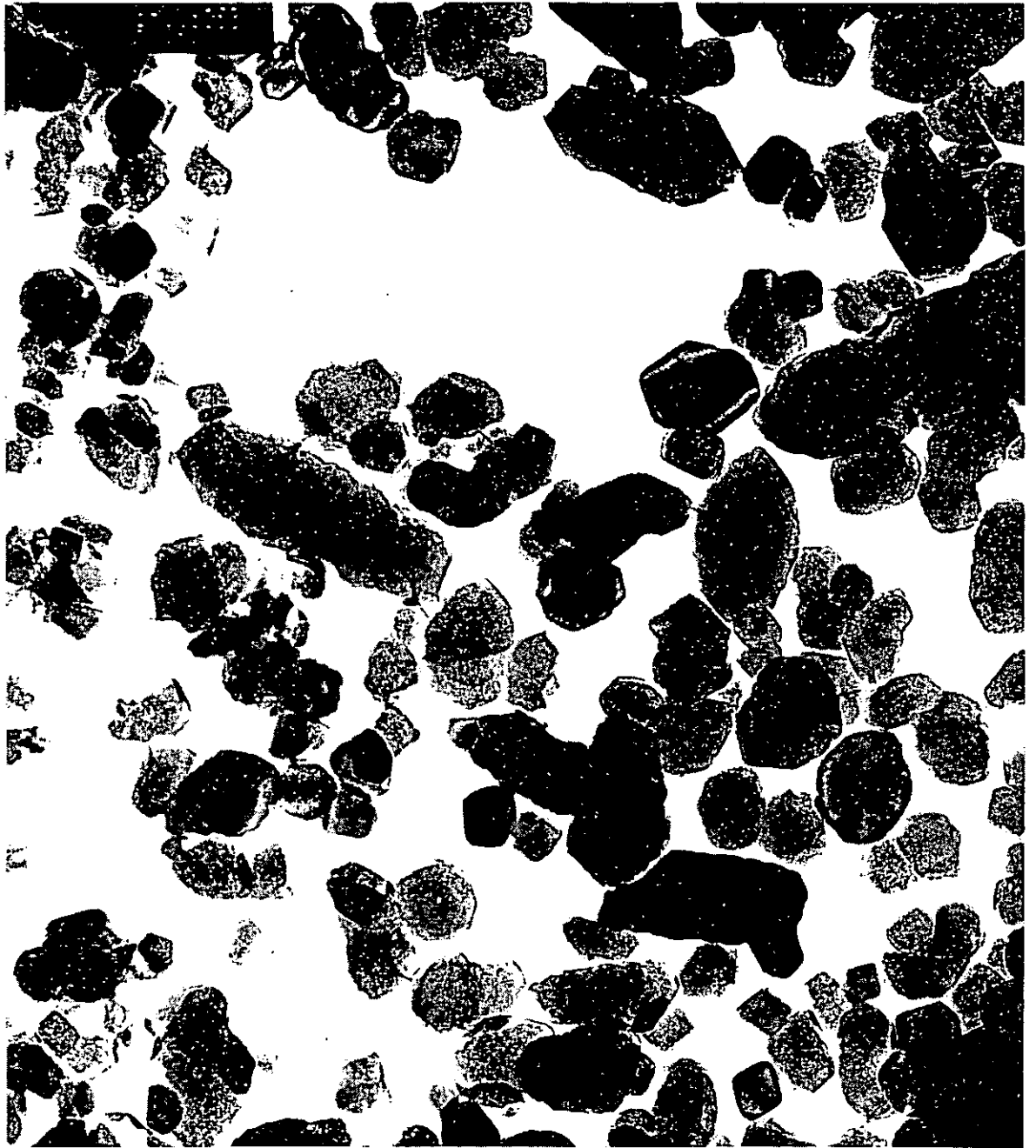


Figure 30 Transmission electron micrograph of badly precipitated calcium carbonate (Scale 1:150,000)

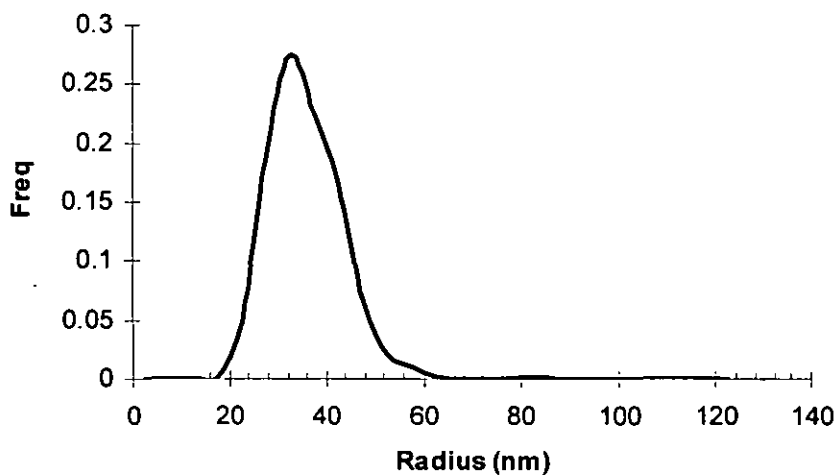


Figure 31 Particle size analysis of transmission electron micrograph of precipitated calcium carbonate

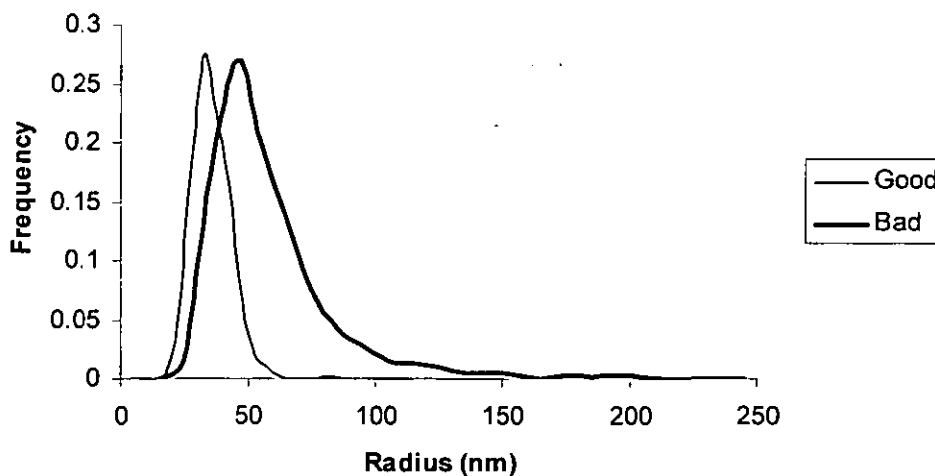


Figure 32 A comparison of transmission electron micrograph particle size analysis distributions of 'good' and 'bad' precipitated calcium carbonate

Further analysis of these distributions (Table 15) enables the direct validation of other experimentally determined phenomena e.g. BET surface area. Variations in

the experimental analysis of the surface area of the filler by gas adsorption and BET analysis can be explained in terms of the particle size distribution.

<b>Parameter</b>	<b>Good Sample</b>	<b>Bad Sample</b>
Mean Radius (nm)	35.57	58.51
Mean Diameter (nm)	71.14	117.02
Surface Area (m <sup>2</sup> /g) (calculated from average radius)	31.12	18.92
Surface Area (m <sup>2</sup> /g) (calculated from individual radius)	28.51	12.83
Surface Area (m <sup>2</sup> /g) (experimental BET estimation*)	25.0	17

\* Single Point BET analysis

Table 15 Particle size analysis of transmission electron micrograph of precipitated calcium carbonate

## 4.1.2 Magnesium Hydroxide

### 4.1.2.1 Scanning Electron Microscopy

A scanning electron micrograph of the filler (Figure 33) has been used to determine magnesium hydroxide filler shape. This filler may be described as being made up of 'plate like agglomerates' with a particle size typically below 1  $\mu\text{m}$ <sup>14</sup>.

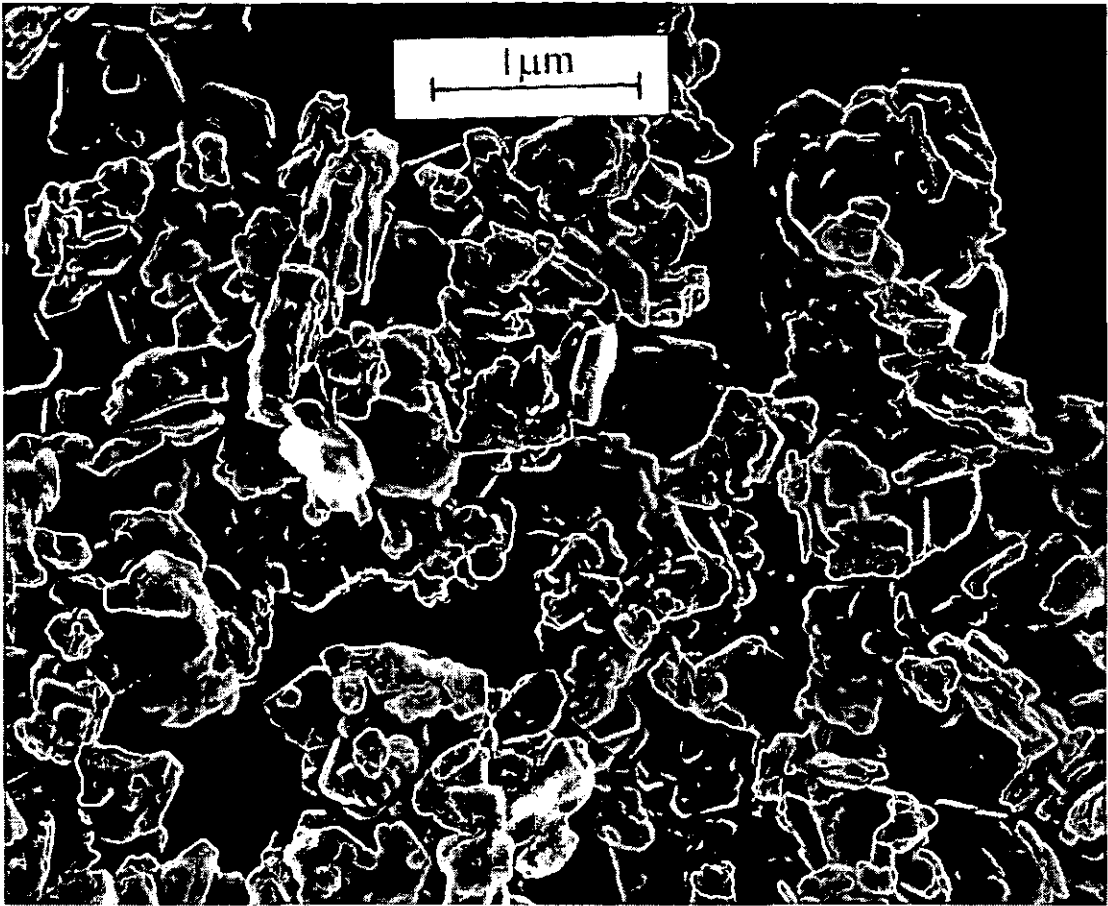


Figure 33 SEM photo-micrograph showing uncoated magnesium hydroxide (Scale 1:20,000)

#### 4.1.2.2 Transmission Electron Microscopy

The complex shape and particle size distribution of the magnesium hydroxide, renders the analysis of the filler by TEM inappropriate.

## **4.2 Thermal Analysis**

Thermal analysis tools allow the analysis of the quantity of coating material present on the coated filler. Neither of the thermal tools used showed the location of the coating. The tools do provide excellent, quick, semi-quantitative tools for the analysis of the stearate coating.

### **4.2.1 CHN Analysis**

CHN analysis is a tool that enables the overall calculation of the quantity of coating present in the system to be calculated.

#### **4.2.1.1 Calcium Carbonate**

Both carbon and hydrogen concentrations from CHN results can be used to analyse the coated material.

Analysis of hydrogen data is the most simple. Data can be easily interpreted in terms of the coating material. Analysis of the carbon contained within the carbonate of the filler is more difficult. The carbon detected from the carbonate must be subtracted if an accurate measure of the coating is to be made. If the composition of the coating and the filler is the same as their empirical formulae, and they undergo complete decomposition, the coated filler would be expected to generate the results shown in Figure 34.

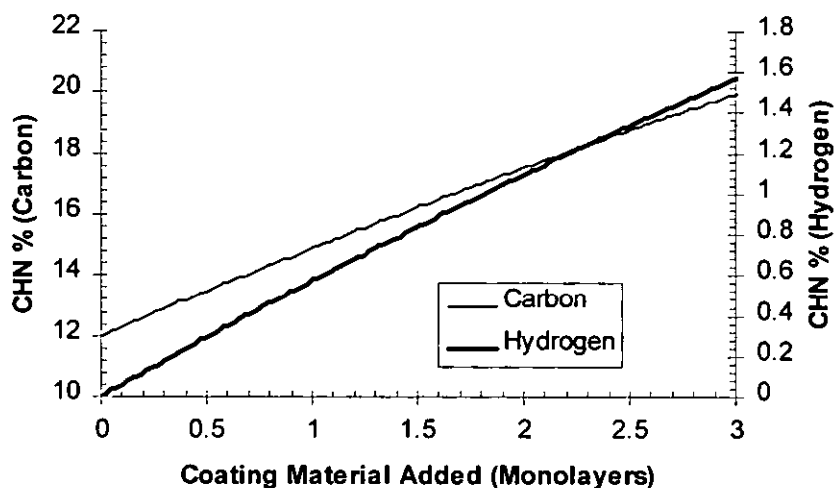


Figure 34 Theoretical CHN decomposition profile for stearic acid coated calcium carbonate (assuming empirical composition)

The theoretical decomposition is based on the empirical formula of calcium carbonate i.e. 12 % of the weight of the atoms present in the molecule are due to carbon. In experimental analysis of uncoated calcium carbonate this value is calculated to be 11.7 %. In modeling the data this figure is used to subtract the carbon produced by the decomposition of the calcium carbonate from the total carbon produced during the decomposition of the coated filler.

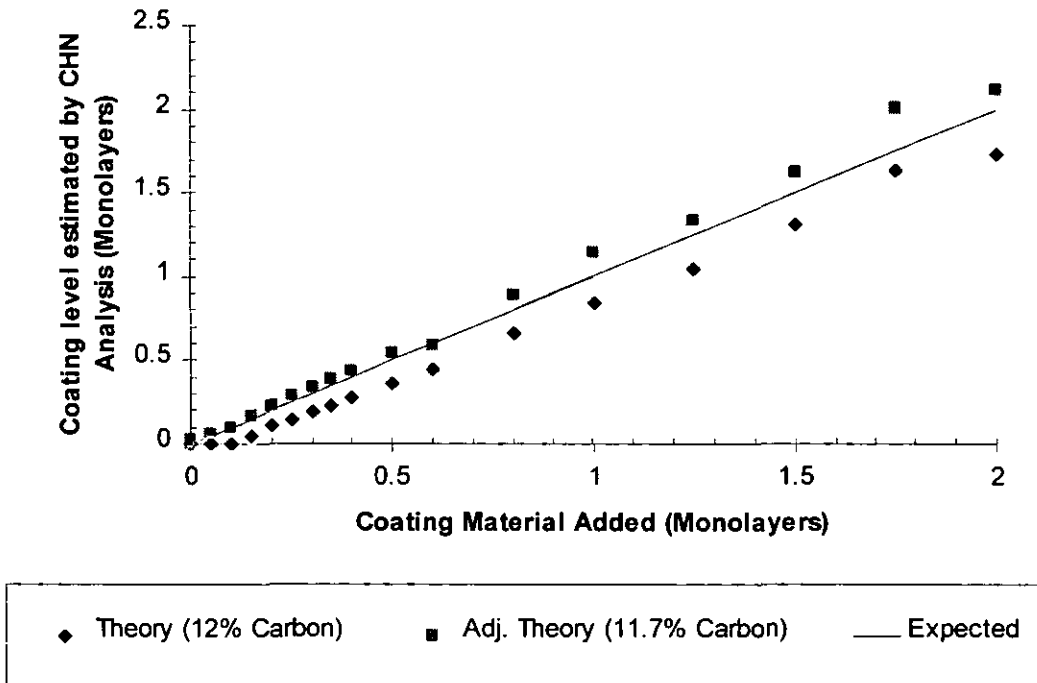


Figure 35 Coating level estimation by carbon CHN analysis of stearic acid coated calcium carbonate

The results of the carbon CHN analysis are shown in Figure 35. Analysis of the carbon data can be made by either the subtraction of carbonate carbon by an estimation based on the empirical formula of calcium carbonate (Theory (12 % carbon)), or by an experimentally determined values (Adj. Theory (11.7 % carbon)).

The results of the hydrogen CHN analysis are shown in Figure 36. Two calculations have been made. One is based on the assumption that all the hydrogen detected is the result of the coating, the other is based on a constant amount of hydrogen (0.1 % (the result of water)) being subtracted from the total hydrogen detected.

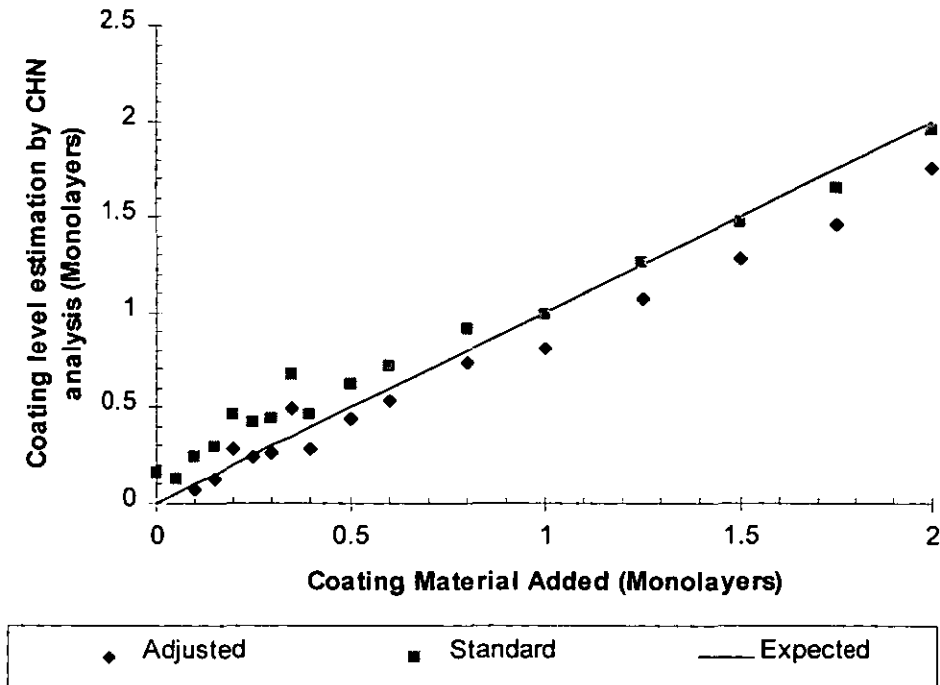


Figure 36 Coating level estimation by hydrogen CHN analysis of stearic acid coated calcium carbonate

#### 4.2.1.2 Magnesium Hydroxide

Both carbon and hydrogen CHN results can be used to analyse the coating material. Analysis of the hydrogen data is less accurate, and must also undergo subtraction to account for the hydrogen contained in the hydroxide.

The coatings estimated by the analysis of the carbon detected are shown in Figure 37.



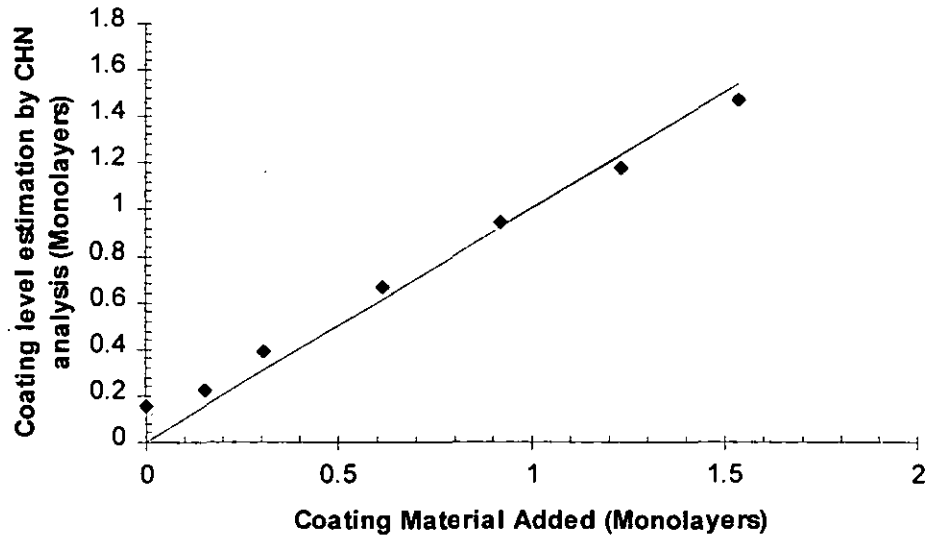


Figure 37 Coating level estimation by carbon CHN analysis of stearic acid coated magnesium hydroxide

## 4.2.2 Thermogravimetric Analysis

The thermogravimetric technique developed by Zeneca for the quality control of the production plant coating was applied to a number of laboratory and batch production samples. This technique consists of a two stage heating process, and is described in further detail in Section 3.3.2.2 Thermogravimetric Experimental Analysis. This technique indicates that coatings produced by dry coating the sample often result in the presence of acid.

### 4.2.2.1 Zeneca Batch Coated Samples

The analysis of coatings by thermogravimetric methods produced by the ammonium stearate method, are shown in Figure 40. No acid was detected by this technique in the range of samples analysed. Examples of the thermogravimetric analysis are shown in Figure 38 and Figure 39.

UNCOATED PCC D MATON

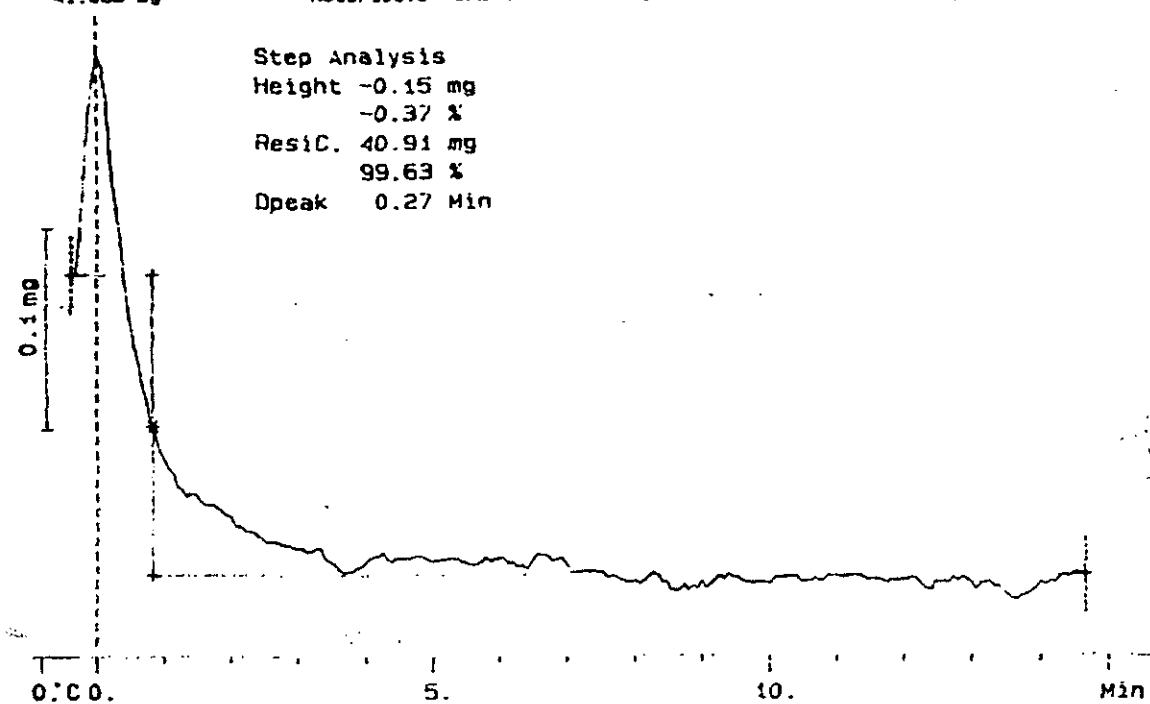
41.065 mg

Rate: 100.0 °C/min

File: 96002.001 TG METTLER 21-Nov-96

Ident: 0.0

WINNOFIL LABORATORY



UNCOATED PCC D MATON

41.065 mg

Rate: 100.0 °C/min

File: 96002.002 TG METTLER 21-Nov-96

Ident: 0.0

WINNOFIL LABORATORY

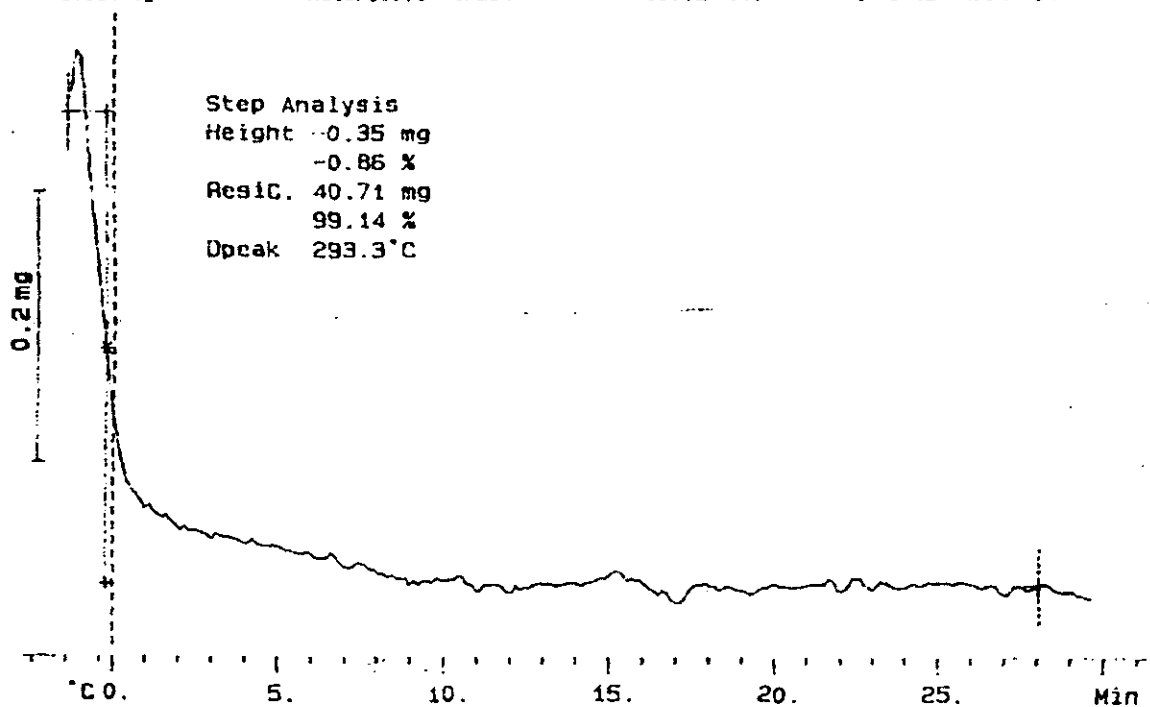
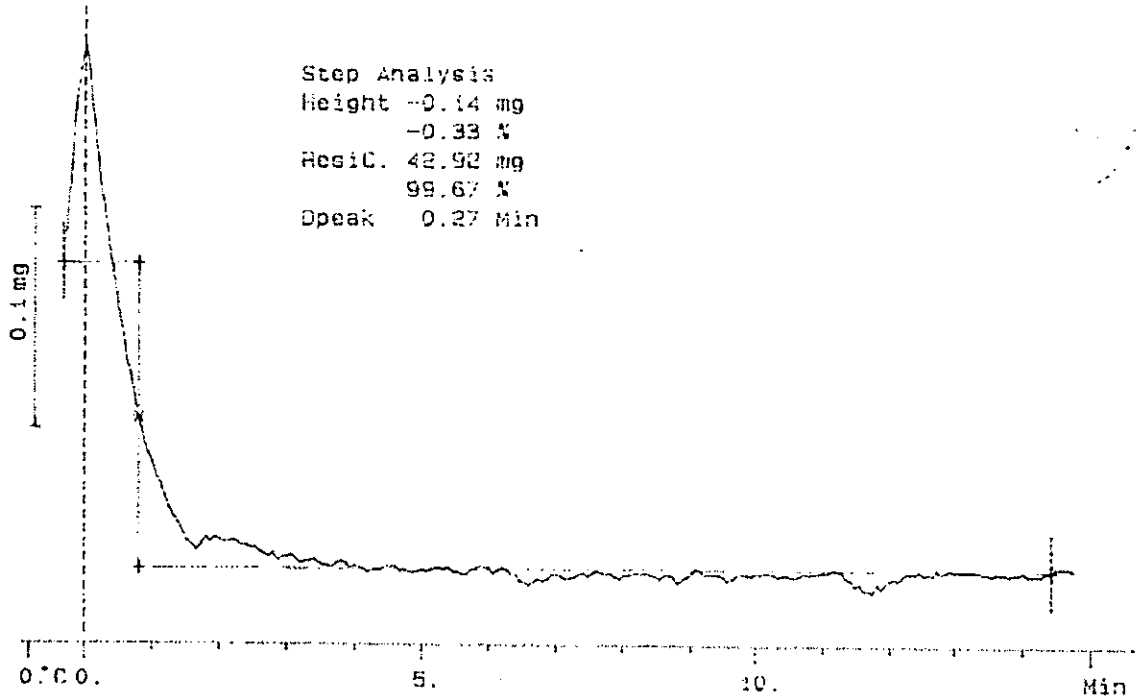


Figure 38 Thermogravimetric analysis of uncoated calcium carbonate

LAB SAMPLE DM3 APPROX 4%SA W/W  
43.064 mg

Rate: 100.0 °C/min

File: 96031.001 T6 METTLER 20-Nov-96  
Ident: 0.0 WINNUPIL LABORATORY



LAB SAMPLE DM3 APPROX 4%SA W/W  
43.064 mg

Rate: 100.0 °C/min

File: 96031.002 T6 METTLER 20-Nov-96  
Ident: 0.0 WINNUPIL LABORATORY

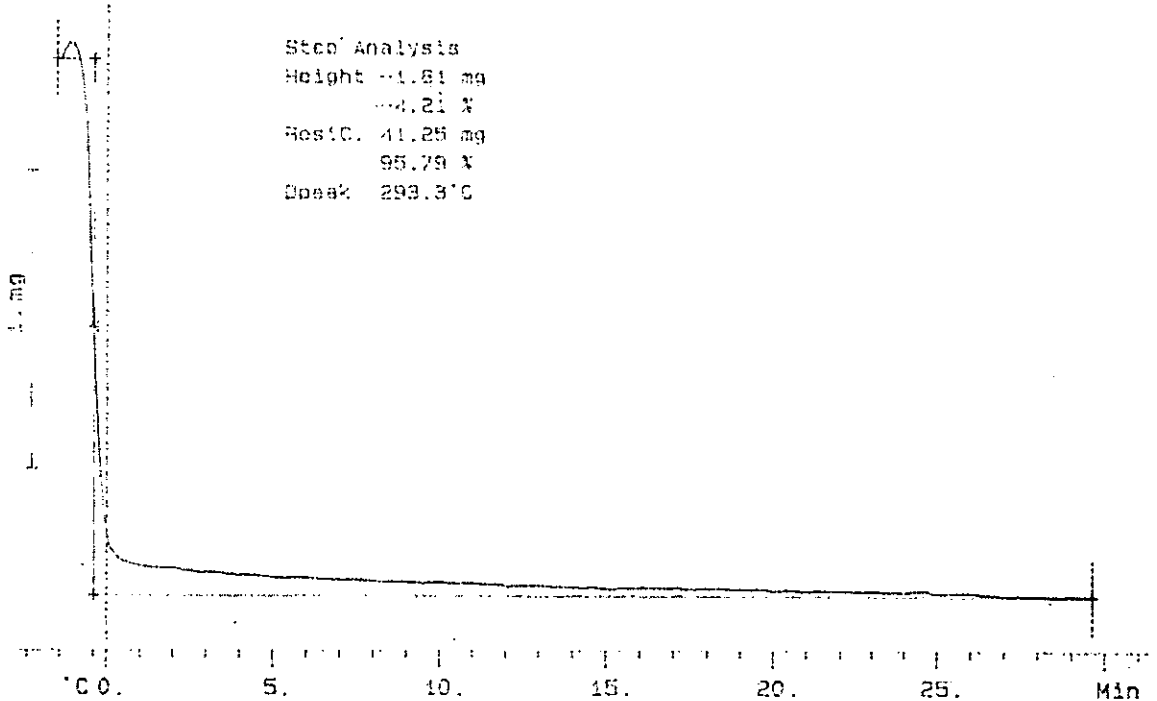


Figure 39 Thermogravimetric analysis of coated calcium carbonate

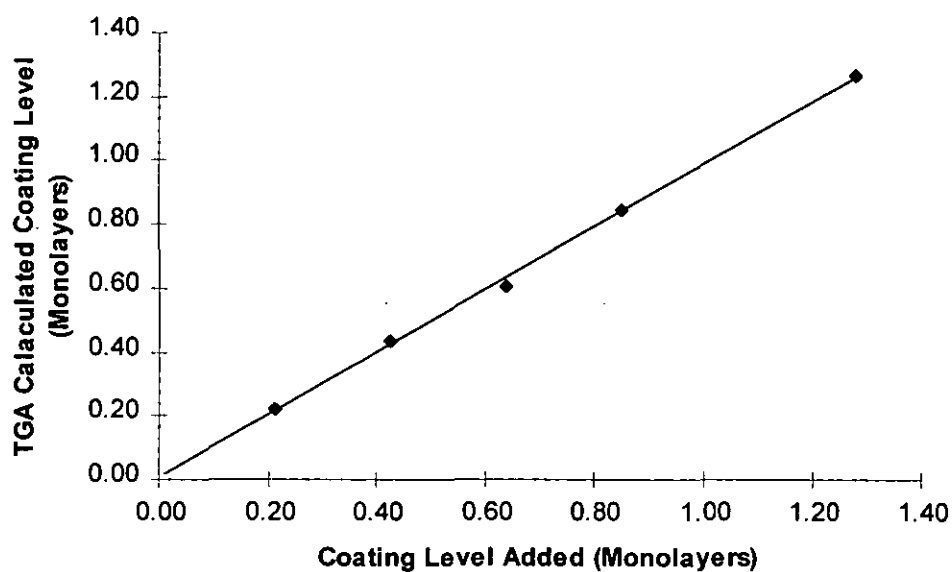


Figure 40 Coating level calculated by thermogravimetric analysis of ammonium stearate coated calcium carbonate

#### 4.2.2.2 Sodium Stearate Coated Samples

The analysis of coatings produced by the sodium stearate method using thermogravimetric methods are shown in Figure 41. A decomposition in the first heating phase, with a profile similar to stearic acid was detected by this technique for a sample with a coating level of 4 monolayers (this was determined to be approximately equivalent to 3700 ppm stearic acid).

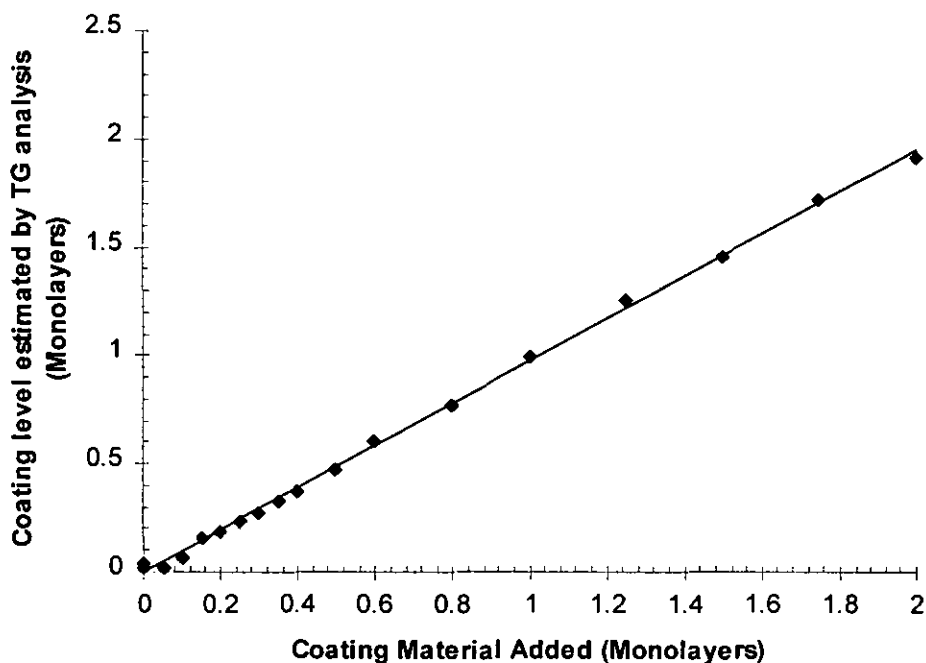


Figure 41 Coating level calculated by thermogravimetric analysis of sodium stearate coated calcium carbonate.

#### 4.2.2.3 Stearic Acid Coated Samples

The analysis by thermogravimetric methods of coatings produced by the stearic acid method are shown in Figure 42. These samples displayed a greater scatter than those seen in other TG analysis (Figure 40 & Figure 41). A decomposition in the temperature range normally expected for stearic acid was detected by this technique for a sample with a coating level of 0.75 monolayers (this was determined to be approximately equivalent to 8200 ppm stearic acid).

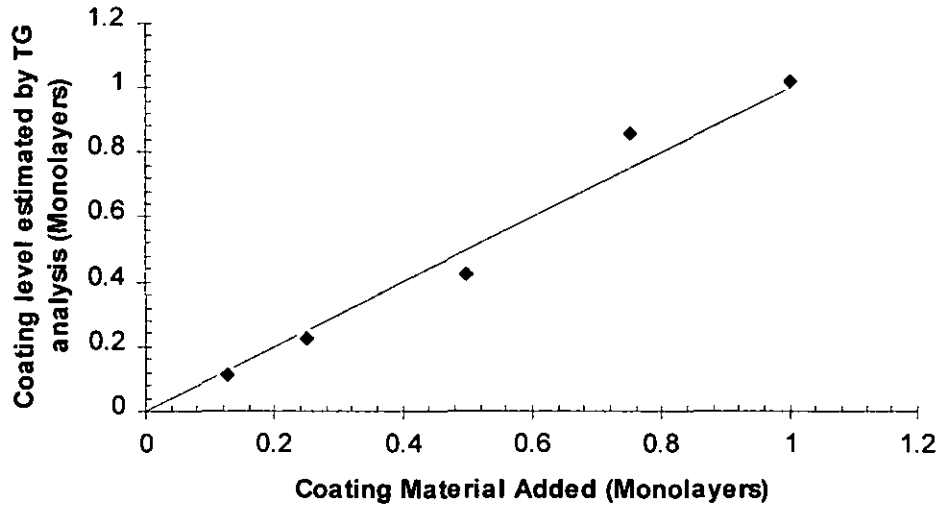


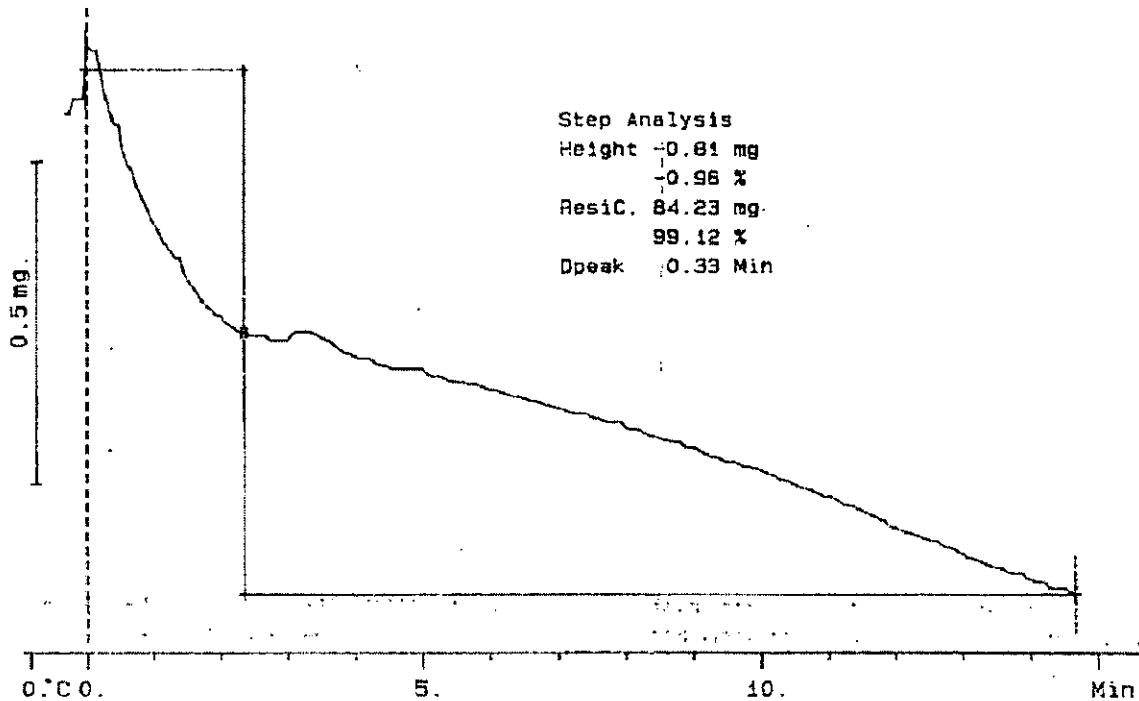
Figure 42 Coating level calculated by thermogravimetric analysis of stearic acid coated calcium carbonate

#### 4.2.2.4 Dry Stearic Acid Coated Samples

Thermogravimetric analysis can be easily used to identify the presence of unreacted stearic acid. When precipitated calcium carbonate is dry coated with sufficient stearic acid to produce a 1 monolayer coating. Approximately 15 % is found not to have reacted to form calcium stearate. The thermogravimetric trace for a sample coating stearic acid and calcium stearate can be seen in Figure 43.

DM015 DRY COAT 3-6-98  
84.975 mg Rate: 100.0 °C/min

File: 99019.001 TG METTLER 03-Jun-98  
Ident: 0.0 WINNDFIL LABORATORY



DM015 DRY COAT 3-6-98  
84.975 mg Rate: 100.0 °C/min

File: 99019.002 TG METTLER 03-Jun-98  
Ident: 0.0 WINNDFIL LABORATORY

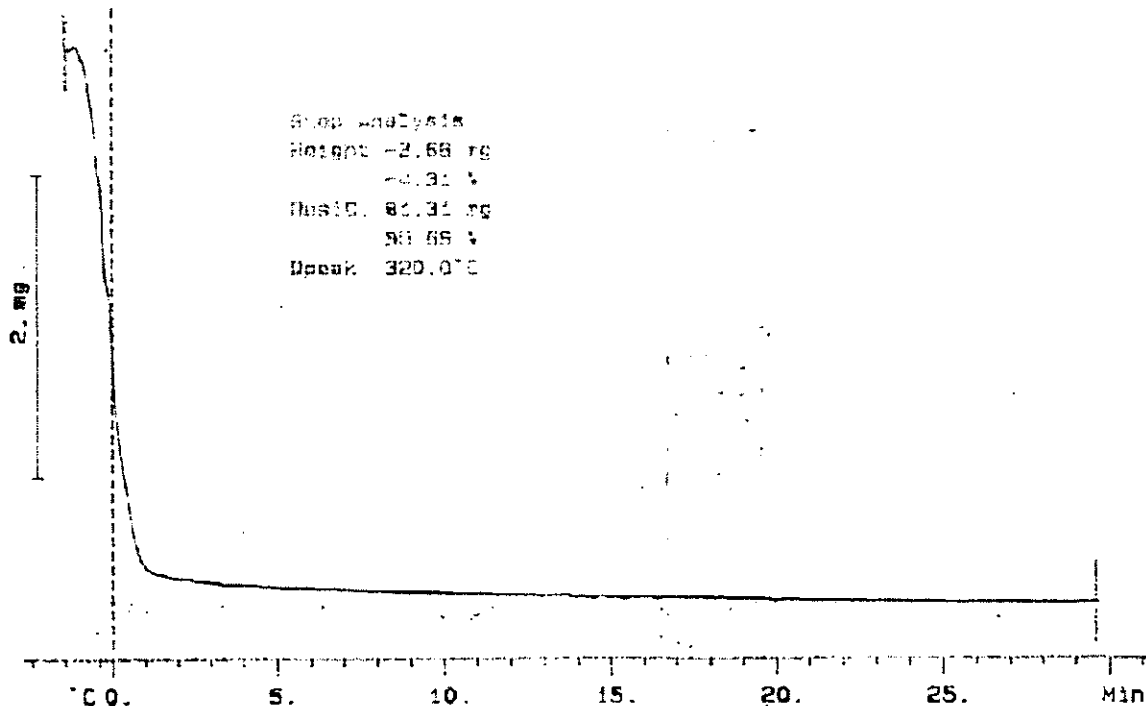


Figure 43 Thermogravimetric analysis of dry stearic acid coated calcium carbonate

### 4.3 Gas Adsorption Results

Analysis of gas adsorption data is usually done using either the BET or Langmuir models. Both the BET and the Langmuir models, assume the adsorption of a gas on a homogeneous surface. For a partially coated filler we know this to be untrue.

If we assume the high surface energy ( $c_H$ ) has a  $c$  constant of 580 and the low surface energy surface ( $c_L$ ) a  $c$  constant of 20 the adsorption isotherms shown in Figure 44 would be expected (These values were experimentally calculated.).

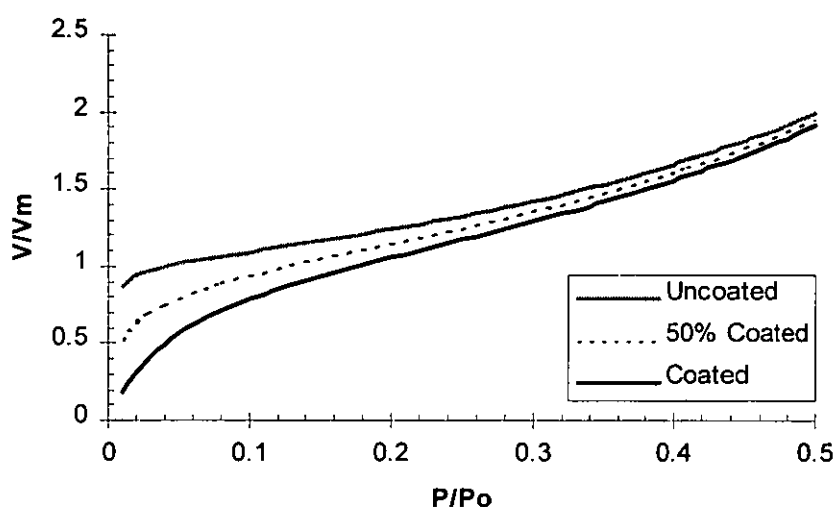


Figure 44 Calculated BET adsorption isotherms for a uncoated, partially coated and coated filler

If these isotherms are then analysed using the BET equation, allowing the volume of gas required to form a monolayer ( $V_m$ ) to remain constant for all samples, then the partially coated sample is calculated to have a  $c$  value of 58. The relationship between the level of coverage and the calculated  $c$  value is not a linear relationship.



### 4.3.1 Dual BET Adsorption Isotherm Theory

As discussed, the homogeneous energy or single site adsorption model is inappropriate for the analysis of partially coated fillers. As a result the single site adsorption models has been expanded to a dual site model to take into account heterogeneous nature of the surface.

#### 4.3.1.1 Single Site Adsorption

The BET equation for a single energy site is written as,

$$V = \frac{V_m c p}{(p_0 - p) \left[ 1 + (c - 1) \cdot \left( \frac{p}{p_0} \right) \right]}$$

Equation 37

where

$V$  is the volume of gas adsorbed,

$V_m$  is the volume of gas required to form a monolayer,

$p$  is the gas pressure,

$p_0$  is the standard pressure,

$c$  is a constant (defined in Equation 22).

This is rewritten in a linear form as:

$$\frac{p}{v(p_0 - p)} = \frac{1}{V_m c} + \frac{c - 1}{V_m c} \cdot \frac{p}{p_0}$$

Equation 38

From this the  $V_m$  ( $\text{cm}^3 \cdot \text{g}^{-1}$ ) and the  $c$  constant can be calculated. From this information the surface area and the latent heat of adsorption of the first layer can

be calculated.

$$Area_{BET} = \left( \frac{V_m}{1000} \times \frac{1}{V_m^\ominus} \right) \times N_A \times \varnothing$$

Equation 39

where

$V_m^\ominus = 24790 \text{ cm}^3 \text{ mol}^{-1}$  is the volume occupied by 1 mole of gas at 1 bar pressure at 298.15K,

$N_A = 6.022 \times 10^{23} \text{ mol}^{-1}$  is Avogadro's constant,

$\varnothing = 0.1620 \text{ nm}^2$  is the molecular cross section of nitrogen.

$$c = e^{(E_A - E_V)/RT}$$

Equation 40

where:

$E_A$  is the latent heat of adsorption of the first layer,

$E_V$  is the latent heat of vaporisation of the adsorbate in the liquid state.

#### 4.3.1.2 Multi Site Adsorption

We consider a mixture of high and low energy sites on discrete bodies and neglect lateral interactions of adsorbed molecules. The model assumes there is adsorption at specific energy sites, or that the adsorption at each site is a function of surface energy, temperature and pressure.

For two different energy sites, there are two different  $c$  constants,  $c_H$  and  $c_L$ , for the high and low energy sites. The fraction of high energy sites is defined as  $H$  and the fraction of low energy sites is known as  $L$ . We can rewrite the amount adsorbed at a relative pressure in terms of the sum of the fractional coverage of

each site.

$$\frac{V}{V_m} = H \left[ \frac{c_H p}{(p_0 - p) \cdot \left[ 1 + (c_H - 1) \cdot \left( \frac{p}{p_0} \right) \right]} \right] + L \left[ \frac{c_L p}{(p - p_0) \cdot \left[ 1 + (c_L - 1) \cdot \left( \frac{p}{p_0} \right) \right]} \right]$$

Equation 41

If the sum of the sites is given as  $H + L = 1$ , then the fractional coverage of low energy sites is given as,

$$L = \frac{\frac{V}{V_m} - \left[ \frac{c_H \left( \frac{p}{p_0} \right)}{\left( 1 - \left( \frac{p}{p_0} \right) \right) \cdot \left[ 1 + (c_H - 1) \cdot \left( \frac{p}{p_0} \right) \right]} \right]}{\left[ \frac{c_L \left( \frac{p}{p_0} \right)}{\left( 1 - \left( \frac{p}{p_0} \right) \right) \cdot \left[ 1 + (c_L - 1) \cdot \left( \frac{p}{p_0} \right) \right]} \right]} - \left[ \frac{c_H \left( \frac{p}{p_0} \right)}{\left( 1 - \left( \frac{p}{p_0} \right) \right) \cdot \left[ 1 + (c_H - 1) \cdot \left( \frac{p}{p_0} \right) \right]} \right]}$$

Equation 42

The fractional level of coverage  $L$  can also be described as the level of coverage or the coating coverage.

The determination of the fraction of the total number of sites that is of a specific energy can be achieved by allowing the developed model to estimate all variables, or to restrict the number of variables, and specify either theoretical or experimental constants. In this work we have chosen to use the values of the constants determined by experimental means.

The value of  $V_m$  used in the experiments was measured from the single BET adsorption isotherm analysis of an uncoated calcium carbonate sample. The value of the  $c$  constant corresponding to the high energy site ( $c_H$ ) 580 was calculated at the same time. A fully coated sample was used to calculate the value of the  $c$  constant corresponding to the low energy site ( $c_L$ ). The  $c$  constant was calculated using the  $V_m$  calculated earlier and was found to equal 22.

### 4.3.2 Dual BET Adsorption Isotherm Validation

BET isotherm assumes no lateral interactions of the gas molecules that are adsorbing on to the surface. From this we may assume that it is not possible to determine the exact surface coating configuration using gas adsorption data alone. A partially coated filler can be experimentally compared to a mixture of coated and uncoated fillers. The coating equivalence is described in Figure 45.

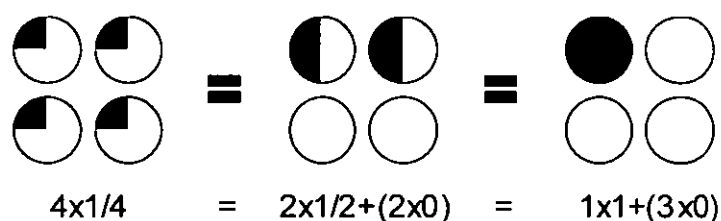


Figure 45 Diagrammatic representation of the ‘coating equivalence’. A partially coated filler can be experimentally compared to a mixture of coated and uncoated fillers

From this we may conclude that the dual BET adsorption isotherm model proposed can be tested by fitting the proposed adsorption isotherm model to measured adsorption isotherms of mixtures of coated and uncoated calcium carbonate.

When this is done and the isotherms fitted using a least squares regression analysis, the following results are obtained

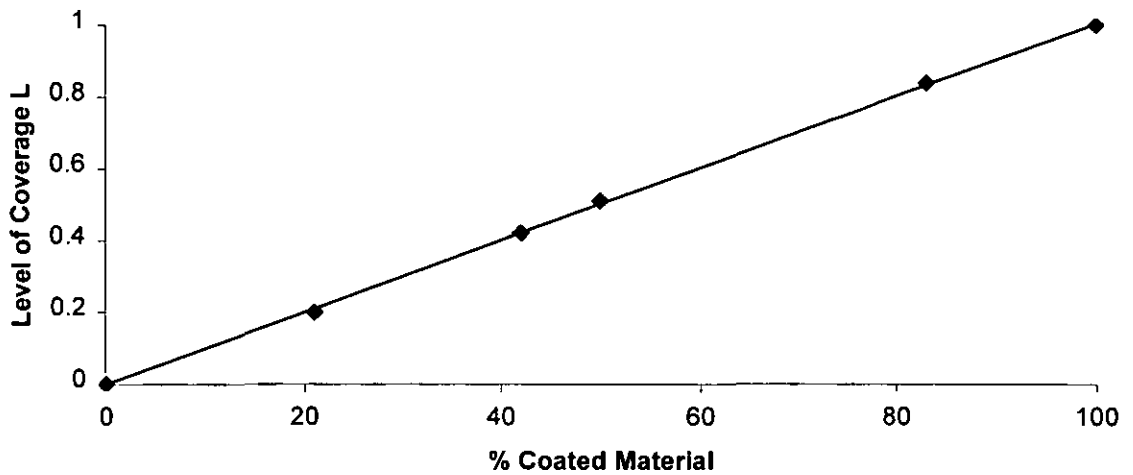


Figure 46 Validation of the dual BET adsorption isotherm model using mixtures of coated and uncoated calcium carbonate

By using regression analysis and the dual BET adsorption model, we are able to show that the fraction of coated material in the analysed mixture can be estimated. The fit of the expected and estimated values for the level of coverage L is almost perfect.

### 4.3.3 Calcium Carbonate - Sodium Stearate Coatings

Using the dual adsorption isotherm approach the level of coverage of the coating material added to the filler can be estimated.

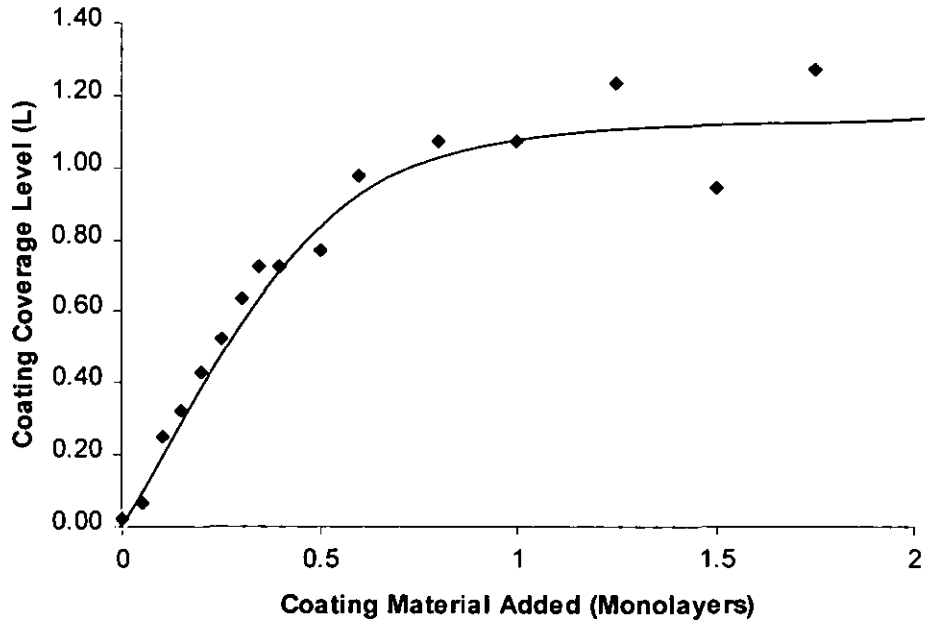


Figure 47 Figure showing the level of coverage calculated for fillers coated with different amounts of sodium stearate using the Dual Adsorption BET Isotherm

From this we may conclude that the 'complete' coverage of the filler by the coating material occurs when enough coating material is added to form 0.6 theoretical monolayers.

For this type of coating system the model will fail above a coating coverage of 1. It does not take into account the 'alternative' locations of the additional coating material in the system and the effect of this on the initially specified constants.

## 4.4 DRIFT Results

DRIFT can be used to provide data that quantifies the amount of coating present in the near surface region of the substrate. DRIFT may also be used to provide some information on the chemical environment of the coating.

By measuring peaks characteristic of the coating and the substrate we are able to calculate the amount of coating material present and standardize that quantity as a function of the substrate present, as a result calculate the quantity of coating material on the substrate.

$$FTIR_{RATIO} = \frac{I_{COAT}}{I_{SUBSTRATE}}$$

Equation 43

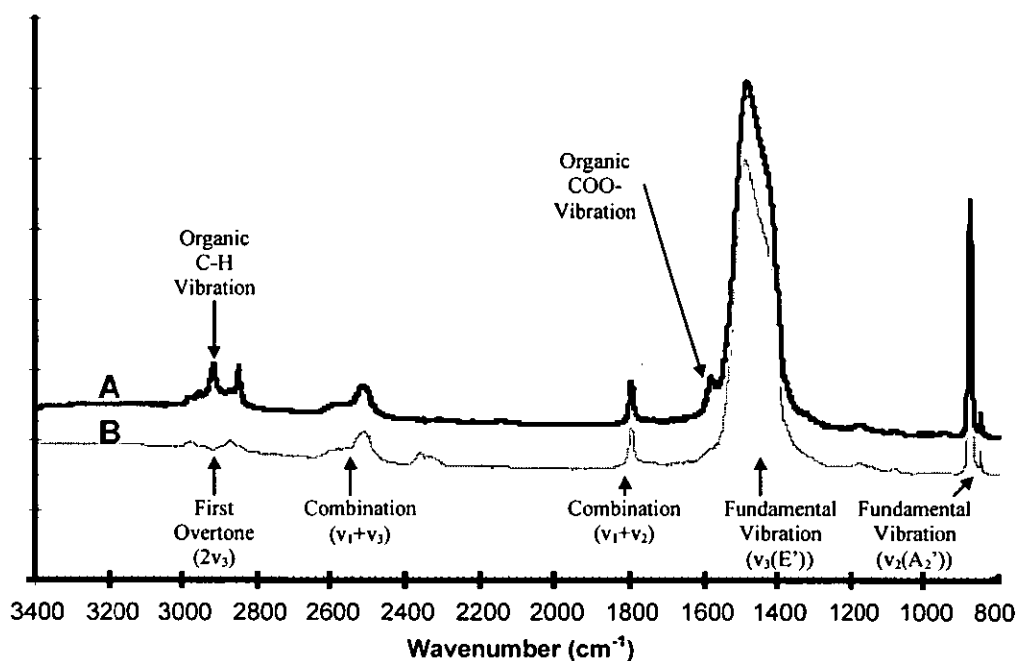
This ratio must be carefully calculated if the peak used for the calculation of the coating intensity also contains part of a substrate peak (e.g. calcium carbonate, see Figure 48). In these situations the substrate should be subtracted from the coating. Care should also be taken in selecting a substrate peak that is not effected by the coating process (e.g. magnesium hydroxide, see Figure 65).

### 4.4.1 Calcium Carbonate

The addition of the stearate group to the surface of the calcium carbonate as a coating agent can be detected. The change in infrared spectra that occurs on addition of the coating is in general the same. Small differences do occur, and these are discussed further in other sections.

Figure 48 shows DRIFT spectra of stearate coated and uncoated calcium carbonate. The experimental values obtained for the precipitated calcium carbonate agree well with the literature values for calcite<sup>126,127</sup>. Coating the surface with stearate gives rise to new bands at 2800-3000 cm<sup>-1</sup>, which may be assigned to C-H vibrations in the alkyl chain of the stearate. Residual stearic acid

(1700  $\text{cm}^{-1}$ ) can be detected if it is present.



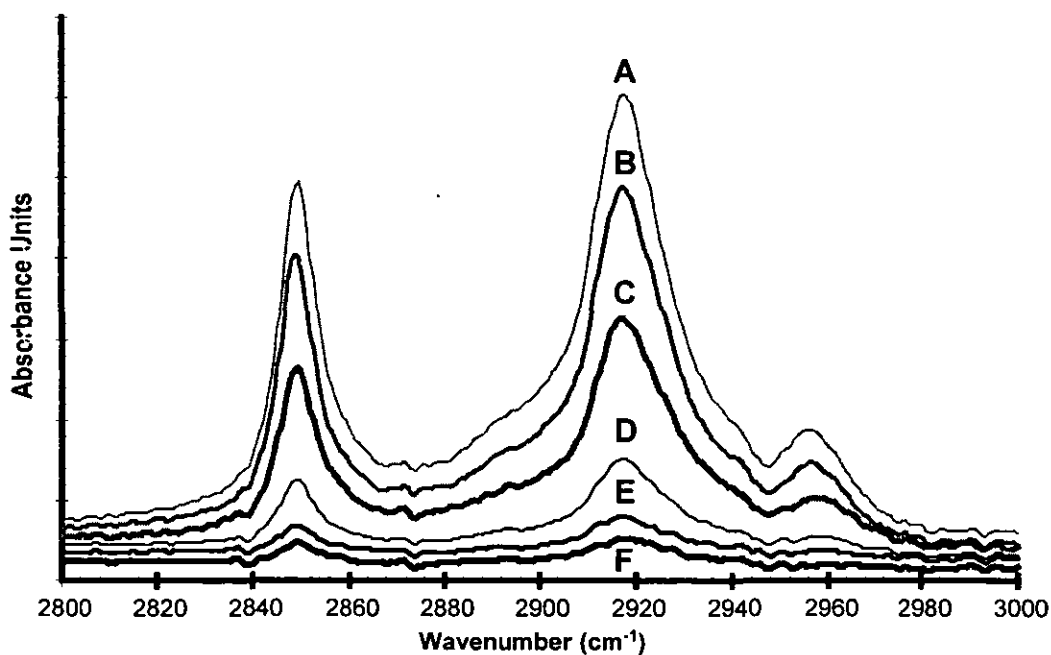
(A - coated, B - uncoated)(ammonium stearate)

Figure 48 DRIFT spectra of stearate coated and uncoated calcium carbonate

On the precipitated calcium carbonate particles used detection limits of 0.05 of a monolayer and less can be achieved. For a single monolayer coating the measurement has a standard deviation of 2%.

The intensity of the C-H vibrations of the alkyl chains can be seen visually to increase as a function of the amount of coating material added (Figure 49).





(A -  $\frac{3}{2}$  Monolayer, B - 1 Monolayer, C -  $\frac{1}{2}$  Monolayer, D -  $\frac{1}{4}$  Monolayer, E -  $\frac{1}{8}$  Monolayer, F -  $\frac{1}{16}$  Monolayer)

Figure 49 Quantitative DRIFT for ammonium stearate coated calcium carbonate showing the increase in C-H bands with coating level

#### 4.4.1.1 Ammonium Stearate

Coating the surface using ammonium stearate gives rise to new bands at 2800 – 3000 $\text{cm}^{-1}$ . This can be assigned to C-H vibrations in the alkyl chain of the stearate. No signals attributable to ammonium ions are detected and the presence of absorption at 1580  $\text{cm}^{-1}$  indicates the coating has reacted on the surface to produce calcium stearate. No unreacted stearic acid (1700  $\text{cm}^{-1}$ ) could be detected.

By comparing the intensities of the peaks that are a direct result of the coating (Section 3.3.4.1 DRIFT Experimental) a measure of the extent of coating can be

achieved. The ratio of the peaks measured in absorbance units is shown in Figure 50.

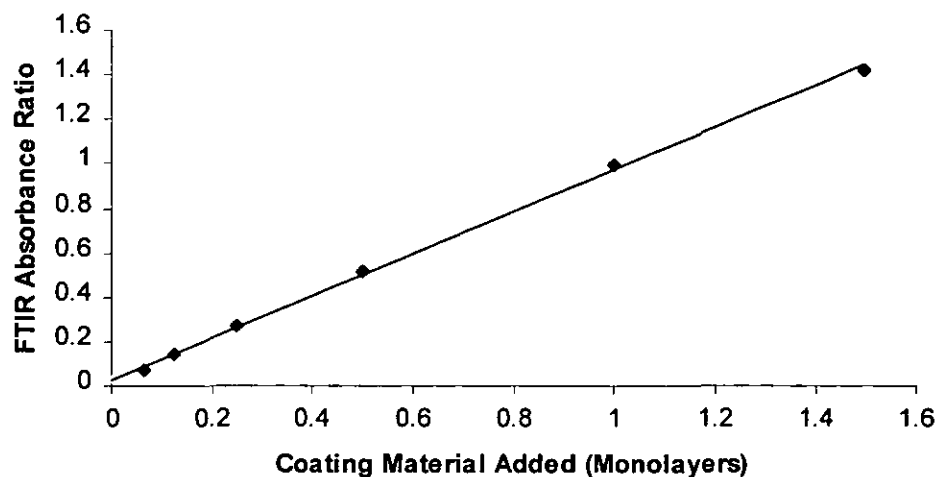


Figure 50 Effect of the quantity of coating material added (as ammonium stearate) on the FTIR absorbance ratio (C-H band ( $3000-2800\text{ cm}^{-1}$ ) divided by the carbonate band ( $2450-2650\text{ cm}^{-1}$ ))

When working in the DRIFT mode, Kubelka-Munk units are commonly used as an alternative to absorbance units. Both Kubelka-Munk and absorbance ratios are seen to increase linearly as a function of the coating material added.

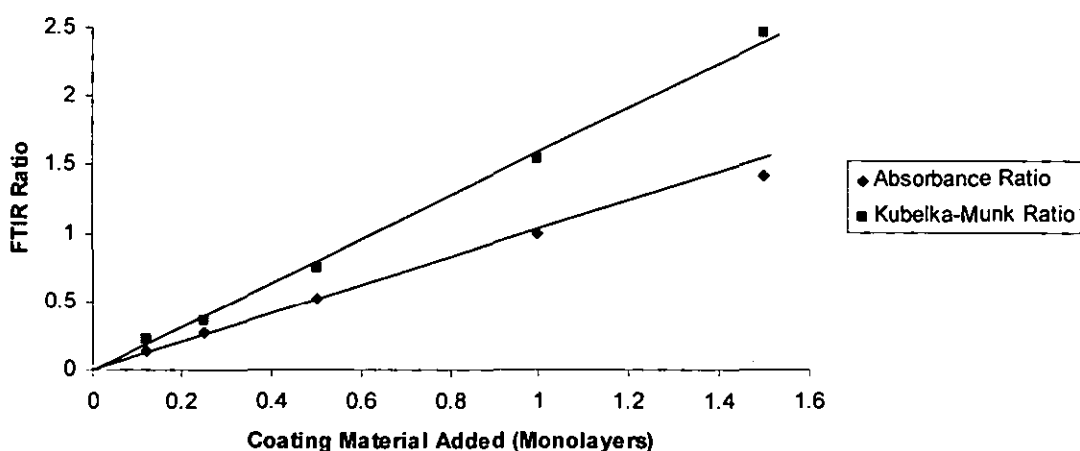


Figure 51 Comparison of the absorbance and Kubelka-Munk ratios calculated during FTIR analysis (C-H band ( $3000-2800\text{ cm}^{-1}$ ) divided by the carbonate band ( $2450-2650\text{ cm}^{-1}$ ))

#### 4.4.1.2 Sodium Stearate

Coating the surface using sodium stearate gives rise to new bands at  $2800-3000\text{ cm}^{-1}$  which may be assigned to C-H vibrations in the alkyl chain of the stearate. No residual stearic acid ( $1700\text{ cm}^{-1}$ ) could be detected.

By comparing the intensities of the peaks that are a direct result of the coating (Section 3.3.4.1 DRIFT Experimental) a measure of the coating can be achieved. The intensities of the absorbance ratios are shown in Figure 52. The variation in the FTIR absorbance ratio as a function of the coating material added is a constant.

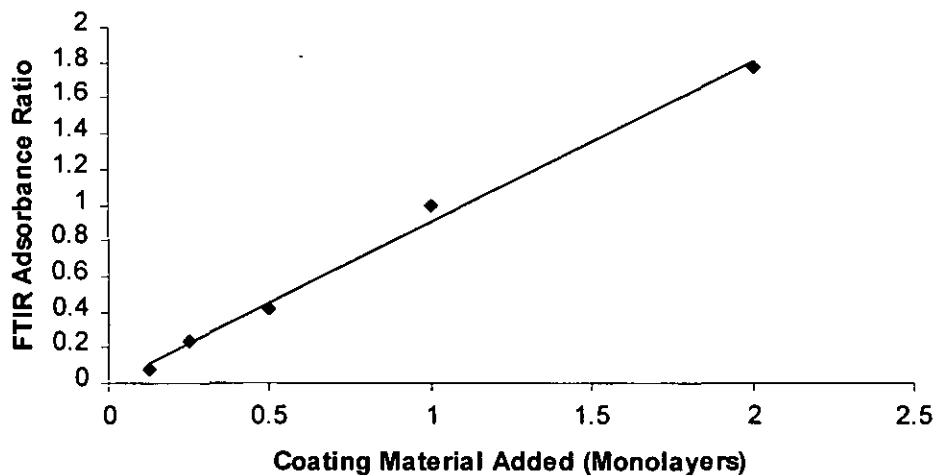


Figure 52 Effect of the quantity of coating material added (as sodium stearate) on the FTIR absorbance ratio (C-H band ( $3000-2800\text{ cm}^{-1}$ ) divided by the carbonate band ( $2450-2650\text{ cm}^{-1}$ ))

Sodium stearate is partially soluble in water. Over a fixed period of time (30 minutes) the coating produced is seen to vary as a function of the coating temperature.

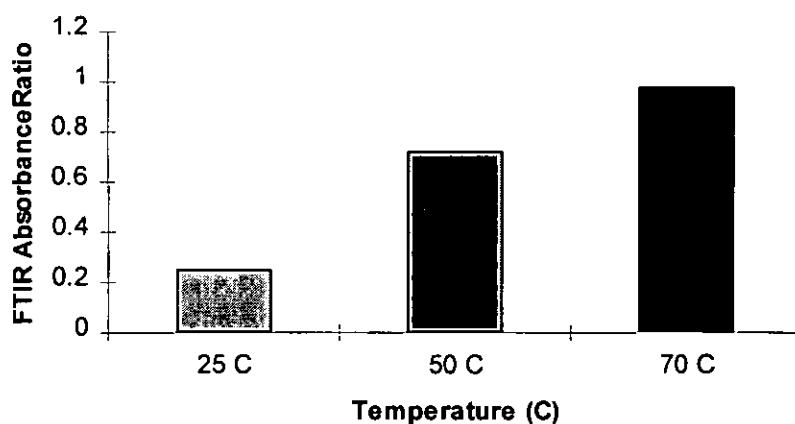


Figure 53 Effect of temperature on the FTIR absorbance ratio (C-H band ( $3000-2800\text{ cm}^{-1}$ ) divided by the carbonate band ( $2450-2650\text{ cm}^{-1}$ )) produced when sufficient sodium stearate is added to produce a coating equivalent to a monolayer

### 4.4.1.3 Stearic Acid Coatings

Coating the surface with stearic acid gives rise to new bands at  $2800\text{-}3000\text{ cm}^{-1}$ , which may be assigned to C-H vibrations in the alkyl chain of the stearate. Unreacted stearic acid ( $1700\text{ cm}^{-1}$ ) could be detected in those samples produced at room temperature.

By comparing the intensities of the peaks that are a direct result of the coating (Section 3.3.4.1 DRIFT Experimental) a measure of the coating can be achieved. The intensities of the absorbance ratios are shown in Figure 54.

When stearic acid is added at different temperatures, the level of the organic matter increases as the temperature increases. Unreacted stearic acid is visible at temperatures below that of the melting point of the stearic acid.

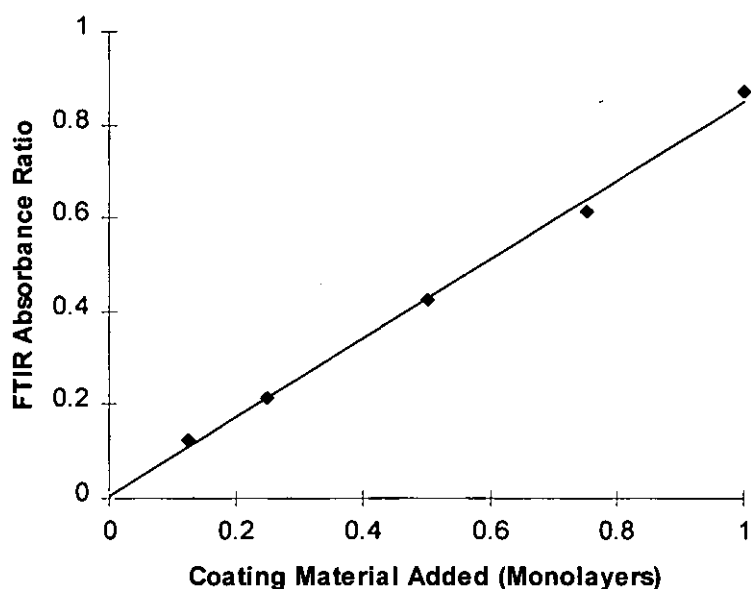


Figure 54 Effect of the quantity of coating material added (as stearic acid) on the FTIR absorbance ratio (C-H band ( $3000\text{-}2800\text{ cm}^{-1}$ ) divided by the carbonate band ( $2450\text{-}2650\text{ cm}^{-1}$ ))

#### 4.4.1.4 Zeneca Ammonium Stearate Coatings

Large batch samples (1 kg) of coated calcium carbonate were produced using the Zeneca facilities at Lostock. The level of stearate detected is seen to increase as a function of the coating material added in the coating process. It is known that during the batch coating procedure different levels of coating can be measured if samples are collected at different sample 'run-off' times (different positions in the reaction vessel).

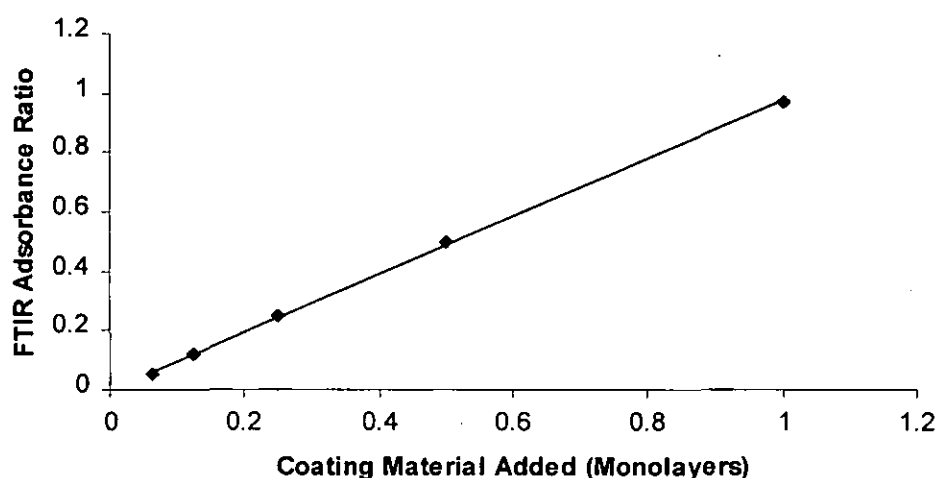


Figure 55 Effect of the quantity of coating material added (as ammonium stearate) on the FTIR absorbance ratio (C-H band ( $3000-2800\text{ cm}^{-1}$ ) divided by the carbonate band ( $2450-2650\text{ cm}^{-1}$ )) when produced on a batch scale

#### 4.4.1.5 Stearic Acid Dry Coated

As discussed in Section 2.2.3.1 Coating Methods, stearate coatings are often produced by a dry coating procedure. The FTIR spectra of the dry coated filler (Figure 56) is similar to that of the wet coated filler (Figure 48), except that close inspection of the spectra indicates a residual stearic acid peak (approximately  $1700\text{ cm}^{-1}$ ). This is discussed further in Section 4.4.1.9 Comparison Of Coating Peaks.

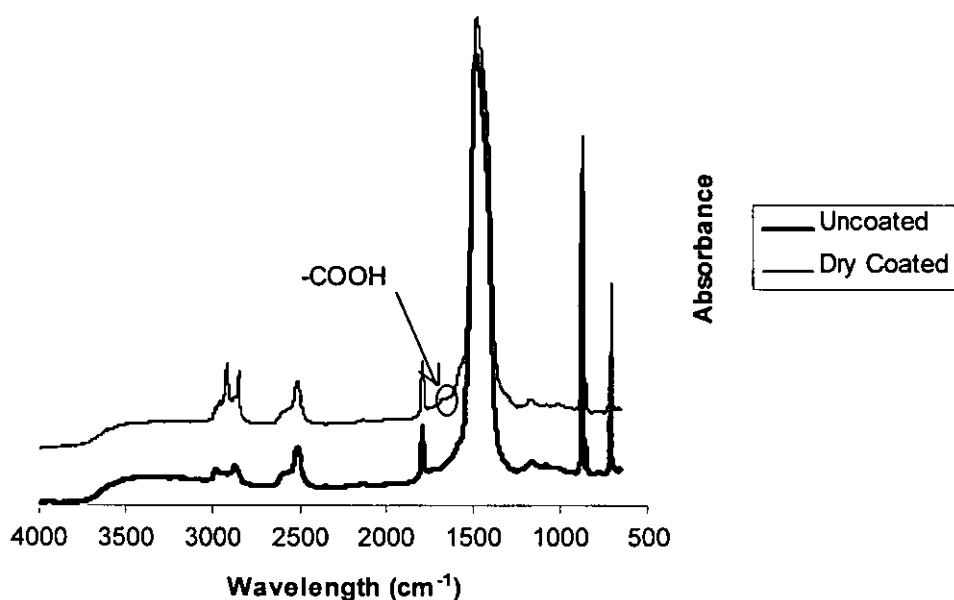


Figure 56 DRIFT spectra of dry stearate coated and uncoated calcium carbonate

#### 4.4.1.6 Sodium Stearate Blended

DRIFT analysis is sensitive to the location of the stearate within the system. To test this sodium stearate was blended (mixed with no heating, just shaking) with precipitated calcium carbonate, and then analysed. As expected, the blended samples had a lower level of absorbance when compared with the wet coated samples. This can be seen in Figure 57. This would indicate that FTIR has some surface specificity.

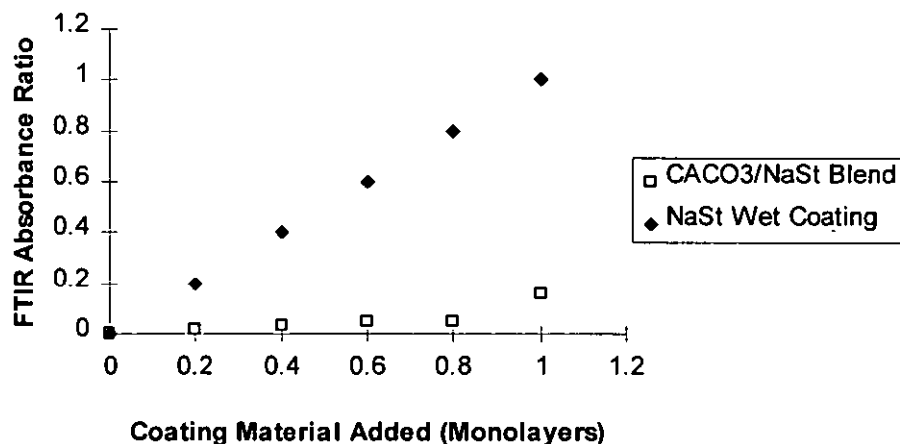


Figure 57 Diagram showing the FTIR absorbance ratio of a sodium stearate/calcium carbonate mixture compared to a wet coated sodium stearate sample

#### 4.4.1.7 Comparison Of Wet Coating Methods

A number of methods have been used in attempts to produce a stearate coating. When a comparison of the FTIR absorbance ratios is made for the same level of stearate addition (1 monolayer) a variation in the absorbance ratio measured is detected (Figure 58).



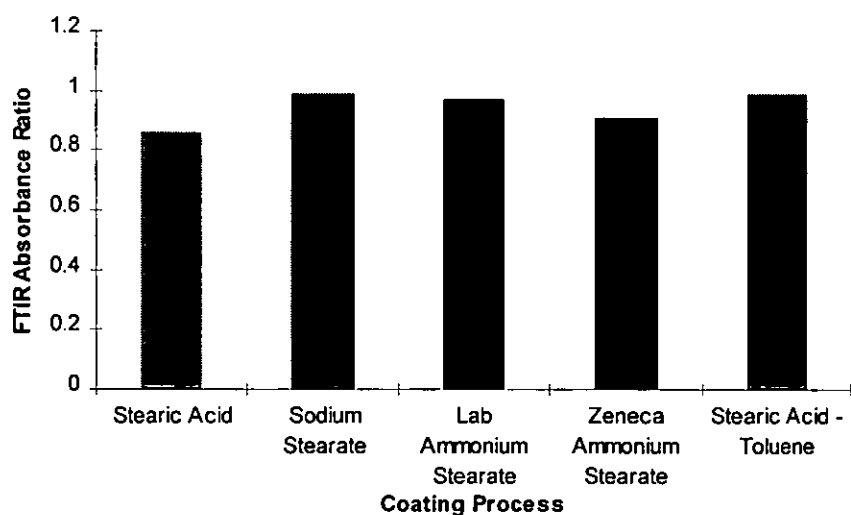


Figure 58 Comparison of stearate coatings produced by different methods measured by FTIR absorbance ratio (C-H band ( $3000-2800\text{ cm}^{-1}$ ) divided by the carbonate band ( $2450-2650\text{ cm}^{-1}$ ))

It has been found that under the same controlled laboratory conditions the sodium and ammonium stearate preparations produce the same absorbance ratio and were found to be the most efficient methods.

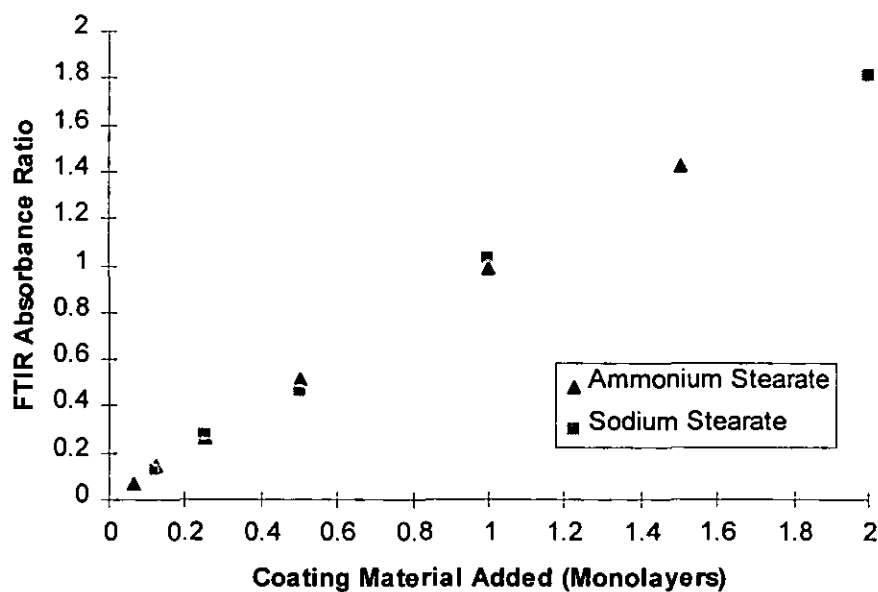


Figure 59 Comparison of the FTIR absorbance ratios (C-H band ( $3000-2800\text{ cm}^{-1}$ ) divided by the carbonate band ( $2450-2650\text{ cm}^{-1}$ )) produced, by the varying quantities of sodium and ammonium stearate added

#### 4.4.1.8 Comparison Of Coating Material Peaks

To aid in the assignment of the characteristic coating peaks the coating materials have been analysed (Figure 60). The environment of the carbonyl group can be seen to have a profound effect on the position of the peak. Ammonium stearate has been manufactured but exists in equilibrium with stearic acid.

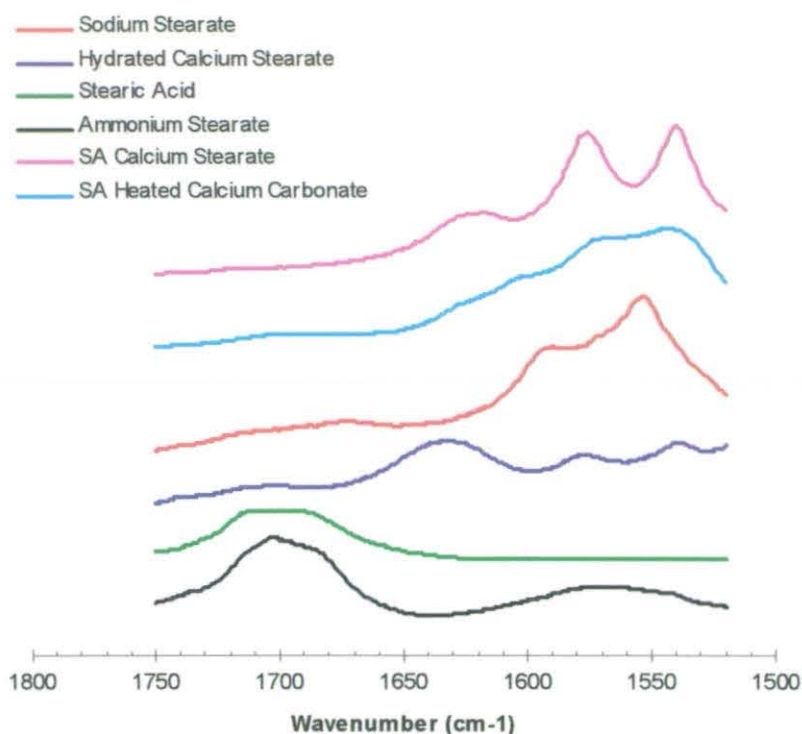


Figure 60 DRIFT spectra of different coating compounds. (Please note peak sizes are not comparable (SA = Sigma Aldrich))

#### 4.4.1.9 Comparison Of Coating Peaks

One of the principal advantages of FTIR is the high signal to noise ratio in the spectra which allows spectral subtraction to detect weak absorbances. The characteristic stearate peaks are obscured by a fundamental stretching frequency of the calcium carbonate. This fundamental band can be subtracted allowing the resultant spectrum to be analysed. Example subtraction spectrum can be seen in Figure 61. A summary of the peak positions can be found in Table 16.

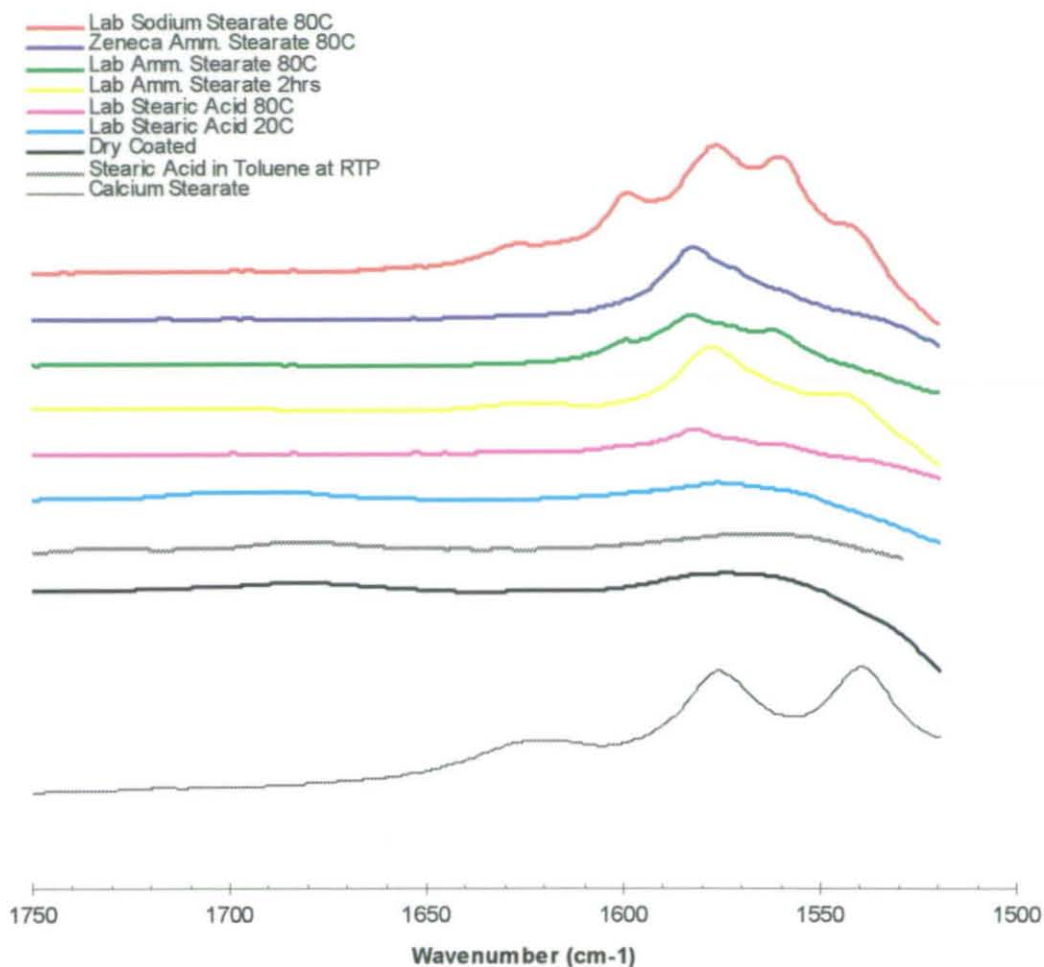


Figure 61 Comparison of the carbon-oxygen bond absorption frequency as a function of the stearate coating process

Similar peak structures can be seen at different coating levels within each coating technique. Different peak positions signify either different physical or chemical environments. The main bond type investigated is the carbonyl bond characteristic of the acid and the stearate. The different environments may be due to the change in the nature of the calcium ion; free or surface bound, hydrated or unhydrated. The environment of the coating can be modified (Figure 62).

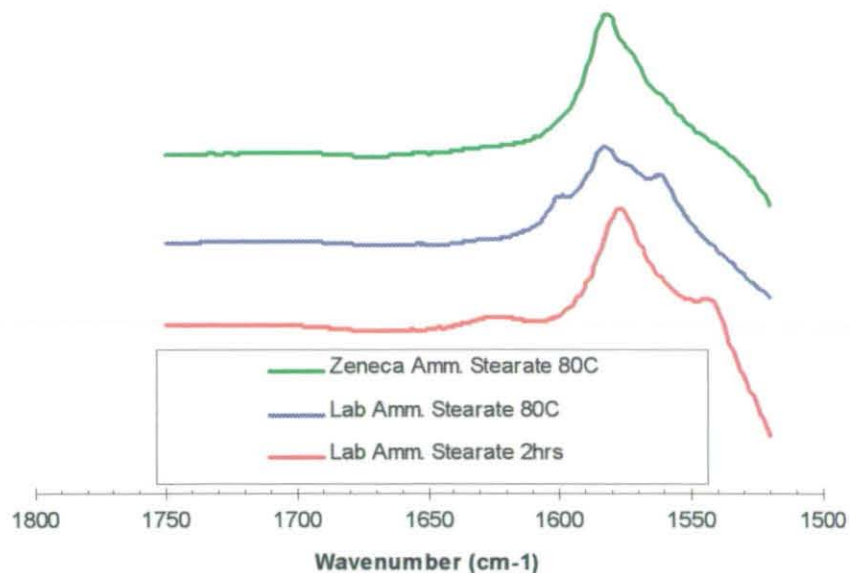


Figure 62 Comparison of the carbonyl bond absorption frequency for different coating conditions

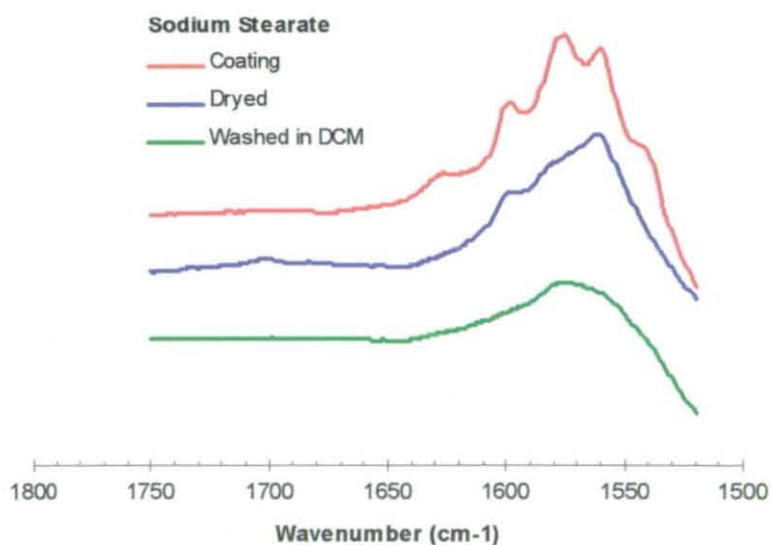


Figure 63 Comparison of the sodium stearate coated calcium carbonate, C=O bond absorption frequency, as a function of the washing process



By comparing peaks that are characteristic of the particular coating processes with the reactants and the reference materials it is possible to propose chemical assignments to the peaks. These proposed assignments are discussed in Section 5.4.2 .

## 4.4.2 Magnesium Hydroxide

### 4.4.2.1 Sodium Stearate

Coating the surface using sodium stearate gives rise to new IR absorption bands at 2800-3000  $\text{cm}^{-1}$ . These may be assigned to C-H vibrations in the alkyl chain of the stearate. Signals that could be attributed to sodium stearate (1553  $\text{cm}^{-1}$ ) are not detected. The presence of an absorption at 1578  $\text{cm}^{-1}$  indicates the coating has reacted to produce magnesium stearate.

The experimental values obtained for the magnesium hydroxide agree well with the literature values<sup>128,129</sup>.

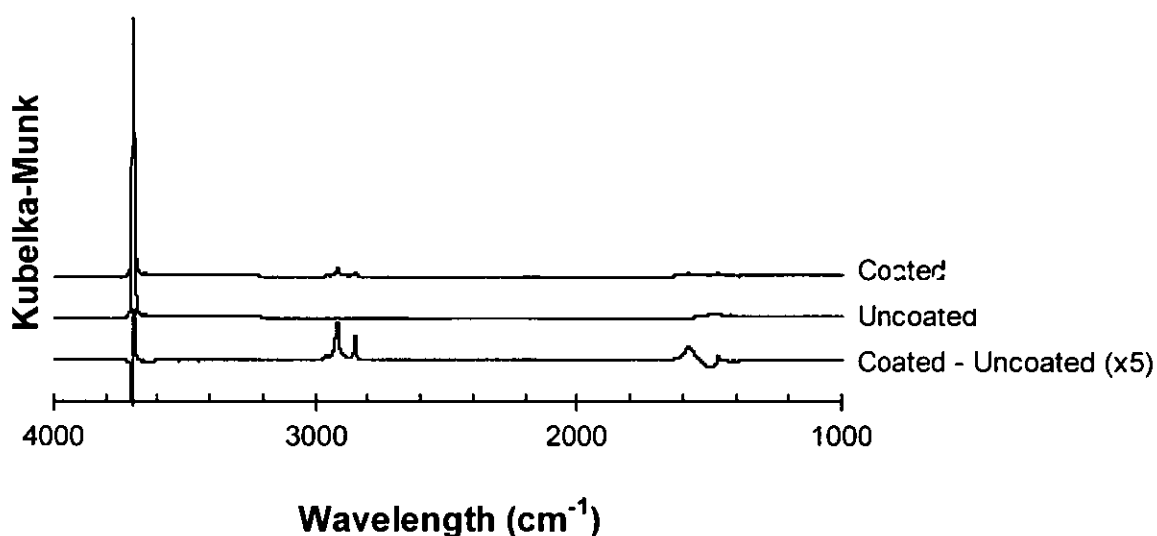


Figure 64 DRIFT spectra (4000 – 1000  $\text{cm}^{-1}$ ) of sodium stearate coated and uncoated magnesium hydroxide

Studying samples by DRIFT results in the analysis of bulk, surface and coating chemistry. Spectral subtraction works effectively if the chemistry of the filler and the coating remains unaltered during the coating process. If a bond is formed



between the surface of the filler and the coating, the coated filler will not exhibit these characteristics. The surface chemical characteristics of the filler can be said to have changed.

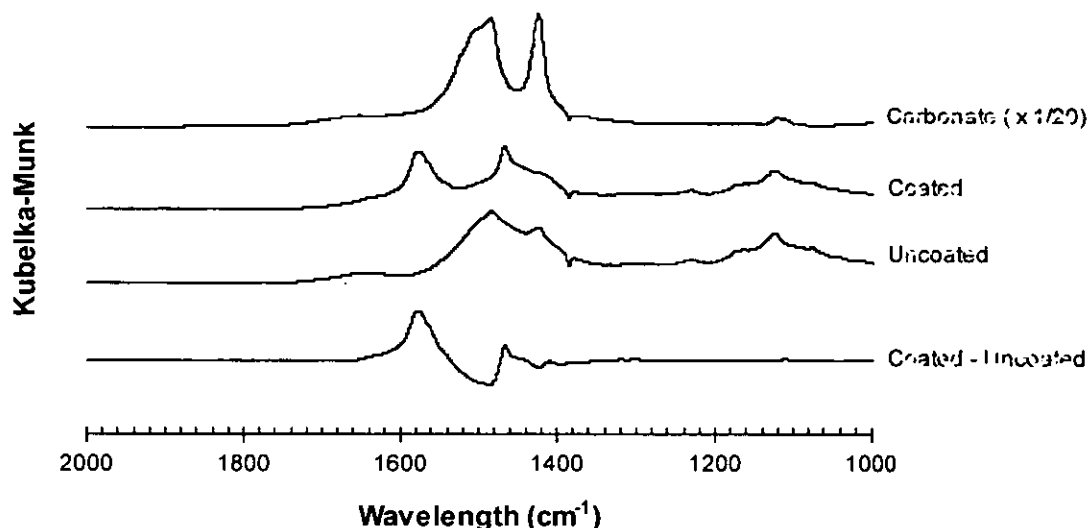


Figure 65 DRIFT spectra ( $2000 - 1000 \text{ cm}^{-1}$ ) of magnesium carbonate, sodium stearate coated and uncoated magnesium hydroxide, and the resultant spectral subtraction

In Figure 65 peaks at  $1484$  and  $1423 \text{ cm}^{-1}$  in the uncoated sample are not present in the coated sample. The absence of these peaks in the coated spectra will give rise to negative data points in the spectral subtraction of these regions. These peaks are indicative of magnesium carbonate being present in the uncoated filler, but not in the coated filler. As this is a surface reaction it is thought that the carbonate species consumed in the coating process are surface specific species.

Diffuse reflection spectra can be used quantitatively but samples must be prepared and the results interpreted with care. The infra-red spectra obtained depend strongly on the shape and size of the powder particles used and the size of the diluent particles. One practical problem is that it can be difficult to achieve the same degree of dispersion of the coated and uncoated filler in KBr. It is necessary

to establish whether the technique can be used quantitatively for the filler coating system studied. In some instances it is convenient to take ratios of peaks, one characteristic of the coating and another characteristic of the powder.

In Figure 66 the area under the C-H band ( $3000-2800\text{ cm}^{-1}$ ) has been ratioed to that under the hydroxide band ( $3750-3600\text{ cm}^{-1}$ ). The linear increase in both formats is only applicable to thin coatings. At higher coating levels linearity would not necessarily be expected.

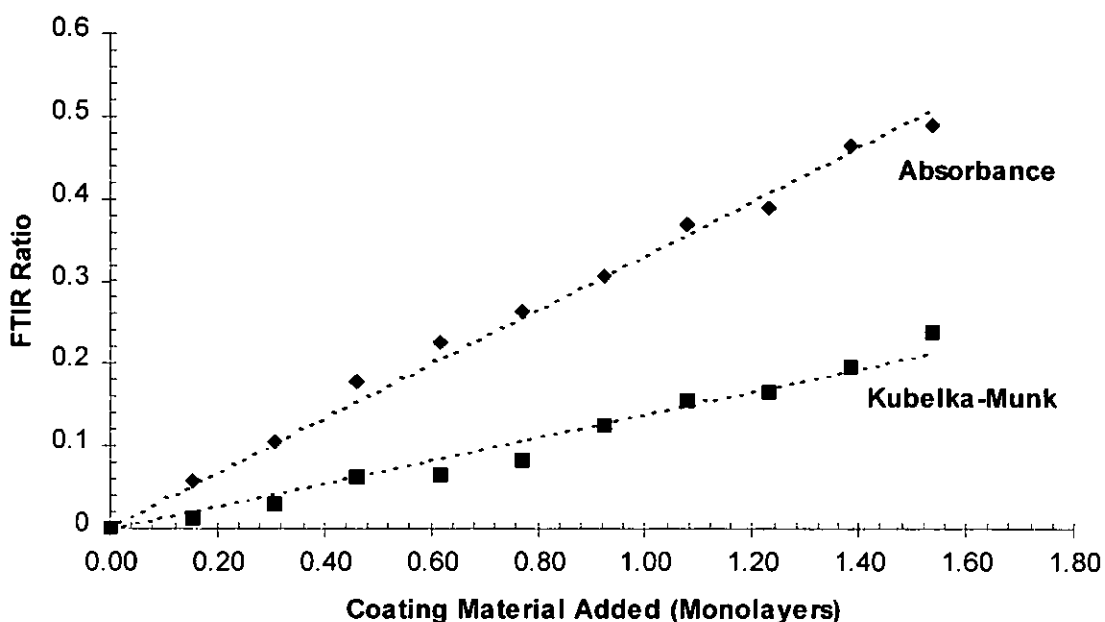


Figure 66 DRIFT ratio analysis of sodium stearate coated magnesium hydroxide (C-H band ( $3000-2800\text{ cm}^{-1}$ ) divided by the hydroxide band ( $3750-3600\text{ cm}^{-1}$ ))

## 4.5 XPS Results

XPS offers the user a high level of surface specificity and chemical selectivity (see Section 2.7.5 X-ray Photoelectron Spectroscopy). If the location of the coating is unknown a multi technique approach can be used to solve this problem. This level of specificity enables the user to determine if the coating is present at the surface and how thick the coating is. The chemical selectivity enables the user to gather some data that can indicate the type of coating.

To utilize XPS to its fullest potential, the system to be analysed must first be evaluated and modelled if appropriate, to enable maximum knowledge to be extracted from the data.

In the analysis of the XPS data as discussed in Section 2.7.5 X-ray Photoelectron Spectroscopy the CS2 approximation of the attenuation length has been used as the most appropriate method for the calculation of the attenuation length <sup>146</sup>.

The following values have been calculated using an MS Excel template.

System Source	Stearate Coating on Calcium Carbonate						
	Al	Al	Al	Al	Al	Al	
Photon Energy	1486.6	1486.6	1486.6	1486.6	1486.6	1486.6	eV
Element	C	C	O	C	C	O	
Level	1s	2p	1s	1s	2p	1s	
Binding Energy	287	347	531	287	347	531	eV
Material	Coating	Coating	Coating	Calcite	Calcite	Calcite	
Density	777	777	777	2710	2710	2710	kgm <sup>-3</sup>
RMM of Matrix	284.48	284.48	284.48	100.09	100.09	100.09	amu
E	1199.6	1139.6	955.6	1199.6	1139.6	955.6	eV
A	0.8472	0.8472	0.8472	0.3944	0.3944	0.3944	
AL (a)	44.1	42.7	38.1	20.6	19.8	17.5	Å

Table 17 Summary of attenuation length calculated using the CS2 equation <sup>146</sup> used in the coating thickness analysis of stearate coatings on calcium carbonate (calcite)

System	Stearate Coating on Magnesium Hydroxide					
Source	Al	Al	Al	Al	Al	
Photon Energy	1486.6	1486.6	1486.6	1486.6	1486.6	eV
Element	C	Mg	O	Mg	O	
Level	1s	2p	1s	2p	1s	
Binding Energy	287	90	531	90	531	eV
Material	Coating	Coating	Coating	Brucite	Brucite	
Density	777	777	777	2360	2360	kgm <sup>-3</sup>
RMM of Matrix	284.48	284.48	284.48	58.33	58.33	Amu
E	1199.6	1396.6	955.6	1396.6	955.6	eV
A	0.8472	0.8472	0.8472	0.3450	0.3450	
IMFP (a)	44.1	48.9	38.1	23.2	17.5	Å

Table 18 Summary of attenuation length calculated using the CS2 equation<sup>146</sup> used in the coating thickness analysis of stearate coatings on magnesium hydroxide (brucite)

System	Stearate Coating on Magnesium Oxide					
Source	Al	Al	Al	Al	Al	
Photon Energy	1486.6	1486.6	1486.6	1486.6	1486.6	eV
Element	C	Mg	O	Mg	O	
Level	1s	2p	1s	2p	1s	
Binding Energy	287	90	531	90	531	eV
Material	Coating	Coating	Coating	Periclase	Periclase	
Density	777	777	777	3580	3580	kgm <sup>-3</sup>
RMM of Matrix	284.48	284.48	284.48	40.31	40.31	amu
E	1199.6	1396.6	955.6	1396.6	955.6	eV
a	0.8472	0.8472	0.8472	0.2654	0.2654	
IMFP (a)	44.1	48.9	38.1	18.2	13.7	Å

Table 19 Summary of attenuation length calculated using the CS2 equation<sup>146</sup> used in the coating thickness analysis of stearate coatings on magnesium oxide (periclase)

## 4.5.1 XPS Thickness Models

### 4.5.1.1 Geometric XPS Theory

The intensity of a photoelectron peak is given by

$$I_A \propto \chi \sigma_A \gamma_A T(E_A) n_A \int_0^{\infty} \exp\left(-\frac{x}{\lambda_A \sin \theta}\right) dx$$

Equation 44

where:

$I_A$  is the intensity of the photoelectron peak,

$\chi$  is the X-ray flux,

$\sigma_A$  is the photoelectron cross section,

$\gamma_A$  angular asymmetry parameter,

$T(E_A)$  is the transmission function of the spectrometer,

$n_A$  is the number density of atoms of type A,

$x$  is the depth perpendicular to the surface from which the electron escapes,

$\lambda_A$  is the electron escape depth,

$\theta$  is the take off angle.

This assumes the sample has a uniform composition as a function of depth, and that there is equal illumination of the sample by the X-rays.

#### 4.5.1.1.1 Flat Model

A general description of the intensities of photoelectrons emitted from the substrate and coating at take-off angle  $\theta$  can be developed.

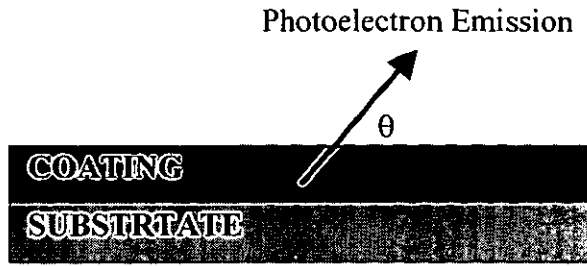


Figure 67 Diagram representing the photoemission from a flat coated surface

The intensity of the coating is given by

$$I_c = \chi \sigma_c \gamma_c T(E_c) n_c \int_0^d \exp\left(-\frac{x}{\lambda_c \sin \theta}\right) dx$$

Equation 45

where;

$I_c$  is the intensity of the coating from photoelectron peak per unit area of surface,

$\lambda_c$  is the attenuation lengths of the photoelectron in the coating,

$n_c$  is the number density of coating atoms present in the coating,

$d$  is the thickness of the coating.

On integration this gives

$$I_c = \chi \sigma_c \gamma_c T(E_c) n_c \left[ -\lambda_c \sin \theta \cdot \exp\left(-\frac{x}{\lambda_c \sin \theta}\right) \right]_0^d$$

Equation 46

which equates to

$$I_c = \chi\sigma_c\gamma_c T(E_c) n_c \lambda_c \sin\theta \left( 1 - \exp\left(-\frac{d}{\lambda_c \sin\theta}\right) \right)$$

Equation 47

The intensity of the substrate through the coating is given by

$$I_s = \chi\sigma_s\gamma_s T(E_s) n_s \cdot \exp\left(-\frac{d}{\lambda_{sc} \sin\theta}\right) \int_0^\infty \exp\left(-\frac{x}{\lambda_s \sin\theta}\right) dx$$

Equation 48

where;

$I_s$  is the intensity of the substrate photoelectron peak per unit area of surface,

$\lambda_s$  is the attenuation length of the photoelectron in the substrate,

$n_s$  is the number density of substrate atoms present in the substrate,

$\lambda_{sc}$  is the attenuation length of the substrate element in the coating,

$d$  is the thickness of the coating.

On integration this gives

$$I_s = \chi\sigma_s\gamma_s T(E_s) n_s \cdot \exp\left(-\frac{d}{\lambda_{sc} \sin\theta}\right) \left[ -\lambda_s \sin\theta \cdot \exp\left(-\frac{x}{\lambda_s \sin\theta}\right) \right]_0^\infty$$

Equation 49

which equates to

$$I_s = \chi\sigma_s\gamma_s T(E_s) n_s \lambda_s \cdot \sin\theta \cdot \exp\left(-\frac{d}{\lambda_{sc} \sin\theta}\right)$$

Equation 50

Combining Equation 47 and Equation 50 gives the general equation for the analysis of coating thickness of a coated flat substrate at take off angle  $\theta$ .

$$\frac{I_c}{I_s} = \frac{\sigma_c \gamma_c T(E_c) n_c}{\sigma_s \gamma_s T(E_s) n_s} \cdot \frac{\lambda_c \cdot \sin \theta \cdot \left( 1 - \exp\left(-\frac{d}{\lambda_c \sin \theta}\right) \right)}{\lambda_s \cdot \sin \theta \cdot \exp\left(-\frac{d}{\lambda_{sc} \sin \theta}\right)}$$

Equation 51

In the case of no coating on a flat surface Equation 50 reduces to

$$I_s = \chi \sigma_s \gamma_s T(E_s) n_s \lambda_s \sin \theta$$

Equation 52

#### 4.5.1.1.2 Spherical Model

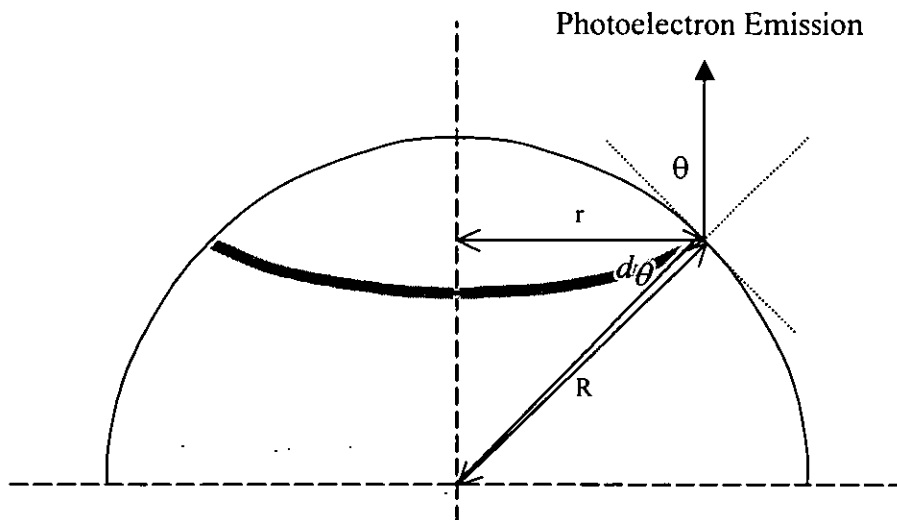


Figure 68 Diagram representing the photoemission from a coated sphere



To analyse the photoelectron emission from the sphere one must consider the emission in the direction of the analyser. As can be seen from the diagram this results in different take off angles from the surface. As a result we must consider rings of radius  $r$ , on a sphere of radius  $R$ . The intensity of the photoemission from the sphere is then the sum of the intensities of the emissions from the rings in the direction of the analyser.

The relationship between the radius of the rings and the radius of the sphere is given by

$$\frac{r}{R} = \cos \theta$$

Equation 53

The area of the ring is given by

$$A_{RING} = 2\pi r \times R.d\theta$$

Equation 54

Substitution of Equation 53 in Equation 54 gives

$$A_{RING} = 2\pi R^2 \cos \theta.d\theta$$

Equation 55

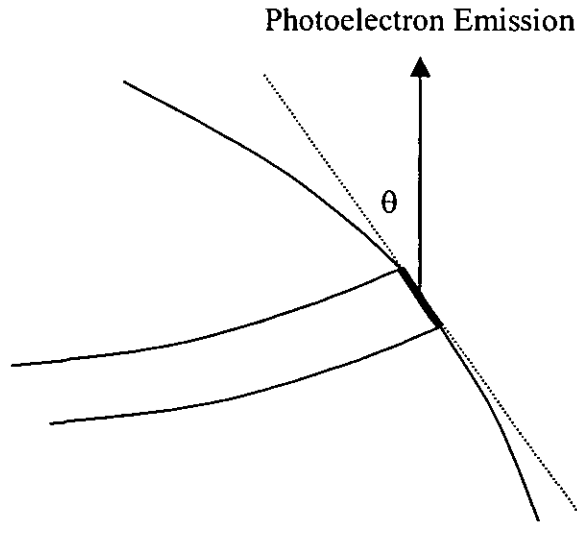


Figure 69 Diagram representing the photoemission of the infinitely small ring

A ring of infinitely small area can be considered to be flat. Therefore the intensity of the emission from the coating, on a surface at a take off angle  $\theta$ , is given by the combination of Equation 47 and Equation 55. The total intensity of the coating is given by

$$I_C^{TOTAL} = \chi\sigma_c\gamma_c T(E_c)n_c\lambda_c.2\pi R^2 \int_0^{\frac{\pi}{2}} \sin\theta \left( 1 - \exp\left(-\frac{d}{\lambda_c \sin\theta}\right) \right) \cos\theta.d\theta$$

Equation 56

The total intensity of the emission from the substrate, at a take off angle  $\theta$ , is given by the combination of Equation 50 and Equation 55. The total intensity from the substrate is given by

$$I_S^{TOTAL} = \chi\sigma_s\gamma_s T(E_s)n_s\lambda_s.2\pi R^2 \int_0^{\frac{\pi}{2}} \sin\theta.\cos\theta.\exp\left(-\frac{d}{\lambda_{sc} \sin\theta}\right).d\theta$$

Equation 57

Combining Equation 56 and Equation 57 gives the general equation for the analysis of coating thickness on a coated sphere

$$\frac{I_C^{TOTAL}}{I_S^{TOTAL}} = \frac{\sigma_C \gamma_C T(E_C) n_C}{\sigma_S \gamma_S T(E_S) n_S} \cdot \frac{\lambda_C \int_0^{\frac{\pi}{2}} \sin \theta \cdot \cos \theta \cdot \left(1 - \exp\left(-\frac{d}{\lambda_C \sin \theta}\right)\right) d\theta}{\lambda_S \int_0^{\frac{\pi}{2}} \sin \theta \cdot \cos \theta \cdot \exp\left(-\frac{d}{\lambda_{SC} \sin \theta}\right) d\theta}$$

Equation 58

In the case of no coating on a sphere Equation 57 reduces to

$$I_S^{TOTAL} = \chi \sigma_S \gamma_S T(E_S) n_S \lambda_S \cdot 2\pi R^2 \int_0^{\frac{\pi}{2}} \sin \theta \cdot \cos \theta \cdot d\theta$$

Equation 59

On integration this gives

$$I_S^{TOTAL} = \chi \sigma_S \gamma_S T(E_S) n_S \lambda_S \cdot 2\pi R^2 \left[ \frac{\sin^2 \theta}{2} \right]_0^{\frac{\pi}{2}}$$

Equation 60

Which reduces to

$$I_S^{TOTAL} = \chi \sigma_S \gamma_S T(E_S) \pi R^2 \cdot n_S \lambda_S$$

Equation 61

This is the same as Equation 52, except the area subtended in Equation 61 is a circle ( $\pi R^2$ ).

### 4.5.1.2 'First' Generation Models

The following equations have been used to estimate the layer thickness; for the flat model (Equation 62) (assuming normal take off from the flat surface) and for the spherical model (Equation 63).

If the photoelectrons characteristic of the substrate and coating are of a similar nature Equation 51 and Equation 58 can be reduced to give,

$$\frac{I_C}{I_S} = \frac{n_C}{n_S} \cdot \frac{\lambda_C \cdot \sin \theta \cdot \left( 1 - \exp\left(-\frac{d}{\lambda_C \sin \theta}\right) \right)}{\lambda_S \cdot \sin \theta \cdot \exp\left(-\frac{d}{\lambda_C \sin \theta}\right)}$$

Equation 62

$$\frac{I_C^{TOTAL}}{I_S^{TOTAL}} = \frac{n_C}{n_S} \cdot \frac{\lambda_C \int_0^{\frac{\pi}{2}} \sin \theta \cdot \cos \theta \cdot \left( 1 - \exp\left(-\frac{d}{\lambda_C \sin \theta}\right) \right) \cdot d\theta}{\lambda_S \int_0^{\frac{\pi}{2}} \sin \theta \cdot \cos \theta \cdot \exp\left(-\frac{d}{\lambda_C \sin \theta}\right) \cdot d\theta}$$

Equation 63

The first generation model allows coating thickness calculations when the relative sensitivity factors of elements are unknown. This can be achieved by generating a theoretical graph on which the intensity ratio calculated can be interpreted in terms of the coating thickness (d).

### 4.5.1.3 'Second' Generation Models

In the 'second' generation model we attempt to take into account the systems in which the two elements analysed are of different binding energies.

Equation 62 and Equation 63 are only valid for the analysis of two chemically shifted peaks of the same energy, one each from the coating and substrate. The equations must be modified to take into the other factors shown in Equation 44. The following equations have been used to estimate the layer thickness; for the flat model (Equation 64) (assuming normal take off from the flat surface); for the spherical model (Equation 65).

$$\frac{I_C}{I_S} = \frac{\sigma_C \gamma_C T(E_C) n_C}{\sigma_S \gamma_S T(E_S) n_S} \cdot \frac{\lambda_C \cdot \left(1 - \exp\left(-\frac{d}{\lambda_C}\right)\right)}{\lambda_S \cdot \exp\left(-\frac{d}{\lambda_{SC}}\right)}$$

Equation 64

$$\frac{I_C^{TOTAL}}{I_S^{TOTAL}} = \frac{\sigma_C \gamma_C T(E_C) n_C}{\sigma_S \gamma_S T(E_S) n_S} \cdot \frac{\lambda_C \int_0^{\frac{\pi}{2}} \sin \theta \cdot \cos \theta \cdot \left(1 - \exp\left(-\frac{d}{\lambda_C \sin \theta}\right)\right) d\theta}{\lambda_S \int_0^{\frac{\pi}{2}} \sin \theta \cdot \cos \theta \cdot \exp\left(-\frac{d}{\lambda_{SC} \sin \theta}\right) d\theta}$$

Equation 65

#### 4.5.1.4 'Third' Generation Models

In the 'third' generation model we attempt to take into account the systems in which the two elements analysed are of different binding energies, and one of the elements analysed is present in both the substrate and the coating.

Equation 64 and Equation 65 must be modified if the element used in the coating is also present in the substrate. A simple formula of the photoemissions can be applied.

$$\frac{I_{COATING\_ELEMENT}}{I_{SUBSTRATE\_ELEMENT}} = \frac{I_{COATING} + I_{(COATING\_IN\_SUBSTRATE)-COAT}}{I_{SUBSTRATE}}$$

Equation 66

Equation 64 and Equation 65 can then rewritten as

$$\frac{I_{COATING\_ELEMENT}}{I_{SUBSTRATE\_ELEMENT}} = \frac{\sigma_C \gamma_C T(E_C) \left[ \left( n_C \lambda_C \left( 1 - \exp\left(-\frac{d}{\lambda_C}\right) \right) \right) + \left( n_{CS} \lambda_{CS} \exp\left(-\frac{d}{\lambda_C}\right) \right) \right]}{\sigma_S \gamma_S T(E_S) n_S \lambda_S \exp\left(-\frac{d}{\lambda_{SC}}\right)}$$

Equation 67

$$\frac{I_{COATING\_ELEMENT}^{TOTAL}}{I_{SUBSTRATE\_ELEMENT}^{TOTAL}} = \frac{\sigma_C \gamma_C T(E_C)}{\sigma_S \gamma_S T(E_S)} \cdot \frac{\left[ \left( n_C \lambda_C \int_0^{\frac{\pi}{2}} \sin \theta \cdot \cos \theta \cdot \left( 1 - \exp\left(-\frac{d}{\lambda_C \sin \theta}\right) \right) \cdot d\theta \right) + \left( n_{CS} \lambda_{CS} \int_0^{\frac{\pi}{2}} \sin \theta \cdot \cos \theta \cdot \exp\left(-\frac{d}{\lambda_C \sin \theta}\right) \cdot d\theta \right) \right]}{n_S \lambda_S \int_0^{\frac{\pi}{2}} \sin \theta \cdot \cos \theta \cdot \exp\left(-\frac{d}{\lambda_{SC} \sin \theta}\right) \cdot d\theta}$$

Equation 68

where:

$n_{CS}$  is the number density of the element characteristic of the coating in the substrate,  $\lambda_{CS}$  is the attenuation length of the element characteristic of the coating in the substrate.

#### 4.5.1.5 'Fourth' Generation Models

##### 4.5.1.5.1 'Fourth' Generation Model Extended (Part 1)

The 'second' and 'third' generation equations assume that the signal comes from a uniformly coated sample. At low levels of coverage this cannot be true. The intensity of a photoelectron peak ratio is not only dependent on the parameters listed in Equation 44, but it is also dependent on the area of analysis. A modified set of equations is required. In this model we attempt to take into account the systems in which the substrate is partially coated and the two elements analysed are of different binding energies.

When XPS is used in conjunction with a technique capable of determining the fractional coverage (Dual BET Isotherm) further information can be obtained.

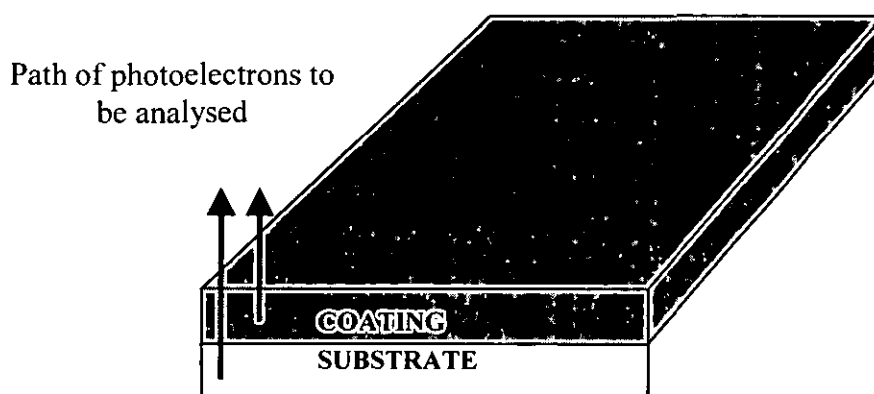


Figure 70 Diagram showing the origins of photoelectron peaks analysed using the simple flat and spherical models

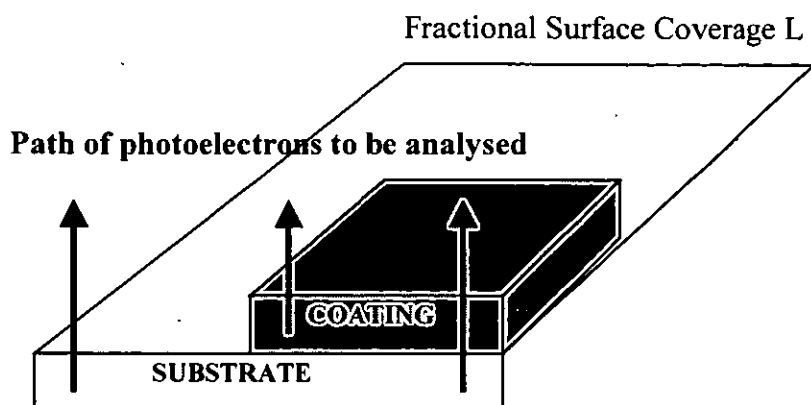


Figure 71 Diagram showing the origins of photoelectron peaks analysed using the 'fourth' generation (part 1) flat and spherical models

Similar models can be drawn for the spherical surface. In the case of the spherical model shadowing effects of the coating on the substrate peak are neglected.

This model is an extension of the 'second' generation model. The 'second' generation equations can be further rewritten if the level of sample coverage is taken into account. Simple coverage theory can be summarised in Equation 69.

$$\frac{I_{COAT\_TOTAL}}{I_{SUBSTRATE\_TOTAL}} = \frac{L(I_{COAT})}{L(I_{SUBSTRATE-COAT}) + (1-L)(I_{SUBSTRATE})}$$

Equation 69

where the intensities  $I$  are the unit area intensities. When this summary is reapplied to the simple flat (Equation 64) and spherical models (Equation 65) equations can be rewritten.

Combining Equation 64, Equation 52 and the simple coverage theory gives



$$\frac{I_{COATING}}{I_{SUBSTRATE}} = \frac{\sigma_C \gamma_C T(E_C)}{\sigma_S \gamma_S T(E_S)} \cdot \frac{L \left( n_C \lambda_C \left( 1 - \exp \left( -\frac{d}{\lambda_C} \right) \right) \right)}{L \left( n_S \lambda_S \cdot \exp \left( -\frac{d}{\lambda_{SC}} \right) \right) + (1-L) n_S \lambda_S}$$

Equation 70

Combining Equation 65, Equation 61 and simple coverage theory gives

$$\frac{I_{COATING}^{TOTAL}}{I_{SUBSTRATE}^{TOTAL}} = \frac{\sigma_C \gamma_C T(E_C)}{\sigma_S \gamma_S T(E_S)} \cdot \frac{L \left( n_C \lambda_C \int_0^{\frac{\pi}{2}} \sin \theta \cdot \cos \theta \cdot \left( 1 - \exp \left( -\frac{d}{\lambda_C \sin \theta} \right) \right) d\theta \right)}{L \left( n_S \lambda_S \int_0^{\frac{\pi}{2}} \sin \theta \cdot \cos \theta \cdot \exp \left( -\frac{d}{\lambda_{SC} \sin \theta} \right) d\theta \right) + (1-L) \frac{n_S \lambda_S}{2}}$$

Equation 71

#### 4.5.1.5.2 'Fourth' Generation Model Extended (Part 2)

The 'second' and 'third' generation equations assume that the signal comes from a uniformly coated sample. At low levels of coverage this cannot be true. A modified set of equations is required. In this model we attempt to take into account the systems in which the substrate is partially coated and the two elements analysed are of different binding energies and one of the elements analysed is present in both the substrate and the coating.

This model is an extension of the 'third' generation model. When the simple coverage theory (Equation 69) is applied to the 'third' generation models, Equation 67 and Equation 68 must be rewritten.

### Path of photoelectrons to be analysed

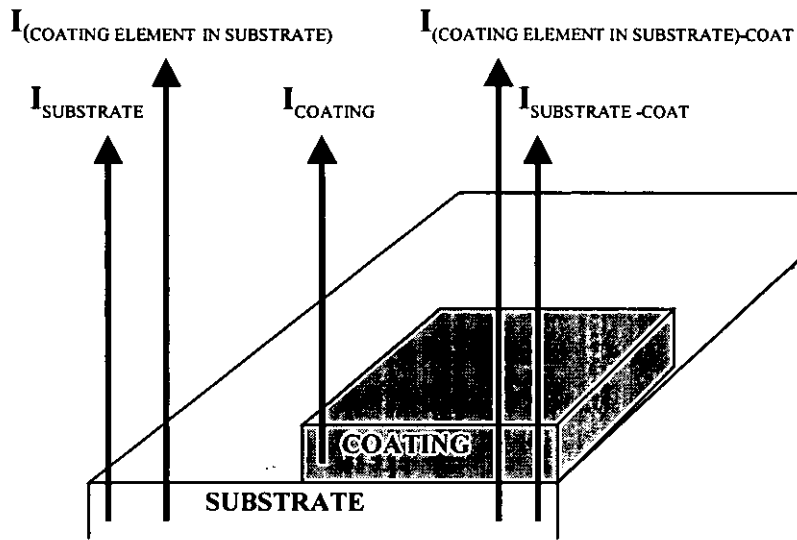


Figure 72 Diagram showing the origins of photoelectron peaks analysed using the 'fourth' generation (part 2) flat and spherical models

Simple coverage theory (Equation 69) when applied to the 'third' generation models must be expanded. When expanded Equation 72 is obtained

$$\frac{I_{\text{COAT\_TOTAL}}}{I_{\text{SUBSTRATE\_TOTAL}}} = \frac{L(I_{\text{COATING}} + I_{\text{(COATING\_ELEMENT\_IN\_SUBSTRATE)-COAT}}) + (1-L)I_{\text{(COATING\_ELEMENT\_IN\_SUBSTRATE)}}}{L(I_{\text{SUBSTRATE-COAT}}) + (1-L)I_{\text{SUBSTRATE}}}$$

Equation 72

Combining Equation 72 and Equation 67 gives

$$\frac{I_{COATING\_ELEMENT}}{I_{SUBSTRATE\_ELEMENT}} = \frac{\sigma_C \gamma_C T(E_C) \left[ L \left[ n_C \lambda_C \left( 1 - \exp\left(-\frac{d}{\lambda_C}\right) \right) \right] + \left[ n_{CS} \lambda_{CS} \exp\left(-\frac{d}{\lambda_C}\right) \right] \right] + (1-L)n_{CS} \lambda_{CS}}{\sigma_S \gamma_S T(E_S) \left[ L \left[ n_S \lambda_S \exp\left(-\frac{d}{\lambda_{SC}}\right) \right] + (1-L)n_S \lambda_S \right]}$$

Equation 73

Combining Equation 72 and Equation 68 gives

$$\frac{I_{COATING\_ELEMENT}^{TOTAL}}{I_{SUBSTRATE\_ELEMENT}^{TOTAL}} = \frac{\sigma_C \gamma_C T(E_C)}{\sigma_S \gamma_S T(E_S)} \frac{(1-L) \frac{n_{CS} \lambda_{CS}}{2}}{\left[ L \left[ n_S \lambda_S \int_0^{\frac{\pi}{2}} \sin \theta \cdot \cos \theta \cdot \exp\left(-\frac{d}{\lambda_{SC} \sin \theta}\right) d\theta \right] + (1-L) \frac{n_S \lambda_S}{2} \right]} + \frac{\sigma_C \gamma_C T(E_C)}{\sigma_S \gamma_S T(E_S)} \frac{L \left[ \left[ n_C \lambda_C \int_0^{\frac{\pi}{2}} \sin \theta \cdot \cos \theta \cdot \left( 1 - \exp\left(-\frac{d}{\lambda_C \sin \theta}\right) \right) d\theta \right] + \left[ n_{CS} \lambda_{CS} \int_0^{\frac{\pi}{2}} \sin \theta \cdot \cos \theta \cdot \exp\left(-\frac{d}{\lambda_C \sin \theta}\right) d\theta \right] \right]}{\left[ L \left[ n_S \lambda_S \int_0^{\frac{\pi}{2}} \sin \theta \cdot \cos \theta \cdot \exp\left(-\frac{d}{\lambda_{SC} \sin \theta}\right) d\theta \right] + (1-L) \frac{n_S \lambda_S}{2} \right]}$$

Equation 74

The effect of partial coverage on the XPS ratio and the estimate coating thickness can be seen in Figure 73 and Figure 74. The coating coverage can be seen to have most effect on the flat model.

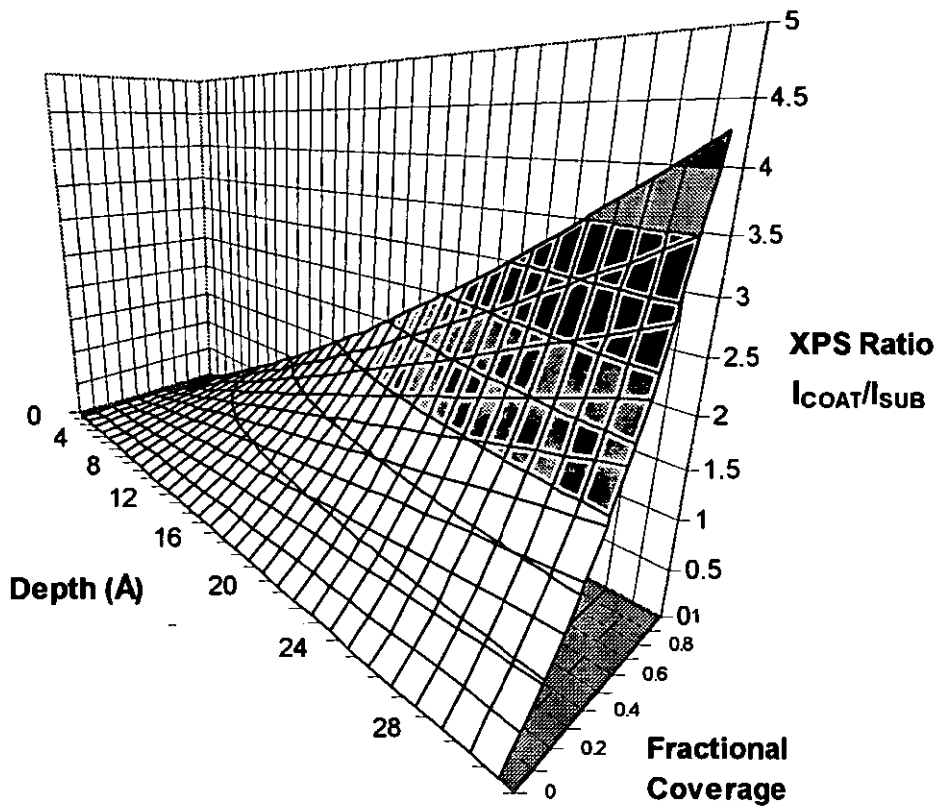


Figure 73 Effect of the fractional coverage on the 'fourth' generation flat model XPS carbon/carbon ratio

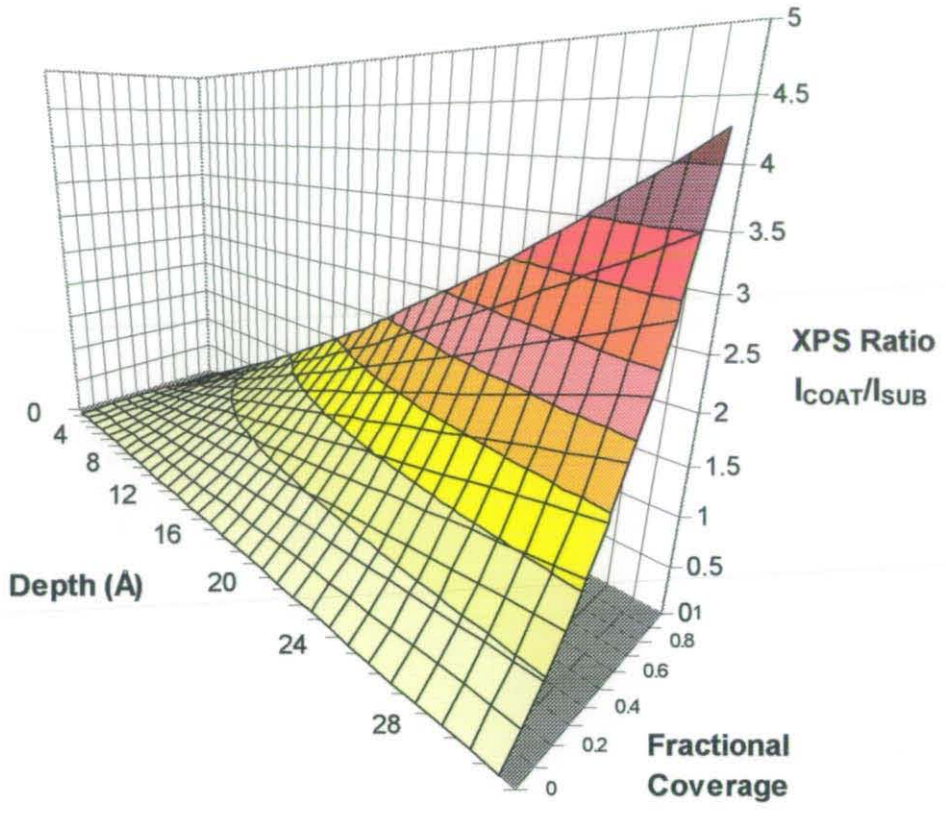


Figure 73 Effect of the fractional coverage on the 'fourth' generation flat model XPS carbon/carbon ratio

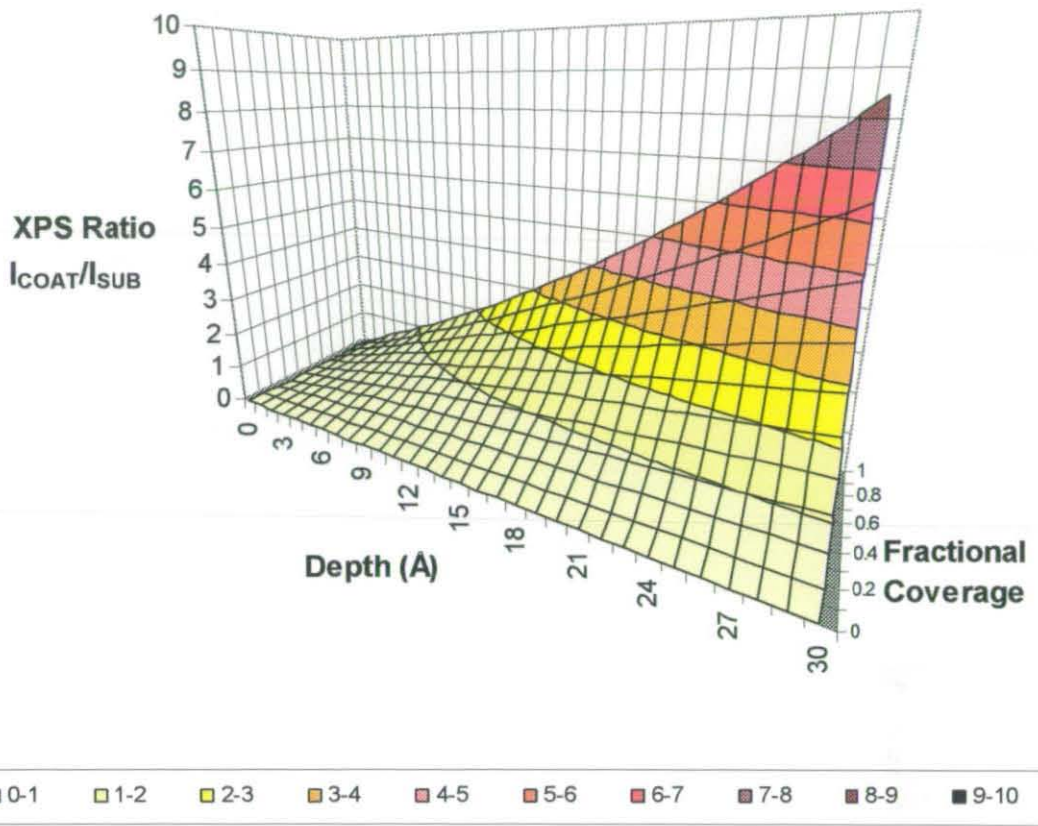


Figure 74 Effect of the fractional coverage on the 'fourth' generation spherical model XPS carbon/carbon ratio

### 4.5.1.6 Effect of Density

The results of the data are open to interpretation, as a number of the parameters are based on semi-quantitative estimations. There are two parameters that fall into this class. The effect of the density on the model is shown in Figure 75.

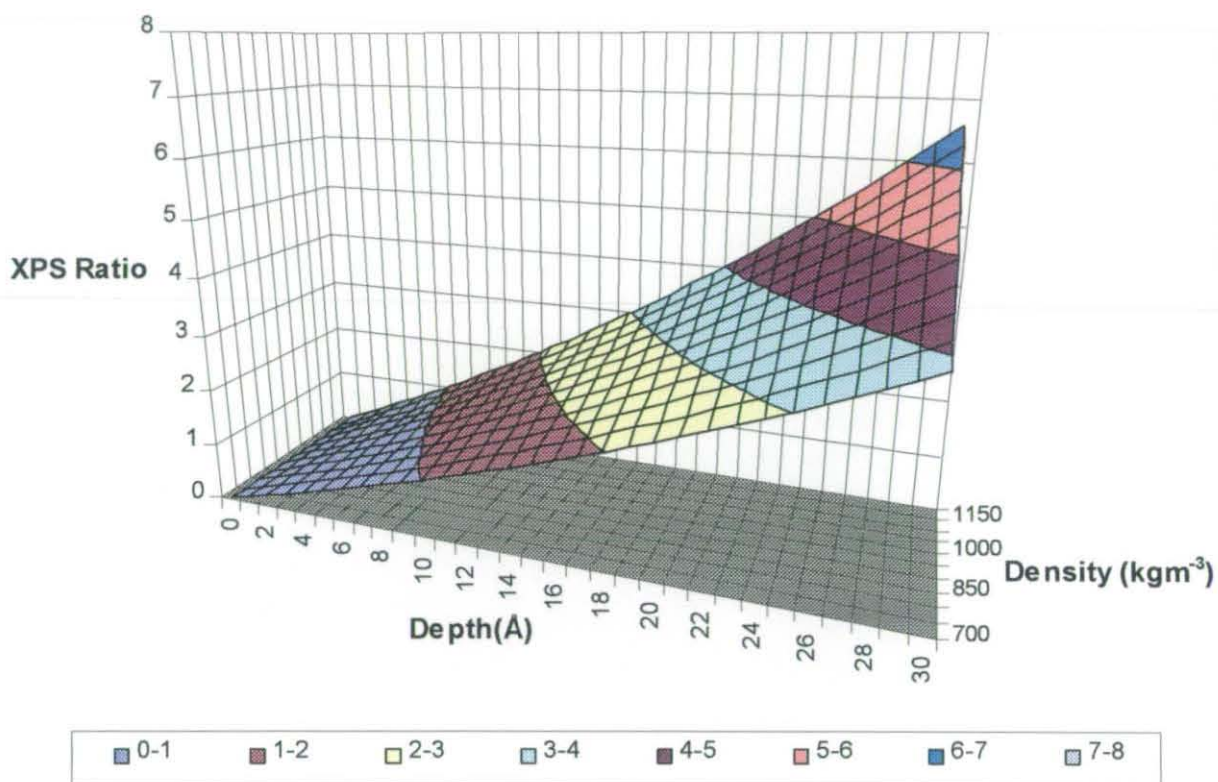


Figure 75 Graph showing the effect of coating density on the thickness estimated from a carbon/carbon XPS ratio calculated for the flat model



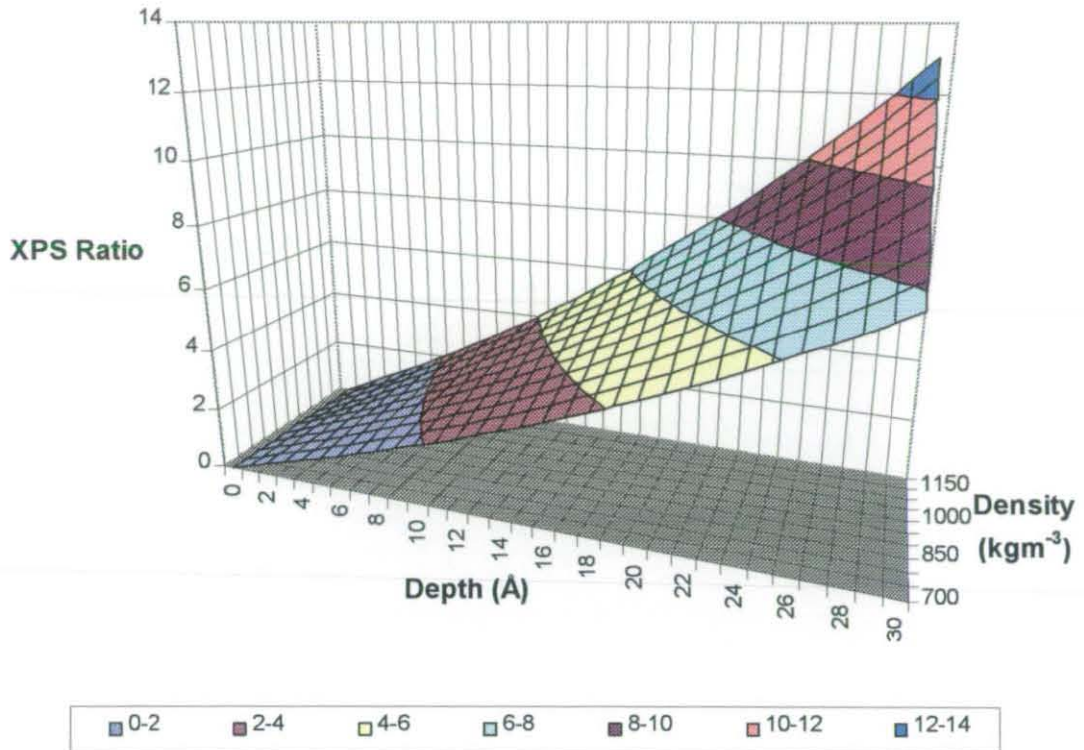


Figure 76 Graph showing the effect of coating density on the thickness estimated from a carbon/carbon XPS ratio calculated for the spherical model

As can be seen from Figure 75 and Figure 76, the effect of density can be quite pronounced. For a flat model, if the density used is  $800 \text{ kgm}^{-3}$  and the thickness is calculated to be  $20 \text{ \AA}$ , and the coating is  $1000 \text{ kgm}^{-3}$  the estimation would have been incorrect by approximately 20 %, the correct answer would have been  $16.5 \text{ \AA}$ . For a spherical model, if the density used is  $800 \text{ kgm}^{-3}$  and the thickness is calculated to be  $10 \text{ \AA}$ , and the coating is  $1000 \text{ kgm}^{-3}$  the estimation would have been incorrect by approximately 20 %, the correct answer would have been  $8 \text{ \AA}$ .



#### 4.5.1.7 Effect of Escape Depth

The effect of the method used to calculate the attenuation length can also effect the thickness of the coating that calculated (Figure 77). For example if we use the method proposed by Seah<sup>143</sup> to calculate this figure the values are some 10-25 % higher than that calculated by Cumpson<sup>146</sup>.

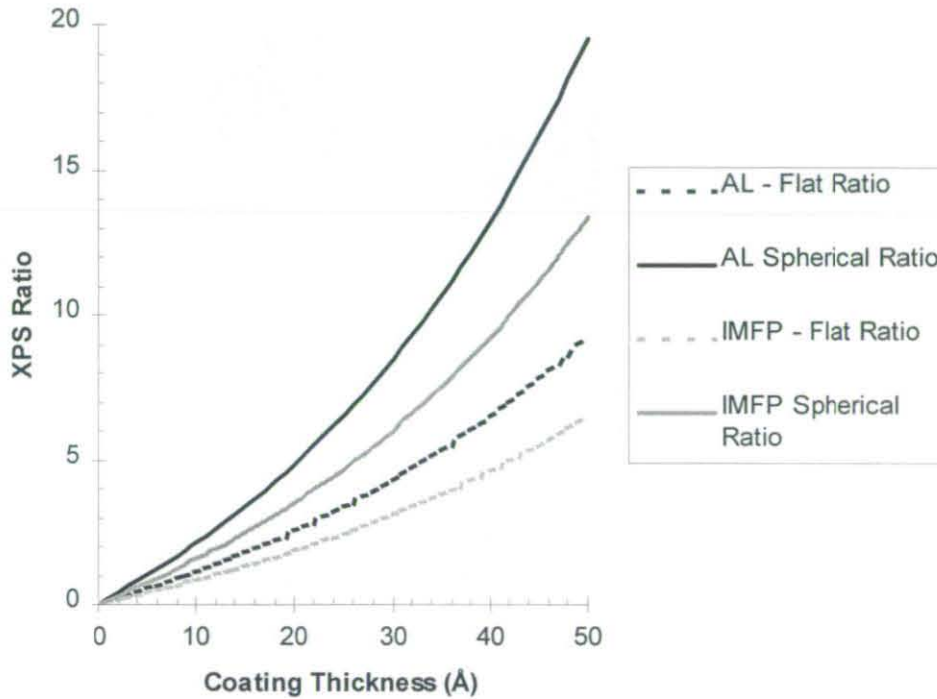


Figure 77 Effect of method used to calculate the escape depth of a photoelectron (IMFP<sup>143</sup> or AL<sup>146</sup>)

As can be seen Figure 77, the effect of escape depth chosen can be quite pronounced. For a flat model, if the AL was used and the thickness is calculated to be 20 Å, and the IMFP provided a better estimation the answer would have been 26 Å. For a spherical model, if the AL was used and the thickness is calculated to be 10 Å, and the IMFP provided a better estimation the answer would have been 13 Å.

### 4.5.1.8 Model Summary

The models described in Section 4.5.1 XPS Thickness Models are summarized in Table 20.

<b>Model Title</b>	<b>Description</b>	<b>Example</b>
<i>'First'</i> Generation	Simple geometric model, based on one element present in different chemical forms in the coating and substrate. (Makes use of high resolution XPS data.)	CaCO <sub>3</sub> - Substrate (C analysed) Stearate - Coating (C analysed)
<i>'Second'</i> Generation	Extension of <i>'first'</i> generation model, but uses two elements exclusive to the substrate or coating.	Mg(OH) <sub>2</sub> - Substrate (Mg analysed) Stearate - Coating (C analysed)
<i>'Third'</i> Generation	Extension of <i>'second'</i> generation model, but takes into account the presence of the coating element in the substrate.	CaCO <sub>3</sub> - Substrate (O or Ca analysed) Stearate - Coating (C analysed)
<i>'Fourth'</i> Generation (Part 1)	Model takes into account partial coverage of a substrate by a coating normally analysed using a <i>'first'</i> or <i>'second'</i> generation model.	Mg(OH) <sub>2</sub> - Substrate (Mg analysed) Stearate - Coating (C analysed)
<i>'Fourth'</i> Generation (Part 2)	Model takes into account partial coverage of a substrate by a coating normally analysed using a <i>'third'</i> generation model.	CaCO <sub>3</sub> - Substrate (O or Ca analysed) Stearate - Coating (C analysed)

Table 20 Summary of XPS models

## 4.5.2 Calcium Carbonate

Once a system has been modelled the experimental work and the analysis of that data begins. The treatment of XPS data is complicated as only specific models can be used in the analysis of calcium carbonate. The models that can be used are summarized in Table 20.

### 4.5.2.1 Ammonium Stearate Coatings

Broad scan spectrum of stearate coated calcium carbonate allows the elemental analysis of the sample. In the analysis of ammonium stearate coated calcium carbonate, no nitrogen due to the ammonium can be detected. No nitrogen peaks at 400 eV can be seen in Figure 78.

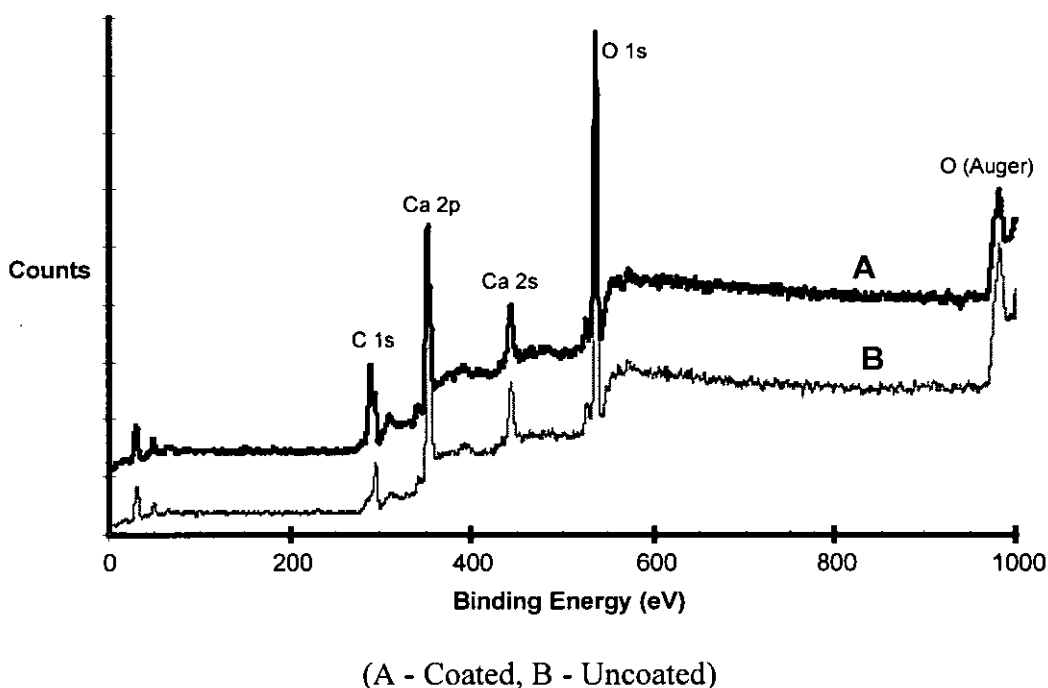


Figure 78 Broad scan XPS spectra of ammonium stearate coated and uncoated calcium carbonate

### 4.5.2.2 Sodium Stearate Coatings

The broad scan XPS spectra of sodium stearate coated calcium carbonate is identical to that of ammonium stearate coated calcium carbonate. No residual sodium can be detected following the coating process.

#### 4.5.2.2.1 Sodium Stearate Coatings and the Geometric Model

The geometric model is the simplest method for analyzing XPS data. Thickness data is not extracted, only atomic composition. The trends of rapidly increasing carbon content until approximately 0.6 monolayer has been added can be seen in Figure 79.

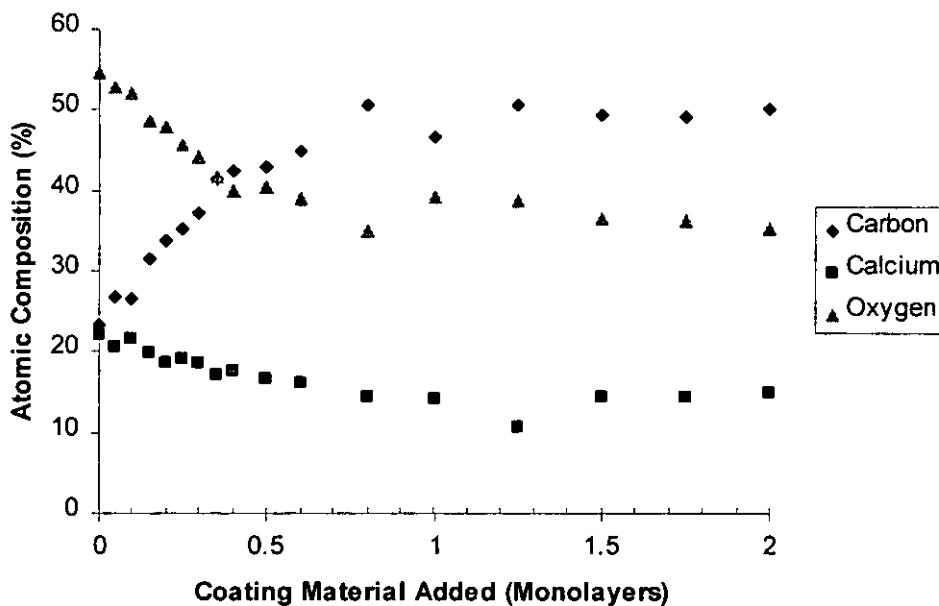


Figure 79 Atomic composition calculated by XPS of a precipitated calcium carbonate filler coated with sodium stearate

This type of analysis is good for the analysis of homogeneous materials where

composition does not vary as a function of depth. The coated filler is by nature non-homogeneous material, with the level of coating varying as a function of depth.

This analysis is able to give an indication of the increasing carbon content at the surface of the material as the level of coating material added is increased.

#### 4.5.2.2.2 Sodium Stearate Coatings and the First Generation Model

In coated calcium carbonate fillers we are able to gather photoelectrons characteristic of the substrate and the coating that are of a 'similar' energy. By using high resolution XPS, a small chemical shift can be seen. This allows curve fitting of the carbon 1s peaks and the analysis of the areas of each peak by the 'first' generation model. By analysis of the intensity ratio an estimation of the thickness of the coating can be made.

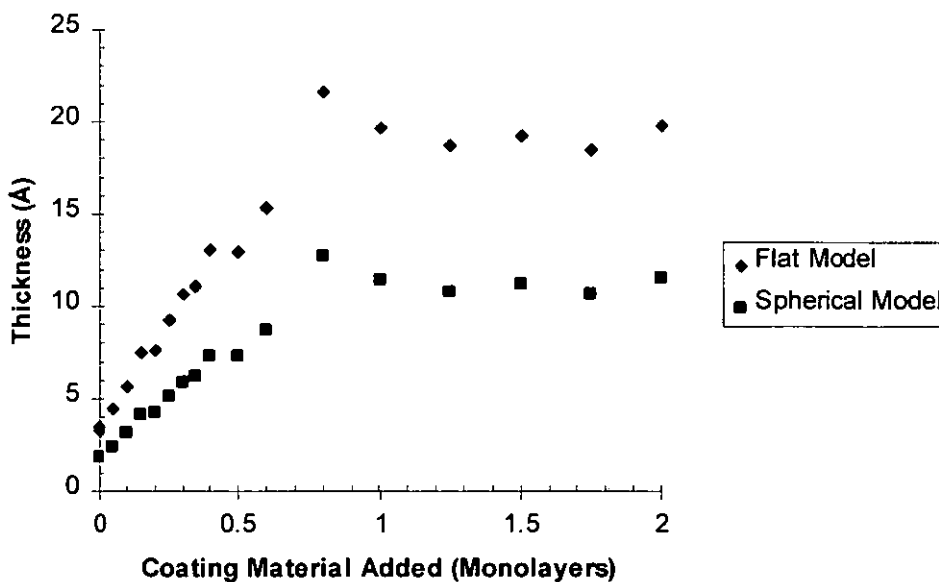


Figure 80 Coating thickness of sodium stearate coated calcium carbonate calculated using the 'first' generation XPS model

Using the *'first'* generation model the flat model calculates a coating with a thickness of 20 Å, the spherical model estimates a thickness of 11 Å.

#### **4.5.2.2.3 Sodium Stearate Coatings and the Second Generation Model**

The first generation model cannot always be used in the analysis of coatings, as not all systems have an element common to both substrate and coating, where the photoelectrons are distinguishable by a small chemical shift.

If the oxygen and calcium data is used in the analysis of the coating thickness the *'second'* generation model is not applicable. The element used in the analysis of the coating is also present in the substrate. If the model is used the result will over-estimate the thickness.

In the case of carbon data, the *'second'* generation model reduces to the *'first'* generation model.

#### **4.5.2.2.4 Sodium Stearate Coatings and the Third Generation Model**

To make maximum use of the broad scan spectra, the *'second'* generation model, can be easily modified to take into account the over estimate, caused by the fact that the intensity of the 'coating' peak also includes some intensity generated by the substrate. This is discussed in more detail in Section 4.5.1.4 *'Third'* Generation Models.

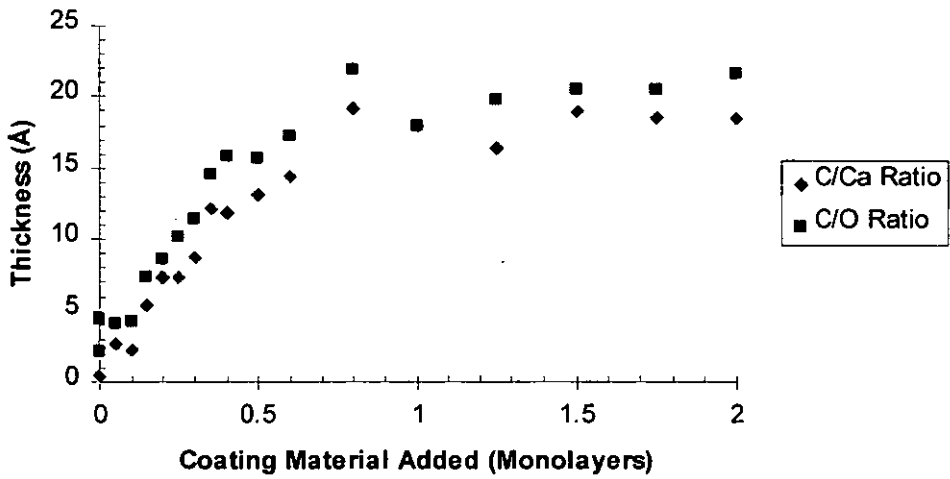


Figure 81 Coating thickness of sodium stearate coated calcium carbonate calculated using the 'third' generation flat XPS model

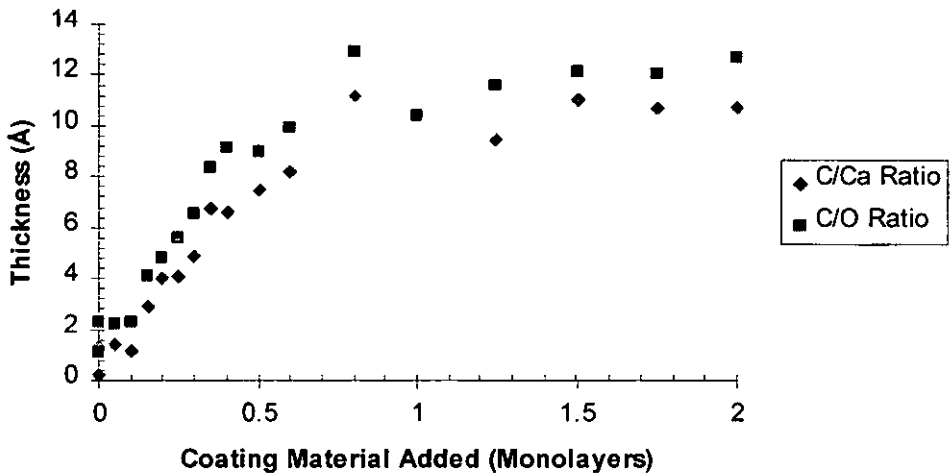


Figure 82 Coating thickness of sodium stearate coated calcium carbonate calculated using the 'third' generation spherical XPS model

As expected both flat (Figure 81) and spherical (Figure 82) *'third'* generation models are in good agreement with the results obtained from the *'first'* generation model (Figure 80). Using the *'third'* generation model the flat models calculate a coating with a thickness of approximately 20 Å and the spherical models estimate a thickness of approximately 11 Å.

#### **4.5.2.2.5 Sodium Stearate Coatings and the Fourth Generation Model**

As discussed in Section 4.5.1 XPS Thickness Models, more data can be extracted from the XPS spectra if the data is interpreted as part of a multi technique approach.

If we use the data shown in Figure 47 and assume it that the increase in coverage as a function of coating material added is linear up to 0.6 monolayers, and then becomes constant, the *'fourth'* generation model can be applied to the coatings, and the coating thickness calculated.

Using the *'fourth'* generation model (part 1) that is an extension of the *'second'* generation model we are able to interpret the data contained in Figure 80 in terms of the fractional coverage (Figure 47).



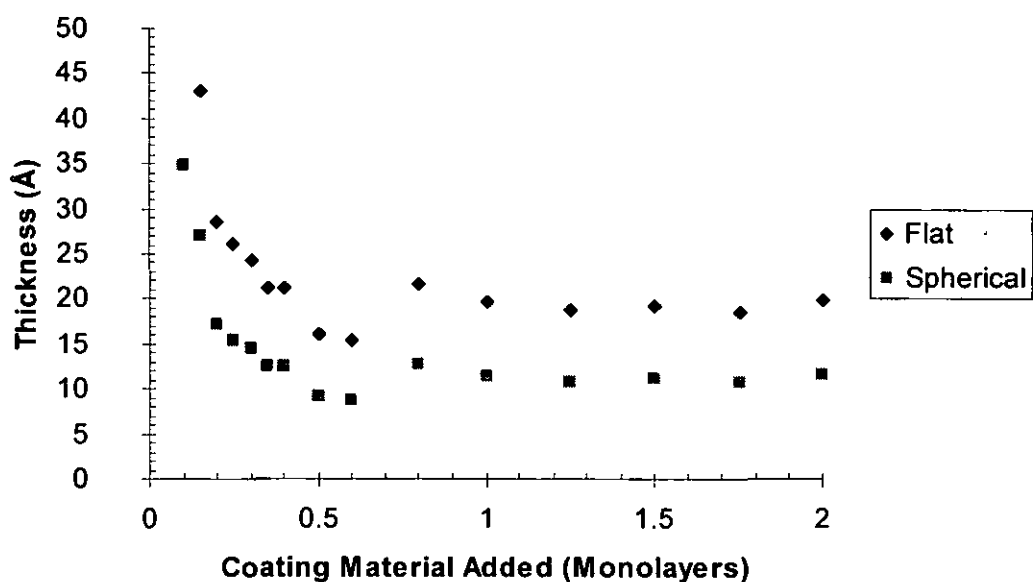


Figure 83 Coating thickness of sodium stearate coated calcium carbonate calculated using the carbon/carbon ratio and the *'fourth'* generation (part 1) XPS models

Using the *'fourth'* generation model that is an extension of the *'second'* generation model we are able to interpret the data contained in Figure 81 in terms of the fractional coverage (Figure 47).

Using the *'fourth'* generation model (part 1) the flat model calculates a coating with a thickness of 20 Å and the spherical model calculates a thickness of 10 Å.

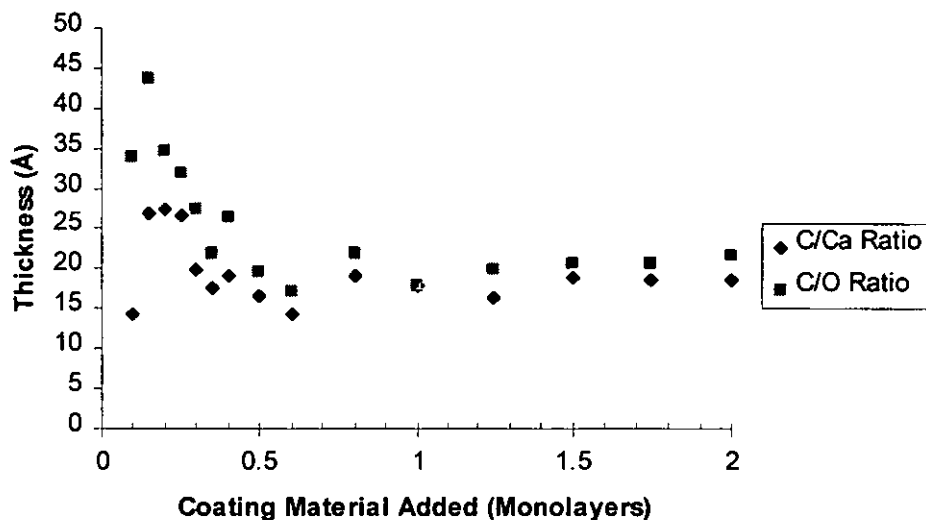


Figure 84 Coating thickness of sodium stearate coated calcium carbonate calculated using the 'fourth' generation (part 2) flat XPS model

Using the 'fourth' generation model (part 2) the flat model calculates a coating with a thickness of 20 Å.

Using the 'fourth' generation model that is an extension of the third generation model we are able to interpret the data contained in Figure 82 in terms of the fractional coverage (Figure 47).

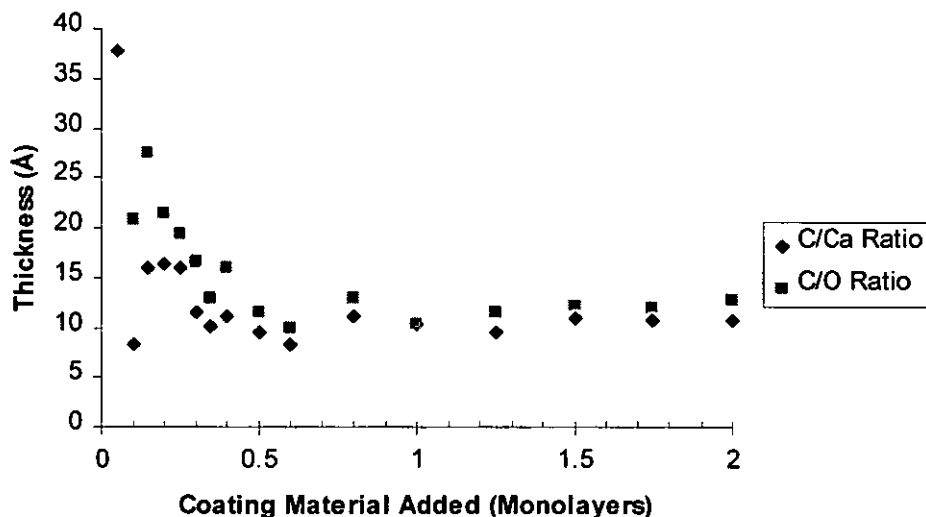


Figure 85 Coating thickness of sodium stearate coated calcium carbonate calculated using the *'fourth'* generation (part 2) spherical XPS model

Using the *'fourth'* generation model (part 2) the spherical model calculates a coating with a thickness of 10-12 Å.

#### 4.5.2.3 Comparison Alternative Coating Methods

A number of coating methods have been analysed. They each generate a different coating thickness. For comparison the carbon/carbon ratios have been analysed using the *'second'* generation model. The results of this analysis can be seen in Figure 86.

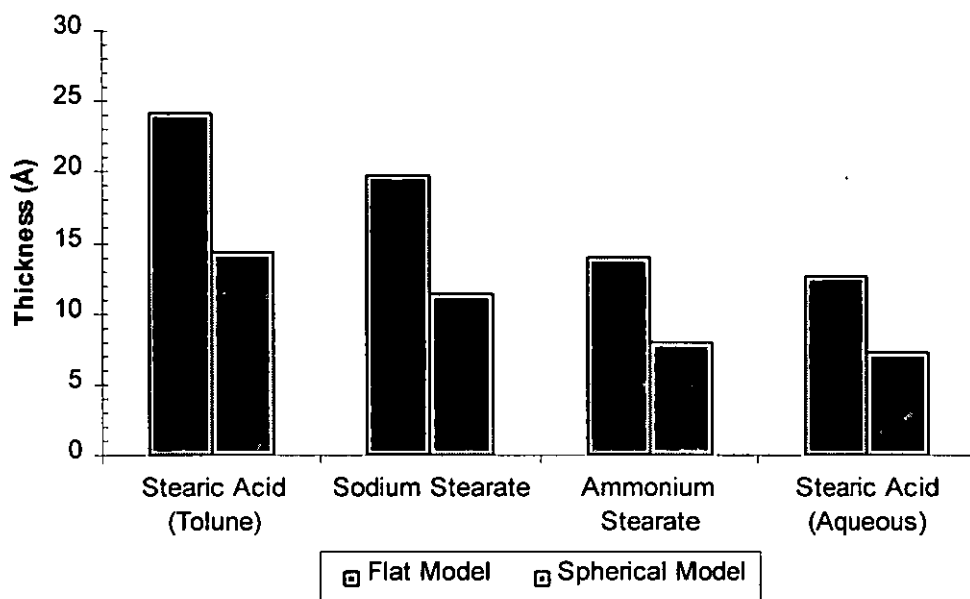


Figure 86 Comparison of the coating thickness produced using different coating methods calculated using the carbon/carbon ratio and the 'second' generation model

When the stearic acid in toluene coating method is used, the thickest coating is produced. This coating process is known to produce some non-bound calcium stearate<sup>19</sup>. On washing the coated PCC with toluene a lower thickness is obtained. This is calculated to be 16.3 Å for the flat model and 9.3 Å for the spherical model.

#### 4.5.2.4 Sample charging

During XPS sample analysis a trend in the charging induced in the photoemission process was detected. Charging is seen to reduce as the coating level is increased. This is consistent with the theory that a coated surface is a less intense photoemitter i.e. if less photoelectrons are emitted the sample is seen to charge less. This reduction is seen to be valid in the range of coating material addition from 0–0.6 monolayers. Above this level no further reduction is seen. The point

at which this occurs is consistent with the trends found by other techniques.

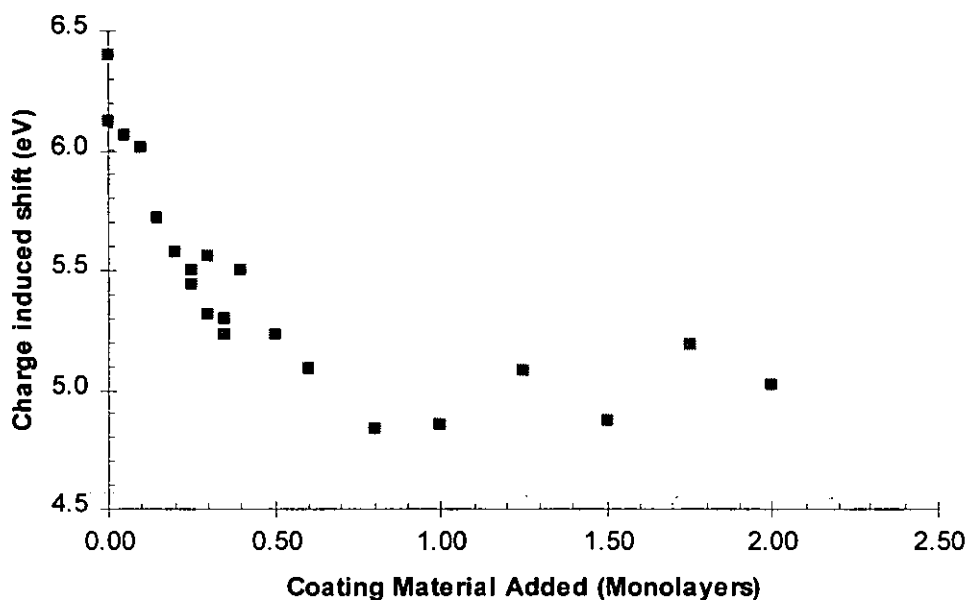


Figure 87 Coated Precipitated calcium carbonate, organic carbon peak charging referenced to adventitious carbon at 284.6 eV

### 4.5.3 Magnesium Hydroxide

Figure 88 shows two broad scan XPS spectra for coated and uncoated magnesium hydroxide. Spectra of this type will detect all elements other than hydrogen. No sodium could be detected (Na(A) B.E. 497 eV). As a result all the sodium stearate has reacted to produce magnesium stearate.

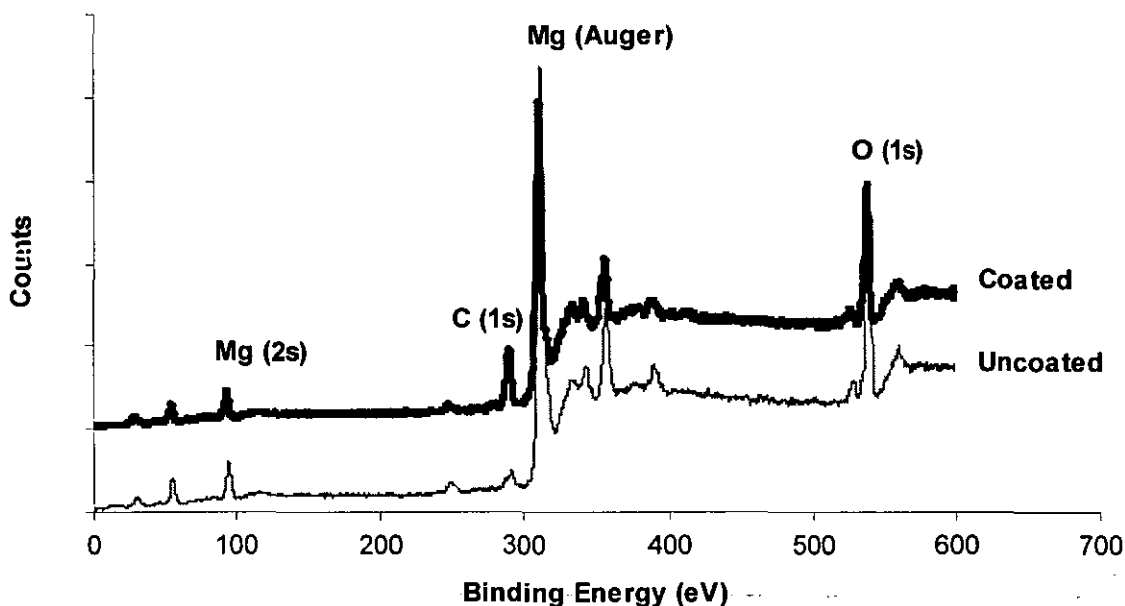


Figure 88 Broad scan XPS spectra of sodium stearate coated and magnesium hydroxide

### 4.5.3.1 Sodium Stearate Coatings

#### 4.5.3.1.1 Sodium Stearate Coatings and the Geometric Model

The basic analysis of the magnesium hydroxide filler indicates a surface structure that is different from the expected bulk magnesium hydroxide (brucite) structure. This would suggest that the natural filler has a magnesium to oxygen ratio of approximately 1:1, which is twice the ratio (1:2) expected for magnesium hydroxide. If the atomic composition of the surface is taken as an indication of surface structure, we might assume that the surface has a chemical composition equivalent to magnesium oxide (MgO). FTIR has also indicated the presence of carbonate. The concentration of the magnesium indicated by the atomic composition is in excess of this estimation.

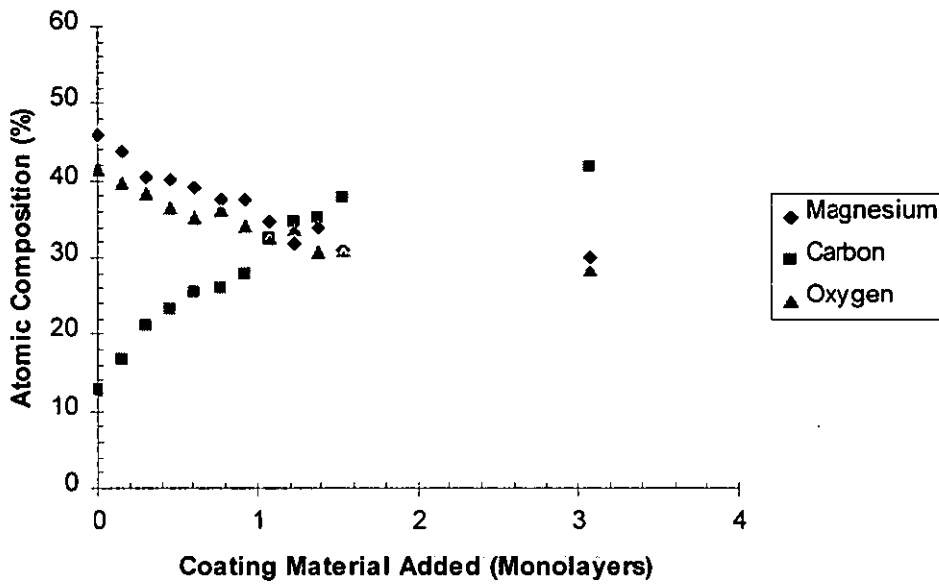


Figure 89 Atomic composition calculated by XPS of a magnesium hydroxide filler coated with sodium stearate

#### 4.5.3.1.2 Sodium Stearate Coatings and the 'Second' Generation Model

The parameters chosen as the basis on which the 'second' generation model are based are important. As a result of the information obtained in Figure 89 analysis of the filler is based on the surface composition of the filler being closer to magnesium oxide rather than magnesium hydroxide. The CS2 and the solid properties (magnesium oxide) are based on the physical data contained in Table 19.

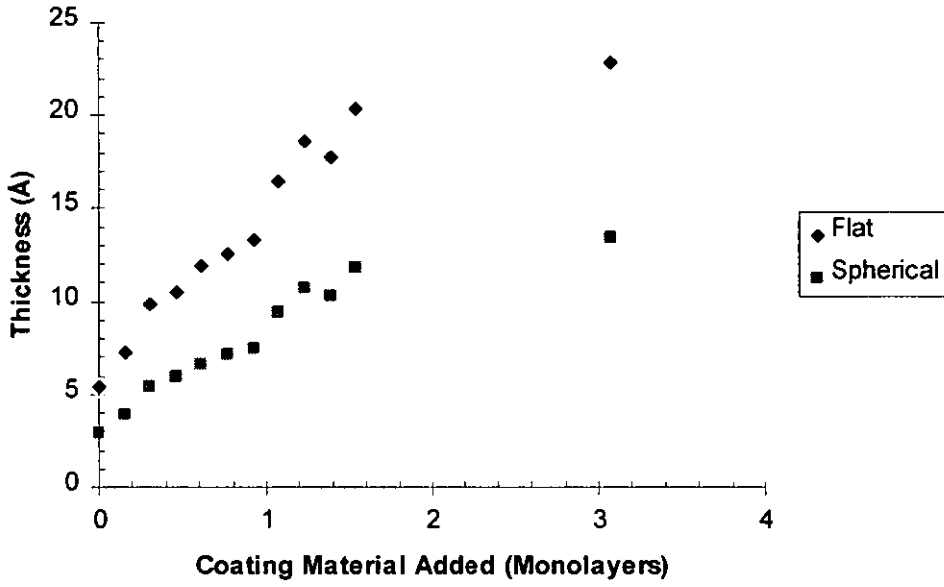


Figure 90 Coating thickness of sodium stearate coated magnesium hydroxide calculated using carbon/magnesium ratio and the 'second' generation models

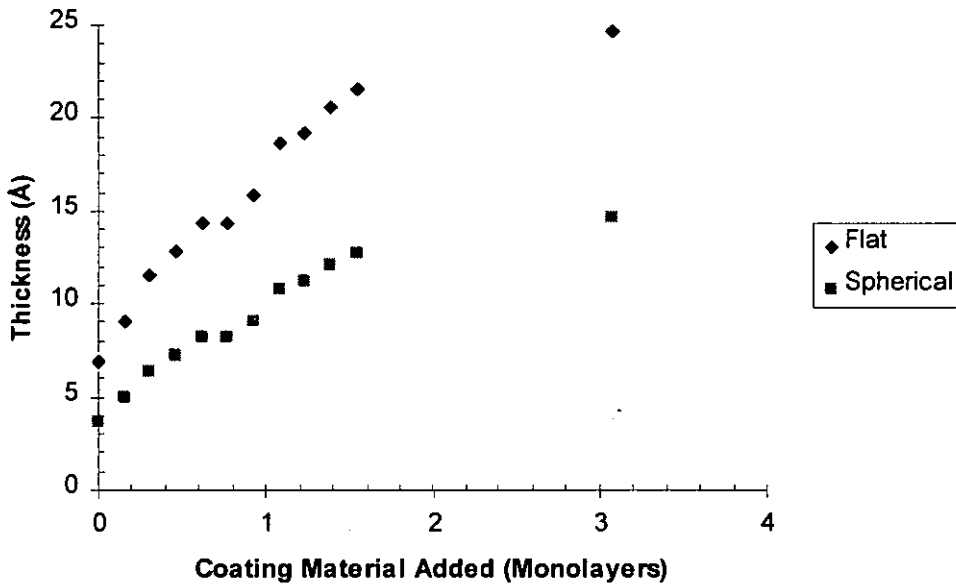


Figure 91 Coating thickness of sodium stearate coated magnesium hydroxide calculated using carbon/oxygen ratio and the 'second' generation models



The coating was analysed assuming that the surface was composed of magnesium hydroxide and the thickness of the coating calculated from the carbon/oxygen ratio was found to be approximately twice that which would have been expected from the carbon/magnesium ratio.

Using the spherical model, the thickness of a coating after sufficient material is added to produce a theoretical monolayer is calculated to be 9 Å and in the case of the flat model 15 Å. Both values fall short of the 24.3 Å calculated<sup>64</sup> for the length of an 18-carbon alkyl chain extended perpendicular to the surface, which would be expected at theoretical monolayer coverage. The coating thickness is seen to increase as more coating material is added above the theoretical monolayer. The plateau is achieved when approximately one and half times the material required for a theoretical monolayer is added. The coating thickness at which the plateau is achieved is calculated to be 19 Å for the spherical model and 27 Å for the flat model. These values are in good agreement with the theoretical value of 24.3 Å calculated<sup>64</sup> for a close packed monolayer.

## 4.6 XRD

### 4.6.1 Sodium & Calcium Stearate

X-Ray diffraction patterns were obtained for the starting stearate form, sodium stearate, and the final stearate form, calcium stearate. Diffraction patterns are caused by a repeated crystalline structure. If this is formed it should be visible in the X-ray diffraction patterns of the coated material. The position at which this peak occurs is dependent on the lattice spacing.

The diffraction patterns obtained for the sodium and calcium stearate are shown in Figure 92.

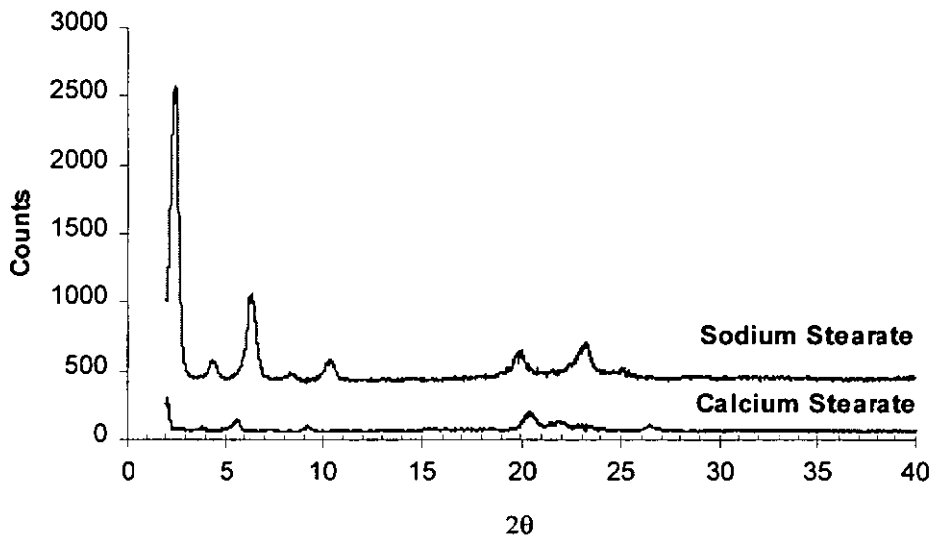


Figure 92 X-Ray diffraction pattern of sodium and calcium stearate

The diffraction pattern obtained for these stearates is weak in comparison to that of the inorganic filler. The most intense calcium stearate diffraction occurs when  $2\theta$  is approximately  $20.5^\circ$ , this can be seen in greater detail in Figure 93. The calcium stearate diffraction pattern is in good agreement with that expected<sup>153</sup>.

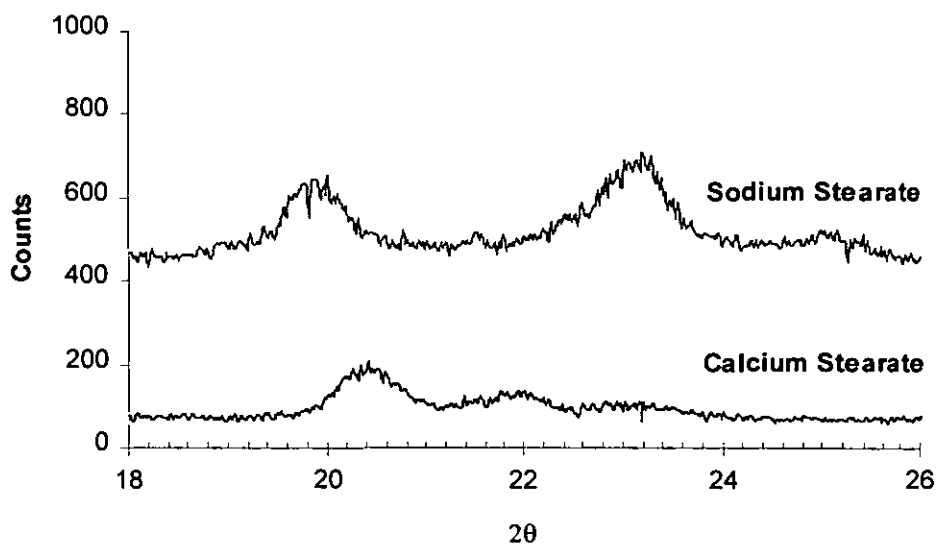


Figure 93 X-Ray diffraction pattern of sodium and calcium stearate

#### 4.6.2 Calcium Carbonate

X-Ray diffraction patterns were obtained for uncoated and coated calcium carbonate fillers. Coatings in the range of 0 to 2 monolayers showed little or no change on coating (Figure 94).

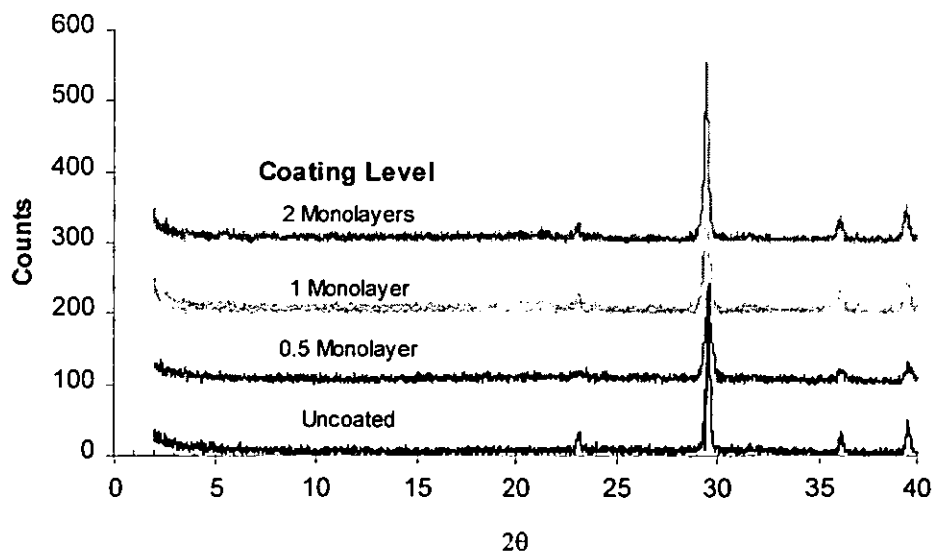


Figure 94 X-Ray diffraction pattern of sodium stearate coated calcium carbonate (0 –2 monolayers)

The calcium carbonate diffraction pattern is in good agreement with that expected  
153

To test this technique higher coating levels were produced. These spectra also showed little/no crystalline calcium stearate structure as expected from Figure 92 and Figure 93.

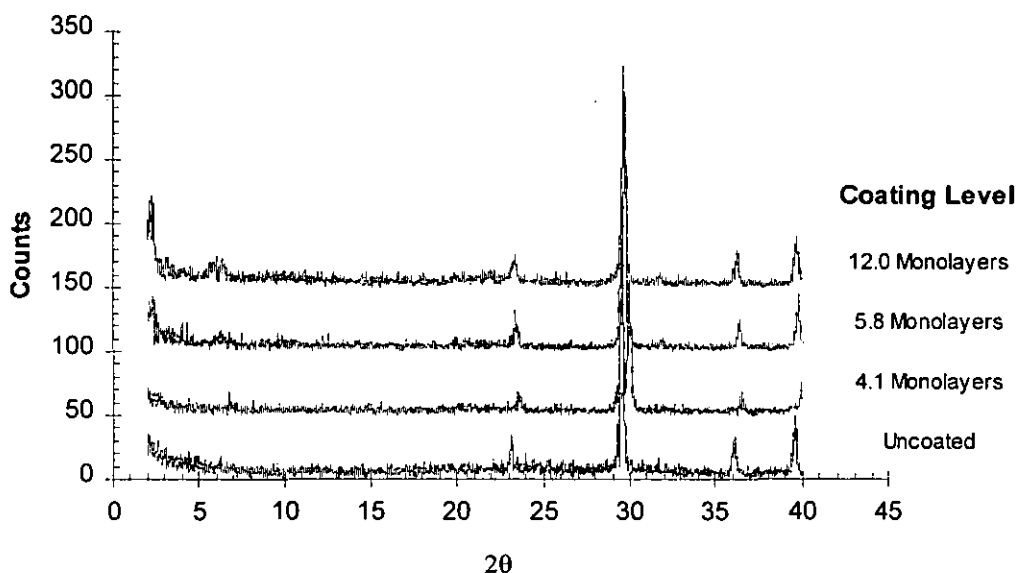


Figure 95 X-Ray diffraction pattern of sodium stearate coated calcium carbonate (4 –12 monolayers)

A small change in the diffraction pattern is detected at the low diffraction angles. These angles are at the limit of the machines detection range, and should be interpreted with care.

## 4.7 DMTA Analysis

In understanding the effect of surface coating we must also understand the effect that this has on the mechanical properties related to the surface or composite. Characterisation of the composites properties in terms of the interfacial and interphase interactions is difficult (see Section 2.7.7 Dynamic Mechanical Analysis (DMA)). By keeping as many parameters as possible constant, an attempt has been made to characterise the mechanical properties of a composite as a function of only either the coating level, or the volume of filler.

### 4.7.1. Dynamic Mechanical Response of uPVC.

When templates are produced and analysed as described in Section 3.3.7 DMTA Experimental Analysis, the samples are found to have one transition in the temperature range of  $-50$  to  $100^{\circ}\text{C}$ . This occurs at approximately  $50^{\circ}\text{C}$  (Figure 96).

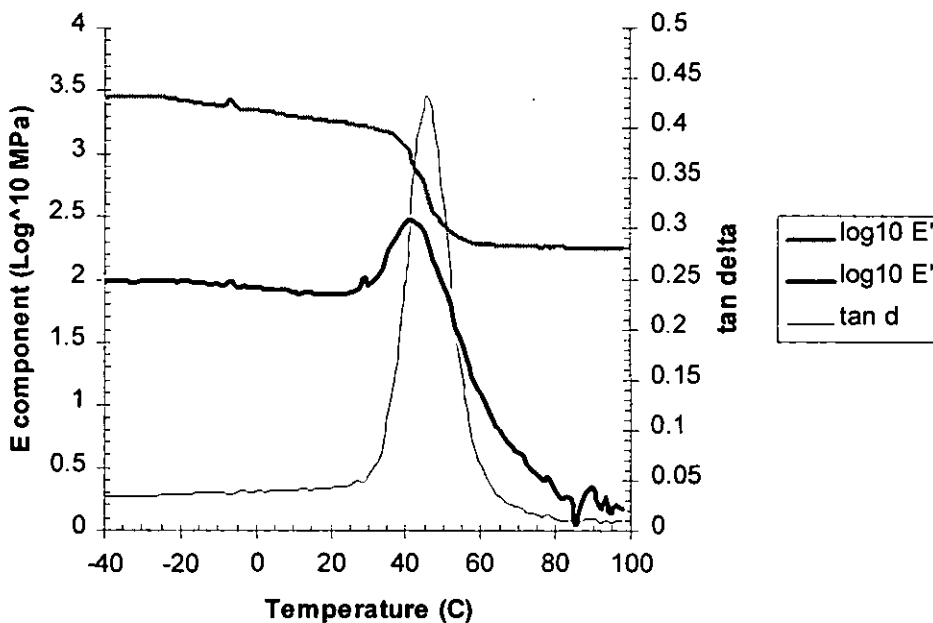


Figure 96 Dynamic mechanical response of uPVC

The position of the  $\tan \delta$  peak is at a higher temperature than the  $T_g$  shown in DSC analysis. The analysis by DSC of samples of unprocessed and processed uPVC indicates that there is no change in transition caused as a result of the solvent processing.

## 4.7.2 Dynamic Response of uPVC Composites

### 4.7.2.1 Dynamic Response as a function of filler loading

On loading the polymer with different amounts of uncoated filler, the response of the composite produced is seen to change. The different levels of filler additions are compared in terms of the components of their dynamic mechanical response in Figure 97, Figure 98 and Figure 99.

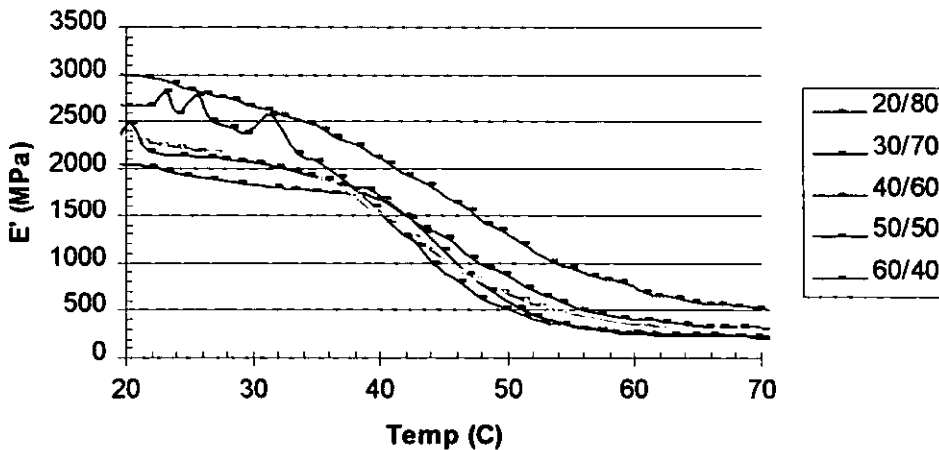


Figure 97  $E'$  Component of the dynamic mechanical response of uPVC – uncoated filler composites (Filler composition varying as a weight filler/weight polymer)

The storage modulus results shown in Figure 97 suggest that at low temperatures the thermal history apparently effects the recorded storage modulus. At low temperatures the storage modulus is also known to be more sensitive to variations

The position of the  $\tan \delta$  peak is at a higher temperature than the  $T_g$  shown in DSC analysis. The analysis by DSC of samples of unprocessed and processed uPVC indicates that there is no change in transition caused as a result of the solvent processing.

## 4.7.2 Dynamic Response of uPVC Composites

### 4.7.2.1 Dynamic Response as a function of filler loading

On loading the polymer with different amounts of uncoated filler, the response of the composite produced is seen to change. The different levels of filler additions are compared in terms of the components of their dynamic mechanical response in Figure 97, Figure 98 and Figure 99.

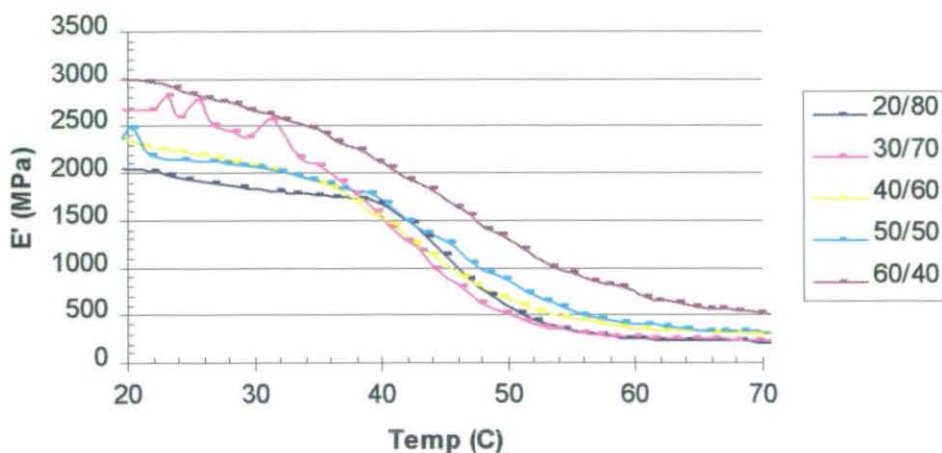


Figure 97  $E'$  Component of the dynamic mechanical response of uPVC – uncoated filler composites (Filler composition varying as a weight filler/weight polymer)

The storage modulus results shown in Figure 97 suggest that at low temperatures the thermal history apparently effects the recorded storage modulus. At low temperatures the storage modulus is also known to be more sensitive to variations

in sample size. The variation in the 60/40 sample is most likely the result of the loading limit of the composite with filler being reached. As the point at which the  $\tan \delta$  maxima is approached (approx. 50 °C), the thermal history becomes less important and is eliminated. At temperatures above the  $\tan \delta$  maxima the increase in filler loading results in an increase in storage modulus.

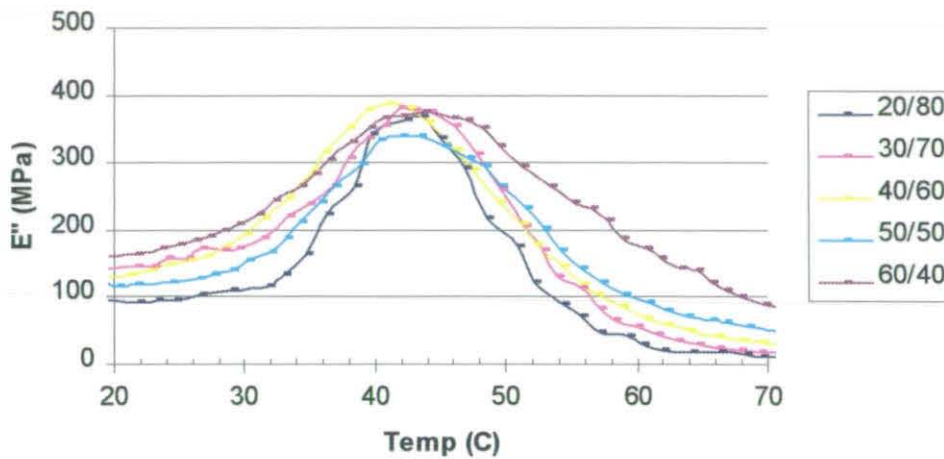


Figure 98 E'' Component of the dynamic mechanical response of uPVC – uncoated filler composites (Filler composition varying as a weight filler/weight polymer)

From the interpretation of the loss modulus peaks (Figure 98) we might conclude that as the filler loading increases the position of the loss modulus peak remains almost constant, but the width of the peak increases with filler loading.



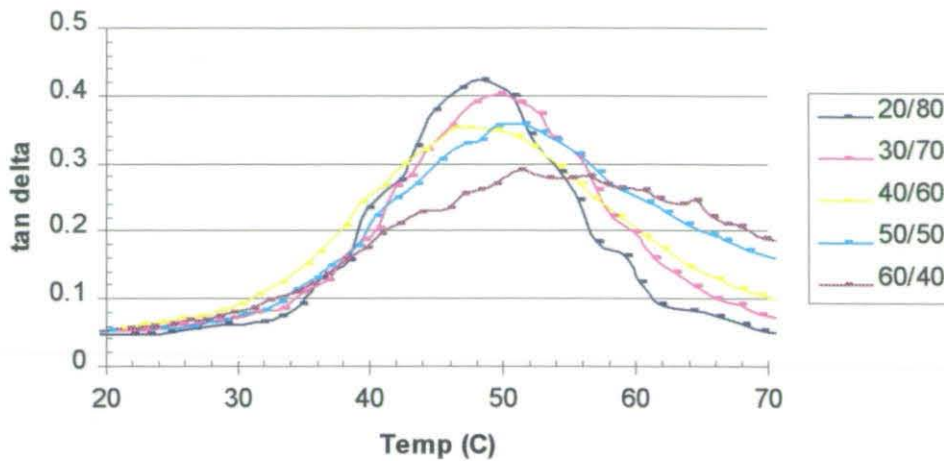


Figure 99 Tan  $\delta$  of the dynamic mechanical response of uPVC – uncoated filler composites (Filler composition varying as a weight filler/weight polymer)

From Figure 99 we might conclude that as the filler loading increases the maximum value of the tan  $\delta$  decreases. This can be interpreted as a direct result of the decrease of the quantity of polymer in the composite. The broadening is consistent with some chains becoming more constrained.

#### 4.7.2.2 Dynamic Response as a function of coating level

On loading the filler with different amounts of uncoated filler the response of the composite produced is seen to change. The different levels of filler additions are compared in terms of the components of their dynamic mechanical response in Figure 100, Figure 101 and Figure 102.

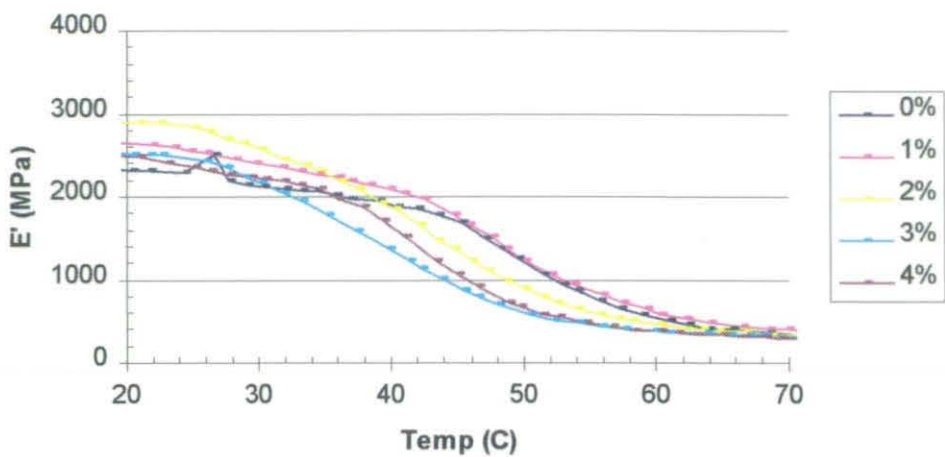


Figure 100 E' Component of the dynamic mechanical response of uPVC – filler composites (50/50 Filler/Polymer loading, coating levels in w/w%)

Above the glass transition point the storage modulus of the different samples become very similar, with the coated samples having a slightly lower storage modulus (Figure 100).

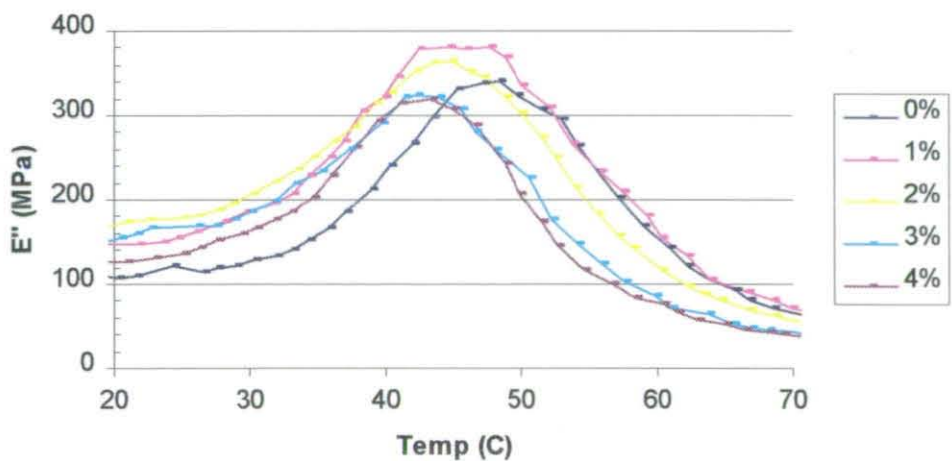


Figure 101 E'' Component of the dynamic mechanical response of uPVC – filler composites (50/50 Filler/Polymer loading, coating levels in w/w%)

These results show a shift in the loss modulus to lower temperatures as the coating level increases (Figure 101).

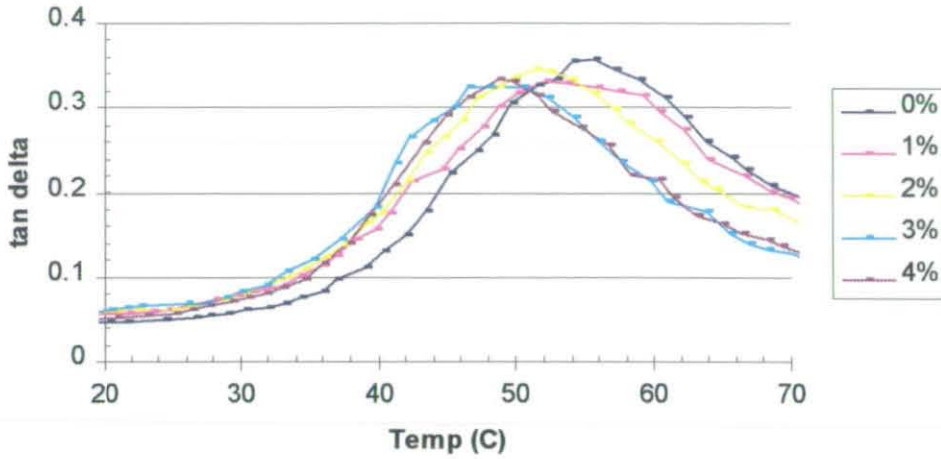


Figure 102 Tan  $\delta$  component of the dynamic mechanical response of uPVC – filler composites (50/50 Filler/Polymer loading, coating levels in w/w%)

These tan  $\delta$  profiles can be separated into 2 basic profiles and one composite profile. A basic profile being the result of either a coated or a uncoated filler, and the composite being a mixture of the two.

The effect of coating on the composite properties is a lowering in temperature of the point at which the tan  $\delta$  maximum occurs.

# Chapter 5 Discussion

Each analytical technique is discussed individually. The use of each technique as part of a multi-technique analysis is made.

## 5.1 Electron Microscopy

Electron Microscopy allows a visual analysis of the particle shape. Statistical analysis of these images enables an analysis of the particle size distribution and an approximation of the surface area to be made.

### 5.1.1 Electron Microscopy and Gas Adsorption Analysis

Transmission electron microscopy distribution analysis results may be used to verify experimentally measured BET surface area values.

A wide particle size difference often has a detrimental effect on composite properties.

Variations in particle size distribution, are often not immediately visible during normal quality assurance e.g. coat level analysis. These variations are easily detected by TEM particle size analysis. The operational cost of this technique is too high for the filler industry to make it a practical quality assurance technique.

Analysis of these distributions (Table 15) allows a validation of other experimentally observed surface area phenomena e.g. specific surface area. Variations in the experimental analysis of the surface area of the filler by gas adsorption and BET analysis can be explained in terms of the particle size distribution.

By establishing a link between TEM and BET analysis we are able to improve our knowledge of the morphology of the calcium carbonate. Under controlled

conditions this can be a powerful quality assurance tool.

## 5.2 Thermal analysis

Thermal analysis is a commonly used tool in many areas of chemistry for the analysis not only of decomposition profiles but to measure the organic material present within a system. Both techniques offer a comparably quick and simple way to calculate the quantity of stearate within the filler system. (TGA requires more preparation than CHN). Neither technique allows the distribution of the coating over the filler to be determined.

The CHN method, although simple and based on a semi-quantitative technique, suffers especially in the case of calcium carbonate from additional carbon decomposition products and also from low levels of sensitivity. Additional assumptions regarding the decomposition of the substrate have to be made when analysing the results and no account is taken for the amount of water contained in the system. With some improvement in analytical technique this approach has some possibilities as a method of quick and simple analysis.

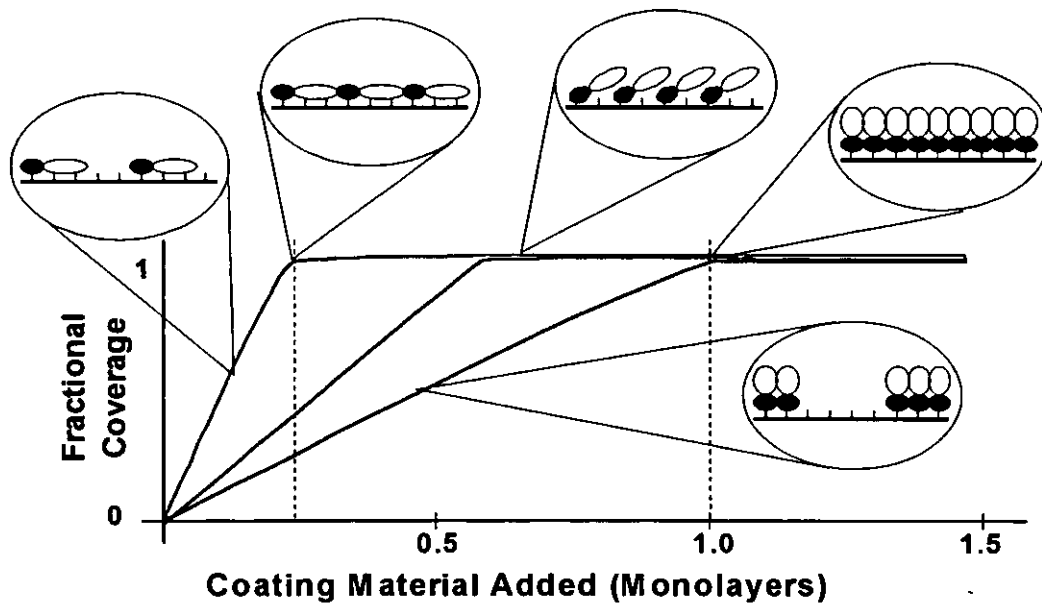
The TGA method has been developed <sup>175</sup> to enable accurate calculation of the level of coating material within the system. The major advantage of this technique over CHN is that one does not need to consider the decomposition of the filler substrate. The TGA tool has been developed so that a visual inspection of the TGA decomposition profile also enables the user to gather some information on the level of water content with the filler system and also the level of stearic acid conversion to stearate.

### **5.3 Gas Adsorption Analysis**

Gas adsorption is routinely used as a method of specific surface area determination. The values obtained have been confirmed using TEM analysis (see Section 4.1.2.2 Transmission Electron Microscopy). More information than just the specific surface area can be obtained from the adsorption isotherm. This technique is routinely used in industry, and the additional information that can be obtained from the adsorption isotherm is often not exploited.

Gas adsorption isotherm analysis also allows the analysis of the surface energy of the material (see Section 2.7.3 Gas Adsorption Isotherm Analysis). Using the new Dual BET adsorption isotherm tool, the fractional coverage of the coating has been estimated. It has been found that, for the calcium carbonate filler, complete coverage, or a maximum reduction in surface energy occurs when approximately 0.5-0.6 theoretical monolayers of coating material have been added to the system.

To fully understand the dual BET adsorption we must first consider the possible scenarios.



(Assuming the maximum packing model is the final conformation)

Figure 103 Possible coating confirmation scenarios and the effect on the coverage  $L$  calculated using the BET dual adsorption isotherm equation

As discussed in section 2.6.1 A 'Monolayer' Coating, two extremes of coating chain conformation can be imagined. If the chains occupied a conformation similar to the layer model we would have expected to have seen the coating coverage level  $L$  reach 1 when 0.2 monolayer of coating material had been added to the system. As a result the layer model (described in Section 2.6.1 A 'Monolayer' Coating) can be eliminated as a possible coating structure. The exact confirmation of the chains after the coating has been completed cannot be determined by Dual BET adsorption analysis alone.

## 5.4 IR analysis

It has been shown that IR analysis in the diffuse reflectance mode is suitable for the analysis of the filler powders. Both quantitative data and chemical information can be obtained by IR analysis.

### 5.4.1 Quantitative IR analysis

Quantitative IR analysis (see Section 4.4.1 Calcium Carbonate) of the powders demonstrates that the coating material added to the filler is in the close vicinity of the surface. IR analysis alone is not able to indicate the formation of a monolayer. The analysis demonstrates that the coating material is still being deposited in the surface region above the level expected for a monolayer. Some deviation from this is seen at high coatings because at these levels the limited surface specificity of the DRIFT technique become apparent. The comparably low absorbance of individual stearate particles present in a mixture with the coated/uncoated calcium carbonate, have been shown to be a possible reason (Figure 57). A constant efficiency is seen for all stearate coatings on calcium carbonate and magnesium hydroxide. A slight variation in coating efficiency is seen for different coating methods.

The difference between reacted and unreacted acid is easily detectable. This is useful in determining the 'real' efficiency of the coating process as a direct quantitative analysis does not take into account the unreacted acid that is still present at the surface.

DRIFT is both surface specific and very sensitive. On  $20 \text{ m}^2\text{g}^{-1}$  particles detection limits of 0.05 of a monolayer and less can be achieved. This means that the technique is more sensitive to coatings than XPS.

### 5.4.2 Surface Chemistry

It has been shown that FTIR can be used to determine not only the quantity of the stearate present but also whether or not it has reacted. In the case of the dry



coating method, unreacted stearic acid can be detected (Section 4.4.1.5 Stearic Acid Dry Coated).

It has been shown that differences in the stearate end group configuration (the environment of the stearate ion) can be detected (Section 4.4.1.9 Comparison Of Coating Peaks). A summary of possible assignments is given in Table 21.

Peak Position (cm <sup>-1</sup> )	Coating Process	Chemical Nature of Peak
1700	N/A	Unreacted acid
1680	Dry coating	Unknown
1625–1630	High level sodium stearate coating	Hydrated calcium stearate
1575–1580	Calcium stearate	Unhydrated calcium stearate Ca(C <sub>18</sub> H <sub>35</sub> O <sub>2</sub> ) <sub>2</sub>
1560	Calcium stearate	Surface bound calcium stearate lattice-Ca-C <sub>18</sub> H <sub>35</sub> O <sub>2</sub>

Table 21 Proposed assignment of the IR characteristic coating peaks

It has been shown that the peak at 1700 cm<sup>-1</sup> is the result of unreacted stearic acid (Figure 60). If it assumed that heating or washing removes water of crystallization, we may assume that the peak at 1625-1630 cm<sup>-1</sup> is the result of water of crystallization (Figure 63)

The reaction of the stearate to form calcium stearate can occur at either the surface or in solution. Due to the insolubility of calcium stearate the time period over which the coating occurs increases the likelihood of producing bound stearate decreases. An unbound stearate is more likely to be at the surface, but not bonded directly to the surface (Figure 62). If this assumption is correct we can assume that the 1575 cm<sup>-1</sup> peak is caused by a non-bound stearate and the 1560 cm<sup>-1</sup> is caused by a surface bound stearate.

Using these peak assignments we might conclude that the Zeneca ammonium

stearate preparations produce less lattice bound calcium stearate than other wet coating techniques. The spectra of the Zeneca ammonium stearate coating has more in common with the 2 hour laboratory based ammonium stearate preparation.

This assignment is not conclusive. The peaks that occur at  $1580\text{-}1570\text{ cm}^{-1}$ , although distinct, are in most cases broad thus obscuring peaks that are listed in Table 16. Analysis of this region of the coated calcium carbonate filler spectrum is difficult as the subtraction is affected by the presence of the large carbonate band. This band is not present in magnesium hydroxide to such an extent. The change in spectrum (Figure 65) of the carbonate region actually provides more information regarding the coating process. As discussed in Section 4.4.2.1 Sodium Stearate, a loss of a substrate peak would actually suggest a reaction at the surface at magnesium sites previously occupied by carbonate ions. This would be expected as the carbonate ion is more soluble than the hydroxide ion. No additional information regarding the mechanism could be obtained from this set of results. A more in-depth analysis of the magnesium stearate peak might provide information that could be applied to different aqueous based stearate coating processes.

### **5.4.3 FTIR and Gas Adsorption Analysis**

Both FTIR (and also CHN and TGA) can be used to give a quantitative analysis of how much stearate is contained in the filler system. Unlike CHN and TGA that are entirely non-surface specific, FTIR does confirm that the stearate is present close to the surface.

This means that one might assume that, as the coating level has been shown to increase uniformly at a constant rate of coating material addition, the coating forms in a maximum packing model configuration and then perhaps develops a multilayer and/or cluster formation. This assumption cannot be made using FTIR technique as it is not sufficiently surface specific. The information regarding the

orientation of the coating can be best obtained using a more surface specific technique such as XPS.

## 5.5 XPS analysis

### 5.5.1 Coating Characterisation

Broad scan analysis enables an overview of the elemental nature of the coating and the substrate. In most cases the chemical information obtained is limited. The analysis of all samples has shown the removal of any elements indicative of the stearate precursor.

### 5.5.2 Coating Thickness Characterisation

The thickness of the coating can be calculated in a number of different ways and it is up to the user to select the most appropriate technique. The models are summarized in Section 4.5.1.8 Model Summary.

For sodium stearate coated calcium carbonate all of the second and third generation models the results are consistent. The flat model predicts a thickness of approximately 20 Å, and the spherical model predicts a thickness of approximately 11 Å. Both these figures are below the 24.3 Å<sup>64</sup> that which would have been expected if the stearate was on the surface in the maximum packing model confirmation. As a result we may conclude that either the coating produced is 'patchy' and the models used are invalid, or the coating produced is not in the maximum packing model confirmation and is in fact located at an angle to the surface (approximately 45-60 degree) or is not fully extended. Due to the nature of a sphere and the volume available to the coating at a fixed radius/surface area you would expect a coating to fall short of the expected value of 24.3 Å, but not half that which would be expected.

The question of the validity of the models can be answered by the use of a multi technique approach (Section 5.5.3 XPS and Gas Adsorption Analysis).

In the case of magnesium hydroxide the coating thickness is seen to increase above that which would be expected for a monolayer. This would suggest that not all of the stearate ends up in a uniform layer and that the coating process is not

100% effective. This would possibly suggest that some independent magnesium stearate particles are formed. The plateau is achieved when approximately one and half times the material required for a theoretical monolayer is added. This would suggest the coating process had a coating effectiveness of around 60-70 %. The coating thickness at which the plateau is achieved is calculated to be 19 Å for the spherical model and 27 Å for the flat model. These values are in good agreement with the theoretical value of 24.3 Å calculated<sup>64</sup> for a close packed monolayer. The magnesium hydroxide filler is plate-like in nature. If the thickness is correct it would suggest that the stearate head group size is most likely the determining factor in controlling the amount adsorbed, and therefore the coating thickness, alternatively there is less than one available reactive site per  $20 \times 10^{-20} \text{ m}^2$  of surface.

### 5.5.3 XPS and Gas Adsorption Analysis

When XPS is used in conjunction with Gas Adsorption the maximum layer model shown in Figure 103, must be reviewed depending on the final position of the stearate chains. The final position of the stearate chains can be determined from the '*second*' and '*third*' generation XPS models i.e. the thickness at which the intensity ratio plateaus.

For sodium stearate coated calcium carbonate the '*fourth*' generation flat model predicts a thickness of approximately 20 Å, and the spherical model predicts a thickness of approximately 11 Å. Both these figures are below the 24.3 Å<sup>64</sup>. As discussed in Section 5.5.2 Coating Thickness Characterisation this would suggest that the coating chain is located at an angle to the surface.

When this information is used in conjunction with the '*fourth*' generation models we are able to understand the way in which the coating attaches itself to the surface.

The profile of the intensity ratio for the '*fourth*' generation model can then be

interpreted as follows.

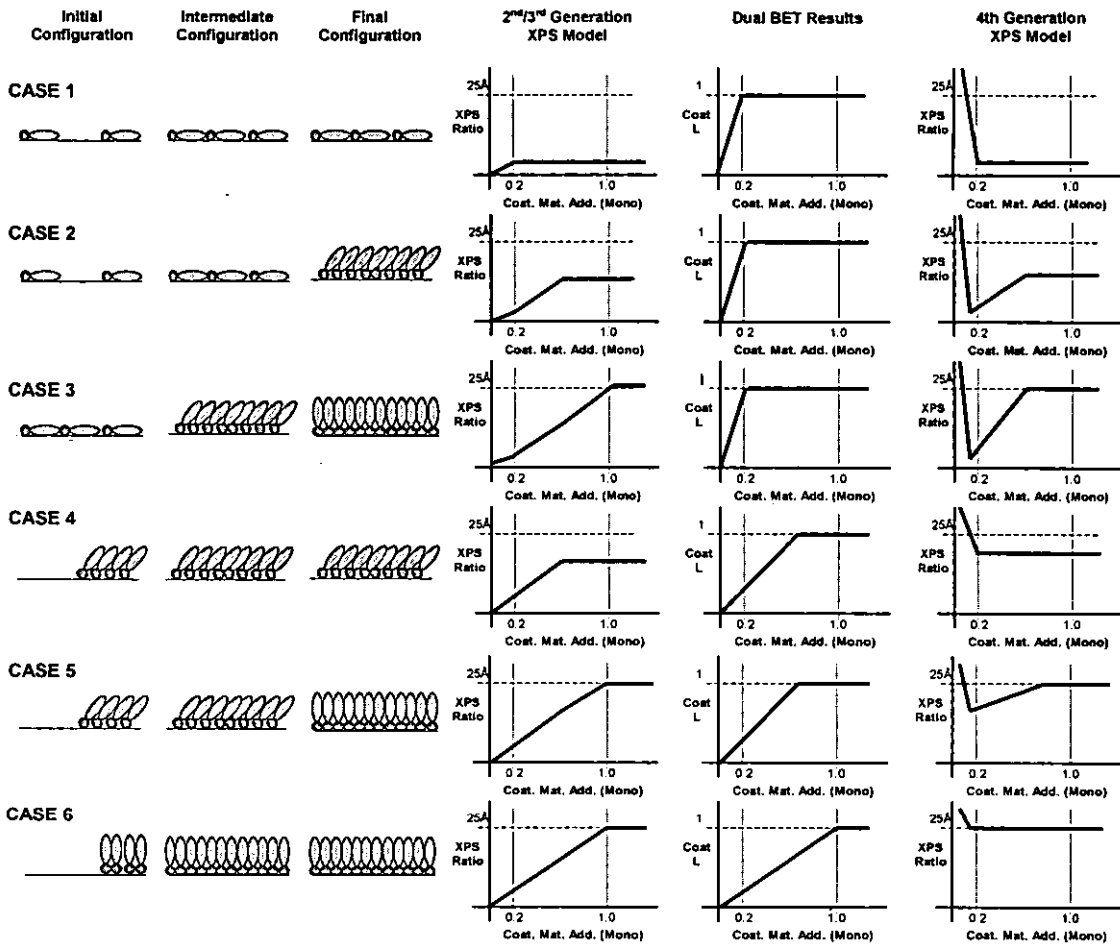


Figure 104 Summary of the XPS and dual BET results expected for different coating configuration

From the data we might conclude that we have a coating that is described by case 4 (Figure 104); the chains being located at the surface, but not in the maximum packing model as initially expected. The combined XPS-BET result would suggest that the formation of the coating is not by the formation of a flat layer of chains but by the build up of chains, close to existing chains. The chains are most likely laying at approximately a 45-60 degree angle to the surface.

With this information in mind we might consider the reason for this. If we consider the initial assumptions of surface area, head group area and chain length to be correct, then we might conclude (as discussed in Section 2.6.2 Surface Reactive Sites) that for a aqueous based coating method that the number of surface reactive sites per unit surface area available is less than would be required for a maximum packing model.

If we take into account the errors discussed in Section 4.5.1.6 Effect of Density and Section 4.5.1.7 Effect of Escape Depth we might conclude that there is approximately 1 available site per  $40 \times 10^{-20} \text{ m}^2$ . This is equivalent to approximately twice the area of the stearate headgroups.

#### **5.5.4 XPS and FTIR Coating Characterisation**

Using chemical information obtained from both XPS and FTIR we are able to more conclusively understand the chemical form of the stearate on the surface. Neither technique alone provides all the information.

In the analysis of sodium and ammonium stearate coated calcium carbonate neither nitrogen nor sodium ions are detected in the XPS broad scan spectra. This would suggest that no pre-cursor material is present in the coated material. Quantitative FTIR shows that the stearate is being added to the system and that the material added is not present as stearic acid. From this may conclude that the stearate present on the filler surface is present as calcium stearate. This calcium stearate must be in particles in the vicinity of the surface (because it detected by DRIFT) but not in the form of a multilayer (as it is not detected by XPS).

## 5.6 XRD analysis

X-Ray diffraction data was inconclusive. No crystalline calcium stearate was detected in the coated filler system using the XRD facilities available. Layer structures approaching 10–100 nm are required for the generation of a sharp X-ray line. This is consistent with the formation of amorphous disordered layers or small numbers of layers. It is possible that in the high coating level samples that we are analyzing concentrations below the minimum detection levels of the apparatus.

Slight differences in the diffraction patterns were noticed at low values of  $2\theta$ . These variations were inconclusive and require further investigation. Small angle X-ray scattering, or neutron scattering would perhaps be better techniques for analysing these variations.



## 5.7 Mechanical Properties

The results obtained in Section 4.7.2.2 Dynamic Response as a function of coating level are consistent with those that would be expected for a range of materials with different coating levels.

As expected in this case it has been shown that immobilized layers are formed on particles in which there is a large energy of interaction<sup>65,79</sup>. These immobilized layers are reduced on coating as the energy of interaction between the filler and polymer decreases. It is well understood that at a molecular level coating the filler particles with an aliphatic chain will reduce the energy of interaction between filler and polymer. For a non-polar polymer these interactions are dominated by dispersion forces and the thermodynamic work of adhesion is given by the Fowkes equation,

$$W_{AD} = 2(\gamma_S^D \gamma_L^D)^{1/2}$$

Equation 6

where  $\gamma_S^D$  and  $\gamma_L^D$  are the dispersion components of the surface excess free energy of the filler and polymer respectively.

$\gamma_L^D$  is about 40 mJ m<sup>-2</sup><sup>179</sup>. It is more difficult to obtain a value for  $\gamma_S^D$ . Filler surfaces that have been exposed to air will have some hydroxylation and adsorbed impurities. A value of 58 mJm<sup>-2</sup> has been measured<sup>19</sup> by IGC. This is significantly lower than that calculated for an ideal clean surface, but is probably more representative of the situation in practice. Similarly, values of about 28 mJm<sup>-2</sup> have been obtained<sup>19</sup> for stearic acid coated fillers, which is in good agreement with theory and other measurements<sup>64</sup>. Using these values the thermodynamic works of adhesion for uncoated and coated filler are estimated to be 96 mJm<sup>-2</sup> and 67 mJm<sup>-2</sup> respectively. Thus coating reduces the thermodynamic

work of adhesion between filler and polymer by 30 %.  $W_{AD}$  of a coated filler is now slightly below that expected for polymer / polymer interactions of  $80 \text{ mJm}^{-2}$ .

The coating of the filler is seen to affect the immobilized layer. The  $T_g$  of the majority of the immobilized layer has been identified, and is about 4-5 degrees higher than that of the bulk polymer.



## Chapter 6 Conclusion

It has been long established that the coating of the filler can alter the properties of a composite. Although well known this effect has often been poorly documented.

The multi-technique approach to analysis has allowed a more detailed analysis of the filler coating. During this project it has been shown that not only the amount of coating present but the level of coverage can be determined.

Electron Microscopy has been used to verify the particle size and to validate the gas adsorption data. Thermal techniques offer a quick and easy approach to the analysis of the quantity of coating material. FTIR DRIFT has been successfully shown to allow the quantification of the extent of system coating. FTIR DRIFT spectra provides detailed information on the surface chemistry of the filler. The use of spectral subtraction and the analysis of different fillers has enabled, a more detailed analysis of the coating process, than that which has been carried out before. The analysis has shown that chemical changes occur at the surface, and that altering the coating process, can have an effect on the coating. While not as surface specific as XPS, FTIR has a high signal to noise ratio allowing lower levels of coatings to be detected.

The surface specificity of XPS allows the thickness of the surface coating to be estimated. Four models have been developed, and software designed that enables the calculation of the coating thickness for a number of different systems. These *'fourth'* generation models are the first models published that take into account the surface coverage of the coating, when calculating the coating thickness.

In the case of magnesium hydroxide the stearate coating thickness is similar to that which could have been expected ( $24.3 \text{ \AA}$ <sup>64</sup>). In the case of stearate coated calcium carbonate the coating thickness is considerably lower than that which would have been expected for a monolayer. The flat model predicts a thickness of

approximately 20 Å, and the spherical model predicts a thickness of approximately 11 Å. From this we might conclude that there are insufficient reactive sites on the calcium carbonate surface to form a theoretical monolayer that conforms to the maximum packing model.

The development of a new approach using the Dual BET adsorption isotherm model allows the calculation of the extent of coverage of the coating. This approach could be easily incorporated into routine surface area measurements, to give an indication of the surface coverage.

For a true estimate of coating thickness at low levels, a combined Dual BET adsorption isotherm model and XPS model has been developed which allows for the 'patchy' nature of the surface. It has been shown that the thickness of the coating is constant, and that the build up of the coating is by addition of coating material to the surface next to existing coating material.

The effect of filler content and coating on the mechanical properties of uPVC filled polymer composites has been demonstrated. This has been interpreted in terms of the change in filler surface energy and the reduction in the filler-polymer interaction. The change in mechanical properties is consistent with that which would have been expected from the surface coverage data.

This work has shown that the mechanism of coating, although not yet fully known is one step closer. A more in-depth, multi-coating process, multi-analytical analysis of coated fillers will enable the understanding of the coating to progress further. The mechanical analysis of samples as discussed is difficult and the work completed in this thesis pushed the limits of the available equipment. Although a correlation between the coating coverage and the mechanical modulus has been made, an alternative mechanical analysis tool will be required to analyse the effect of the coating/surface energy on the filler-polymer interphase region.

# **Chapter 7 Appendices**

## **Appendix 1 Presentations & Publications**

### **Presentations**

**Loughborough Fillers Symposium II**, Loughborough, UK.

17<sup>th</sup> – 18<sup>th</sup> September 1996

Extended Abstract & Presentation

**International Symposium EURO-FLLERS '97**, Manchester, UK.

8<sup>th</sup> – 11<sup>th</sup> September 1997

Extended Abstract, Presentation & Poster

**Chemistry Research For Britain 98'**, London, UK.

17<sup>th</sup> March 1998

Abstract & Poster

**5<sup>th</sup> International Conference on Adhesion and Surface Analysis**,

Loughborough, UK.

31<sup>st</sup> March – 2<sup>nd</sup> April 1998

Extended Abstract & Poster

**7<sup>th</sup> International Symposium on Chemically Modified Surfaces**, Illinois, USA.

24<sup>th</sup> – 26<sup>th</sup> June 1998

Abstract & Presentation

**ESCA Users Group**, Chester, UK.

6<sup>th</sup> January 1999

Presentation

**International Symposium EURO-FILLERS '99**, Lyon, France.

6<sup>th</sup> – 9<sup>th</sup> September 1999

Extended Abstract & Poster.

### **Publications**

**Composite Interfaces**,

VSP, Holland

*Composite Interfaces*, Vol. 5, No.6, pp 493-502 (1998)

“Filler Surfaces and Composite Properties”

D. Maton, I. Sutherland, Department of Chemistry, Loughborough University, UK

D.L.Harrison, Zeneca Resins UK

**Fundamental and Applied Aspects of Chemically Modified Surfaces,**

RSC Publications, UK

Edited by J.P. Blitz & C.B. Little. Published 1999. ISBN 0-85404-714-X

“Filler surface Characterisation and its relation to Mechanical Properties of Polymer Composites”

D. Maton, I. Sutherland, Department of Chemistry, Loughborough University, UK

D.L.Harrison, Zeneca Resins UK

# Appendix 2 Visual Basic XPS Thickness Calculation Program

## User Interface

**XPSTC - Main Screen**

File Analysis Theory Help

**Method**

- 1) Enter XPS Machine Parameters
- 2) Enter all data applicable to the substrate and coating
- 3) Press calculate to calculate the unknown parameters
- 4) Data has been exported to XPSTC.csv in the program directory

**Calculate**

**XPS Machine Parameters**

X Ray Source:

Work Function:

Machine Type:

**Coating Characteristics**

Element:

Peak:

Binding Energy:

IMFP:

MWT:

Number Density:

Coating Density:

RSF:

KE:

**Substrate Characteristics**

Element:

Peak:

Binding Energy:

IMFP in substrate:

IMFP in coating:

MWT:

Number Density:

Substrate Density:

RSF:

KE:

**Coating in Substrate**

Coating element present in substrate

Number Density:

IMFP in substrate:

**Coating Level**

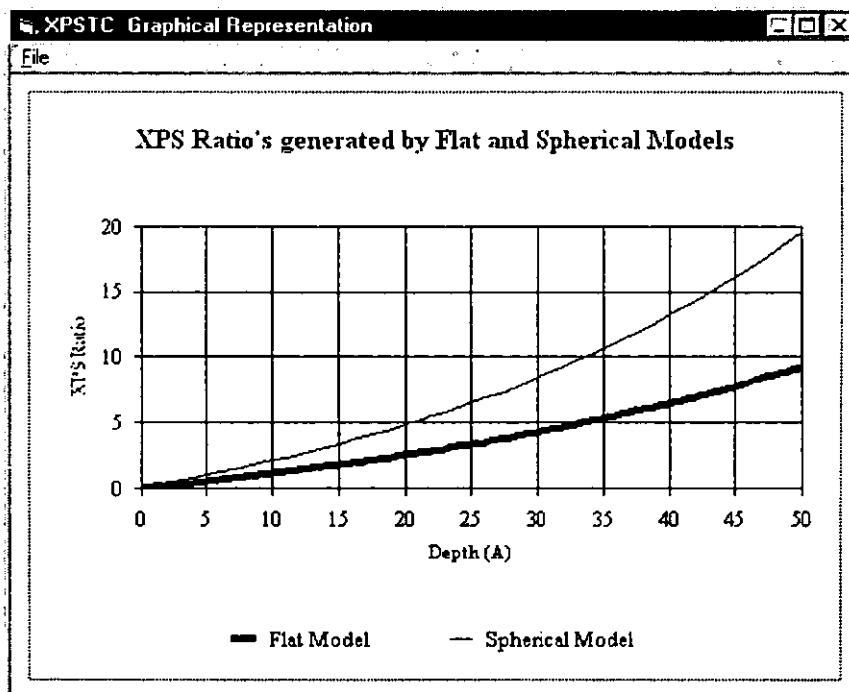
Non uniform coating level

Level of coverage:

**Model**

**Status**

## Result Presentation



## Program Code



Only the model sub routines are listed. Excluded are print, save results, save variables, graphing, KE calculations, RSF data file upload, experimental data analysis, and error checking sub routines.

'Flat Model

Public Sub flatmodel()

txtstatus.Text = "Starting Flat Model v2"

Dim top As Single

Dim bot As Single

For d = 1 To 500

top = coatimfp \* (coatdensity / coatmwt) \* coatnd \* (1 - Exp(-(d / 10) / coatimfp))

bot = subimfps \* (subdensity / submwt) \* subnd \* Exp(-(d / 10) / subimfpc)

RatioArray(d).ratioflat = mpara \* top / bot

Next d

txtflatmodel.Text = "Flat v2"

End Sub 'flatmodel()

'Flat Model

Public Sub flatmodelv2()

txtstatus.Text = "Starting Flat Model v3"

Dim top As Single

Dim bot As Single

For d = 1 To 500

top = (coatimfp \* (coatdensity / coatmwt) \* coatnd \* (1 - Exp(-(d / 10) /  
coatimfp))) + ((subcoatimfps \* (subdensity / submwt) \* subcoatnd \* Exp(-(d / 10)  
/ coatimfp)))

bot = subimfps \* (subdensity / submwt) \* subnd \* Exp(-(d / 10) / subimfpc)

RatioArray(d).ratioflat = mpara \* top / bot

Next d

txtflatmodel.Text = "Flat v3"

End Sub 'flatmodel v2()

```

'Spherical Model
Public Sub sphericalmodel()
txtstatus.Text = "Starting Spherical Model v2"

Dim top As Single
Dim bot As Single
Dim i As Integer
Dim a As Single
Dim pi As Single
pi = 3.1415926535

For d = 1 To 500

top = 0
bot = 0

For i = 1 To 2000

a = (pi / 2) * (i / 2001)

top = top + (coatimfp * (Sin(a) * Cos(a)) * (coatedensity / coatmwt) * coatnd * (1 -
Exp(-(d / 10) / (coatimfp * Sin(a))))))
bot = bot + (subimfps * (Sin(a) * Cos(a)) * (subdensity / submwt) * subnd *
(Exp(-(d / 10) / (subimfpc * Sin(a))))))

Next i

RatioArray(d).ratiospherical = mpara * top / bot
Next d
txtsphericalmodel.Text = "Spherical v2"

End Sub 'sphericalmodel()

```

```
'Spherical Model version 2
Public Sub sphericalmodelv2()
txtstatus.Text = "Starting Spherical Model v3"
```

```
Dim top As Single
Dim bot As Single
Dim i As Integer
Dim a As Single
Dim pi As Single
pi = 3.1415926535
```

```
For d = 1 To 500
```

```
top = 0
bot = 0
```

```
For i = 1 To 2000
```

```
a = (pi / 2) * (i / 2001)
```

```
top = top + (coatimfp * (Sin(a) * Cos(a)) * (coaldensity / coatmwt) * coatnd * (1 -
Exp(-(d / 10) / (coatimfp * Sin(a)))))) + (subcoatimfps * (Sin(a) * Cos(a)) *
(subdensity / submwt) * subcoatnd * (Exp(-(d / 10) / (coatimfp * Sin(a))))))
bot = bot + (subimfps * (Sin(a) * Cos(a)) * (subdensity / submwt) * subnd *
(Exp(-(d / 10) / (subimfpc * Sin(a))))))
```

```
Next i
RatioArray(d).ratiospherical = mpara * top / bot
Next d
```

```
txtsphericalmodel.Text = "Spherical v3"
End Sub 'sphericalmodelv2()
```

```
Public Sub flatmodelv3()  
'Fourth Generation Model (Part1)  
txtstatus.Text = "Starting Flat Model v4.1"
```

```
Dim top As Single  
Dim bot As Single
```

```
For d = 1 To 500
```

```
top = coatinglevel * (coatimfp * (coatdensity / coatmwt) * coatnd * (1 - Exp(-(d /  
10) / coatimfp)))
```

```
bot = coatinglevel * (subimfps * (subdensity / submwt) * subnd * Exp(-(d / 10) /  
subimfpc)) + ((1 - coatinglevel) * (subimfps * (subdensity / submwt) * subnd))
```

```
RatioArray(d).ratioflat = mpara * top / bot
```

```
Next d
```

```
txtflatmodel.Text = "Flat v4.1"
```

```
End Sub
```

Public Sub flatmodelv4()

'Fourth Generation Model (Part2)

txtstatus.Text = "Starting Flat Model v4.2"

Dim top As Single

Dim bot As Single

For d = 1 To 500

top = ((coatinglevel \* ((coatimfp \* (coatdensity / coatmwt) \* coatnd \* (1 - Exp(-(d / 10) / coatimfp))) + ((subcoatimfps \* (subdensity / submwt) \* subcoatnd \* Exp(-(d / 10) / coatimfp)))))) + ((1 - coatinglevel) \* (subcoatimfps \* (subdensity / submwt) \* subcoatnd)))

bot = ((coatinglevel \* (subimfps \* (subdensity / submwt) \* subnd \* Exp(-(d / 10) / subimfpc))) + ((1 - coatinglevel) \* (subimfps \* (subdensity / submwt) \* subnd)))

RatioArray(d).ratioflat = mpara \* top / bot

Next d

txtflatmodel.Text = "Flat v4.2"

End Sub

```
Public Sub sphericalmodelv3()
'Fourth Generation Model (Part1)
txtstatus.Text = "Starting Spherical Model v4.1"
```

```
Dim top As Single
Dim bot As Single
Dim i As Integer
Dim a As Single
Dim pi As Single
pi = 3.1415926535
```

```
For d = 1 To 500
top = 0
bot = 0
```

```
For i = 1 To 2000
a = (pi / 2) * (i / 2001)
```

```
top = top + ((coatimfp * (Sin(a) * Cos(a)) * (coatdensity / coatmwt) * coatnd * (1
- Exp(-(d / 10) / (coatimfp * Sin(a)))))) * (pi / 4000)
bot = bot + ((subimfps * (Sin(a) * Cos(a)) * (subdensity / submwt) * subnd *
(Exp(-(d / 10) / (subimfps * Sin(a)))))) * (pi / 4000)
```

```
Next i
```

```
RatioArray(d).ratiospherical = mpara * ((coatinglevel * top) / (((coatinglevel *
bot) + ((1 - coatinglevel) * (subimfps * (subdensity / submwt) * subnd) / 2))))
```

```
Next d
```

```
txtsphericalmodel.Text = "Spherical v4.1"
End Sub
```

```
Public Sub sphericalmodelv4()
'Fourth Generation Model (Part2)
txtstatus.Text = "Starting Spherical Model v4.2"
```

```
Dim top As Single
Dim bot As Single
Dim i As Integer
Dim a As Single
Dim pi As Single
pi = 3.1415926535
```

```
For d = 1 To 500
top = 0
bot = 0
For i = 1 To 2000
a = (pi / 2) * (i / 2001)
```

```
top = top + ((coatimfp * (Sin(a) * Cos(a)) * (coatdensity / coatmwt) * coatnd * (1
- Exp(-(d / 10) / (coatimfp * Sin(a)))))) + (subcoatimfps * (Sin(a) * Cos(a)) *
(subdensity / submwt) * subcoatnd * (Exp(-(d / 10) / (coatimfp * Sin(a)))))) * (pi /
4000)
```

```
bot = bot + ((subimfps * (Sin(a) * Cos(a)) * (subdensity / submwt) * subnd *
(Exp(-(d / 10) / (subimfpc * Sin(a)))))) * (pi / 4000)
```

```
Next i
```

```
RatioArray(d).ratiospherical = mpara * (((coatinglevel * top) + ((1 - coatinglevel)
* (subcoatimfps * (subdensity / submwt) * subcoatnd) / 2))) / (((coatinglevel *
bot) + ((1 - coatinglevel) * ((subimfps * (subdensity / submwt) * subnd) / 2))))
```

```
Next d
```

```
txtsphericalmodel.Text = "Spherical v4.2"
```

```
End Sub
```



## Chapter 8 References

---

- <sup>1</sup> D.Hull. An introduction to composite materials. Cambridge University Press. Cambridge. (1981)
- <sup>2</sup> I.S.Miles & S.Rostami (Ed.). Multicomponent polymer systems. Longman Scientific and Technical. (1995)
- <sup>3</sup> A.W. Birley, J.Batchelor & B. Howarth. Physics of plastics. Hanser Publishers. (1991)
- <sup>4</sup> R.Rothon (Ed.). Particulate-filled polymer composites. Longman Scientific and Technical. (1995)
- <sup>5</sup> P.R.S.Gibson, C.P.Pratt. Rubber J. Sept 3 (1969)
- <sup>6</sup> R.B.Bjorklund. App. Surf. Sci. 75 197 (1993)
- <sup>7</sup> M.B.Evans, R.N.Rothon, T.A.Ryan. Plastics Rubber Process Appl. 9 215 (1988)
- <sup>8</sup> D.S.Keller. Conference Proceedings, TAPPEI. 349 (1992)
- <sup>9</sup> D.Maton. BSc Project Report, Loughborough University, (1995)
- <sup>10</sup> A.Seville. BSc Project Report, Loughborough University, (1994)
- <sup>11</sup> R.N.Rothon, A.M.Ryder, T.A.Bourke. European patent. 0,568,488 (1993)
- <sup>12</sup> A.Packter. Crystal Res. Technol. 20 3 329 (1985)
- <sup>13</sup> Kyowa Chemical Industry. British patent. 1,514,081 (1978)
- <sup>14</sup> C.Birchenough. PhD Thesis, Loughborough University, (1997)
- <sup>15</sup> J.Kolarik, J.Jancar. Polymer. 33 23 4961 (1992)
- <sup>16</sup> Z.Demjen, B.Pukansky, E.Foldes, J.Nagy. J. Colloid and Int. Sci. 190 427 (1997)
- <sup>17</sup> E.Fekete. B. Pukansky, A.Toth, I.Bertoti, J. Coll. Int. Sci. 135 200 (1990)

- 
- <sup>18</sup> K.Liao, X.Chen, C.Zheng. *J. Appl. Polym. Sci.* 57 1245 (1995)
- <sup>19</sup> E.Papirer, J.Schultz, C.Turchi. *Eur. Polym. J.* 20 12 1155 (1984)
- <sup>20</sup> J.B.Griffiths. *Plastics and Rubber Processing and Applications.* 13 3 (1990)
- <sup>21</sup> L.Domka. *Colloid. Polym. Sci.* 272 1190 (1994)
- <sup>22</sup> T.Nakaatsuka, H.Kawasaki, K.Itandi, S.Yamashita. *J. Appl. Polym. Sci.* 27  
259 (1982)
- <sup>23</sup> H.P.Schreiber, J.Viau, A.Fetoui, Z.Deng. *Polym. Eng. Sci.* 30 5 263 (1990)
- <sup>24</sup> E.W.Washburn. *Phys. Rev* 17 273 (1921)
- <sup>25</sup> P.S.Murfitt. *Conference Proceedings, Fillers.* 8/1 (1986)
- <sup>26</sup> J.Jancar. *J. Materials Chem.* 24 3947 (1989)
- <sup>27</sup> J.W.Ess, P.R.Hornsby, S.Y.Lin, M.J.Bevis. *Plastics and Rubber Processing and Applications.* 4 7 (1984)
- <sup>28</sup> M.W.Darlington, R.S.V.Nascimento. *Conference Proceedings, Fillers.* 15/1 (1986)
- <sup>29</sup> R.W.Campbell. *Conference Proceedings, 36<sup>th</sup> Annual Technical Conference; Reinforced Plastics/Composites Institute.* 4-A 1 (1981)
- <sup>30</sup> J.Kolarik, B.Pukanzsky, F.Lednicky. *Conference Proceedings, Interfaces in Polymer and Ceramic Composites.* (1988)
- <sup>31</sup> W.A.Zisman, *ACS Adv. Chem. Series.* 43 1 (1964)
- <sup>32</sup> L.A.Girafalco, R.J.Good *J. Phys. Chem.* 61 904 (1957)
- <sup>33</sup> R.J.Good, L.A.Girafalco, G.Kraus *J. Phys. Chem.* 62 1418 (1958)
- <sup>34</sup> R.J.Good, L.A.Girafalco *J. Phys. Chem.* 64 561 (1960)
- <sup>35</sup> R.J.Good, *ACS Advances Chem.Ser.* 43 74 (1964)
- <sup>36</sup> R.J.Good, *Treatise on Adhesion vol. 1, Ed. R.L.Patrick, Dekker* (1967)
- <sup>37</sup> F.M.Fowkes, *Ind. Eng. Chem.* 56 40 (1964)

- 
- <sup>38</sup> F.M.Fowkes, J. Phys. Chem. 66 1863 (1962)
- <sup>39</sup> F.M.Fowkes, J. Adhesion. 4 155 (1972)
- <sup>40</sup> F.M.Fowkes, J.Phys.Chem. 67 2538 (1963)
- <sup>41</sup> D.K.Owens, R.C.Wendt J. Appl. Poly. Sci. 13 1741 (1969)
- <sup>42</sup> D.K.Owens, J. Appl. Poly. Sci. 14 1725 (1970)
- <sup>43</sup> J.Kloubek, Advances Colloid Int. Sci. 38 99 (1992)
- <sup>44</sup> S.Wu, J. Polym. Sci. Part C 34 19 (1971)
- <sup>45</sup> S.Wu, J. Adhesion. 5 39 (1973)
- <sup>46</sup> S.Wu, J. Macromol. Sci. Part C 10 1 (1974)
- <sup>47</sup> F.M.Fowkes, Polymer Sci. Tech. 12A, Ed. L.H.Lee, Plenum Press (1980)
- <sup>48</sup> F.M.Fowkes, J. Adhesion Sci. Technol. 1. 7 (1987)
- <sup>49</sup> C.J. van Oss, R.J.Good, M.K.Chaudhury, Langmuir, 4 884 (1988)
- <sup>50</sup> H.P.Schreiber, J. Adhesion, 37 51 (1992)
- <sup>51</sup> R.S.Drago, B.J.Wayland. J. Amer. Chem. Soc. 112 3259 (1965)
- <sup>52</sup> R.S.Drago, G.C.Vogel, T.E.Needham J. Amer. Chem. Soc. 93 6014 (1971)
- <sup>53</sup> R.S.Drago, L.B.Parr, C.S.Chamberlain J. Amer. Chem. Soc. 99 3203 (1977)
- <sup>54</sup> R.H.Bradley, I.Sutherland, E.Sheng. J.Coll. Int. Sci. 179 561 (1996)
- <sup>55</sup> H Balard, E Papirer, Conference Proceedings, MOFFIS-93, (1993)
- <sup>56</sup> E.Papirer, H.Balard, A.Vidal, Eur. Pol. J. 4 783 (1988)
- <sup>57</sup> J.Schultz, K.Tsutsumi, J.Donnet. J. Coll. Int. Sci. 59 2 272 (1977)
- <sup>58</sup> Z.Kessaissia, E.Papirer, J.Donnet. J. Coll. Int. Sci. 82 2 526 (1981)
- <sup>59</sup> A.C.Zettlemoyer. ~~Ind. Eng. Chem.~~ 57 27 (1965)
- <sup>60</sup> C.M.Liau, S.J.Hurst, G.C.Lees, R.N.Rothon, D.C.Dobson, Prog. Rubber Plas. Tech. 11 137 (1995)
- <sup>61</sup> E.Chibowski, L.Holysz. Langmuir. 8 710 (1992)

- 
- <sup>62</sup> E.Chibowski, L.Holysz. *Langmuir*. 8 717 (1992)
- <sup>63</sup> A.Siebold, A.Walliser, M.Nardin, M.Oppliger, J.Schultz. *J. Coll. Int. Sci.* 186  
60 (1997)
- <sup>64</sup> J.Israelachvili. *Intermolecular and surface forces*. Academic Press. 9 139  
(1985)
- <sup>65</sup> K.Kendall, F.Sherliker. *British Polym. J.* 12 85 (1980)
- <sup>66</sup> J.Jancar, A.T.DiBenedetto, A.DiAnselmo. *Polym. Eng. Sci.* 33 559 (1993)
- <sup>67</sup> P.G. De Gennes. *Macromolecules*, 13 1069 (1980)
- <sup>68</sup> G.C. Eastmond, G. Mucciariello. *Polymer*, 23 164 (1982)
- <sup>69</sup> E. Helfand (Ed). *Polymer compatability and incomptability*. Harwood  
Academic. (1982)
- <sup>70</sup> L.Domka. *J. Adhesion Sci. Technol.* 10 5 407 (1996)
- <sup>71</sup> M.S.Boaira & C.E.Chaffey. *Polym. Eng. Sci.* 17 715 (1977)
- <sup>72</sup> A.Einstein. *Investigations on the theory of Brownian motion*. Dover. (1956)
- <sup>73</sup> E.Guth. *J. Appl. Phys.* 16 20 (1945)
- <sup>74</sup> E.H.Kerner. *Proc. Phys. Soc: London.* B69 808 (1956)
- <sup>75</sup> T.S.Chow. *J. Mater. Sci.* 15 8 1873 (1980)
- <sup>76</sup> T.S.Chow. *Polymer*. 20 1576 (1979)
- <sup>77</sup> T.S.Chow. *J. Polym. Sci.* 20 2103 (1982)
- <sup>78</sup> D.M.Bigg. *Poly. Comp.* 8 2 (1987)
- <sup>79</sup> K.Iisaka, K.Shibayama. *J. Appl. Polym. Sci.* 22 3135 (1978)
- <sup>80</sup> J.J.Kipling, E.H.M.Wright. *J. Chem. Soc.* 160 855 (1962)
- <sup>81</sup> R.C.Weast (Ed). *Handbook of Chemistry and Physics*. The Chemical Rubber  
Company, Cleveland (1972)
- <sup>82</sup> P.Somasundaran, G.E.Agar. *J. Coll. Int. Sci.* 24 433 (1967)

- 
- <sup>83</sup> D.S.Cicerone, A.E.Regazzoni, M.A.Blesa. *J. Coll. Int. Sci.* 154 2 423 (1992)
- <sup>84</sup> N.Vdovic, J.Biscan. *Coll. Surf.* 137 7 (1998)
- <sup>85</sup> P.Siffert, P.Fimbel. *Coll. Surf.* 11 377 (1984)
- <sup>86</sup> M.Raetzsch, H.Jacobasch, K.Freitag, K.Grundke, G.Hermel. *J. Adhesion Sci. Technol.* 3 8 595 (1989)
- <sup>87</sup> C.N.Banwell. *Fundamentals of Molecular Spectroscopy*. McGraw-Hill, Maidenhead, (1983)
- <sup>88</sup> D.Briggs, M.P.Seah. *Practical Surface Analysis. Volume 1: Auger and X-ray Photoelectron Spectroscopy*. John Wiley & Sons Ltd. (1990)
- <sup>89</sup> D.Briggs, M.P.Seah. *Practical Surface Analysis. Volume 2: Ion and Neutral Spectroscopy*. John Wiley & Sons Ltd. (1992)
- <sup>90</sup> D.P.Ashton, R.N.Rothon, H.Ishida. *Controlled Interfaces in Composite Materials*, Elsevier, Amsterdam, (1990)
- <sup>91</sup> A.V.Kiselev, Y.I.Yashin. *Gas Adsorption Chromatography*, Plenum Press, New York, (1969)
- <sup>92</sup> G.D.Gray, U.B.Mohlin. *J. Coll. Int. Sci.* 47 747 (1974)
- <sup>93</sup> S.W.Sinton, J.C.Crowley, G.A.Lo, D.M.Kalyon, C.Jacob. *Soc. Plastics Eng. Ann. Technical Conf.* 116 (1990)
- <sup>94</sup> V.J.McBrierty. *Conference Proceedings, Eurofillers.* 67 (1997)
- <sup>95</sup> D.C.Douglas, V.J.McBrierty, T.A.Weber. *J. Chem. Phys.* 64 1533 (1977)
- <sup>96</sup> D.C.Douglas, V.J.McBrierty, T.A.Weber. *Macromolecules* 10 178 (1977)
- <sup>97</sup> T.H.Ferrigno, E.J.Wickson. *Handbook of PVC Formulating*. Wiley, New York, (1993)
- <sup>98</sup> British Standard BS3483: Part B7, (211)
- <sup>99</sup> T.Gren, C.Nystrom. *Int. J. Pharmaceutics.* 74 49 (1991)

- 
- <sup>100</sup> The Analysis of Fatty Acids and Fatty Alcohols. Technical publication No.6, Prices Ltd, Bromborough (1965)
- <sup>101</sup> T.Ashan. Colloids and Surfaces. 64 167 (1992)
- <sup>102</sup> Y.Wang, W.J.Thomson. Thermochemica Acta. 255 383 (1995)
- <sup>103</sup> F.W.Wilburn, J.H.Sharp, D.M.Tinsley, R.M.Mcintosh. J Therm. Anal. 37 9 2003 (1991)
- <sup>104</sup> J.Luhr, F.Janowski. Angewandte Makromolekulare Chemie. 205 1 (1993)
- <sup>105</sup> J.L.Whitcombe. Determination of coating level by thermogravimetry. Zeneca Resins (1995)
- <sup>106</sup> A.W.Adamson, A.P.Gast. Physical Chemistry of Surfaces, Wiley-Interscience, New York, (1997)
- <sup>107</sup> M.J.Jaycock, G.D.Parfitt. Chemistry of Interfaces, Ellis Horwood, Chichester, (1986)
- <sup>108</sup> S.Brunauer, L.S.Deming, W.S.Deming, E.Teller. J. Am. Chem. Soc. 62 1723 (1940)
- <sup>109</sup> A.W.Adamson, L.Dormat. J. Am. Chm. Soc. 88 2055 (1966)
- <sup>110</sup> I.Langmuir. J. Am. Chem. Soc. 40 1361 (1918)
- <sup>111</sup> S.Brunauer, P.H.Emmett, E.Teller. J. Am. Chem. Soc. 60 309 (1938)
- <sup>112</sup> T.L.Hill. J. Chem. Phys. 14 263 (1946)
- <sup>113</sup> S.J.Gregg, K.S.W.Sing. Adsorption, Surface area and Porosity. Academic Press. London. (1967)
- <sup>114</sup> S.Ross, J.P.Oliver. On Physical Adsorption, Interscience, New York, (1964)
- <sup>115</sup> A.W.Adamson, I.Ling. Adv. Chem. 33 51 (1961)
- <sup>116</sup> W.A.House, M.J.Jaycock. Coll. Polym. Sci. 256 52 (1978)
- <sup>117</sup> S.Ross, I.D.Morrison. Surf. Sci. 52 103 (1975)

- 
- <sup>118</sup> J.Koenig. *Adv. Polym. Sci.* 44 88 (1983)
- <sup>119</sup> H.Ishida. *Rubb. Chem. Tech.* 60 497 (1987)
- <sup>120</sup> R.G.Messerschmidt. *App. Spec.* 39 4 737 (1985)
- <sup>121</sup> A.L.Smith. *Chem. Anal.* 84 175 (1986)
- <sup>122</sup> H.G.Hecht, *J. Res.* 80A 4 (1976)
- <sup>123</sup> G.Socrates. *Infrared characteristic group frequencies: tables and charts.* Wiley. Chichester. (1994)
- <sup>124</sup> D.H.Williams, I.Fleming. *Spectroscopic methods in organic chemistry.* McGraw-Hill. London. (1995)
- <sup>125</sup> D.F.Hornig. *J. Chem. Phys.* 16 11 (1948)
- <sup>126</sup> W.Forsling et al. *Spec. Acta.* 50A 11 1857 (1994)
- <sup>127</sup> W. Sterzel, E. Chorinsky. *Spec Acta.* 24A 353 (1967)
- <sup>128</sup> H.A. Bensi, *J. Chem. Phys.* 30 852 (1959)
- <sup>129</sup> R.T.Mara, G.B.B.M.Sutherland. *J. Opt. Soc. Amer.* 43 1100 (1953)
- <sup>130</sup> L.L. Shevchenko. *Russian. Chem. Rev.* 32 4 201 (1963)
- <sup>131</sup> F.Vratny, M.Dilling. *Ana. Chem.* 33 10 1455 (1961)
- <sup>132</sup> D.W.Deamer, D.W.Meek, D.G.Cornwell. *J. Lipid Res.* 8 255 (1967)
- <sup>133</sup> R.J.Jakobsen, J.E.Katon. *Spec. Acta.* 29A 1953 (1973)
- <sup>134</sup> R.C.Lord, F.A.Miller. *Appl. Spec.* 10 115 (1956)
- <sup>135</sup> L.M.Coyne, S.W.S.McKeever, D.F.Blake. *Spectroscopic Characterisation of Minerals and their surfaces.* American Chemical Society. (1989)
- <sup>136</sup> W.Neagle, C.H.Rochester. *J. Chem. Soc. Faraday Trans.* 86 1 181 (1990)
- <sup>137</sup> A.Holmgren, L.Wu, W.Forsling. *Spectrochimic Acta.* 50A 11 1857 (1994)
- <sup>138</sup> M.Gilbert, I.Sutherland, A.Guest. *Conference Proceedings, Filplas '92.* Manchester (1992)

- 
- <sup>139</sup> D.A.Taylor, C.D.Paynter. Conference Proceedings, Fillers Symposium. (1994)
- <sup>140</sup> C.M.Liau, G.C.Lees, S.J.Hurst, R.N.Rothon, D.C.Dobson. *Plast. Rubb. Compos. Process Applns.* 24 211 (1995)
- <sup>141</sup> I.Sutherland, D.Maton. Conference Proceedings, Loughborough Fillers Symposium 2. (1996)
- <sup>142</sup> L.E.Davis, N.C.Macdonald, P.W.Palmberg, G.E.Riach, R.E.Weber. *Handbook of Auger Electron Spectroscopy.* Physical Electronics Industries Inc. Minnesota (1976)
- <sup>143</sup> M.P.Seah, W.A.Dench. *Surf. Int. Anal.* 1 2 (1979)
- <sup>144</sup> C.J.Powell, A.Jablonski, I.S.Tilinin, S.Tanuma, D.R.Penn. *J. Electron Spectrosc. Relat. Phenom.* 98-99 1 (1999)
- <sup>145</sup> O.A.Baschenko, V.I.Nefedov. *J. Electron Spectrosc. Relat. Phenom.* 27 109 (1982)
- <sup>146</sup> P.J.Cumpson, M.P.Seah. *Surf. Int. Anal.* 25 430 (1997)
- <sup>147</sup> A.Jablonski. *Surf. Sci.* 364 380 (1996)
- <sup>148</sup> H.Bethe. *Ann. Physik* 5 325 (1930)
- <sup>149</sup> S.Tanuma, C.J.Powell, D.R.Penn. *Surf. Interface Anal.* 21 165 (1994)
- <sup>150</sup> A.Jablonski, C.J.Powell. *J. Vac. Sci. Technol. A* 15 4 2095 (1997)
- <sup>151</sup> J.E.Fulghum, R.Stokell, G.McGuire, BiPatnaik, N.Yu, Y.J.Zhao, N.Parikh. *J. Electron Spectrosc. Relat. Phenom.* 60 117 (1992)
- <sup>152</sup> S.Tougaard. *Surf. Interface Anal.* 8 257 (1986)
- <sup>153</sup> Powder diffraction file (CD-ROM). JCPDS International Centre for Diffraction Data, Swarthmore. (1997)
- <sup>154</sup> C.M.Liau, R.N.Rothon, S.J.Hurst, G.C.Lees. *Composite Interfaces.* 5 6 503 (1998)



- 
- <sup>155</sup> Y.Wada, T.Matsubara. Powder Tech. 78 109 (1994)
- <sup>156</sup> K.D.Ertel, J.T.Carstensen. J. Pharmaceutical Sci. 77 7 625 (1988)
- <sup>157</sup> J.D.Ferry. Viscoelastic properties in polymers” 3<sup>rd</sup> Ed. J.Wiley, New York. (1980)
- <sup>158</sup> R.E.Wetton. Eur. Polym. J.. 2/3 131 (1993)
- <sup>159</sup> J.V.Dawkins (Ed). Developments in polymer characterisation. Chpt. 5 Elseiver . Applied Science (1993)
- <sup>160</sup> R. Wetton et al. Thermochimica Acta. 175 1 1 (1991)
- <sup>161</sup> R. Wetton et al. Journal de Physique. 46 5 689 (1985)
- <sup>162</sup> R.E.Wetton et.al. American Laboratory. 25 1 15 (1993)
- <sup>163</sup> L.E.Nielsen. Mechanical properties of polymers and composites. Marcel Dekker Inc. New York. (1974)
- <sup>164</sup> K.Pournoor, J.C.Seferis. Polymer. 32 3 445 (1991)
- <sup>165</sup> J.L.Thomason. Polymer Composites. 11 2 105 (1990)
- <sup>166</sup> T.B.Lewis, L.E. Nielsen. J. Appl. Polym. Sci.. 14 1449 (1970)
- <sup>167</sup> L.E.Nielsen. J. Polym. Sci.. 17 1897 (1979)
- <sup>168</sup> M.Y.Bolouk, H.P.Schreiber. Polym. Comp. 7 5 (1986)
- <sup>169</sup> A.Yim, R.S.Chahal, L.E. St-Pierre. J Colloid Interf. Sci.. 43 583 (1973)
- <sup>170</sup> P.S.Theocaris, G.D.Spathis. J. App. Polym. Sci. 27 3019 (1982)
- <sup>171</sup> J.Kubat, M.Rigdahl, M.Welander. J. App. Polym. Sci. 39 1527 (1990)
- <sup>172</sup> M.Sumita, H.Tsukihi, K.Miyasaka, K.Ishikawa. J. App. Polym. Sci.. 29 1523 (1984)
- <sup>173</sup> J.L.Acosta, M.C.Ojeda, A.Linares, M.Romero. Die Angewandte Makromolekulare Chemie. 139 201 (1986)
- <sup>174</sup> V.P.Chacko, F.E.Karasz, R.J.Farris. Polym. Eng. Sci.. 22 15 968 (1982)

- 
- <sup>175</sup> J.L. Whitcombe. Determination of coating level by thermogravimetry. Zeneca Resins Internal Document: Ref. RES.WI.049 Issue 1.1. (1996)
- <sup>176</sup> J. H. Schofield, J. El. Spec. Rel. Phenom. 8 129 (1976).
- <sup>177</sup> M. P. Seah, Surf. Int. Anal. 2 222 (1980)
- <sup>178</sup> R. F. Reilman, A. Msezane, S. T. Manson, J. Electron Spectrosc. Relat. Phenom. 8 389 (1976)
- <sup>179</sup> D. M. Brewis & D. Briggs. Industrial Adhesion Problems. Orbital Press, Oxford (1985)

